PH.D. THESIS IN CHEMICAL ENGINEERING

XXVI Cycle

Cyclonic Flows for Reactor Applications with High Engulfment Levels

Scientific Committee

Prof. Antonio Cavaliere
Dr. Maria Rosaria de Joannon
Dr. Raffaele Ragucci

Candidate

Eng.Alfonso Chinnici

Cyclonic Flows for Reactor Applications with High Engulfment Levels

Table of Contents

Abstract

This thesis aims at designing, developing and optimizing novel cyclonic vortex reactor configurations in the context of innovative technologies development for increasing the efficiency and reducing the environmental impact of energy systems. Furthermore, not depending on the specific engineering application, the thesis aims at improving our knowledge on cyclonic vortex flows, clarifying several aspects of their aerodynamic. In particular, the interaction mechanism between a jet and the vortex structure generated by jet itself and/or by cross interference process of multiple jets is investigated. The mixing process between inlet and recirculated fluid, due to the presence of a vortex flow is analyzed with the aim to identify reactor configurations for which the mixing process results maximized, strong, fast and easy to control. Mixing process rate analysis has been carried out by means of engulfment process quantification, a process that governs the mass exchange between a jet and fluid coming from the environment. Furthermore, the identification of the key parameters and the assesment of their effects on the cyclonic vortex structure in terms of vortex characterization and stabilization have been performed.

MILD Combustion and Solar Thermal Gasification are the technologies investigated in this thesis. Cyclonic flows can be naturally coupled with such a processes due to peculiar characteristics.

The first study is related to the development of a novel Vortex burner configuration for a MILD post-combustion process for the purification of CO_2-rich exhaust streams from non-condensable reactive species in the context of Carbon-Capture and Storage Technologies (CCS).

The process requires strong and fast mixing of fuel and oxidant to be stabilized and it is characterized by kinetic times longer than a conventional combustion process. The proposed configuration matches with all these constrains. Furthermore, with the configuration proposed, the cyclonic vortex is characterized by a quasi 2D fluid-dynamic structure, so that the scale up/down of the vortex burner can be easily performed.

Vortex structure characterization and the mixing process analysis have been performed by means of Particle Image Velocimetry and a CFD analysis with RANS approach. The effect of the inlet jet Reynolds number, number of inlet jets, jet type, level of confinement and total inlet flow rate on the engulfment process has been assessed. Results highlighted that

the engulfment process is enhanced by increasing the inlet jet Reynolds number and the number of inlet jets, by adopting low level of confinement and an off-set wall jet.

The second study investigates the use of a cyclonic flow to couple Lean Premixed (LP) and MILD Combustion concepts, for gas turbine applications. This type of process need to take place in combustion chamber where the internal recirculation is significantly enhanced to yield a high level of mixing and subsequent heating of the fresh air-fuel by means of recirculated hot products. Strong and fast mixing of inlet fluid with the hot products is necessary for stabilizing lean and ultra-lean mixture in MILD conditions and represents the critical point for the successful application of this concept to LP gas turbines. The novel vortex reactor configuration proposed allows to analyze some key aspects of mixing process in a vortex combustor. In particular, the effects of inlet jet Reynolds number, number and position of inlet jets are investigated by means of Large Eddy Simulation (LES) approach with the aim to analyze the mixing process between inlet and recirculated fluid. The reactor configuration proposed ensures intense, fast and stable engulfment process.

Results highlighted that the engulfment process is enhanced for a jet that interacts with a vortex structure with respect to a free jet, due to an increase of the local vorticity. Furthermore, it has been found that a strong/stable mixing is achieved for a vortex reactor configuration with two or four inlet jets meanwhile a not stable mixing and a not stable vortex structure is obtained for one single inlet reactor configuration.

Also the presence of fluid-dynamic flow instabilities such as Precessing Vortex Core (PVC) phenomena, generally connected with a strong 3D cyclonic vortex structure has been investigated. Results showed that with the proposed reactor configuration, characterized by a $H/d_{reactor} < 1$ and a sudden contraction as outlet section, a stable quasi 2D vortex structure is obtained, so that PVC is avoided.

Finally, the third study concerns the development of a novel Solar Vortex Gasifier (SVG) configuration. In a directly irradiated solar gasifier, the reactor window is a critical part being used to control the atmosphere in the reactor and prevent particles egress from it. The window can be subjected to overheating due to particles deposition, leading to a reduction in the solar power absorption (decreased transparency) and potential failure. The second issue that needs to be addressed is the short residence time of the particles within the SVG. The effectiveness of this reactor concept can be increased by increasing the residence time of the gas. This prolonged resident time of the particles in the reactor can be

achieve by either reducing the inlet volumetric flow rate or generating stronger vortices that keep the particles in the reactor for a longer time. In a conventional SVG configuration, residence time distribution (RTD) of the particles are principally related to the main flow rate, and it is not easy to control. For a successful application of this process is mandatory that RTD results a function of other parameters, principally the particle size and that it can be easily controlled.

In this view, a novel design of a solar vortex gasifier is proposed in order to develop an efficiently and flexible reactor in which at the same time the window appears clear, long particles residence time can be obtained and the particle RTD results a function of the particle size. To address this scope, a CFD Analysis has been performed with RANS approach coupled with a Lagrangian particle tracking in order to evaluate the effects of changing key parameters, namely geometrical factors, total flow rate and particle size, on window state, mean residence time and the residence time distribution of solid particles.

Chapter 1

Introduction

1.1 - Cyclonic Flows

Cyclonic flows are present both in nature and in practical facilities. In nature, typical example are tornadoes, dust devils or waterspouts, while they have a wide range of applications in engineering. In systems for energy production, such as combustion and gasification processes, cyclonic flow is widely used, due to a variety of advantages like longer residence time, improving and control of mixing rate between fuel and oxidant streams, a better flame stabilization and a cleaner burning (Weber et al., 1986; Syred and Beer, 1974; Gupta, 1984). Pratical uses of reactive cyclonic flows can be found in industrial furnaces, utility boilers, gasifiers and gas turbines combustors with internal recirculation. Design and development of novel systems for energy applications based on cyclonic flow concept is the main topic of interest of this thesis.

1.2 - Motivation of studying Cyclonic Flows

As reported previously, cyclonic flows exhibit several peculiar characteristics that are of interest for energy applications. Even though cyclonic flows have been intensively studied due to their industrial applications, several aspects of their aerodynamics have to be understood further, as it will become evident from the literature review in Chapter 2. The thesis aims at investigating the aerodynamics of cyclonic flow for reactor applications in detail. More specifically, cyclonic flow has been investigated in order to characterize residence time distribution of gas and particle flow subjected to a vortex flow, to evaluate mixing process between fresh mixture and recirculated fluid, to highlight presence/absence of fluid-dynamic instabilities connected with this peculiar flow. All of these processes and phenomena have been connected with key variables affecting a cyclonic flow such as

geometrical reactor parameters, number and position of inlet jets, jet Reynolds number and cyclone Swirl number.

This study has as its final goal the design and development of novel vortex reactor configurations for energy applications.

1.3 - Methods of Investigation

The work presented in this thesis is based both on CFD and experimental approach in order to analyze and characterize a cyclonic flow within the framework of engineering applications for energy production systems .

CFD modeling approach was adopted to predict the features of the cyclone flow field in great details, which providing a better understanding of the fluid dynamics inside cyclone apparatus. CFD was adopted since it is a reliable and relatively inexpensive method of examining the effects of a number of design changes with respect to experimental approach, representing a cost-effective route for geometry optimization.

The different numerical investigations presented in the thesis were conducted using both Large-Eddy Simulation (LES). and Reynolds Averaged Navier-Stokes (RANS). In particular RANS was used to obtain information on the average flow field, define and optimize cyclone devices, meanwhile LES model was principally adopted to evaluate time-series flow fields, to reveal fluid-dynamic coherent structures and time-depending processes in the flow.

A part of this thesis concerns the development of novel design of combustion chambers for MILD Combustion applications. As it will pointed out in the next chapters this combustion "mode" is a very promising process in the framework of new combustion technologies development aimed to enhance the efficiency and reduce the environmental impact of combustion systems. In order to design and dimension novel vortex reactors, it is mandatory to assess the characteristic times of the chosen system in terms of the auto-ignition time and oxidation time. Kinetic analysis presented in the next chapters were carried out by means of several applications of the CHEMKIN software.

1.4 - Scope of the thesis

In the context of novel technologies aimed to enhance the efficiency and reduce the environmental impact of energy systems, MILD Combustion and Solar Thermal Gasification processes are gaining attention due to their ability to provide an alternative, cleaner and more efficient pathway to process derived-fossil fuels and alternative fuels with respect to conventional combustion and gasification processes.

In MILD Combustion processes a clean and efficient utilization of fuel is achieved by mixing hot gases with fresh combustible mixture in diluted conditions, by means of a strong recirculation in the combustion chamber, which leads to a reduction in pollutants emissions.

In Solar thermal gasification the advantages of using solar energy to drive the endothermic gasification process are numerous and include upgraded calorific value of the carbonaceous feedstock, higher H_2 to CO ratio in the product syngas compared with the syngas derived in conventional auto-thermal gasification, reduced pollutants discharge due to the lack of combustion, and the elimination of oxygen input.

Due to peculiar characteristics, cyclonic flows can be naturally coupled with MILD Combustion and Solar Thermal Gasification processes in order to improve and develop such a technologies, in the framework of a continuos growth of novel energy production systems aimed to reduce pollutants emission, to increase the process efficiency, and consequently to reduce fuel consumption and thus, CO_2 emission.

In this view, one of the aim of this thesis is to project, design and develop novel cyclonic vortex reactor configurations for MILD Combustion and Solar Thermal Gasification process.

Furthermore, not depending on the specific engineering application, key aspects of cyclonic flows aerodynamic aspects that have to be understood further are investigated. In particular, a part of this study has been devoted to the mixing process analysis between inlet reactor jets and the vortex flow, with the aim of finding vortex reactor configurations for which mixing process results maximized, strong, fast and easy to control. Mixing process analysis has been carried out by means of engulfment process quantification, a process that governs the matter exchange between a jet and the fluid coming from the environment. A more clear definition and quantification of engulfment process will be provided in chapter 4. Also presence/absence of fluid-dynamic instabilities connected with

a cyclonic flow has been investigated in order to develop cyclonic vortex reactors where fluid-dynamic instabilities are absent, since they can affect vortex and combustion stabilization, mixing process and combustion process efficiency.

Finally, main parameters affecting a cyclonic vortex structure have been identified and investigated. Characterization of vortex structure has been carried out with the final aim to identify possible reactor configurations for which a quasi 2D-fluid-dynamic structure is established. In such a way, scale up/down of vortex reactor can be easily performed, basing on the concept of modularity.

Chapter 2 presents a review of the different aspects of cyclonic flows that will be investigated through-out the thesis as well as the challenges that the design of cyclonic vortex reactors faces. A part of this chapter is dedicated to numerical aspect issues in modeling cyclonic flows.

Chapter 3 presents the approach used to perform this work. In particular, a comprehensive description of numerical codes and methods used in this thesis is provided, and Particle Image Velocimetry technique, which has been used throughout this work for the experimental campaign, is presented.

Chapter 4 is related to the studies carried out for developing a new Vortex burner configuration for MILD Combustion applications. As it will be highlighted in this chapter, MILD Combustion process can be naturally involved in the context of Carbon-Capture Technologies (CCT) for CO_2 capture and sequestration. The process under investigation requires a strong fast mixing of fuel and primary stream to be stabilized and it is characterized by kinetic times longer than conventional combustion process. Cyclonic flow concept has been chosen in this study since it matches with all the peculiar characteristic of the process. Furthermore, this study extends our knowledge on confined vortex flow behavior and it represent one of the first studies on a cyclone combustion devices that adopt gaseous fuel (literature is principally related to liquid, solid fuels and waste materials). The novel configurations proposed, based on cyclonic flow concept, allow to analyze some key aspects of mixing process in a vortex combustor. In particular, the effects of inlet jet Reynolds number, number and position of inlet jets are investigated by numerical and experimental approach with the aim to analyze the mixing process and identify geometrical configuration that lead to a mazimization of such a process. As final remark of this activity, possible reactor configurations for establishing a quasi-2D fluid-dynamic structure have been identified and investigated.

Chapter 5 investigates the use of cyclonic flow to couple Lean Premixed (LP) and MILD Combustion concepts, for gas turbine applications. This type of process need to take place in combustion chamber where internal recirculation are significantly enhanced to yield a high level of mixing and subsequent heating of the fresh air-fuel by means of recirculated hot products. Strong and fast mixing of primary flow with the hot products is necessary for stabilizing lean and ultra-lean mixture in MILD conditions and represents the critical point for successful application of this concept to LP gas turbines. The primary purpose of this study is to develop novel combustion chamber configurations in which the rate of engulfment process is maximized but at the same time, stable and easy to control. Presence of fluidynamic flow instabilities such as precessing vortex core phenomena, revealing of coherent structures and their characteristic frequencies are the other goal of this activity.

Finally, Chapter 6 focuses on the development of a new design for Solar Vortex Gasifier applications. The effectiveness of this reactor concept can be increased by increasing the residence time of the gas and particles. This prolonged resident time of the particles in the reactor can be achieve by either reducing the inlet volumetric flow rate or generating stronger vortices that keep the particles in the reactor for a longer time. In a conventional Solar Vortex Gasifier configuration, residence time distribution (RTD) of the particles are principally related to the main flow rate, and it is not easy to control. For a successful application of this process is mandatory that RTD results a function of other parameters, principally the size of the particle and it can be easily controlled. In this study a sensitivity analysis of the main geometry factors affecting the RTD, the effect of the particles size and total flow rate on the RTD were carried out by means of RANS approach coupled with a lagrangian particle tracking, in order to propose new configurations for Solar Vortex Gasifier technology development.

Finally, the main findings, as well as some general discussion of cyclonic vortex structure characterization and conclusions from this PhD work are summarized in Chapter 7.

Chapter 2

Literature Review

In this chapter, we briefly present the different aspects of flows that will be analysed in this thesis. In particular, the first part of this chapter presents a classification of the main cyclone devices, depending on the application field and how the swirl is generated into the chamber.. The second part is, instead, a state of the art of. CFD studies of cyclonic flows aimed to highlight critical issues concerning the modeling of these flows. As it has been pointed out .in the first chapter, a part of this thesis is devoted to the analysis of mixing process inside of a cyclonic flow with the aim to obtain a fast and strong mixing inside the chamber configurations tested. In this view, the last paragraph of this chapter is a brief review of the main solutions adopted in engineering applications to increase mixing process rate. A detailed description of the energy processes analyzed in this thesis will be provided in the next chapters.

2.1 - General Concepts

Local recirculation or extensive regions of reversed flow, periodic fluctuations in pressure and velocity, and high levels of kinetic-energy dissipation are the principal characteristics of confined vortex flows.

The flow patterns in a confined vortex are of importance for several practical devices and industrial equipment. These include vortex separators (Gupta et al., 1984), the oldest of the industrial applications, the dust collector, Ranque-Hilsh vortex tube (Hilsch, 1947), the spray dryer, the liquid atomizer, the vortex valve, the vortex combustor (Tanasana and Nakamira, 1971), the gas-core nuclear rocket and many others. Problems of heat and mass transfer in swirl flows are of technologically important in designing different heat and mass transfer exchangers, submerged burners, heat transfer promoters and chemical reactors. Better utilization of vortex flows may lead to an enhancement of heat and mass transfer (De Sa et. al, 1991; Martemianov and Okulov, 2002,2004).

Two basic types of vortex flows can be distinguished:

1. forced vortex flow, which is a swirling flow with the same tangential velocity distribution as a rotating solid body

2. free vortex flow, which is the way a frictionless fluid would swirl.

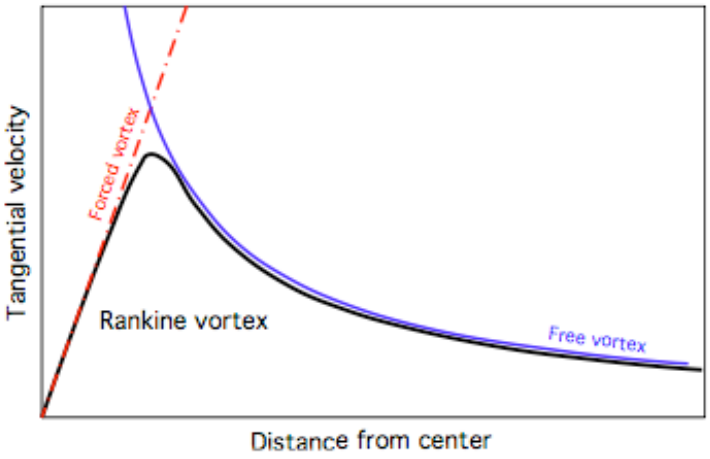

Fig. 2.1 - Distribution of tangential velocity in a real vortex.

The tangential velocity distribution in a real vortex chamber is intermediate between these two extremes. Now imagine first that the swirling fluid has an infinite viscosity (behaves like a solid body). Hence, no shearing motion exists between fluid layers at different radii. In this case, the fluid elements at all radial positions are forced to have the same angular velocity Ω which equals to v_θ/r where v_θ is the tangential velocity. This is the forced vortex flow or solid-body rotation:

$$v_\vartheta = \Omega r \tag{1}$$

In the other extreme, if the swirling fluid has no viscosity, the motion of a given fluid element is not influenced by the neighboring elements at smaller and larger radii. If in such a fluid, we bring an element to a smaller radius, its tangential velocity will increase, since its moment-of- momentum ($mv_\theta r$) will be conserved. Such a vortex is called a free or frictionless vortex. In such a flow, we have $rv_\theta = C$, with C a constant, so that:

$$v_\vartheta = \frac{C}{r} \tag{2}$$

This is the second basic swirl flow. A real swirling flow normally has a core of near solid-body rotation surrounded by a region of near loss-free rotation as sketched in Fig. 2.1. This is called a Rankine vortex.

A radial as well as an axial pressure gradient develops as a result of the vortex motion and the tangential velocity in a cyclone device. These pressure gradients, in turn, influence the flow field and lead to a complex flow phenomenon. If the swirling motion is strong enough, a positive pressure gradient in the axial direction could result in the development of flow reversal in the main flow. At the limit, when the swirl intensity decays to nearly zero, the flow becomes purely axial (pipe flow).

Three axial flow regimes have been reported in the literature, depending on the swirl intensity and the inlet conditions, namely:

1) For low swirl intensity, forward flow over the entire cross sectional area of the pipe, as shown in Fig. 2.2;
2) For a high swirl intensity, backward flow near the pipe axis (r/R = 0) and forward flow near the wall (r/R = 1), (see Fig. 2.3);
3) Double flow reversal with forward flow near the axis and the wall and backward flow in the intermediate region as depicted in Fig. 2.4. There are few references about this regime and the conditions for its development appear to be affected by the inlet geometry (Guo and Dhir, 1990).

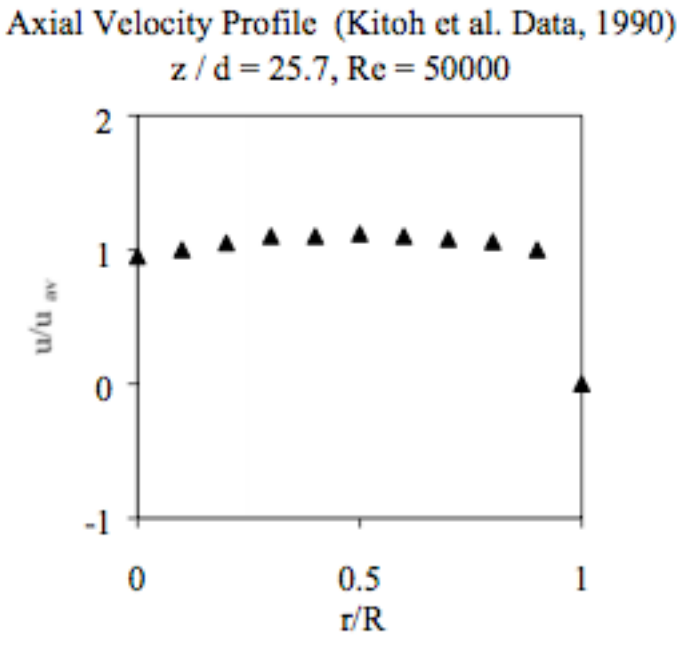

Fig. 2.2 - Type 1 Axial velocity profile.

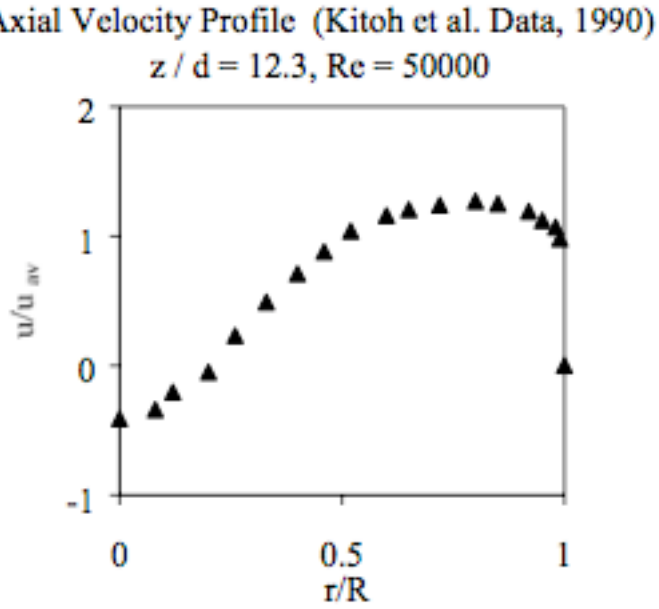

Fig. 2.3 - Type 2 Axial velocity profile.

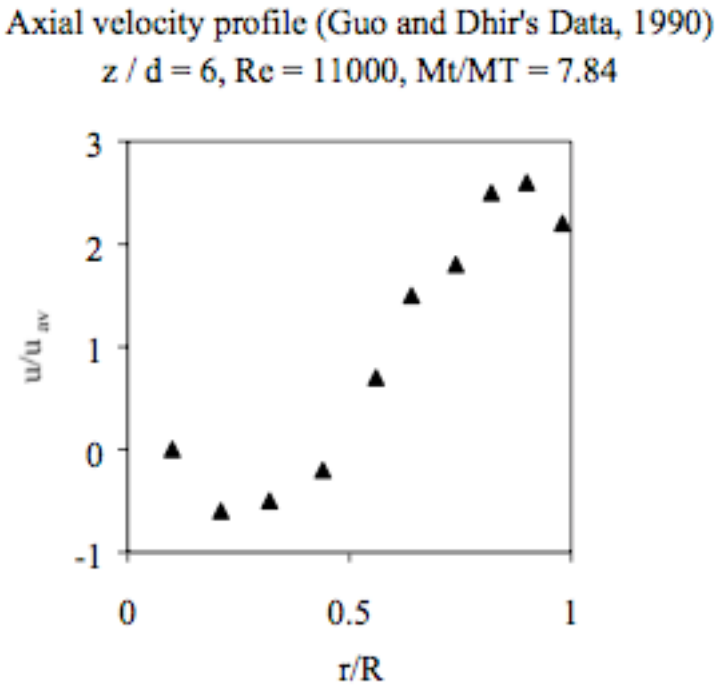

Fig. 2.4 - Type 3 Axial velocity profile.

For with concerning the radial velocity inside a cyclone device, generally the magnitude of the radial velocity, according to experimental data and CFD simulations, is two orders of magnitude smaller than the corresponding tangential or axial velocities.
The flow and pressure distribution within cyclones is more easily under- stood if we make clear the relation between static and dynamic pressures; p and $1/2\varrho v^2$, respectively, with ϱ the density. The well-known Bernoulli equation for steady flow of a frictionless, constant density fluid, which can be derived from the Navier-Stokes equations, states that:

$$\frac{p}{\rho} + gh + \frac{1}{2}v^2 = C - along - a - streamline \tag{4}$$

In this equation, we recognize the static and dynamic pressures as the first and third terms on the left-hand side. They have been divided by the fluid density. This equation shows that static and dynamic pressures can be interchanged in the flow field (Hoffman and Stein, 2008). In areas where the velocity is high, the static pressure will be low and vice versa. It is especially important to appreciate this interdependence between static and dynamic pressure when dealing with vortex flows. The left-hand side of the previous equation is called Bernoulli's trinomial. The second term is unimportant relative to the two others when discussing dust separators and vortex burners since the fluid density is relatively low, and height differences not very large. In an actual flow situation, the fluid is not fric tionless. Frictional dissipation of mechanical energy will therefore cause Bernoulli's trinomial to decrease in the flow direction, i.e. the trinomial is no longer constant, but decreases along a streamline. Frictionless flow is, nevertheless, a reasonably good approximation in the outer part of the swirl in a cyclone; Bernoulli's trinomial does not change in a sensible way in this part.

2.2 - Cyclonic Flows in Combustion

In combustion systems, such as in gas turbine engines, diesel engines, industrial burners, and boilers, cyclonic flows (or vortex flows) were originally used to improve and control the mixing rate between fuel and oxidant streams in order to achieve flame geometries and

heat release rates appropriate to the particular process application (Weber et al., 1986). At sufficient degree of swirl, an internal recirculation zone is generated, which allows high rate of heat release, as products of combustion are recirculated and ignite the incoming fuel/oxidant streams. This provides a stable, compact flame (Swithebank and Chigier, 1969), with a good performance for difficult carboneous materials and poor quality gases (Syred and Beer, 1974).

Swirling flows result from the application of a spiraling motion, with a tangential velocity component (also known as a tangential or azimuthal velocity component) being imparted to the flow via swirl vanes (Wang et al., 2007),in axial plus tangential entry swirl generator (Kempf et al., 2008), direct tangential entry into the combustion chamber. (Gupta, 1984) .Experimental studies show that swirl has large-scale effects on flow fields: jet growth, entrainment, and decay (for inert jets) and flame size, shape, stability, and combustion intensity (for reacting flows) are affected by degree of swirl imparted to the flow.

Two main types of vortex combustor can be identified as follows:

1) Swirl Burner, here swirling flow exhausts into a furnace or cavity and combustion occurs in and just outside the burner exit;

2) Cyclone Combustion Chamber, here air is injected tangentially into a large, usually, cylindrical chamber and exhausts through a centrally located exit hole in one end. Combustion mostly occurs inside the cyclone chamber.

Swirl burners are typically adopted to increases considerably the stability limits of most flames; in fact with certain swirl burners, the blow-off limits are virtually infinite. Cyclone combustion chambers have large internal reverse flow zones which provide very long residence times for the fuel/air mixture. They are typically used for the combustion of difficult materials such as poor quality waste or vegetable refuse. In contrast to the swirl burner which usually has one central toroidal. recirculation zone, the cyclone combustor often has up to three concentric toroidal recirculation zones. Sufficient information is also available to indicate that stratified or staged fuel or air entry may be wed to minimize noise, hydrocarbon, and NO_x emissions from swirl combustors.

2.2.1 Swirl Burner-

For non-premixed combustion applications, in order to maintain the flame, a continuous source of ignition must be provided to the fresh reactants located at the root of the flames. At high velocity, blow-off occurs if the heat received by the recirculating eddies from the hot combustion gases is insufficient to maintain a temperature high enough to cause ignition.

In jets with high swirl number, when the angular-to-linear-momentum ratio exceeded a critical value, a toroidal vortex type recirculation zone appeared in the central region of the flow and close to the nozzle. This toroidal vortex plays a key role in the stabilization of flames. The high-intensity turbulence that occurs in the vortex region increases the mixing which can be enhanced by up to a factor of 5 (Valera-Medina et al.,2009; Al-Abdeli and Masri, 2007). The hot gases and active chemical species recirculate back to the burner due to the Central Recirculation Zone (CRZ). Heat and mass are thus transported effectively from combustion products to fresh combustible mixture (Gupta, 1984). The improved mixing allows to push back the blow-out limits of non-premixed flames and to short both the flame length and the distance from the burner at which the flame is stabilized (Valera-Medina et al.,2009).

Other benefits of using a swirl for flame stabilization come from the compact flame and the high level of mass recirculation that are obtained compared to non-swirling flow. Therefore, all industrial combustors feature a swirl that is intense enough to create a large central recirculation zone.

Flame stabilization by means of the development of a Central Recirculation Zone is the main concept that underlie the development of a swirl burner. A schematic diagram of such a device is reported in Fig. 2.5. This is of simple configuration with two circular inlets firing into a circular chamber, which leads via a sudden contraction to the exhaust, normally 50% of the diameter of the main chamber. The area of the tangential inlets can be varied by removable inserts to give swirl numbers in the range 0.75 upwards. Fuel can be introduced by several methods, including axially along the centre line and premixed with the air by introduction via a premixing system just before the tangential inlets. This device normally produces a central recirculation zone (CRZ) in the exhaust over its operational range giving excellent flame holding capabilities.

Several factors influence the size of the recirculation zone, namely the degree of swirl, the blockage ratio of the flame holder in the stream, divergent walls if there is no separation of the flow from the walls and the shape of the flame holder. Changing the amount and nature of fuel injected allows to control the temperature and the gas composition into the reverse flow zone while variations of the degree of swirl controlled by the swirl number allows an aerodynamic control for mixing and reaction (Gupta, 1984).

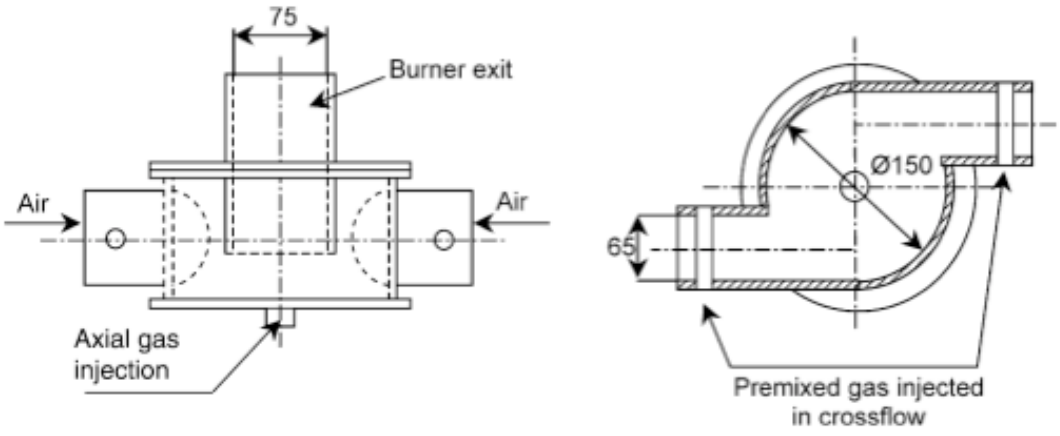

Fig. 2.5 - Schematic diagram of a generic swirl burner (adapted from Valera Medina et al., 2009).

Swirl flows, and their effects on the combustion process are all strongly dependent on the degree of swirl imparted to the flow. This degree of swirl is characterized by the swirl number S. The swirl number is a non-dimensional number defined as the ratio of the axial flux of swirl momentum to the product of the axial flux of axial momentum and the injector radius R (Syred and Beer, 1974):

$$S = \frac{\int \rho U_{\vartheta} U_x r \, dA}{R \int \rho U_x^2 \, dA} \tag{5}$$

where Ux and U_θ are the axial and the tangential components of the mean velocity respectively, A is the section of the injector and R is a characteristic length, typically the radius of the cross section plane or the equivalent radius in case of a non-cylindrical shape. Other important dimensionless parameters characterizing a swirl flow are the Strouhal number St and the Reynods number Re with:

$$St = \frac{fD}{U} \quad (6)$$

and

$$\mathrm{Re} = \frac{UD}{\nu} \quad (7)$$

with f being the precession frequency, D a characteristic diameter (typically D = 2R), U the flow velocity and ν the kinematic viscosity of the fluid.

A typical toroidal recirculation zone formed at the exhaust of a swirl burner is shown in Fig. 2.6 for a swirl number of 1.57 and shows the large bubble of time mean recirculated flow that is formed with here 12% of the flow being recirculated (Chigier and Beer, 1964).

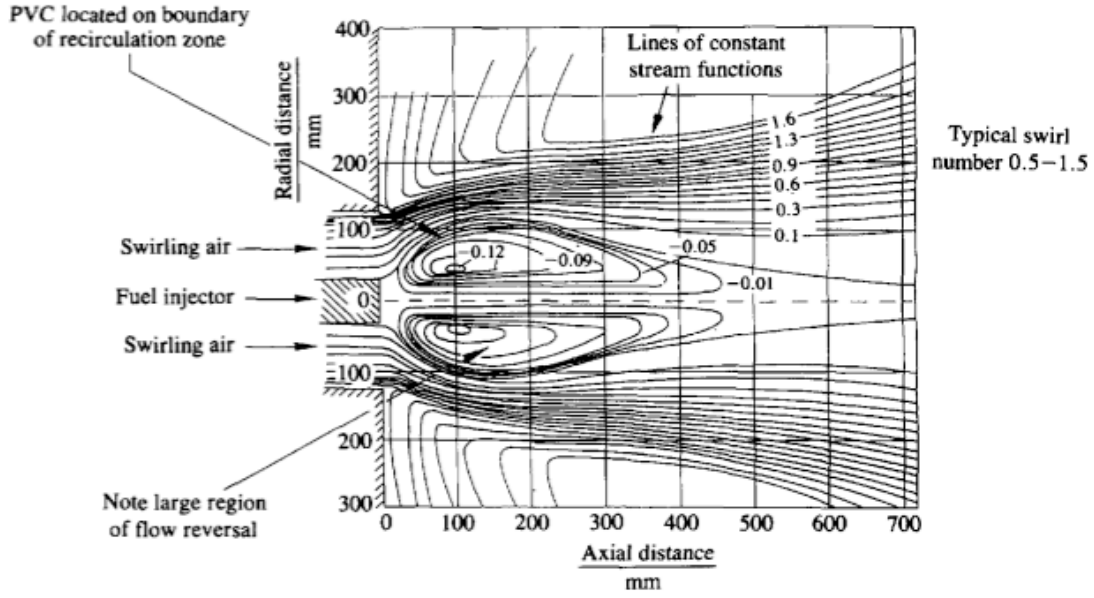

Fig. 2.6 - Stream function distribution at swirl burner exhaust (adapted from Gupta, 1984).

With confinement this process is modified, the rate of decay of swirl velocity is considerably reduced, hence the size and strength of the CRZ formed. This is illustrated by results from a swirl burner furnace system for the combustion of low calorific values gases from carbon black plants (Syred et al., 1997).

2.2.2 Cyclone Combustion Chamber

The cyclone combustor has usually been used for the combustion and processing of materials that are normally considered difficult to burn or process efficiently such as vegetable refuse, high ash content coals, anthracite, high sulfur oils, low calorific value waste gases (.Syred et al., 1977; Tsarev,et al., 18, 12, 1971; Madhiyanon et al., 2006)

The main characteristic of the cyclone combustor are:

1) long residence times, which depends upon swirl number and chamber length;

2) a long, thin annular recirculation zone formed internally close to the walls that can be used to enhance flame stabilization;

3) due to the very high swirl levels, exceptionally high levels of artificial gravitational acceleration are imposed on the entering fuel/air mixture, with considerable benefit to flame speed;

4) they can be adapted in a two-stage combustor arrangement, the swirl burner type flow in the exit being used to provide an after burning process which ensures complete fuel burnout.

The swirl numbers in cyclone combustors are appreciably higher than for the corresponding swirl burners. Typically, the range of swirl numbers lie in between 3 and 20, depending on the geometry configuration and field of application (Gupta, 1984). A sketch of a typical cyclone combustion chamber is reported in Fig. 2.7.

In most occasions, for a cyclone combustion chamber the exact calculation of Swirl number is too involved. But using reasonable approximations, in the constant-density case, it has been showed that this parameter can be reduced to a geometric factor (Gupta, 1984):

$$S = \frac{\pi D_e D_c}{4 A_i} \tag{8}$$

with A_i,the inlet area, D_e the exit chamber diameter and D_c the chamber diameter. Compared with other types of combustors a cyclone combustor can be considered to occupy an intermediate position between pulverized-fuel flames and bed combustion. The advantages of cyclone combustors are:

1) excellent fuel oxidizer mixing;

2) heat release concentrated over a reduced volume (high thermal load);

3) low excess air operation; high temperature level with high calorific value fuels

There is little information concerning combustion effects in cyclone combustors as compared to swirl burners. The main reason for this is that all practical cyclone combustors have been used exclusively for the combustion of solid fuels, hence making aerodynamic and most other measurements difficult.

Tangential fuel introduction is preferential for better fuel/air mixing and combustion efficiency. Either blue flames or yellow, highly radiative, flames could be produced inside the cyclone combustor by varying the respective positions of the air introduction along the chamber walls. Flame photographs showed that the position of the flame front inside the cyclone combustor could also be varied by varying the inlet velocity and the position of fuel introduction. Final burnout of the flame sometimes appeared to occur in the exit with a flame very similar to that produced by many types of swirl burners. Highest combustion efficiency occurred when some 2 to 3 per cent of the air was admitted on the axis of symmetry. Two-stage combustion was also utilized for enhancing residence times and combustion efficiency.

The results of detailed measurements of flow aerodynamics within cyclone combustor conditions reveal that the internal flow patterns under non-combustIve and combustive conditions have some similarities (Schimdt,1970; Mansurov et al., 1970) and, in general, non-combustive results can be extrapolated to combustive conditions with a fair degree of success. The main reason is that the combustion process occupies most of the cyclone chamber volume and therefore does not produce the strong radial density and pressure gradients that are responsible for the differences between the non-combustive and combustive states (contrary to that in swirl burners).

The swirl number, S,of most cyclone combustors is very high (typically > 10) under non-combustive conditions. Under combustion conditions the inlet angular momentum to the cyclone chamber remains approximately constant.

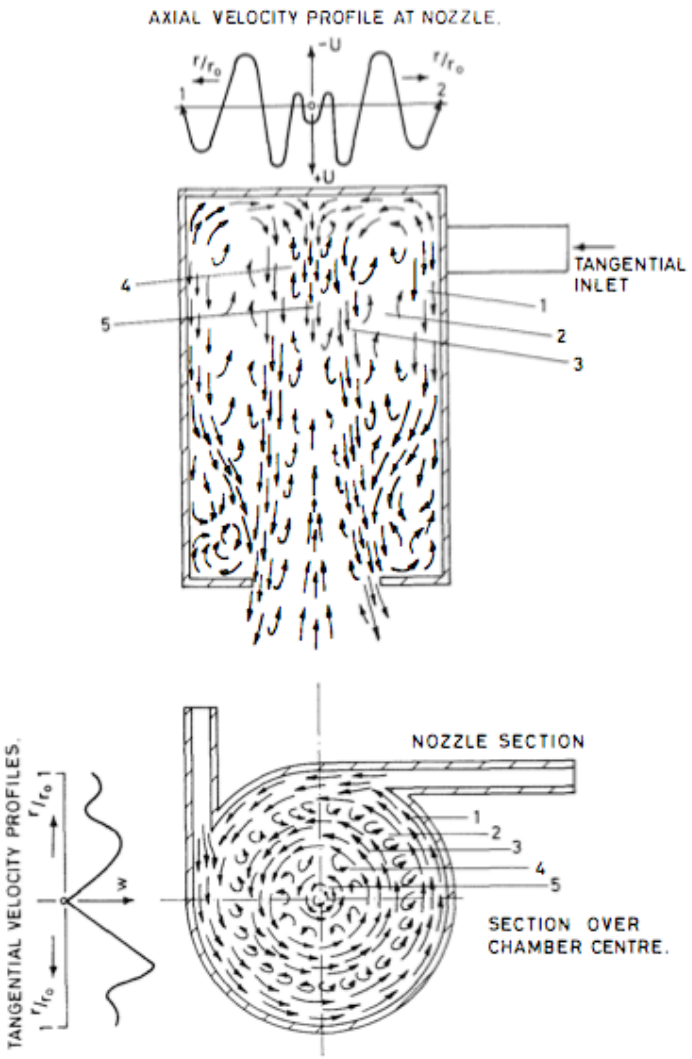

Fig. 2.7 - Schematic diagram of a generic cyclone combustion chamber (adapted from Gupta, 1984).

Nevertheless, the axial momentum of the outlet fluid stream is considerably increased due to exothermic reactions and dynamic confinement of the gases in the cyclone chamber. The swirl number is reduced according to

$$S = S_{isothermal} \frac{T_{inlet}}{T_{outlet}} \tag{4}$$

where T_{inlet} and T_{outlet} are the average inlet and outlet temperature of gases. Confirmation of this conclusion has also come from Beltagui and MacCallum (1976) that found that the main effect of combustion in a cyclone combustor was to reduce the exit swirl number and

thus the size of the internal recirculation zone in the exhaust region. Nevertheless, the internal flow structure is not significantly altered for $r/r_0 > 0.5$.

Cyclone combustion chamber can be classified depending on the degree of swirl, inlet injection configuration and application field. .An extensively review of the different configurations present in literature together with detailed information about.combustion efficiency, flow field and pressure drops of these devices can be found in Gupta (Gupta, 1995).

2.3 - Stability Regimes and Recirculation Zone

2.3.1 Vortex breakdown and recirculation zone

In a Swirl Burner, at low swirl level, $S < 0.4$ (Gupta, 1984) or $S < 0.6$ (Lucca-Negro and O'Doherty, 2001), the centrifugal forces can create significant radial pressure gradients at any axial position compared to axial pressure gradient. This adverse axial pressure gradient is not large enough to cause axial recirculation. There is also no coupling between axial and tangential velocity components (Lucca-Negro and O'Doherty, 2001).

As the swirl number is increased, a strong coupling develops between the axial and tangential velocity components. Both strong axial and radial pressure gradients are set up near the nozzle exit. When there is a change in the cross-sectional area, such as when the flow enters the combustion chamber, the flow expansion results in a decrease of the radial pressure gradient. This leads to an increase in the pressure along the centerline as we go downstream (Syred, 2006). When the axial momentum of the fluid cannot any longer overcome the axial pressure gradient along the jet axis, a flow reversal occurs and a central toroidal recirculation zone is set-up.. The formation of this recirculation zone, through a vortex breakdown process (Syred and Beer, 1974), acts as an aerodynamic blockage or like a three dimensional bluff body and helps to stabilize the flame [115]. The formation mechanism of a recirculation zone induced by swirl is summarized in Fig. 2.8.

The presence of a confinement affects the vortex breakdown process as it modifies the tangential velocity and thus the pressure gradients (Syred, 2006). The mechanism of vortex swirl generation by devices such as swirlers is due to strong inertial effects. However, once the vortex flow is generated, the mechanism that leads to vortex breakdown in high-Reynolds number flows is related largely to inviscid (dynamical) effects (Valera-Medina et

al.,2009). Vortex breakdown is a highly unstable and transient flow pattern which occurs due to the instabilities present in swirl flows such as shear-layer instabilities (like Kelvin-Helmholtz instability) similar to axial jets and azimuthal shear-layer instabilities created by the radial gradient in azimuthal velocity.

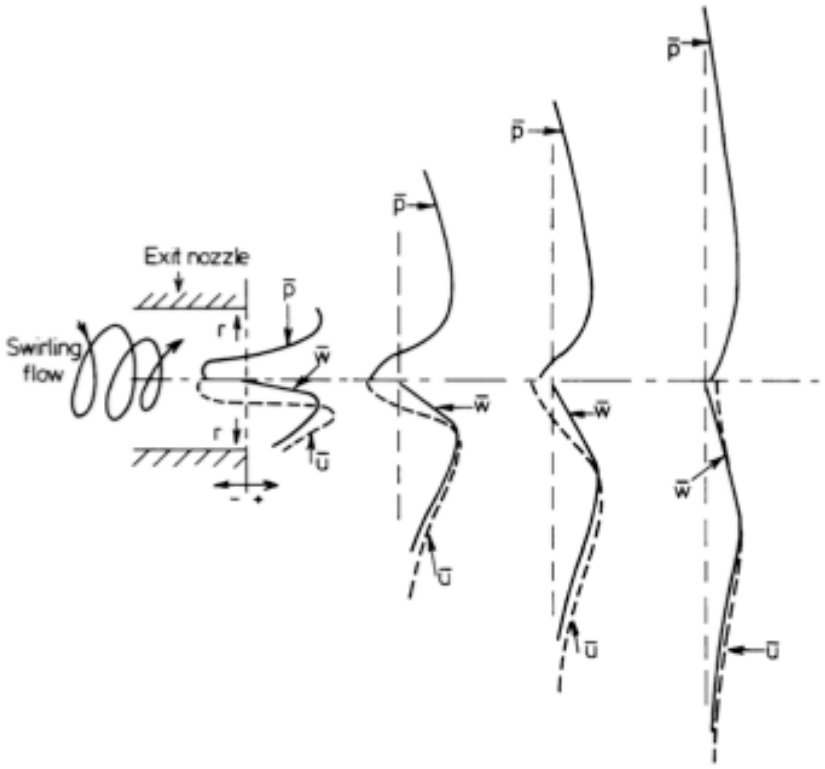

Fig. 2.8- Schematic diagram of processes leading to CRZ formation (adapted from Syred, 2006).

The centrifugal force is another source of instability and leads to a flow profile corresponding to a vortex (Kempf et al., 2008), Rusak and Wang. (1996) propose criteria to predict the stability and the dynamics of vortex breakdown in high Reynolds number swirl flows. One first defines the inlet swirl ratio as $\Omega = \theta \cdot R_i/U$ with R_i as the inlet section radius, θ as the rotation rate and U as the uniform axial velocity. Ω represents the swirl number of the swirler at the swirler exit plane. Two critical swirl ratios, $\Omega_0 < \Omega_1$, are found to exist for a swirl flow in a pipe. For $\Omega < \Omega_0$, a columnar flow is found to develop throughout the pipe, which is the unique solution of the unsteady and axisymmetric Navier-Stokes equations. For $\Omega_0 < \Omega < \Omega_1$ two stable steady-state solutions can develop. One of them describes a columnar swirl flow while the other one is a swirl flow with a

stagnation breakdown region. Which solution appears will depend on initial disturbances introduced to the columnar flow inlet. If small perturbations decay in time it is the columnar state which will prevail while large disturbances enforce a transition to the breakdown state. This transition is called the breakdown process. At last, when $\Omega > \Omega_1$, the columnar swirling flow is unstable and the flow always develops a vortex breakdown state (Valera-Medina et al.,2009). Using the work of Rusak et al. (1996), these critical swirl levels can be computed.

2.3.2 Precessing Vortex Core

The vortex breakdown can sometimes display strongly time dependent characteristics, whereby the recirculation zone itself becomes unstable and starts to precess about its own axis. This situation refers to a Precessing Vortex Core (PVC) (Syred and Beer, 1972). In any swirl burner flow where a vortex breakdown has occurred, a large three-dimensional periodic flow structure can appear that is also referred to as a precessing vortex core (Gupta, 1984; Valera-Medina et al.,2009). PVC (Fig. 2.9) is usually found at the boundary of the reverse flow zone. It forms when the forced vortex region of the flow becomes unstable and the axis of the rotation of the flow inside the swirling recirculation zone starts to precess around the axis of symmetry. As a consequence, the vortex breakdown becomes asymmetric and highly time-dependent (Lucca-Negro and O'Doherty, 2001),

The vortex breakdown can take on several forms, including the appearance of multiple helical vortices formed in the swirl stream shear layer. It has been reported that the unsteady dynamics of these particular features can play an important role in combustion induced oscillations (Midgley et al., 2005; 78; Spencer et. al, 2008).

The combustion process tends to dampen a structure that is present under isothermal conditions, especially in non-premixed configuration (Fig. 2.10). Even when the vortex core precession is suppressed, the resulting swirling flame is unstable and tend to wobble in response to minor perturbations in the flow, most importantly close to the burner exit (Syred, 2006).

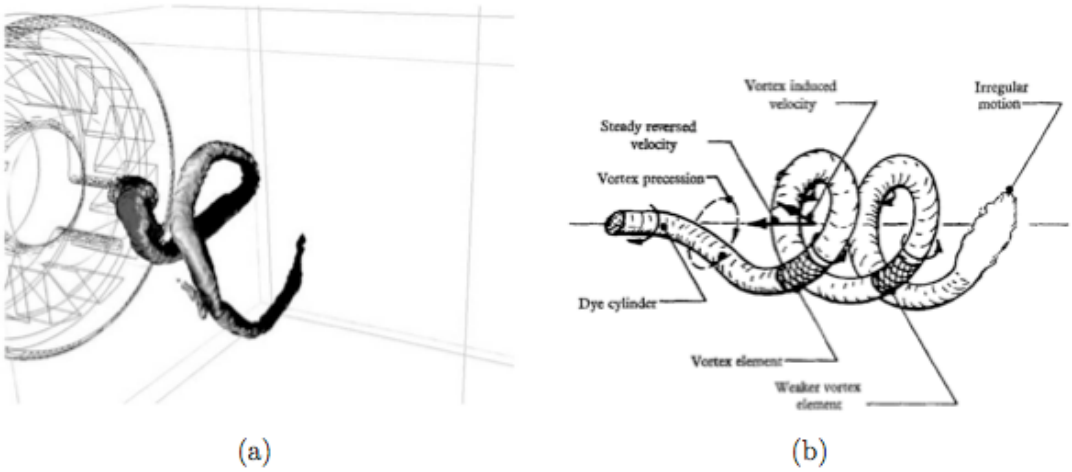

Fig. 2.9- (a) Visualization of a PVC structure as predicted by LES at the exit of the swirler using an iso-surface of low pressure (adapted from Roux et al., 2005); (b) A sketch of a PVC (adapted from Lucca Negro and O'Doherty, 2001).

Premixed or partially premixed combustion can also produce large PVC similar in structure to that found isothermally. In that case, it has been reported that the Strouhal number associated with the PVC in reactive conditions at equivalence ratios around 0.7 may increase by a factor of 2 compared to isothermal conditions (Syred, 2006).

The effect of confinement has an extremely important effect upon the PVC and its related instabilities. Confinement can dramatically alter the size and shape of the CRZ formed as the swirl burner flow expands into a furnace or combustion vessel (Syred and Beer, 1974, Gupta et al.,1984). It can also induce weak regions of forward axial flow on the central axis inside the CRZ. Confinement ratio, D_o/D_e, is the dominant factor, the smaller this ratio the larger is the effect.

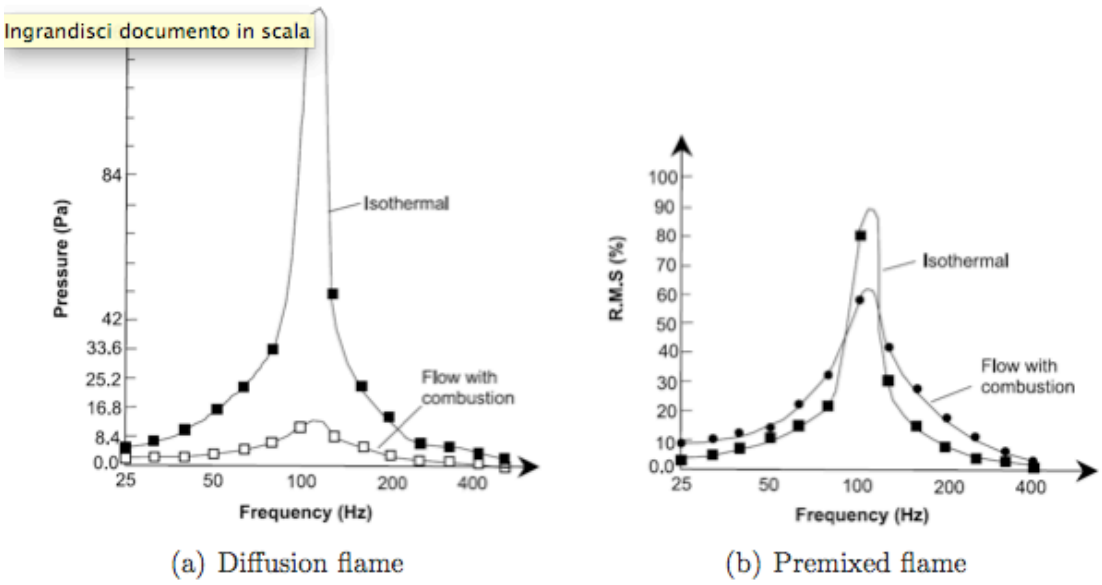

Fig. 2.10- Effect of combustion upon the PVC with (a) 100% axial fuel injection (b) premixing, S = 1.98, equivalence ratio 0.89 (adapted from Syred, 2006).

Other important factors include the level of swirl, equivalence ratio and whether or not a quarl or sudden expansion is used on the burner exit. The CRZ formed by an unconfined swirl burner arises because of the sudden expansion and associated entrainment effects on the edge of the swirling flow (Syred and Beer, 1974). This causes decay in swirl velocity profile, which in turn generates strong radial and axial pressure gradients creating the CRZ. Inevitably, any form of significant confinement will affect this process and alter the size and shape of the CRZ. As the PVC is closely associated with the boundary of the CRZ confinement has considerable effects. (Fick, 1968).

Similar phenomena occur in the exhaust regions of cyclone chambers and combustors, provided they are central and unobstructed. This phenomenon is not well documented in the literature and is often referred to as a kind of fluid dynamic, swirling air jet from a cyclone chamber issuing into free air emitted a characteristic note whose frequency varied with Reynolds number and geometrical configuration. Suzuki (1960) for a vortex whistle, obtained a relationship between the precessional frequency and maximum tangential velocity. Suzuki also showed that the frequency of the vortex whIstle reduces considerably with increase in the L/D_0 ratio. A large diameter rod (d_{rod}/do =0.2, to 0.4) placed on the axis of the whistle destroyed the size of the internal recirculation zone and the PVC . Hence, the effect of the presence of an oil gun on the central axis of a burner is to damp or

destroy PVC, reduce the size of the recirculation zone, increase pressure drop and, sometimes, also reduce combustion efficiency. Hence, the effect of the presence of an oil gun on the central axis of a burner is to damp or destroy PVC, reduce the size of the recirculation zone, increase pressure drop and, sometimes, also reduce combustion efficiency. Similarly, it has been showed that sudden contractions would also stabilize the PVC (Cassidy, 1970).

It has also been demonstrated by flow visualization studies that vortex core precession occurs in especially long cyclone dust separators with $L/D_0 > 4$ (Smith, 1962). The precession always starts away from the tangential inlet deep inside the device; conical contractions seem to reduce the precession. With short cyclone chambers ($L/D_0 <1$) at high degrees of swirl, the very strong radial inflows in the wall boundary layers can affect the PVC. In such a device up to two concentric bands of PVCs may occur around the varying areas of recirculation. In the exit, four distinct PVCs were found, while in the outer part of the chamber at the boundary of the outer reverse flow zone a secondary ring containing many PVCs occurs. Thus, with cyclone chambers, it is evident that the behavior of PVCs is more complex than with simple swirl generators and burners.

2.4 - CFD Studies of Cyclonic Flows

Although experimental and DNS/LES studies provide useful information and insight into the flow physics, the computational methods involving turbulence modeling offers the broadest prospects for several applications. However, the complex flow structure of a cyclonic flow, invalidates some of the assumptions on which simple turbulence models are based. Particularly challenging for modeling are flow features that are absent in simple flows in which the models are usually tuned and validated. But, to be more concrete, the main issue here is rather the necessity of a model of turbulence that simultaneously accounts for:

1. High curvature of the average streamlines;
2. High swirl intensity and radial shear;
3. Adverse pressure gradients and recirculation zones.

These three features make turbulence inside cyclones highly anisotropic, which means that most models based on first order turbulence closure, including two-equation models (i.e., the k-epsilon model), are very weak at capturing the real flow.

Several attempts were made to overcome this limitation. The outcome has been that at least second-order closure, i.e., a Reynolds stresses transport model (RSTM or RSM) is needed to capture anisotropy and achieve a realistic simulation of cyclone flow.

The RSM provides information of all the stress components and contains exact terms for swirling effects in its stress transport equations, so it is capable of capturing most of the physical phenomena. A number of studies (Fu and Qian, 2002; Rumsey et al., 2000; Speziale et al., 2000; Jakirlic et al., 2002; Holzapfel, 2004; Yang et al., 1991) have confirmed that the RSM produced better results than the two equation models for swirling flows. However, the superiority of the RSM used for swirling flows is sometimes overemphasized. While it is true that the RSM is superior to the k-epsilon model for strongly swirling flows, one should not forget that the pressure-strain term is an isotropic assumption in the standard RSM. Although some high order correlation of the pressure-strain have been suggested, they need to be confirmed further for engineering applications.

The high computational costs associated to Reynolds stresses models justified great interest in alternate methods that account for the turbulence anisotropy without excessive computational effort.

The algebraic stress model (ASM) is an economical way of accounting for the anisotropy of Reynolds stress without having to solve the full Reynolds stress transport equations. Fu and Qian (2002) and Rumsey et al. (2000) reported their computations of curvature flows in U-type ducts. However, a number of studies (Fu and Qian, 2002; Rumsey et al., 2000; Speziale et al., 2000; Jakirlic et al., 2002) showed that the ASM assumptions cause loss of swirl-related curvature terms and are still insufficient to capture turbulent physics of swirling flows.

Aside from the RNG k-epsilon and the k-epsilon cc, other hybrid models based on two-equation ideas, such as that of (Meier et al., 1999) have been used to obtain more acceptable results. In particular, to improve accuracy of modeling for swirling flows, the k-epsilon model must be modified. Recent studies (He et al., 1999; Malhotra et al., 1994; Hsieh and Rajamani, 1991; Launder et al., 1977) have indicated that after proper modification, the k-epsilon model can have the potential to be used for strongly swirling flows. Launder et al. (1977) introduced a Richardson number and an empirical coefficient

in the dissipation equation used for the curvature correction. He et al. (1999) used the same approach to simulate the flow in a cyclone where a curvature correction term with a single empirical constant was added into the dissipation equation. Snegirev et al. (2004) modified the eddy viscosity coefficient to use a formula with Richardson number instead of the standard one. Launder et al. (1977) indicated that it might have been better to have made the curvature correction on the production term of the epsilon-equation as well as on the destruction part. Malhotra et al. (1994) just used this approach in which the expressions of both the production and destruction terms were altered together. These modifications of the production, destruction or both have been used successfully for the simulation of swirling or curved flows. In spite of numerous successes these modified k-epsilon models are not as widely validated as the standard k-epsilon models and have reduced popularity and generality. To date there is no generic turbulence model applicable to wide ranging applications. Closure coefficients are a choice of the developer (Wilcox, 2002) so that models are optimized for specific applications. In the standard k-epsilon models the standard values of the model constants were obtained using the experimental data from simple flat plate shear flows (Launder and Spalding, 1972) so it is not surprising that the conventional k-epsilon model with the standard values of the model constants produces unrealistic solutions for strong swirl flows in complex geometries. There are two basic approaches to modify the production and destruction terms for the curvature corrections in the standard k-epsilon model: the re-formalization (RNG) of the production and destruction terms and the constant adjustments before the terms. It should be mentioned that both approaches have same the physical grounding, based on the curvature correction of the production and destruction terms. The reformalization approach has been widely studied (Slack et al., 2000; He et al., 1999; Malhotra et al., 1994; Snegirev et al., 2004). The adjustment of the model constants is based on the fact that the model constants affect the eddy viscosity, and the production and destruction of dissipation rate of the turbulent kinetic energy. The modifications of the eddy viscosity, and the production and destruction of the dissipation rate make the Reynolds stresses and eddy viscosity corrected. Thus, the anisotropic swirl flows can be corrected. However, there are few reports and no clear guidelines about how to adjust these constants although there is a certain physical background. A regulation how to adjust model constants has not yet emerged for 3D swirling flows.

In later years, the need of using unsteady solvers and second-order discretization was established; some key papers on this issue are (Montavon et al., 2000; Witt et al., 1999; Slack et al., 2000). In Montavon et al., (2000) a URANS scheme was used to detect that the PVC structure develops thorough the cyclone length, is destroyed at a certain height, and finally stabilizes itself in the form of a quasi-periodic phenomenon. The study reported in Slack et al. (2000), used a stationary RSTM simulation as an initial condition to trigger a LES, to finally capture the PVC phenomenon with great realism. It was also established that the flow was dominated by the greater scales, since the influence of the specific SGS used in the LES solver was minor.

Nickolaus and Smith (2005) analyzed highly swirled flows in dump combustors, with and without a downstream contraction. Using Large Eddy Simulation (LES), they captured the flow features that were observed in the experiments they modeled. A Reynolds averaged Navier–Stokes (RANS) model was also used, but was found to be less accurate than the LES calculations. It should also be noted, however, that a tremendous difference in simulation run-time existed between the RANS and the LES models. Using the same mesh, the LES ran for 3 weeks, while the RANS model only needed 1 day for convergence.

To provide some illustrations to the simulation of PVC phenomena, lets quote recent research on a pilot PFBC cyclone, equipped with a long dipleg (Velilla, 2005). Single-phase gas flow was simulated by three methods: k-epsilon, RNG k-epsilon and the SSG implementation of a RSTM. Predictions were compared with hot-film anemometry and pressure measurements taken at the dipleg. The study discovered that, under normal operating conditions, the vortex enters well within the dipleg, so that the flow possess their many characteristics of the flow in a cyclone body (Gil et al; 2001,2002). In order to simulate it, second- order discretization and a differential RSTM were needed. When the latter was run, however, it did not converge to a stationary solution. With an adequate time step and retaining an adequate number of time iterations, quasi-periodicities were discovered and the simulation transformed itself in a URANS implementation.

Results showed a reasonable agreement in pressure drop and tangential velocity up to the lower part of the dipleg. Velocity data suffered however from the fact that experimental measurements were taken as pure averages, i.e., without acknowledge- in the fact that large oscillations will show up at fixed positions as a consequence of the PVC. Special phenomena associated with cyclone flow were also detected for the PFBC cyclone dipleg, both experimentally and numerically. The position of the vortex end was detected by

pressure measurements and by the numerical simulation. The adopted URANS scheme seemed to capture the PVC in a similar fashion to other unsteady calculations, some of them being also URANS models but including LES as well.

The latest CFD studies [Peng et al., 2001, 2002] continue to show the capacity of CFD models for predicting interesting aspects of vortex flow separators. Further work using RSTMs is reported in (Wang et al., 2006). LES simulation of swirling and cyclone flows is presently becoming a new standard, based as already noted on increased computer capabilities. Derksen and Akker (2000) were among the first to simulate the PVC phenomenon by this method, but only attempting to model small scale cyclones at a moderate inlet Reynolds number of 14000. The capabilities and sensibilities of the particular technique (LES with standard SGS and a lattice-Boltzmann discretization) in simulating confined turbulent vortex flows have been further reported in (Derksen, 2005).

It is not easy to forecast the future of this line of research. On the one hand, LES methods seem to offer a completely realistic simulation barring some minor details. However, the relative competence of URANS with an advanced RSTM has not been established yet, and it should be, given the very relevant cost factor involved. On the other hand, only relatively stable and ordered flows have been simulated. LES and URANS methods must be tested for conditions of a highly incoherent and variable PVC, to ascertain their usefulness under such conditions.

2.5 - Enhanced Mixing Processes

Jet control is a problem of considerable interest in many industrial applications since it regulates the degree of mixing and the efficiency of the process itself .

For a submerged free jet, we can define the process of entrainment defined as the radial flow of the fluid within the direct environment of the jet (Han and Mungal , 2001) . The rate of entrainment regulates the process of mixing between the jet and the ambient fluid . In the context of application of combustion processes the process of entrainment also influence the residence time and the chemical process in general. In this optical control of a jet is of fundamental interest , not only in terms of mixing , but also relatively to the formation of pollutant species. (Chen and Driscoll, 1990). The first studies on the characteristics of entrainment of a jet must be in Ricou in Spalding (1961) , who analyzed

the process of entrainment of a turbulent jet in isothermal conditions , deriving a simple relationship that governs the process of mixing :

$$\frac{m}{m_0} = C\frac{x}{d^*} \quad (5)$$

where m denotes the mass flow of the jet at a distance x from the entrance, m_0 is the initial flow rate , C is the entrainment coefficient equal to 0.32 for the problem analysis and d* is the equivalent diameter which links the environment density with the initial moment of the jet. Further work (Hill, 1972) has shown that the coefficient of entrainment is not a constant but is a function also of the initial mass flow rate of the jet. In particular, the author found that this coefficient varies from 0 to the asymptotic value of 0.32 within 13 diameters from the entrance. Becker and Yamazaki (1978) have analyzed the effect of buoyancy on the entrainment process of a submerged jet, finding that the presence of the buoyancy dramatically increases the speed of entrainment . Other authors (Muniz , 2000) have studied the effect of heat release and the buoyancy on the entrainment process of a jet in a coflow configuration finding that both the release of heat and the presence of a coflow reduce the capacity of jet entrainment. Summarizing , the process of entrainment that regulates the process of mixing, is an extremely complex problem and the entrainment local rate appears to be affected by several factors , such as the release of heat, the buoyancy , the presence of a coflow and the relative speed of the latter and the axial position of the entrance of the jet.

In the context of novel reactor development linked to combustion processes, the problem of the increase of the mixing ("enhanced mixing process") has played and still plays a primary role. First of all, it has to be stressed that the word “enhanced” means to make better, which is not necessarily the same thing as to increase the mixing rates. As discussed by Nathan et al., (2006), increased mixing rates reduce flame luminosity, which may or may not be desirable depending on the application, and typically also reduces flame stability. The optimal mixing characteristic general depend on the application and can not be “enhanced” in a general sense simply by ever-increased mixing rates.

A practical possibility to increase the mixing in the combustion process is the use of systems capable of generating zones of recirculation, so as to increase the local vorticity in the vicinity of the jet to control (Driscoll, 1987). As reported in the introduction,

combustion processes with the use of swirl (Marzouk and Huckaby , 2010) are based on this principle. In particular, the unsteady motions in large scale for areas of recirculation act as a big vortex , engulfed quickly fluid from the surrounding areas (Driscoll, 1987) and increasing the entrainment rate. In addition, this application allows to dramatically reduce the time of the mixing process and therefore of residence in the combustion chamber. Other applications based on this principle , are the sudden expansion, through which it is possible to realize controlled recirculation zones . An exhaustive work on increasing the entrainment level, the spread of a jet in the presence and absence of an abrupt expansion, linked to an increase in the local vorticity is provided by Iyougun and Birouk (2009) .

Other devices are to be found in the bluff-body, that through the creation of zones of recirculation allow the stabilization of a flame in a variety of application of combustion processes (Kiya et al., 2001).

Precessing jet (PJ) is an aerodynamic way to increase the entrainment rate. Studies on PJ have carried out at the University of Adelaide and their application to burners in cement kilns and similar installations (Nathan et. al, 1998; Manias et al., 1994; Newbold et al., 1997; Smith et al., 1998; Lee et al., 2003). Significant advantages in terms of reduced NO_x emissions have been shown on gas fired cement kilns and promise is shown when firing pulverized coal. A Precessing Jet unit consists of a cylindrical chamber with a small axisymmetric sharp edged inlet orifice at one end and an exit lip at the other. Flow enters the sharp edged orifice and expands into the chamber where it attaches asymmetrically to the wall, with substantial internal flow recirculation. The asymmetry causes the reattaching flow to precess about the axis of the device, producing a precessing exit flow. The lip and large transverse pressure gradients near the outlet together steer the exit flow through a large angle, towards the axis and across the face of the nozzle outlet. As a result the PJ entrains large quantities of external fluid, some 5–6.8 that of an equivalent free turbulent jet.

The issue relating to the enhanced mixing is even more stringent for micro-scale applications or in combustion processes with high levels of dilution .

In the case of applications for micro-combustors the problem is extremely important since a rapid mixing between the flows of fuel and oxidizing in laminar flow conditions is needed. In this regard, once again , the use of systems such as perforated plates capable of locally increasing the degree of vorticity (Woodfield et al. , 2003), is a successful strategy to achieve an increase of mixing in these device .

In the case of combustion processes highly diluted and preheated, which in the literature are brought together by the acronym MILD (2004) , the presence of recirculation in the combustion chamber is an essential prerequisite for the establishment of such a regime. The process, in fact, is accomplished through the entrainment of combustion products into the fresh charge, by means of a recirculation (internal or external), which has as result the preheating and the dilution of the fresh mixture feed to the combustor. A state of the art on MILD processes will be provided in Chapter 4.

A key parameter for such a process defined by Wunning and Wunning (1997) is the internal recirculation rate defined as the ratio of the mass flow rate of the internal recirculation gas (M_E) to that of initial fuel and air jet ($M_F + M_A$), namely:

$$K_V = \frac{M_E}{(M_F + M_A)} = \frac{(M_J - M_F - M_A)}{(M_F + M_A)} \tag{19}$$

where $M_E = M_J \cdot (M_F + M_A)$ and M_J is the total mass flow rate of flue gases entrained by both fuel and air jets.

Literature highlighted that high values of this parameter (Kv > 3), which means high levels of entrainment of the combustion products in the combustion chamber are necessary for the onset of a MILD process. In this type of process, the entrainment plays a vital role in regulating the stabilization mechanism. The interaction between the entrainment and the stabilization of a MILD combustion process was analyzed recently by Oldenhof et al. (2011) The experimental apparatus adopted is constituted by a jet of cold fuel that interacts with a coflow of high temperature and lack of oxygen. It has been observed that an increase in the number of Re (and therefore the capacity of entrainment) of the fuel jet , placed at the center of the coflow, leads to a decrease of lift-off height of the flame and an increase of kernel ignition frequency.

For this type application, recirculation in the combustion chamber is usually obtained according to two types reactors. The first (Vervisch et al., 2004), provides the combination of a abrupt expansion, a central jet with high initial momentum and a confined space; in such a way a recirculation zone extended to a wide portion of the combustor is obtained, dictated by the particular aerodynamics of the combustor. A second (Bobba et al., 2007) , however, provides an increase of the entrainment process through the use of a reverse-flow reactor configuration. Here, combustion products are " forced" to recirculate towards the fresh charge, being positioned the exit of the combustor near the entrance of the same .

Another application that is based on the principle of recirculation to increase the mixing , to reduce pollutant emissions and obtain high levels of combustion efficiency is the trapped vortex (TVC), (Patrignani et al., 2010), principally developed for gas turbine applications. In this device we obtain the creation of a vortex within a cavity and the fuel is injected directly into the vortex. Compared to the combustion MILD the value of Kv is about 20 (about 80% of the gas in the combustion chamber is constituted by the combustion products) with all the benefits that ensue . The only problem concerning this configuration is linked to the fact that , once established the vortex within the cavity , only a small fraction of the main flow participates in the reactive process (approximately 3% of the total).

2.6 - Context of the work and its objectives

As it has been highlighted previously, vortex flows can show various aspects of their aerodynamics such as precession or vortex formation, increase of jet entrainment process (and therefore of the mixing process) and longer residence time comparing with non-cyclonic flows. All the above characteristic can be exploited in the context of novel energy processes development and are explored in detail in this thesis. .

Chapter 4 is related to the studies carried out for developing a new Vortex burner configuration for MILD Combustion applications. As it will be highlighted in this chapter, MILD Combustion process can be naturally involved in the context of Carbon-Capture Technologies (CCT) for CO_2 capture and sequestration. The process under investigation requires a strong fast mixing of fuel and primary stream to be stabilized and it is characterized by kinetic times longer than conventional combustion process. Cyclonic flow concept has been chosen in this study since it matches with all the peculiar characteristic of the process. Furthermore, this study extends our knowledge on confined vortex flow behavior and it represent one of the first studies on a cyclone combustion devices that adopt gaseous fuel (literature is principally related to liquid, solid fuels and waste materials).

Chapter 5 investigates the use of cyclonic flow to couple Lean Premixed (LP) and MILD Combustion concepts, for gas turbine applications. This type of process need to take place in combustion chamber where internal recirculation are significantly enhanced to yield a

high level of mixing and subsequent heating of the fresh air-fuel by means of recirculated hot products. Strong and fast mixing of primary flow with the hot products is necessary for stabilizing lean and ultra-lean mixture in MILD conditions and represents the critical point for successful application of this concept to LP gas turbines. The novel configurations proposed, based on cyclonic flow concept, allow to analyze some key aspects of mixing process in a vortex combustor. In particular, the effects of inlet jet Reynolds number, number and position of inlet jets are investigated by Large Eddy Simulation approach with the aim to analyze the mixing process. The primary purpose of this study is to develop novel combustion chamber configurations in which the rate of the entrainment process is maximized but at the same time, stable and easy to control. Presence of fluidynamic flow instabilities such as precessing vortex core phenomena, revealing of coherent structures and their characteristic frequencies are the other goal of this activity.

Finally, Chapter 6 focuses on the development of a new design for Solar Vortex Gasifier applications. The effectiveness of this reactor concept can be increased by increasing the residence time of the gas. This prolonged resident time of the particles in the reactor can be achieve by either reducing the inlet volumetric flow rate or generating stronger vortices that keep the particles in the reactor for a longer time. In a conventional Solar Vortex Gasifier configuration, residence time distribution (RTD) of the particles are principally related to the main flow rate, and it is not easy to control. For a successful application of this process is mandatory that RTD results a function of other parameters, principally the size of the particle and it can be easily controlled. In this study a sensitivity analysis of the main geometry factors affecting a particle RTD, the effect of particles size and total flow rate on the RTD were carried out by means of RANS approach coupled with a lagrangian particle tracking, in order to propose new configurations of Solar Vortex Gasifier for a development of such a technology.

Chapter 3

Models, Codes and Experimental Approach

In this chapter an overview of the numerical tools and experimental techniques used in this thesis, are presented. In particular, the first part of the chapter summarizes the numerical models adopted, while the second part describes the experimental techniques. A detailed description about modeling approach and post-processing methods used is reported in Appendix A.1 .

Details concerning the set-up of the numerical models, description of the experimental systems and construction of the facilities are provided in the next chapters.

All the experimental measurements were conducted in the laboratories of the Institute for Research on Combustion of the National Research Committee in Naples. Numerical simulations were carried out at the Chemical Engineering Department of University Federico II of Naples and at the Centre for Energy Technologies of University of Adelaide in South Australia.

3.1 - Use of Computational Fluid-dynamic in Cyclonic Flows

In this thesis CFD modeling approach was adopted to predict the features of the cyclone flow field in great details, which providing a better understanding of the fluid dynamics inside cyclone apparatus. CFD was adopted since it is a reliable and relatively inexpensive method of examining the effects of a number of design changes with respect to experimental approach, representing a cost-effective route for geometry optimization.

The different numerical investigations presented in the thesis were conducted using both Large-Eddy Simulation (LES). and Reynolds Averaged Navier-Stokes (RANS). In particular RANS was used to obtain information on the average flow field, define and optimize vortex reactor geometry and to quantify the mixing process, meanwhile LES model was principally adopted to evaluate time-series flow fields, to reveal fluid-dynamic coherent structures and time-depending processes (such as mixing process) in the flow. Furthermore, in the context of Solar Vortex Gasifier development and optimization,

Discrete Phase Model (Euler-Lagrange method for dispersed phase motion modeling, one-way coupling) was implemented together with a RANS approach in order to evaluate the particle trajectories through the fluid phase, so that their residence time and behavior can be investigated.
All the simulations were carried out with FLUENT solver of the commercial software ANSYS.

3.2 - Post-Processing Methods

3.2.1 Spectral Analysis

In this thesis spectral analysis is used to obtain information about the frequencies contained in a data set, to analyze the spectral components shared by several signals or to determine the transfer function of a system. Spectra analysis generally used fast Fourier transform (FFT) which is a common tool in practical applications. Actually, efficient computational algorithms are available and allow the implementation of FFT methods on signal processing.

3.2.2 Vortex Definition: Q-criterion

Vortices are a special existence form of fluid motion with origin in the rotation of fluid elements. It can be possible to recognize the existence of vortices first by their intuitive streamline patterns, which are however not Galilean invariant and cannot be used to define a vortex. A natural basis for developing possible rational criteria for identifying a vortex is the symmetric- antisymmetric decomposition of the velocity gradient tensor, ∇u, $\nabla u = D + \Omega$, which suggests that a vortex may be defined as a flow region where the vorticity (symmetric tensor Omega) prevails over the strain rate (symmetric tensor Omega).
The first criterion to reveal vortex structures in a flow (Basdevant and Philipovitch, 1994), for two dimensional incompressible flow (u, v) based on the eigenvalues σ of ∇u, of which the characteristic equation is:

$$\sigma^2 + Q_{2D} = 0 \tag{20}$$

where Q_{2D}

$$Q_{2D} = \left(\frac{1}{2}\|\Omega\|^2 - \|D\|^2\right) \tag{21}$$

is the second invariant of ∇u (and also the negative of the discriminant Δ_{2D}; the first invariant is tr(∇u)=0). When $Q_{2D} > 0$ at a point, the flow is called elliptic and we have purely imaginary eigenvalues $\pm i\sigma_i = \pm\sqrt{Q_{2D}}$; for the case of $Q_{2D} < 0$ the flow is called hyperbolic. Thus, a vortex is defined as a connected fluid region with:

$$Q_{2D} = (-\Delta_{2D}) = \sigma_i^2 > 0 \tag{22}$$

known as Q-criterion. Q-criterion, is related in the literature to the family of Eulerian coherent structure criteria (together with swirling strenght criterion, vorticity and pressure criterion) for the identification of vortex structure in a flow. Such a criterion was adopted in this thesis to reveal the coherent structures in the fluid flow.

3.3 - Kinetic Analysis: Numerical Tools

A part of this thesis concerns the development of novel design of combustion chambers for MILD Combustion applications. As it will pointed out in the next chapters this combustion "mode" is a very promising process in the framework of the development of new combustion technologies aimed to enhance the efficiency and reduce the environmental impact of combustion systems. In order to design and dimension novel burners concepts it is mandatory to assess the characteristic times of the chosen system in terms of the auto-ignition time and oxidation time. Kinetic analysis presented in the next chapters were carried out by means of several applications of the CHEMKIN software.

The CHEMKIN is a software developed by Sandia National Laboratories for the solution of problems and interpretation of gas phase chemical kinetics with elementary. It is a powerful and flexible tool for simulation of systems described by kinetic mechanisms detailed and complex. The software is widely used for the development and optimization of combustion processes. It allows also the study of systems not in thermal equilibrium, called plasma, where the reactions could be due to different temperatures and involve ions and electrons.

3.4 - Particle Image Velocimetry

One of the aim of this thesis concerns the development and design of a novel Vortex Combustion Chamber configuration for MILD Combustion applications. In this thesis Particle Image Velocimetry (PIV) technique was used to characterize the isothermal flow-field inside a Vortex Burner prototype, built coupling PMMA and quartz in order to have a full optical access of the device. In particular PIV was adopted to obtain information on the fluid-dynamic flow field, inlet jet behavior in terms of growth rate and jet width with respect to the main key parameters of the process.(namely, inlet jet Reynolds number and number of the inlet jets). In the following, the basic features of PIV technique are described briefly, meanwhile a full description of experimental facility, optical diagnostic and test conditions used will be provided in the next chapter.

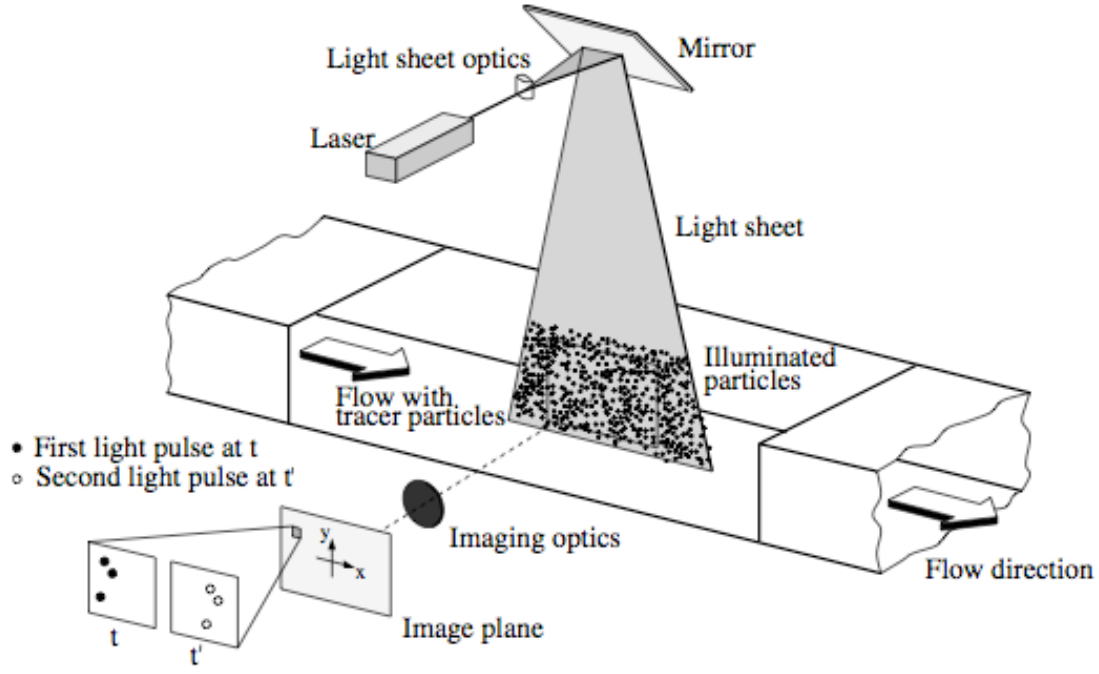

Fig. 3.2 Typical experimental system for particle image velocimetry.

The experimental setup of a PIV system typically consists of different sub- systems. In several applications tracer particles have to be added to the flow. These particles have to be illuminated in a plane of the flow at least twice within a short time interval. The light

scattered by the particles has to be recorded either on a single frame or on a sequence of frames. The displacement of the particle images between the light pulses has to be determined through evaluation of the PIV recordings. In order to be able to handle the great amount of data which can be collected employing the PIV technique, sophisticated post-processing is required.

A typical setup for PIV recording is reported in Fig.3.2 (Clemens, 2002). Small tracer particles are added to the flow. A plane (light sheet) within the flow is illuminated twice by means of a laser (the time delay between pulses depending on the mean flow velocity and the magnification at imaging). It is assumed that the tracer particles move with local flow velocity between the two illuminations. The light scattered by the tracer particles is recorded via a high quality lens either on a single frame (e.g. on a high-resolution digital or film camera) or on two separate frames on special cross-correlation digital cameras. After development the photo-graphical PIV recording is digitized by means of a scanner. The output of the digital sensor is transferred to the memory of a computer directly.

For evaluation the digital PIV recording is divided in small subareas called “interrogation areas”. The local displacement vector for the images of the tracer particles of the first and second illumination is determined for each interrogation area by means of statistical methods (auto- and cross-correlation). It is assumed that all particles within one interrogation area have moved homogeneously between the two illuminations. The projection of the vector of the local flow velocity into the plane of the light sheet (two-component velocity vector) is calculated taking into account the time delay between the two illuminations and the magnification at imaging.

The process of interrogation is repeated for all interrogation areas of the PIV recording. With modern charge coupled device (CCD) cameras (1000×1000 sensor elements and more) it is possible to capture more than 100 PIV recordings per minute. High-speed recording on complementary metal- oxide semiconductor (CMOS) sensors even allows for acquisition in the kHz- range. The evaluation of one digital PIV recording with several thousand instantaneous velocity vectors (depending on the size of the recording, the interrogation area and processing algorithm) is of the order of a second with standard computers. If data is required at even faster rates for online monitoring of the flow, dedicated software algorithms which perform evaluations of reduced precision within fractions of a second are commercially available.

Chapter 4

MILD Vortex Burner: Reactor Design, Modeling and Experimentation

4.1 - Introduction

This chapter presents the design, modeling and experimental analysis of a novel MILD Vortex Burner configuration for MILD Combustion applications. First of all, a state of the art of MILD processes and the identification of the problem is reported. In particular, here, a post-oxidation MILD process to reduce oxygen and non-condensable/oxidizable species concentrations from flue gas of CO_2-capture-ready combustion systems is proposed. Then, the results will be presented by dividing them into paragraphs according to the different aspects of the process investigated. Thus, the first session is related to a kinetic analysis of the process, in order to numerically study the process of typical flue gas of CO_2-capture-ready combustion systems to both assess the practical feasibility and identify the optimal working conditions with the target of reducing oxygen and non-condensable/oxidizable species concentrations below their maximum acceptable values.

Second session reports a preliminary CFD analysis carried out to define the geometry of the reactor. Then, a prototype of the reactor was built coupling quartz-PMMA in order to investigate the mixing process and the jet behavior inside the vortex chamber and to characterize the isothermal flow-field by means of PIV technique. Particular attention was devoted to the mixing process inside the chamber. between the recirculated fluid and the primary jet. Mixing process evaluation was carried out relating such a process to the engulfment process. Definition and quantification of the engulfment process are reported in a specific paragraph. Afterwards, further CFD analysis were carried out to compare experimental and numerical data, testing different closure models. The last session is related to a reactive CFD analysis of the process.

4.2 - MILD Combustion

4.2.1 General Concepts

In the century of global warming causes by greenhouse gases emissions, one of the main purpose in energy production systems development has been to obtain a combustion process that allows to reduce pollutants emission, to increase the process efficiency, and consequently to reduce fuel consumption and thus, CO_2 emission.

However, in processes involving combustion, the abatement, of pollutants often comes at the price of efficiency losses. In other words, the existing combustion system remains to be difficult to simultaneously satisfy the requirements for both high efficiency and low pollution.

MILD (Moderate or intense low-oxygen dilution) combustion processes evolve in a temperature and concentration range outside the sphere of interest of conventional combustion processes and is one of the feasible candidate to simultaneously address thermal efficiency need and pollutant emission restriction. Moreover it represents a trade-off between optimizing fuel conversion in terms of energy saving and pollutant abatement, keeping the configurations of traditional processes. MILD combustion regime operates using contemporaneously high temperatures and high dilution of reacting mixture with inert gases, in order to make use of temperature positive effects and, at the same time, to keep under control their gradients. In fact dilution allows to increase thermal capacity of the system, maintining adiabatic flame temperature in a range that keeps NO_x emission under control. In order to smother the adiabatic flame temperatures reached during combustion process, it is needed to use high mixture dilution levels, in order that mixture composition falls out from LFL-UFL (Lower Flammable Limit – Upper Flammable Limit). To realize the process combustion is hence necessary to keep the pre-heating temperature higher than the auto-ignition temperature of mixture. Heat and flue gas recirculation allow to attain the task about pre-heating temperature. The recirculation of hot combustion products decreases oxygen concentration locally and increases the temperature of the reactants. This slows the reactions and leads to a distributed reaction zone so that combustion occurs in homogeneous conditions with uniform concentration of the chemical species and temperature profiles. Various advantages derive from using high preheating temperatures. First of all, higher temperature allows to obtain higher efficiency of

oxidation process. This leads to an higher speed oxidation in the first part of the process of combustion and for liquids and solids fuel, an acceleration in the physical process of atomization, vaporization and gasification. This means that the use of high initial temperatures implies a higher flexibility in the choice of the fuel. Working temperatures should determine an important reduction in the production of NO_x and soot (Aganfonov, 2011; Song, 1981)

Features of combustion processes, such as maximum temperature, structure of the pyrolytic and oxidative region, species distribution and pollutant formation, are the effects of complex interleaved heat and mass transport phenomena and kinetics. The initial and boundary conditions have a significant influence on the evolution of the whole process. In particular, they become even more significant when the process evolves in conditions that can be considered as occurring at the boundary of an admissible range of parameters. This is the case of MILD combustion processes which, by definition, evolve in different temperatures and concentration ranges from those of conventional combustion processes.

In order to define the conditions in which MILD combustion evolves, we can start by considering a homogeneous charge of fuel, such as methane, and air at stoichiometric conditions and at a temperature of 300 K. The temperature increase ΔT related to complete fuel conversion can be computed by the following heat balance relation:

$$m_{in} \cdot Y_{CH_4} \cdot \Delta H_r = m_{out} \cdot c_p \cdot \Delta T \tag{23}$$

where $m_{in} = m_{out}$ is the mass flow, Y_{CH_4} the fuel mass fraction, ΔH_r the heat of reaction, c_p the specific heat capacity at constant pressure and ΔT the temperature increase during oxidation. The relation between temperatures and mixture compositions is schematically represented in Fig 4.1, where a plane $T_{inlet} - X_{O_2}$ is reported. On this plane the iso-concentration lines can be associated to a well identified temperature increase, such as expressed by relation seen previously and reported for a representative number of X_{O_2} . All the values on this plane are obtained by considering the thermodynamic properties constant with temperature. By such an approximation ΔT corresponding to a fixed X_{O_2} is independent of the initial temperature of the mixture. The final temperature T reached by system will be $T = T_{inlet} + \Delta T$.

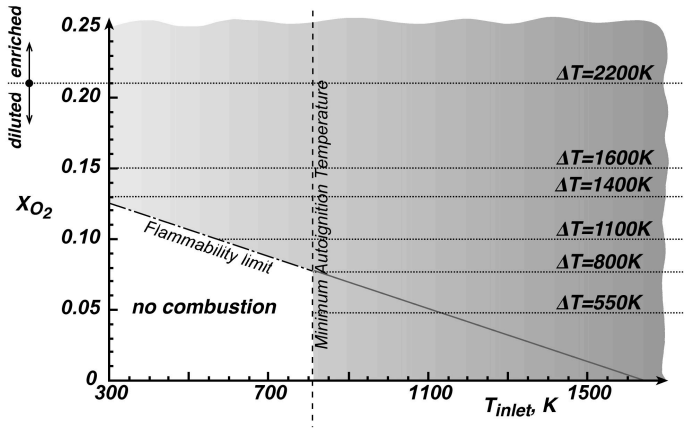

Fig. 4.1 - $T_{inlet} - X_{O_2}$ plane identifying the region at different temperature increases during oxidation (adapted from Cavaliere and de Joannon, 2004).

The temperature increase corresponding to stoichiometric conventional conditions (X_{O_2} = 0.21) is about 2200 K. It can be possible to see that a decrease in the oxygen molar fraction, while keeping the fuel/oxygen ratio constant, corresponds to a decrease in ΔT . For instance, the temperature increase related to X_{O_2} = 0.15 is about 1600K. Starting from X_{O_2} of about 0.125 (ΔT =1400K) the iso-concentration lines intersect a dashed-dotted line. This represents the flammability limit associated with the maximum dilution level allowable for a stoichiometric methane/oxygen/diluent for the propagation of a deflagration structure. It is well known from the literature that this is possible only when the temperature increase due to the oxidative process is high enough to ensure a feedback of radicals and heat so that fresh mixture can reach the ignition temperature and then autoignite. The flammability limit intersects a vertical dashed line, drawn at the minimum auto-ignition temperature $T_{ign}^{\min}$, at T_{inlet} = 800K (Zabetakis, 1965). For $T_{inlet} < T_{ign}^{\min}$ and X_{O_2} below the flammability limit, a deflagration structure cannot be sustained and no combustion occurs without an external permanent source. In contrast, for the same dilution levels the oxidation process can evolve if T_{inlet} is higher than $T_{ign}^{\min}$. In these conditions, very low temperature increases with respect to standard combustion processes are obtained.

On the basis of these indications MILD combustion is defined by Cavaliere A. and de Joannon M. (Cavaliere and de Joannon, 2004) as follows:"A combustion process is termed "mild" when the inlet temperature of a reactant mixture is higher than the self-ignition temperature of the mixture, whereas the maximum allowable temperature increase with respect to the inlet temperature during combustion is lower than self ignition temperature "

As clearly shown in Fig 4.1, the process evolves in a narrow temperature range, which could be placed in an intermediate region between the very fast kinetics of the oxidative undiluted conditions and the relatively slow kinetics linked to low-temperature self-ignition regimes.

By defining $\Delta T_{inlet} = T_{inlet} - T_{ign}^{\min}$ it is possible to summarize the different combustion regimes on the basis of the main macro area of possible processes. They are illustrated in Fig 4.2 in which ΔT and ΔT_{inlet} are reported on the ordinate and abscissa axis respectively.

As we can see in this diagram, main categories are identified. Below the abscissa are processes with a negative maximum temperature increase. They are identified as pyrolysis processes because they are endothermic in nature and are subdivided into two categories, *auto-incepted pyrolysis* and *assisted pyrolysis*. The first needs no external source to make the processes effective and is located in the lower-right quadrant, for $\Delta T_{inlet} > 0$. The second is called *assisted pyrolysis*, because it needs external heating or a catalytic device in order to develop. It is located in the lower-left quadrant, where the inlet temperature is lower than the ignition temperature ($\Delta T_{inlet} < 0$), which in the case of pyrolysis should be called *inception temperature*. In principle and in a rigorous way the maximum temperature should always be higher than the frozen temperature. Therefore, the lower quadrants should not exist. In practice, pyrolytic conditions are obtained for high mixture fraction values.

The upper-left quadrant is the region of assisted ignited combustion for which the maximum temperature difference is positive, whereas the inlet ignition differential is negative. This is the classical, standard combustion condition, in which the first ignition of the mixture is ensured by heat (or other source) by an external source, since reactants do not carry enough sensitive enthalpy to incept the process. This region corresponds to the region on the left side of $T_{ign}^{\min}$ on the plane in Fig 4.1. This region is also divided in two

parts. Feed-back combustion, associated with the region above the flammability line and pilot combustion, associated with the region below it.

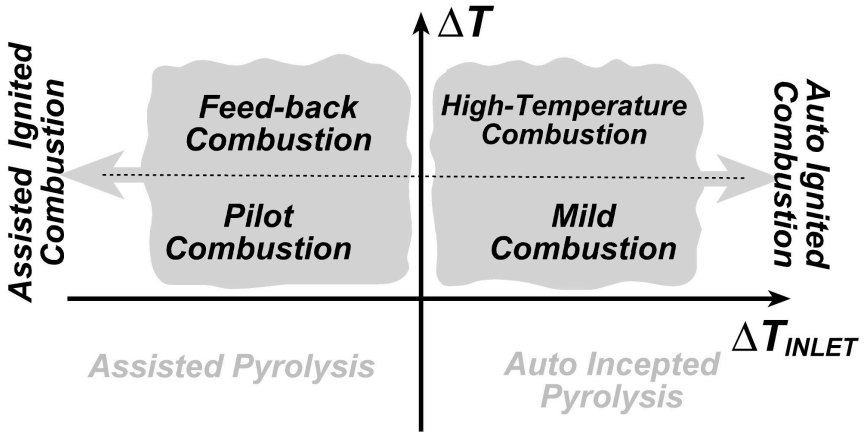

Fig. 4.2 - Combustion categories as a function of ΔT and ΔT_{inlet} (adapted from Cavaliere and de Joannon, 2004).

Spontaneous inception of oxidation occurs in the processes in the upper-right quadrant and are classified as *auto ignited combustion*. In this case the differential inlet temperature is positive and auto-ignition should occur with no external energy input. Also in this case two regions can be identified. The first, known as *high-temperature combustion*, is the region where the system can increase its temperature up to values comparable to air/fuel systems in stoichiometric condition. In contrast, in the second region the maximum ΔT is lower than a certain value, as shown in Fig 4.2. This region has been termed *MILD combustion* (Cavaliere and de Joannon, 2004) both because the temperature increase is quite mild and because reference is made to diluted conditions according to the acronym, Moderate or Intense Level of Dilution. The definition is rigorous in the sense that it is not ambiguous and is based on a conservative criterion identifying approximate conditions in which oxidation is more controlled by auto ignition rather than by the heat released by the oxidation itself. It has to be noted that Figs 4.1 and 4.2 are only indicative of the range of MILD combustion and they are used to clarify the basic concept behind it. A more precise boundary of the region in which it occurs can be obtained only if specific processes have to be analyzed in detail, in terms of fuel type, system composition and configuration considered.

It is possible to give other definitions, available in literature, of the MILD combustion that stresses the peculiar characteristics of such a process. For example, (Peters, 2000) has suggested an analytic definition basing on the absence of ignition and of extinction of oxidation process that occurs for highly diluted and pre-heated mixtures.

On the basis of the definition given above several peculiarities of such combustion mode could be highlighted.

One of main peculiarities of this combustion mode is the absence of a flame front. Actually in the conventional burners the real chemical reactor is the steady front flame, an area stretched by turbulence, on which typical reactions of combustion processes occur. Although the thickness of the front of flame is very tight, it hosts great temperature and species concentration gradients. The location of the flame front and its stability in the combustion chamber depends on many fluidynamic parameters. If mixture is highly diluted (beyond flammability limits) and preheated to temperatures that allow auto-ignition, there will not be a front flame but a reaction volume that extends to the whole combustion chamber. In these operative conditions, there are no problems related to flame instability, leading to a simplification of reactants mixing and stabilization processes.

Combustors working in MILD combustion conditions have been developed and tested in industry and research institutes (J. Yuan 1999; B. Özdemir 2001; A. Cavigiolo 2003; C. Galletti 2007; M. Fantuzzi 2008; P. R. Medwell 2008). When MILD combustion take place, the entire furnace appears bright and transparent, i.e. no flame is visible (J. A. Wunning 1997; M. Katsuki 1998; H. Tsuji 2003; A. Cavaliere 2004), so that this process is often called “flameless combustion” or “flameless oxidation” (FLOX) (J. A. Wunning 1997).

Temperature and species concentration profiles measured in burners working in diluted high-temperature condition show a fairly uniform distribution. For instance in Fig 4.3, the wall temperature of a furnace where natural gas is burnt in MILD conditions (S. Orsino 2001) is reported on the left axis as a function of axial coordinate. It is evident that temperature is quite constant along the whole furnace (A. Milani 17-18 January 2000). This testifies that there is no main reaction zone, associated with strong gradients, localized in a limited region of the combustion chamber, as would be generally expected for a standard furnace . In this case, the reaction zone extends to most of the available volume, thus often leading to the statement that such systems work in almost “well-stirred” conditions (S. Orsino 2001). Distributing heat release to a larger volume results in a nearly

uniform temperature distribution with reduced peak temperatures. As a consequence the net radiation flux can be enhanced by as much as 30% (H. Tsuji 2003) and emissions of some pollutants are lower than from conventional combustion system in which combustion zone is concentrated on a flame front. In the same figure, a third characteristic of MILD combustion process highlighted, namely the relatively high radiative heat flux in the order of 300-350KW/m2 (S. Orsino 2001) measured in the same furnace. Such a high radiative flux is related to high concentrations of species strongly emitting in the infrared region, such as CO_2 and H_2O. Because the whole combustor is filled with such species, the whole medium becomes more emitting with respect to a conventional combustion furnace. This characteristic is of great practical interest because it positively affects heat transfer and contributes to keeping the average temperature low.

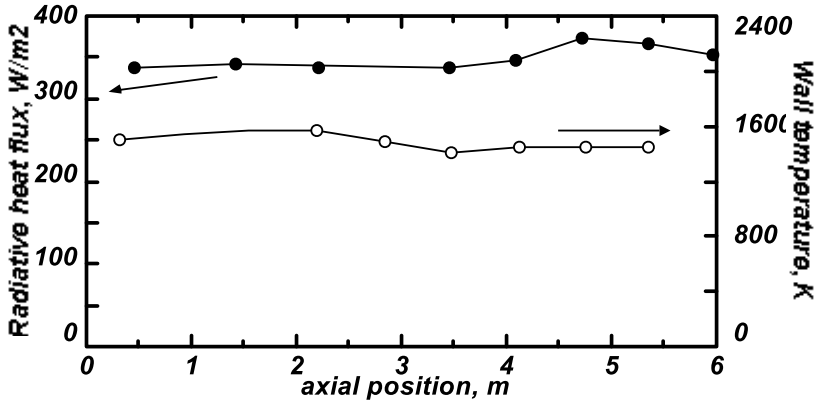

Fig.4.3 - Radiative heat flux (left axis) and wall temperature profile (right axis) in the burner in a mild combustion regime (adapted from Orsino, 2001)

Because of this almost homogeneous distribution of heat, “hot spots” are eliminated and product quality can be improved in some applications.

Several studies have been done on this type of combustion in order to completely understand the process. The aim of these works is to evaluate the stability and the behavior of the combustion process and the performances of the combustion chamber in terms of energy efficiency, pollutants emission and heat flux. All the key parameters such as the pre-heat temperature, the velocity of the jets, type of fuel and percentage of oxygen are related to the system behavior and hence to pollutants emission. Moreover the optimization of the combustion chamber in terms of fuel and pre-heated air injections positions, firing modes (parallel and staggered) is investigated.

In this context, between several methods of application of Mild combustion, two of them seem to be widely used. The first method is characterized by a central jet of fuel and a number of air jets located circumferentially around the central jet supplying preheated combustion air. In this configuration, the air jets entrain large quantities of the recirculated combustion products before mixing with the fuel jet (Wunning and Wunning, 1997). In the second method, the combustion air is provided by a central, high-momentum air jet that is surrounded by a number of low-momentum fuel jets. These weak fuel jets are injected into recirculated combustion products and consequently the fuel is diluted before it mixes with the combustion air (Weber 1999, Tsuji 2003).

A schematic picture of such applications of Mild combustion is shown in Fig. 4.4. Depending on the position of air and fuel injectors, different dilution cases in which the burned gas might entrain into fuel, air or both streams can be considered. Moreover, in these cases dilution and preheating processes are coupled together and their values depend on the amount of entrained burned gas.

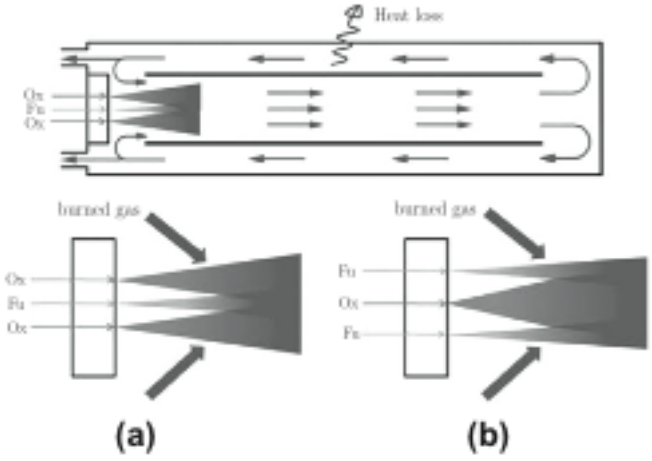

Fig.4.4 - Schematic picture of MILD Combustion (adapted from Wünning and Wünning, 1997).

Degree of dilution of reactants by the flue gas was defined by Wünning et al.(J. A. Wunning 1997) . A relative internal recirculation rate that is the ratio of the mass flow rate of the internal recirculation gas (M_E) to that of initial fuel and air jet ($M_F + M_A$), namely:

$$K_V = \frac{M_E}{(M_F + M_A)} = \frac{(M_J - M_F - M_A)}{(M_F + M_A)} \tag{19}$$

where $M_E = M_J \cdot (M_F + M_A)$ and M_J is the total mass flow rate of flue gases entrained by both fuel and air jets.

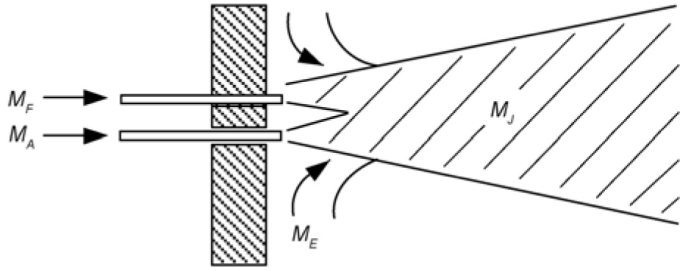

Fig. 4.5 - Stability limits of the non-premixed MILD combustion of methane (adapted from Wünning and Wünning, 1997).

This parameter is critical in defining the influence of gas recirculation on MILD combustion. Fig 4.5 illustrates the axial evolution and radial spread of the fuel-air jet, which results from the entrainment of the surrounding flue gas by the jets and their mixing. The reactants are gradually diluted by the flue gases (e.g., CO_2 and H_2O) and inert gas (N_2). Wünning et al. obtained by experiment the relationship between K_V and the furnace temperature in diffusion combustion, from which a stability limit diagram was constituted for the non-premixed MILD combustion of methane (CH_4) in a particular furnace system (Fig. 4.6).

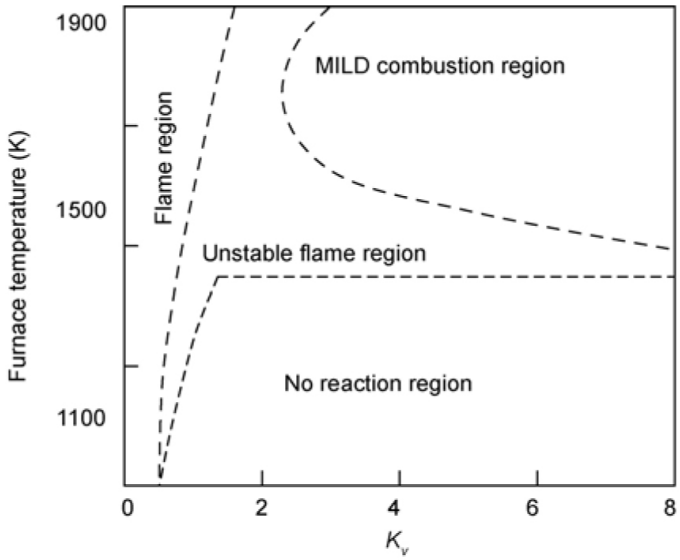

Fig. 4.6 - The relationship between Kv and temperature in methane non-premixed combustion (adapted from Wünning and Wünning, 1997).

.

The majority of previous investigations on MILD combustion was carried out by examining the influence of K_V on combustion and sometimes by comparing it with the diagram.

Fig. 4.6 shows that in the MILD combustion zone, the internal recirculation rate (K_V) is greater than 2.5, and the furnace temperature is greater than 1100 K. Based on this definition there are many works that attempt to classify the conditions under which you can get a MILD combustion as a function of parameters. Cavigiolo et al. (A. Cavigiolo 2003) carried out a detailed study on the influence of K_V on the reaction temperature and formations of NOx and CO in the natural gas combustion process. They found that MILD combustion is extremely stable because the characteristics of NOx and CO emissions reduction do not change with the furnace temperature, fuel type or fuel heat value. They also found that due to differences in the burning point and the calorific value between different fuels, the critical values of K_v are different for different fuels to establish the MILD combustion. For example, for firing methane to obtain MILD combustion, K_V must be greater than 2.3 and the furnace temperature must be greater than 800°C–850°C. An important result was achieved by Galletti et al. (C. Galletti 2007). They found by experiments and CFD simulations that to save the computation time for engineering applications, the 3-D simulation of the MILD combustion should be simplified to the 2-D case. They found quite small differences between the 2-D and 3-D calculations. This consideration allows to assess the spatial uniformity of this combustion mode. Galletti et al. also found that reducing air inlet area can increase the jet momentum, enhance the mixing and entrainment between the reactant jet and the flue gas, and increase the uniformity of the furnace temperature, hence reducing the reaction peak temperature and NOx emissions. Effuggi et al. and Derudi et al. (M. Derudi 2007; M. Derudi 2007; A. Effuggi 2008) revealed that the MILD combustion of biomass gas with low calorific value can be achieved under the condition of high recirculation rate at $K_V > 5$ and high furnace temperature > 800°C. They analyzed the difference between the MILD combustions of natural gas and biomass gas according to the magnitudes of K_V and the furnace temperatures of different fuels.

In the context of optimization, recently Cho et al. (Cho 2011) have investigated the effect of different burner configurations in a regenerative multi-burner flameless furnace. They

found that the parallel firing mode performs better than staggered because it shows lower NO_X emissions for all conditions investigated. Moreover, the horizontal case shows NO_X emissions with respect to vertical, due to the higher temperature uniformity ratio in parallel mode and horizontal configuration.

Further studies have to evaluate the use of different fuels under MILD condition. In particular the use of firing oil and coal was studied (Derudi 2007; Derudi 2007; Wu 2007; Parente 2008; Galletti 2009; Yu, 2010). This suggests that the MILD combustion may be realized broadly by using any types of fuel no matter it is a gas, liquid or solid fuel. For example, the studies on the MILD combustion of hydrogen fuel (Derudi 2007; Derudi 2007; Parente 2008; Galletti 2009) found that as the hydrogen concentration in natural gas increases, the greater initial velocity (>70m/s) and higher flue gas recirculation (K_v>9) must be used to achieve MILD combustion. Yu et al. (Yu, 2010) found that the increase of the reactant dilution will decrease the reaction temperature and that when reactants are highly diluted with the flue gas (K_v>10), NOx and CO emissions are not sensitive to the dilution level. Weber et al. (Weber, 2005) and Zhang et al. (Zhang, 2007) investigated the MILD combustion of the pulverized-coal fuel and confirmed the possibility of occurrence of coal MILD combustion. Stadler et al. (H. Stadler 2009; H. Stadler 2009) investigated the formation mechanisms of NOx for coal combustion under the MILD mode and, especially, the influence of char combustion and gasification on NOx formation. Recently Dally et al. (Dally, 2010) have successfully achieved MILD combustion of firing sawdust in a lab-scale furnace.

Lou et al. (Lou.,2008) tried to achieve the MILD combustion of firing the biomass fuel. They found that when firing rice husk, the NOx emission increased with increasing air preheat temperature, and when the temperature results higher than 1000°C–1050°C, the NOx emission increased with temperature at a higher rate but was still lower than that from the conventional combustion mode. The reason for lower NOx emissions is that the slower reaction of MILD combustion reduces both the fuel and thermal NO emissions. The MILD combustion can decrease the thermal NO emission by 70% and fuel NOx by 40%–60% . This is why NOx emissions can be reduced when coal combustion takes place the MILD mode.

As was highlighted previously, MILD Combustion has potential for use in a number of practical applications, but this limited by a lack of detailed understanding of fundamental aspects, such as autoignition, reaction zone structure, stabilization mechanisms. A big part

of the literature on MILD Combustion is concentrated on large systems. Despite the importance of these systems, such methodology fails to address the fundamental issues of the regime. For this reason in literature, different approach have been developed for better understanding the combustion process in terms of kinetic aspects (characteristic times and kinetic pathways), turbulence-kinetics interactions, the role of the entrainment and the stabilization mechanisms.

Regarding to the kinetic aspects, a part of the literature is related to experimental and numerical studies with model reactors.

Model reactors such as plug flow reactor and well-stirred reactor allow simplifying the study of oxidation reactions since they permit to emphasize particular aspects of the process without a complex fluidodynamic. Furthermore their complementary allow for a global and structured characterization of the process itself. Moreover the behavior of model reactors has been widely modeled since the equations, such as mass or energy conservation, necessary to describe such systems, in ideal conditions, are function of just one coordinate. Hence they allow for a good comprehension of physical and chemical phenomenology and meanwhile for a validation and tuning of predictive models supported by experimental data obtained in precise operative conditions.

De Joannon et al. (De Joannon 2004) analyzed the methane oxidation in the range of interest concerning MILD Combustion processes in a jet-stirred reactor model. They identified different combustion regimes: multiple operating points (hysteresis), steady–unsteady behavior or stable–unstable evolution. Wide ranges of both inlet temperature (875–1275 K) and oxygen/fuel ratio (C/O from 0.01 to 1.4) as well as narrow ranges of dilution (85–90% of nitrogen content) and residence time (0.35–0.5 s) were covered in relation to the identification of regimes. They found that decreasing both residence time and dilution level in a narrow range of values is beneficial in suppressing temperature oscillations, according to the numerical analysis in terms of inlet temperature and air/fuel ratio. Sabia et al. (Sabia 2006) investigated the effect of hydrogen addiction to the methane combustion in Mild conditions for the same reactor, with particular focus on the dynamic behavior, showing that the presence of hydrogen in the system leads to an higher reactivity and a significant reduction of the area in the T_{in}–C/O plane where thermo-kinetics oscillations were observed.

Recently, Sabia et al. (Sabia, 2013) performed an experimental and numerical study on the autoignition of methane and a synthetic bio-gas in a tubular flow reactor at atmospheric

pressure with an high level of dilution, evaluating the auto-ignition delay times and relating such a parameter to the key investigation parameters for MILD Combustion (e.g. level of dilution, inlet temperature system, nature of diluent) creating a set of data for tuning kinetic models in such a non-conventional conditions. In the same context, De Joannon et al. (2012) highlighted the inconsistency of some standard kinetic models for predicting fuel auto-ignition in MILD Combustion conditions because they have been developed on the basis of experimental activities in traditional combustion processes.

Based on different model reactors, a rigorous classification of different processes was done by the Naples's research combustion group (De Joannon et al, 2007, 2008, 2009, 2012). For real applications such as furnaces the HDDI (Hot Diluted Diffusion Ignition in Counter-diffusion Flow Reactor) is proposed. The difference in MILD Combustion conditions for such a configuration is that one or both of reactants can be heated or diluted at a proper level. Four possibilities are possible (Cavaliere and de Joannon, 2004). In these works they clarified the role of diluent nature and diluent ratio identifying different combustion regimes and different flame structures.

On the basis of De Joannon's works, recently Abtahizadeh et al. (Abtahizadeh, 2012) performed a numerical study with a a network of model reactors for obtaining basic knowledge of MILD Combustion in which the fuel stream is preheated and diluted with various amount of burned gas as well as the oxidizer stream. With respect to previous works, they investigated an unsteady problem founding that the autoignition time is delayed by strain rate.

For a deep understanding of the reaction zone structure and the role of the entrainment in MILD Combustion, the Adelaide's combustion group developed an unique lab-scale burner with well controlled conditions in which a wide range of combustion parameters can be easily varied (Dally et al. 2002). The Jet in Hot Coflow (JHC) burner consists of a central insulated fuel jet within an annular coflow of hot exhaust products from a secondary burner mounted upstream of the jet exit plane. The outer annulus is insulated with a fibrous blanket to minimize heat losses to the surrounds. The influences of the coflow persist ~100 mm downstream of the jet exit plane; beyond this the surrounding air begins to mix with the jet and coflow. The surrounding air entrainment facilitates the additional study of these effects on the reaction zone. The O_2 level of the coflow is controlled by the constant flow rate secondary porous burner.

Dally et al. (B. B. Dally 2002; B.B. Dally 2004; G. G. Szegö 2008; G.G. Szegö 2009) found that the reaction peak temperature decreases due to the initial fuel dilution that can increase jet scalar dissipation rate, and influence flame front structure and combustion reaction. Moreover they found that increasing the dilution of oxidants can increase the flame volume and lower the intensity of reaction. They also investigated the relationship between OH and temperature under different oxygen concentrations. Dally found that the mass fraction of OH in MILD combustion is more uniform than that of conventional combustion. Moreover Medwell et al. (Medwell 2005, Medwell 2007; Medwell 2008) also measured the oxygen concentration in different reaction regions and they evaluated OH, formaldehyde and temperature component for different coflow O_2 level, different fuels and jet Reynolds number. They found that the MILD combustion occurred over a much larger space so that the mass fraction of OH was lower and more uniformly distributed in the reaction zone than that from conventional combustion. Moreover the effect of jet Reynolds number was shown to have a marked effect on the formaldehyde levels, while it is less influential on the OH and temperature. These studies thus point to the importance of diluting reactants on MILD combustion.

The Delft's combustion group developed a jet in hot coflow (DJHC) based on that of the Adelaide JHC to gain understanding in the interplay of turbulence and chemistry in MILD Combustion (Oldenhof 2011, Oldenhof 2012). They showed that the chemical reactions have a very weak impact on the velocity field, mean velocities and turbulent stresses. Moreover, they found that the location of first chemical reactions decreases with increasing jet velocity. Finally, they showed that the hottest part of the coflow finds its way into the jet shear layer at an axial location that is around 20 mm lower going from the lowest to the highest jet values of the jet mass flow utilized. This result highlights that the rate with which hot oxidizer fluid is transported towards the edge of the jet where mixing takes place is an important factor in the flame stabilization of the DJHC, according to the dominant role of autoignition in the stabilization of jet-in-hot coflow flames.

Due to the relative geometry, the JHC configurations has been largely used for testing the validity of numerical turbulence- chemistry models when applied to MILD Combustion conditions.

In recent years large attention has been paid of the modeling of MILD combustion especially of gaseous mixtures. A few works can be found on the modeling of MILD

combustion of pulverized coal (Shaffel et al., 2009), but nothing on the modeling of liquid fuels.

One of the key points in the modeling of MILD combustion is the coupling between turbulence and chemistry. In conventional flames, most of the times it can be assumed that the oxidation processes occur nearly instantaneously, and that turbulent mixing governs the reaction rate (following the so called ‘‘mixed is burnt approach’’). Conversely, in MILD combustion the low reactants concentration, which characterizes the reaction region, leads to an increase of the chemical timescales; on the other hand the enhanced turbulence levels due to exhaust gases recirculation reduce the turbulent mixing timescales. Consequently, the turbulent and chemical timescales become similar and it is a generalized opinion that the Damkohler number (turbulent to chemical timescale ratio) approaches unity (Galletti et al., 2007). In such conditions the numerical modeling should take into account both mixing and chemistry, becoming a very challenging task. This has also been proven recently by Parente et al. (Parente 2011) who applied the Principle Component Analysis to a set of measurements taken in MILD combustion conditions. The aforementioned authors showed that at least 4 components were needed to account for more than 90% of the variance contained in the original data; therefore approaches based on single progress variable are not suited for the description of such combustion regime, as proved by the works of (e.g. Coelho and Peters, 2001,)

Some successful predictions (e.g. Christo and Dally, 2005, Parente et al., 2008, 2011, 2012, Galletti et al., 2009) of different MILD combustion burners fed with gaseous mixtures have been obtained in the past by using Reynolds-averaged Navier-Stokes (RANS) equations and the Eddy Dissipation Concept (EDC) model developed by Magnussen (1981) to treat the turbulence-chemistry interaction. One of the main advantages of the EDC model is that it allows a relatively efficient incorporation of skeletal/detailed kinetics into CFD codes, especially in conjunction with ISAT tabulation (Pope, 1997) so that it appears extremely suited for MILD combustion. However Christo and Dally (2005), Frassoldati et al. (2010), De et al. (2011) and Aminian et al. (2011) reported that EDC over-predicted in some locations the maximum temperature even by 200 K when simulating Jet-in-Hot-Coflow typed burners. Such overprediction was observed with different kinetic schemes. Based on this results, both De et al. (2011) and Aminian et al. (2012) proposed a modification of the residence time constant of EDC for MILD conditions.

More recently, Ihme and See (2011) developed and employed a three-stream flamelet/ progress variable (FPV) model together with a Large Eddy Simulation (LES) approach to model the flame characteristics of JHC flame with the 9% O2 mass fraction in the hot coflow of the JHC flames. In such cases the high computational cost of LES forced to a simplification of the oxidation kinetics.

A LES study on a jet in a vitiated hot coflow (Cabra flame) was performed by Domingo et al. (2008) using a combination of tabulated chemistry. LES was found to well predict the turbulent part of the flame, however the model needed to be improved for the diffusion part.

Another interesting aspect in MILD combustion modeling constitute the predictions of pollutant emissions. Because of the low process temperatures and low fluctuations characterizing MILD combustion, the thermal NO formation route (usually the dominant one in conventional flames) is suppressed (Szego et al., 2008). Consequently, the CFD model should include other routes such as Fenimore's prompt and the N_2O intermediate route (which is a low-temperature pathway). Moreover, the presence of H_2 in the fuel may promote NO formation through the NNH intermediate mechanism (Bozzelli and Dean, 1995, Hayhurst and Hutchinson, 1998, Klippenstein et al., 2011). Recently Galletti et al. (2009) showed that the NNH mechanism was the dominant NO formation route in a in a lab-scale burner operating in MILD conditions and fed with a CH_4/H_2 mixture. The same conclusion was drawn for a self-recuperative MILD burner operating in ultra-lean conditions (Parente et al., 2011).

4.2.2 Identification of the problem.

The presence of oxygen and/or other non-condensable species (i.e. nitrogen, argon, methane, hydrogen) in flue gases of CO_2-capture-ready combustion systems is a relevant issue to be faced with for several reasons. More specifically, such impurities have negative effects on purification, transport, injection and storage of CO_2 stream, because they greatly affect the thermodynamic properties of CO2 (i.e. vapor–liquid properties, heat capacity, enthalpy and entropy) (Li et al, 2009).

Firstly, non-condensable species increase the saturation pressure of liquid CO_2 and decrease the critical temperature. As a result, lower temperature and additional

overpressure is required to avoid the risk of two phases behavior during transport and storage of CO_2 (Wang et al., 2011;Yan et al., 2006). It has been highlighted that oxygen as well as other non-condensable species increases the compression work required for CO_2 transport almost linearly with respect to their concentration in the CO_2 stream. The increase in compression work is approximately 2.5%, 3.5% and 4.5% for a concentration of 1% by volume of oxygen, nitrogen and hydrogen respectively (De Visser et al., 2006). Non- condensable species also increase the pressure required for CO_2 injection and reduce the capacity of the storage sites by decreasing the density of CO_2 stream (Wang et al., 2011).

The residual oxygen in the CO_2 streams used for EOR (Enhanced Oil Recovery) operations may react with hydrocarbons in oil field causing both an overheating at the injection point and an increase of oil viscosity thus implying higher extraction cost and more difficulties in refining operation (De Visser et al., 2006; Steeneveldt et al., 2006). Another potential effect of oxygen is the increased biological growth even if the relevance of this effect on oil production has not been thoroughly exploited yet. Moreover, oxygen in presence of small amount of water (order of ppm) in the CO_2 stream used for EOR operations, significantly increases corrosion rates in the oil production and downstream processing equipment .

Also in amine separation processes for CO_2 capture and sequestration, the presence of oxygen has negative effects on both the efficiency and economics of the process. It degrades most of the amine based solvents not allowing for their regeneration, and also determines the formation of corrosive compounds and surfactants (foaming) poisoning the active adsorbing species (Blomen et al.,2009). These effects further increase the relatively high cost related to such a separation process.

Even if it has not yet been established unequivocally the maximum acceptable level of oxygen in the currents of CO_2, many studies, carried out as part of European projects focused on CCS technologies, have showed that the maximum volume fraction of all non-condensable species, such as O_2, N_2 and Ar, in CO_2 stream to be stored, in less restrictive conditions, should not exceed 4% in volume (Pipitone and Bolland, 2009).

Companies as Praxair, Kinder Morgan and Statoil involved in the management and development of plants for CO_2 sequestration impose a maximum concentration of oxygen below 10 ppm as pipeline specification (Pipitone and Bolland, 2009).

There are generally no significant technical barriers to reduce oxygen and non-condensable species and provide high purity of the captured CO_2 (i.e. physical separation). The most common technique to reduce oxygen down to ppm range is to incorporate a distillation column of the liquid CO_2 in the typical purification process of CO_2 streams for sequestration or EOR (White et al., 2008). However, such a technique is likely to induce remarkable additional costs and energy requirements resulting in an overall reduction of power plant efficiency. In particular, White et al. (2008) showed that separation of residual oxygen increases the difficulties in physical separation of non-condensable species in the stream. Therefore, it would be highly desirable the individuation of alternative, more economical techniques to reduce concentration of oxygen and non-condensable species in the CO_2 captured stream to acceptable levels for transport and storage.

Among the other techniques post-oxidation is worth to be considered as a suitable alternative for reducing oxygen and non-condensable/oxidizable species (such as H_2 and CH_4) concentration to one digit ppm (or to ppb) levels, obtaining high purity CO_2 streams that can be used for sequestration or EOR, without additional physical separation processes for such gaseous species. On the other hand, oxy-fuel combustion based technologies are surely among the most promising capture-ready combustion systems allowing for obtaining higher CO_2 concentration in exhaust streams with respect to other CCS technologies (i.e. pre-combustion and post- combustion) (Olajire, 2010). However relatively high levels of impurities, in terms of residual oxygen and non-condensable species, are expected in the CO_2 stream to be captured (Kather et al.,2011). For these systems the fraction of residual oxygen in CO_2-exhaust stream to be treated into post-oxidation stage is a function of fuel used in the primary combustion chamber. In particular, the average volume fraction of residual oxygen in the exhaust stream is variable from 2% to 5% by volume depending on whether the plant is fueled with natural gas or pulverized coal (Bolland, 2009) Such an exhaust gas stream at the exit of oxy-fuel combustion system is also characterized by a high temperature and dilution level (due to high concentrations of CO_2 and H_2O). It can constitute the feed of a post-combustion burner where small quantities of fuel can be added in order to convert the oxygen as well as the other non-condensable/oxidable species to CO_2 and/or H_2O. Additionally, the presence of a post burner also increments global plant efficiency by heat recovery, and in peculiar thermodynamic cycles plant electrical efficiency. For example, power efficiency could

increase when post-burning is coupled with exhausted heat/mass recirculation and supercritical bottoming strategies (Li et al., 2012).

A general layout of the process has been reported in Fig. 4.1. It can be applicable to systems based on either the post-combustion CO_2 capture or oxy-fuel technologies. A hot, diluted stream coming from the main combustion unit is fed to a MILD combustion burner. In both considered systems the stream at the exit of the main combustion unit is at high temperature. Oxygen molar fraction varies from 2% to 5% in the case of oxy-fuel system and can reach about 10% in post-combustion capture technologies (Kvamsdal, et al.,2007). In oxy-fuel systems the MILD post burner can be placed either before or after the recirculation section according to the temperature at the exit of the combustion chamber. Its position has to be time by time evaluated, assuming that the inlet temperature (T_{in}) has to be higher than the autoignition temperature (T_{ign}) of the chosen auxiliary fuel, such as indicated in Fig. 4.7.

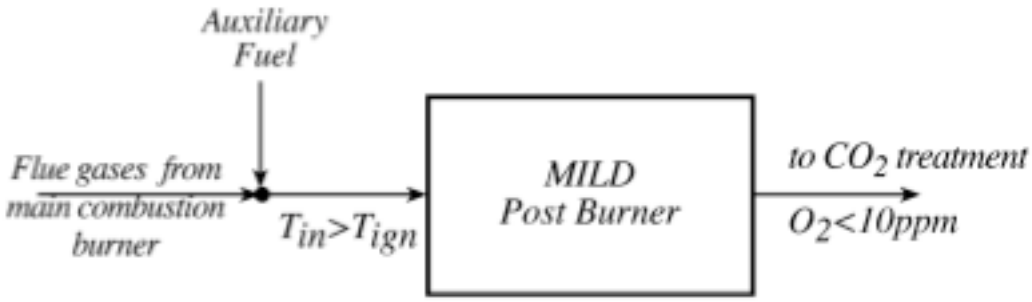

Fig. 4.7 Schematization of MILD Post burner for CO_2 sequestration.

As already summarized previously, there are several reasons for the elimination of non-condensable/reactive gases present in the CO_2 to be sequestered for both typologies of the plants, with particular regard to oxygen. In this perspective, beside the elimination of drawbacks related to presence of oxygen, the insertion of a MILD post-burner downstream of the main combustion chamber potentially shows several advantages that can lead to an increase of the overall efficiency of the plant. In particular, a distillation column is generally used to eliminate oxygen present in concentration lower than 1% for EOR, assuming that N_2 and Ar reach the desired concentrations in the CO_2 stream during the multiple stage compression (Sarofim, 2007). The presence of a MILD post burner allows

for the elimination of the section of the plant devoted to the physical separation of non-condensable gases based on distillation, with a significant economic advantage. In addition, the compression work is reduced by 2.5% for an oxygen concentration reduction of 1%. In the case of CO_2 chemical adsorption with amine based processes, the lower the oxygen content, the higher the cost saving for amine degradation (Blomen et al.,2009). Beside, the reaction of oxygen with additional fuel leads to an energy recovery corresponding to its heat of combustion. In the case of oxy-fuel systems this also allows for a total conversion of the oxygen that derives from an air separation unit with the related cost.

Since very small quantities of fuel (high level of disproportion of inlet streams) need to be added in order to convert the oxygen as well as the other non-condensable/oxidable species to CO_2 and/or H_2O and that reaction proceeds in a high diluted environment so that strong and fast mixing process and longer chemical times can be needed to make effective the process of cleaning. Cyclonic flows due to their peculiar characteristics can be adopted to resolve these issues. Design of a novel MILD Vortex burner for a specific CO_2-stream treatment and cleaning has to address several constraints:

- long residence time of gas flow, compatible with chemical kinetic times:
- strong and fast mixing between inlet streams and recirculated fluid for combustion process stabilization;
- maximization of mixing process, for geometrical reactor optimization;
- establishment of a quasi 2D fluid-dynamic structure for easy reactor scale up/down operations.
- All these issues are investigated in the following sections. In this work dots, previously reported will be connected with the main parameters affecting a cyclonic vortex structure.

4.3 - Results and Discussions

4.3.1 Kinetic Analysis

4.3.1.1 Chemical Kinetic Times and Species Concentration

The aim of this analysis is to numerically study the post-oxidation process of typical flue gas of CO_2-capture-ready combustion systems to both assess the practical feasibility and identify the optimal working conditions with the target of reducing oxygen and non-condensable/oxidizable species concentrations below their maximum acceptable values. Temperatures and composition of the reacting flows make such a post combustion treatment a MILD combustion process. Characteristic kinetic times (auto-ignition, and oxidation) and key species concentrations at steady state were evaluated to study the evolution and the completion of the oxidation process. These parameters are required for designing and dimensioning post-oxidation stages to be used for oxygen reduction in exhaust streams. Initial conditions considered here are those characteristic of the output streams of oxy-combustion plants. Characteristic times and mole fraction of key species at steady state were correlated to the main parameters that influence MILD combustion processes such as inlet temperature system, fed mixture composition, equivalence ratio (ϕ), fuel and/or diluent nature to provide information about optimal operating conditions of post-oxidation process. The evaluation of exploitation of a MILD post combustion process for non-condensable gases has been carried out by means of numerical analyses. The system has been schematized as a tubular flow reactor where a premixed flow of flue gases and additional fuel has been fed, on the basis of the layout reported in Fig. 4.1.

To this aim a standard commercial software was used in order to simulate the system behavior. Computations were performed by means of Chemkin 3.7 package (Kee et al., 2001). Integrations were performed by means of PLUG application of Chemkin 3.7 that simulates the behavior of an ideal tubular flow reactor. Such configuration was chosen in order to study the oxidation process as function of the axial coordinate or equivalently of the residence time and in absence of complex fluid dynamics.

Particular attention was paid to the choice of the kinetic model. In previous works (Picarelli, 2011; Sabia et al., 2012), several oxidation kinetic mechanisms were tested to

investigate oxidation characteristic times of highly diluted CH4/O2 systems at atmospheric pressure. Among the tested mechanisms the c1–c3 (http://creckmodeling.chem.polim- i.it/ POLIMI_C1C31201.CKI/) was found the most reliable in predicting methane oxidation features and characteristic kinetic times in diluted and highly pre-heated systems on the basis of experimental evidences (Sabia et al., 2013).

Numerical simulations were carried out on methane-oxygen systems diluted in carbon dioxide or carbon dioxide/water at atmospheric pressure, varying mixture inlet temperatures and composition. Two residual oxygen molar fractions of 2% and 5% were considered. Methane was chosen as reference fuel since it is a non-condensable/oxidizable species that is likely present in exhaust gases coming out from CCS systems. It has been added to flue gases in such a quantity that the effect of equivalence ratio $\phi = (C/O_{mix})/(C/O_{stoich})$ varying from 1 to 1.4 was evaluated. In the same way, methane/ethylene and methane/propane mixtures were considered as fuel. All the operative conditions considered have been summarized in Table 4.1.

It is necessary to underline that H_2 and CH_4 are generally not explicitly mentioned in the CO_2 capture related literature as non-condensable gases present in flue gases from whatever burners either in oxy-fuel or post combustion capture systems. However CH_4 is reported as the flue gases components in coal combustion systems in several papers (Chagger et al., 1999; Thitakamolet al., 2007). In addition their concentrations are fixed to target values.

The attention was focused on characteristic kinetic times of the process (i.e. auto-ignition delay and oxidation times) and on the final concentrations of species to be eliminated.

Feed stream properties	Value
Mixtures of fuel/CO_2/ H_2O/O_2	
Fuel = CH_4 or CH_4/C_2H_4 or CH_4/C_3H_8	
Auxiliary fuel = C_2H_4 or C_3H_8	
Residual O_2 fraction	2–5% v/v
CO_2	90% v/v
H_2O	0–35% v/v
Equivalence ratio (ϕ)	1–1.4
$X_{ch4}/X_{auxiliary\ fuel}$ (R)	4–9
Temperature (T_{in})	700–1500 K
Pressure (p)	Atmospheric

Tab. 4.1 Flue gases working condition considered in the analysis.

In particular concentration of species at the final section of combustion system is evaluated and compared with the target concentration values, summarized in Table 4.2 and fixed on the basis of the data reported in the literature (Yan et al.,2006; D'Amato et al., 2011).

Species	Target (ppm)
O_2	10
H_2	100
CO	1000
CH_4	/

Tab. 4.2 Target Concentration for Species.

Following a criteria described in details elsewhere (de Joannon et al., 2002), the auto-ignition time (τ_{ign}) was defined as the time corresponding to a temperature increase equal to 10 K with respect to mixture inlet one (T_{in}). The oxidation time (τ_{ox}) is the time needed to reach an oxygen molar fraction of 10 ppm in the exhaust gases or, alternatively, in case such condition is not reachable, it is the time the system needs to reach the steady state.
Fig. 4.8 shows the auto-ignition delay times as a function of α (=1000/Tin) for a $CH_4/O_2/CO_2$ system at atmospheric pressure for a value of equivalence ratio ϕ variable from 1 to 1.4. For these ϕ the fuel oxidation is complete. The investigated temperature range is α = 0.6–1.5 (that corresponds to T_{in} = 700–1500 K) while the residual oxygen molar fractions in the inlet flow are 2% and 5%.

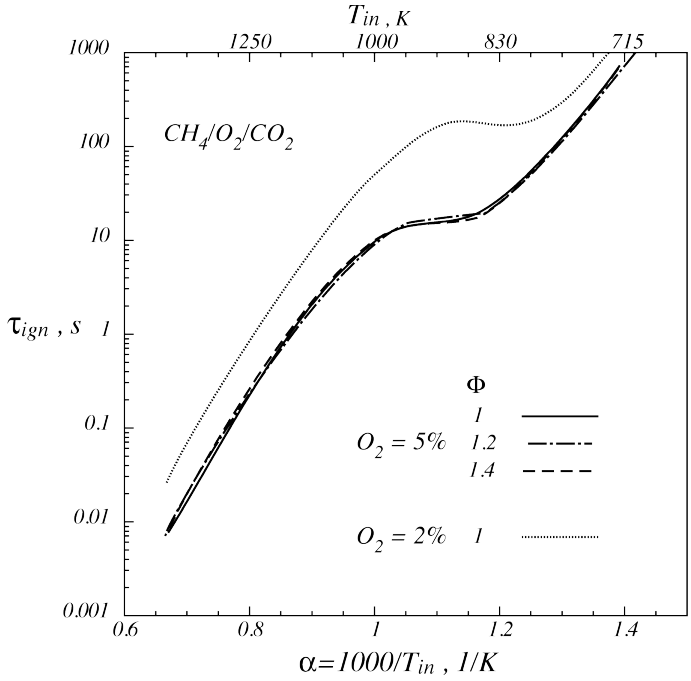

Fig. 4.8 Auto-ignition delay times computed for different equivalence ratio and different residual oxygen mole fraction.

It is clearly shown that the auto-ignition delay time decreases as the system inlet temperature increases. More specifically, three different slopes of the auto-ignition delay time curve are identifiable. In particular for low and high temperatures, the auto-ignition delay time decreases as T_{in} is enhanced, while, for the intermediate temperature range, the auto-ignition delay time is almost independent on the system inlet temperature. Such behavior resembles the well known Negative Temperature Coefficient (NTC) phenomenology that affects the kinetic of aliphatic hydrocarbons, well described for such a case in Sabia et al. (2012).

For a residual oxygen molar fraction of 5% the auto-ignition de- lay time is slightly dependent on the equivalent ratio. As matter of facts, the profiles for ϕ = 1, 1.2 and 1.4 are very close to each other for the whole considered temperature range.

This is also true for a residual oxygen molar fraction equal to 2%. In this case only the curve corresponding to stoichiometric conditions (ϕ = 1) is reported. As expected the auto-ignition delay time is higher at lower oxygen concentration regardless of T_{in} and the NTC region shifts toward higher a values.

As a first indication about actual feasibility of post-combustion processes it has to be noted that inlet temperatures lower than 1000 K ($\alpha = 1$) imply auto-ignition delay times incompatible with practical industrial systems.

It is of interest to evaluate the dependence on the inlet temperature of the oxidation time, τ_{ox}, which is the time needed to reach an oxygen molar fraction of 10 ppm. Fig. 4.9 shows the oxidation times as function of α. According to the previous considerations the analysis is only restricted to $\alpha < 1$ case (i.e. inlet temperature higher than 1000 K).

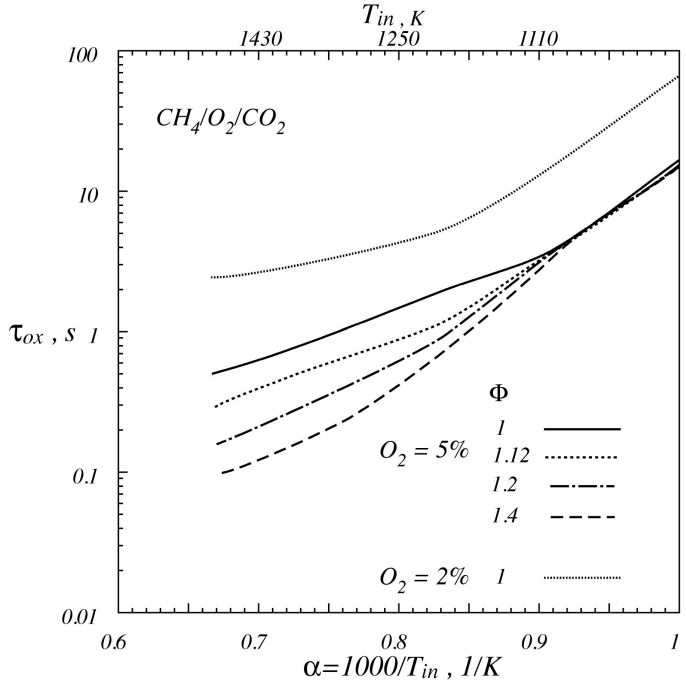

Fig. 4.9 Oxidation times computed for different equivalence ratio and different residual oxygen mole fraction.

In general, the oxidation time decreases as the inlet temperature system is increases and it is sensitive to the equivalence ratio. Curves relative to a residual oxygen molar fraction of 5% are coincident for $0.9 < \alpha < 1$, while for $\alpha < 0.9$ they spread showing that the oxidation time decreases when the mixture enriches in fuel.

For example, for $\alpha = 0.67$, τ_{ox} at $\phi = 1.4$ is about one order of magnitude smaller with respect to the one computed at the stoichiometric condition ($\phi = 1$).

Decreasing the residual molar fraction down to 2%, the oxidation times, as well as auto-ignition delay times, increase with respect to the previous ones in all the temperature range considered.

The O_2 molar fraction (on dry basis) relative to the oxidation time is reported in Fig. 4.10 as function of a, for the system $CH_4/O_2/ CO_2$ with an oxygen molar fraction equal to 5% on curves parametric in the equivalence ratio ϕ (from 1 to 1.4). In the figure, also the oxygen target value in the treated CO_2-rich stream (10 ppm) is indicated.

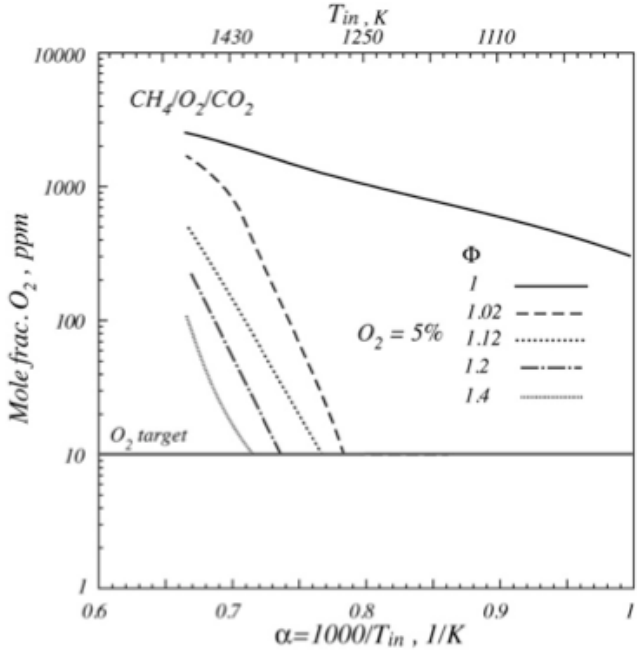

Fig. 4.10 Oxygen mole fraction evaluated at sox for the system $CH_4/O_2/CO_2$.

For the stoichiometric condition, the O_2 mole fraction is greater than 10 ppm for any inlet temperature. This result implies that the post-oxidation process is not realizable with such mixture composition.

For $\phi > 1$ (even slightly greater than the stoichiometric condition) and for $\alpha > 0.77$ (corresponding to T_{in} equal to 1300 K) the tar- get is reachable for all the ϕ values analyzed while, at higher temperatures, the O_2 mole fractions result higher than 10 ppm.

Fig. 4.11 shows the production of CO_2 (in terms of g/s) at τ_{ox} as function of α for the systems so far considered.

Such results highlight that the production of CO_2 is strongly affected by the equivalence ratio and the inlet temperature system. In particular it decreases as / and the inlet system temperature.

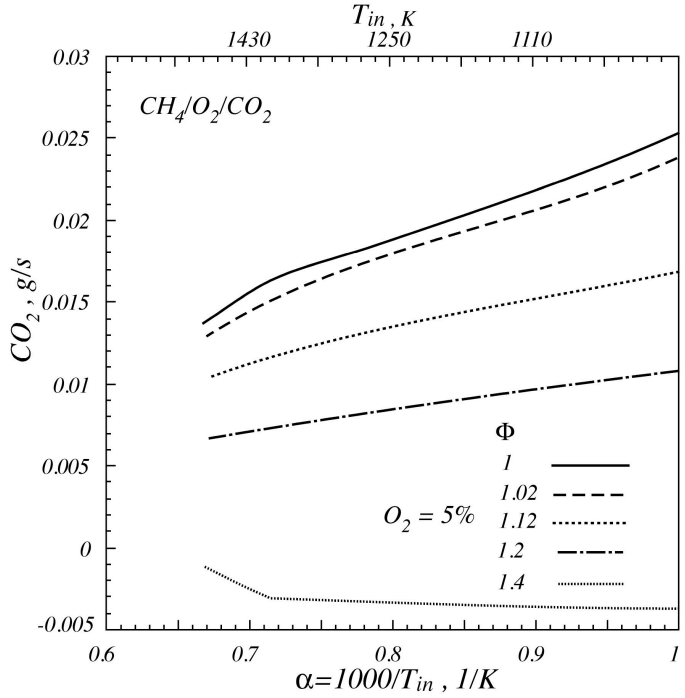

Fig. 4.11 Production of CO_2 at sox for the system $CH_4/O_2/CO_2$.

Such results highlight that the production of CO_2 is strongly affected by the equivalence ratio and the inlet temperature system. In particular it decreases as ϕ and the inlet system temperature increase. For ϕ = 1.4 the production of CO_2 at τ_o becomes negative. In such a condition, the post-oxidation process is useless because a certain amount of the CO_2 to be treated is converted into undesired species, such as CO, negatively affecting the sequestration process.

Figs. 4.12 and 4.13 report the CO and H_2 molar fraction (on dry basis) in the treated CO_2-rich stream as function of a for the system $CH_4/O_2/CO_2$ at τ_{ox} for a residual oxygen molar fraction equal to 5% and different equivalence ratios (from 1 to 1.2). According to literature, CO and H_2 targets were set to 1000 and 100 ppm respectively.

In general, H_2 molar fraction evaluated at τ_{ox} decreases as system inlet temperature increases, while the CO molar fraction exhibits the opposite trend. Moreover both of them increase as the equivalence ratio increases. Results obtained for values of equivalence ratio near stoichiometric conditions (ϕ = 1.02, 1.04) show that in such conditions the H_2 molar

fractions evaluated at τ_{ox} are smaller than the concentration target of 100 ppm. Similar considerations can apply for the CO molar fraction except for higher temperature (T_{in} > 1300) where it is higher than 1000 ppm.

Increasing the equivalence ratio value (ϕ = 1.12, 1.2), the H_2 and CO molar fractions result higher than their targets in all the temperature range considered.

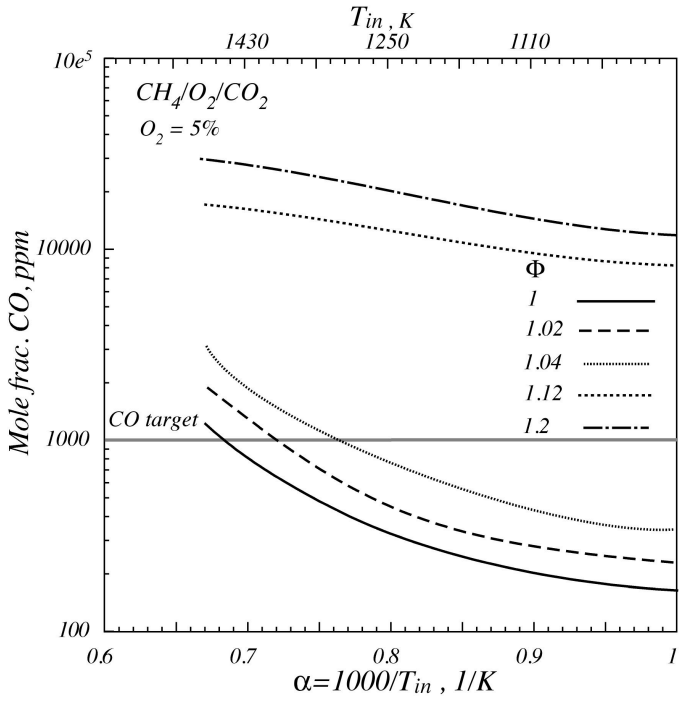

Fig. 4.12 Carbon monoxide mole fraction evaluated at sox for the system $CH_4/O_2/CO_2$.

Figs 4.14 and 4.15 show the effect of the presence of H_2O in the CO_2-rich exhaust stream to be treated on the characteristic kinetic times. Such an effect was considered because water is always present in different amount in the CO_2-rich flue gas streams of real combustion systems.

The system considered is $CH_4/O_2/CO_2/H_2O$ for a residual O_2 molar fraction equal to 5% and ϕ = 1.02. The H_2O molar fraction was varied from 0 up to 35%.

The trend of auto-ignition delay time curves is similar for all the cases analyzed (H_2O molar fraction equal to 0%, 15%, and 35%). At low temperatures the shortest τ_{ign} competes to system with 35% of H_2O, while the longer sign to system diluted totally in CO_2. In the NTC region the trend is inverted. Finally, for $\alpha < 1$ the curves are very close to each other.

The effect of H_2O on auto-ignition delay times of highly diluted CH_4/O_2 systems has been exploited numerically in a previous work (Sabia et al.,2012).

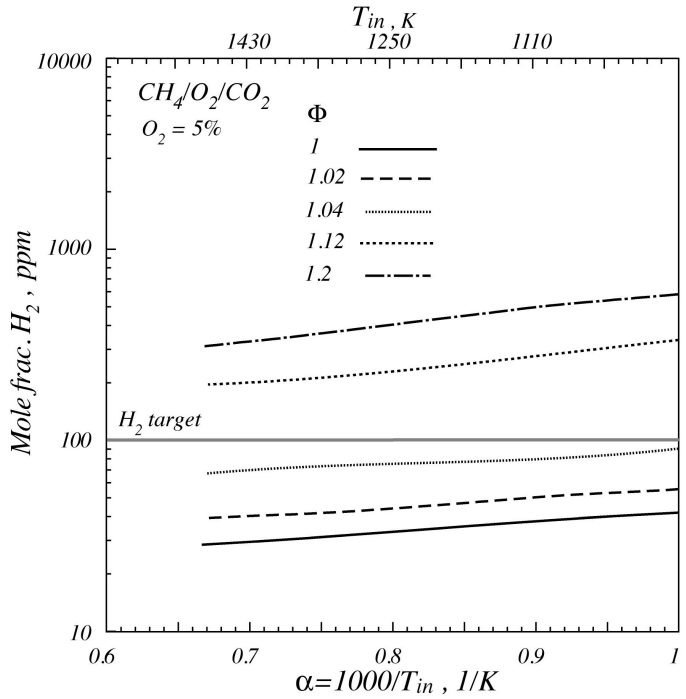

Fig. 4.13 Hydrogen mole fraction evaluated at sox for the system $CH_4/O_2/CO_2$.

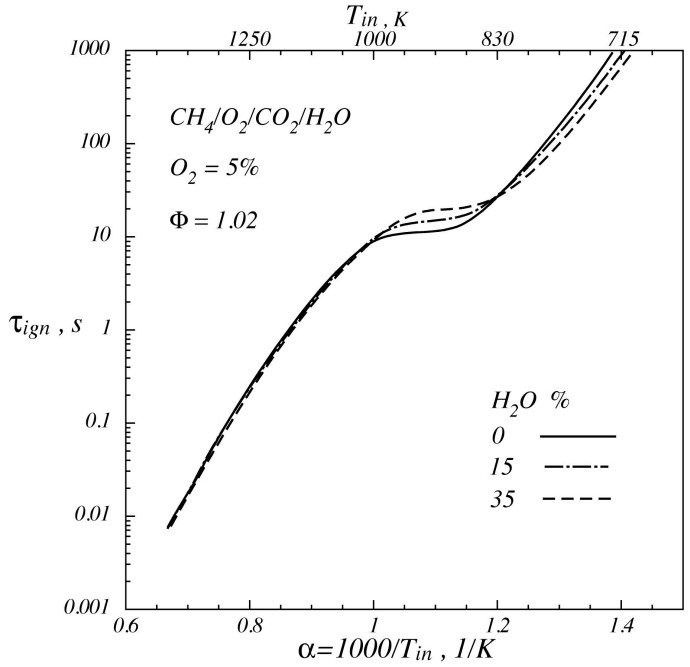

Fig. 4.14Auto-ignition delay times computed for different H_2O mole fraction.

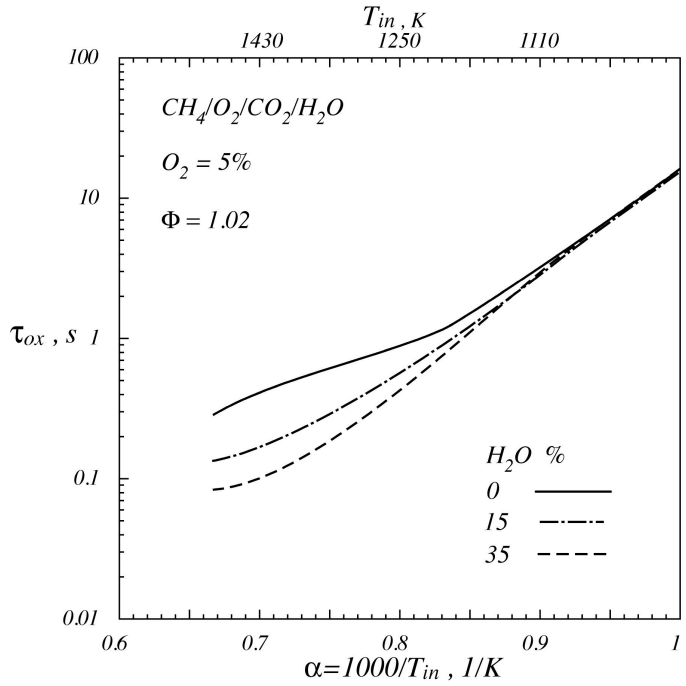

Fig. 4.15 Oxidation times computed for different H_2O mole fraction.

The presence of H_2O in the system shows an effect on the oxidation time similar to that of equivalence ratio described previously.. In particular for $0.9 < \alpha < 1$ the sox is not affected significantly by the presence of H_2O in the system while for $\alpha < 0.9$ it decreases as H_2O molar fraction increases.

For evaluating the effect of the nature of fuel used in the post- oxidation process on kinetic characteristic times and species production numerical simulations were performed considering mixtures of methane/ethylene and methane/propane with different components percentages as fuels, while considering the same equivalence ratios used in previous integrations.

The systems analyzed are fuels/O_2/CO_2/H_2O with a residual O_2 molar fraction equal to 5%, H_2O molar fraction equal to 15% and ϕ = 1.02. The CH_4/auxiliary fuel volume ratio (R) has been set equal to 4 and 9. The trend of O_2, H_2 and CO mole fractions at τ_{ox} as function of α for the systems considered, are not reported but, for such an equivalence ratio and for $\alpha > 0.77$, their concentrations in the treated CO_2-rich stream are below the target thresholds.

Figs. 4.16 and 4.17 show the effect of the nature of fuel used on the characteristic kinetic times. In particular curves in Fig. 4.16 represent the ratio between autoignition delay times

evaluated for $CH_4/O_2/CO_2/H_2O$ system and those obtained for fuels/$O_2/CO_2/H_2O$ systems ($\tau_{ign\ CH4}/\tau_{ignMIX}$), as function of a for parametric values of CH_4/C_2H_4-C_3H_8 ratios.

The values of auto-ignition delay time ratios are higher than 1 for CH_4/C_2H_4 and CH_4/C_3H_8 mixtures considered in all the temperature range investigated. Such a result implies that ethylene or propane strongly increases the system reactivity during the auto- ignition process.

For the CH_4/C_2H_4 mixture with R = 9 the $\tau_{ign\ CH4}/\tau_{ignMIX}$ curve exhibits a nearly bell-shaped trend. In particular for $1.4 < \alpha < 1.2$ it shows a linear trend in a logarithmic scale, later on, decreasing a the ratio $\tau_{ign\ CH4}/\tau_{ignMIX}$ increases reaching a maximum value at $\alpha = 1$ ($\tau_{ign\ CH4}/\tau_{ignMIX} = 20$), then it decreases. At the extreme of the inlet temperature range investigated

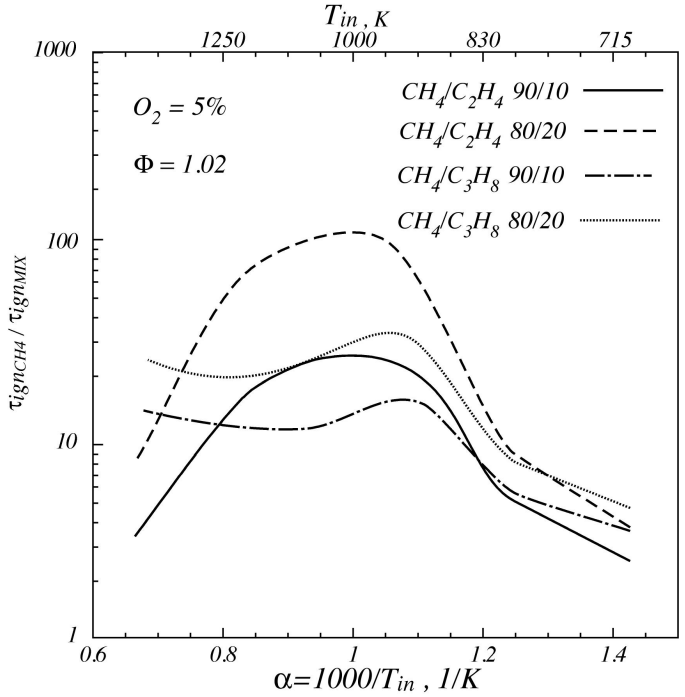

Fig. 4.16 Methane to fuel mixture autoignition delay times ratio.

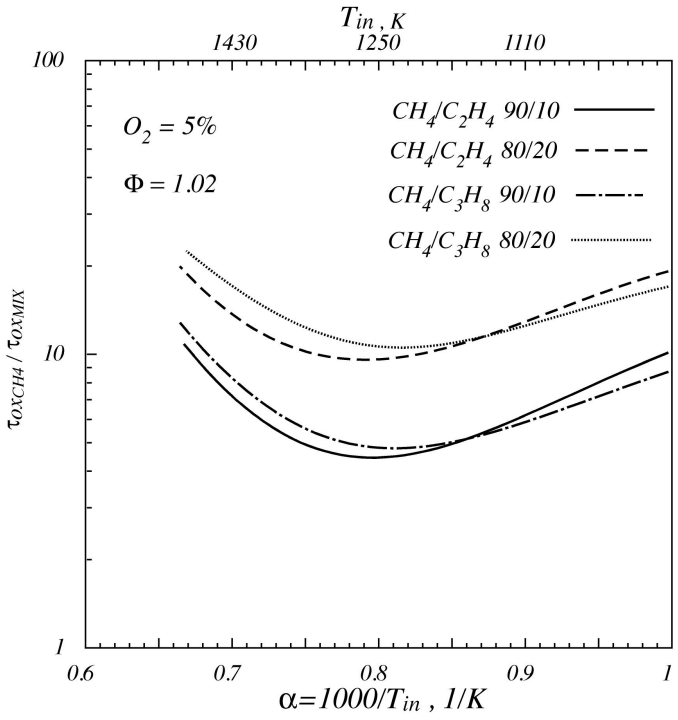

Fig. 4.17 Methane to fuel mixture oxidation times ratio.

the ignition times are comparable ($\tau_{ign\ CH4}/\tau_{ignMIX}$ = 2.5). Increasing the amount of ethylene in the fuel mixture (R = 4), $\tau_{ign\ CH4}/\tau_{ignMIX}$ curve shows a similar behavior with respect to the case just described, but $\tau_{ign\ CH4}/\tau_{ignMIX}$ is higher. In particular for α = 1 the auto-ignition delay time ratio becomes 100.

For the CH_4/C_3H_8 mixture with R = 9 and for 1.4 < α < 1.2, the $\tau_{ign\ CH4}/\tau_{ignMIX}$ shows a linear trend in a logarithmic scale. For α = 1.1 it reaches a maximum, then it slightly decreases down to a constant value of 10.

Decreasing R down to 4, $\tau_{ign\ CH4}/\tau_{ignMIX}$ is similar respect to the case described above with a shift toward higher a values.

At low temperatures (1.4 < α < 1.2) and for a fixed value of R, the s $\tau_{ign\ CH4}/\tau_{ignMIX}$ curves relative to CH_4/C_2H_4 and CH_4/C_3H_8 mixture are very similar while in the intermediate temperature region the $\tau_{ign\ CH4}/\tau_{ignMIX}$ values relative to CH_4/C_2H_4 mixture are higher than those obtained for CH_4/C_3H_8 systems. At high temperature (α < 0.8) the trend is inverted.

Fig. 4.17 shows the ratio between oxidation times evaluated for $CH_4/O_2/CO_2/H_2O$ system and those obtained for fuels/$O_2/CO_2/H_2O$ systems ($\tau_{oxCH4}/\tau_{oxMIX}$), as function of a for parametric values of R.

Results reported in Fig. 4.17 suggest that, as for auto-ignition delay time, the addition of C_2H_4 or C_3H_8 in the system leads to a faster oxidation process respect to CH_4 system.

For the CH_4/C_2H_4 mixture with R = 9 the $\tau_{oxCH4}/\tau_{oxMIX}$ value decreases as inlet temperature increases reaching a minimum for $\alpha = 0.8$ ($\tau_{ox\ CH4}/\tau_{oxMIX} = 5$), then it increases with T_{in}. Decreasing R, down to 4, oxidation time ratio curve shifts to higher values. In such a case the minimum value of $\tau_{ox\ CH4}/\tau_{oxMIX}$ is about 10.

For a fixed value of R, the $\tau_{ox\ CH4}/\tau_{oxMIX}$ curves relative to CH_4/C_2H_4 and CH_4/C_3H_8 mixture are very similar in all the temperature range investigated.

Relating to the CH_4 system, all the results can be summarized in a feasibility map of the post-oxidation process, reported in Fig 4.18. In particular three different zones can be identified A first zone, colored in green, extending for $T_{in} < 1000$ K and for all ϕ values analyzed, where the kinetic times evaluated are too long to be incompatible with an industrial system. A second zone, colored in blue, extending for $T_{in} > 1000$ K and for high values of ϕ, where the key species targets are not respected. Finally, a third region, colored in red, extending for $1000 < T_{in} < 1300$ K and $1.01 < \phi < 1.08$ where the post-oxidation process is feasible.

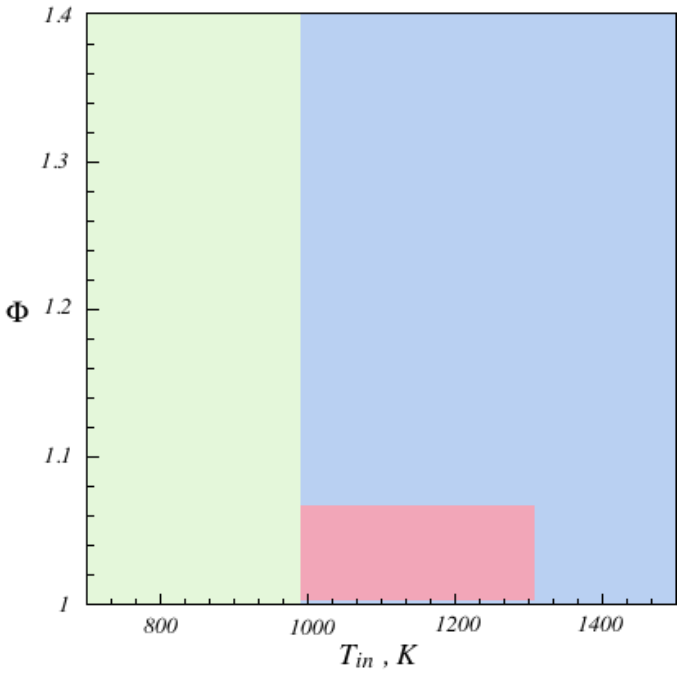

Fig. 4.18 Feasibility Map..

This analysis shows that the elimination of oxygen and non-condensable species from CO_2 streams to be sequestered by means of a post-combustion process in MILD conditions is a feasible alternative to the other CO_2 purification techniques and the process can reach a high efficiency from chemical point of view. Starting from a flue gas stream deriving from an oxy-fuel combustion process, i.e. with a typical composition at the exit of combustion chamber, the evolution of cleaning reactive process has been followed as a function of inlet temperature and fuel/oxygen ratio, with the aim of identifying the optimal range of operative conditions.

Three main parameters have been taken into account during such recognition. A first edging of potential working conditions has been made by fixing the target concentration values of undesired species to be reached, on the basis of market requirement.

Among the potential favorable conditions with respect to target concentrations, an evaluation of corresponding characteristic times of the process has been carried out in order to identify the operation parameters that allow for ignition and oxidation times compatible with residence time of real burners. In such an analysis, it has been shown that both methane and mixtures of methane with C_2 or C_3 species are effective both in reduction of oxygen and in promoting the oxidation of other non-condensable species present in CO_2 stream, even though the presence of the higher molecular weight paraffin strongly reduces ignition and oxidation time. As a consequence, the choice of fuel is related to the design, logistic and economic evaluation in the overall assessment of the sequestration plant. In both cases, the needed initial temperatures of CO_2 enriched streams to be treated are congruent with characteristic temperatures at the exit of the main combustion chambers.

4.3.1.2 Effect of CO_2 Dilution

The use of non-conventional operative conditions and the presence of high level of CO_2 and H_2O in the reaction zone can significantly affect the evolution of low hydrocarbons combustion process (Sabia et al.,2013; Chinnici et al., 2011). More specifically, CO_2 and H_2O can modify the chemical pathways involved in oxidation processes because of thermal and kinetic effects (de Joannon et al.,2012; Glarborg and Bentzen, 2011).

In fact, such species have a higher heat capacity with respect of N_2, thus changing the adiabatic flame temperature, so that kinetic pathways, and then they can participate to chemical reactions as active species or in third-molecular reactions as third body species.

Focusing the attention on CO_2, it has been pointed out that great amount of CO_2 would primarily modify the equilibrium of the reaction $CO_2 + H = CO + OH$ (Park et. al, 2003; Le Cong et al.,2008; Liu et al., 2001-2003; Renard et al.,2003; Mazas et al., 2010). It results in a strong competition for H atoms with the chain-branching reactions $H + O_2 = OH + H$ and $H + HO_2 = OH + OH$, altering the O/H radical pool that control the evolution of oxidation processes (Watanabe et al., 2013; Le Cong et al., 2009). Moreover the CO_2 decomposition reaction, as well as reactions of CO_2 with hydrocarbon radicals (CH, CH_2 species), is responsible of higher CO levels with respect to traditional air combustion (Mardani et al., 2013; Sevault et al., 2012; Heil et al., 2011). Therefore the presence of a great amount of CO_2 in MILD and/or Oxy-fuel combustion can sensible modifies the progression of fuels oxidation.

Even if the chemical and thermodynamic effects of CO_2 on fuels oxidation processes have been discussed in literature, further studies are mandatory to full understand the role of such a species in the progression of fuels oxidation process in MILD/Oxy combustion. This aspect is critical under such operative conditions because as highlighted in the previous paragraph, high dilution levels delay characteristic kinetic times and temperature gradients, associated to the oxidation process, are modest so that the transit among kinetic pathways is slower with respect to traditional flames thus implying that their competition is stressed (Sabia et al.,2012). Therefore the presence of great amount of carbon dioxide would emphasize CO_2 chemical-thermodynamic effects on the progression of the combustion process. Even though the CO_2 reactions are renewed in literature (in particular $CO_2 + H = CO + OH$), the exploitation of combustion processes in systems highly diluted in CO_2 can give rise to peculiar behaviors because carbon dioxide equilibrium reactions may be altered. Furthermore in such operative conditions, even same small uncertainty on kinetic constants and/or the third body efficiency in third-molecular reactions in detailed kinetic schemes would produce meaningful effects on numerical predictions.

Previous studies (de Joannon et al.,2003-2004-2005) were devoted to understand the effect of high dilution and pre-heating levels on the evolution of the combustion process. The oxidation of methane/oxygen mixtures diluted in nitrogen under MILD operative conditions in an atmospheric non-adiabatic perfect stirred flow was experimentally and

numerically studied. Methane was properly chosen as representative of light hydrocarbons because it exhibits combustion chemistry relatively simpler with respect to heavier hydrocarbons. Results highlighted the presence of a complex dynamic behavior in terms of thermo-kinetic temperature oscillations. Because this behavior could limit the application fields technologies based on sensible enthalpy and mass recirculation, the dependence of such instabilities on the main working parameters (e.g. inlet temperature system, dilution level, reactor residence time) was studied. Instabilities were explained on the basis of chemical competition between different kinetic pathways. The CH_3 recombination path present in the CH_4 oxidation mechanism plays a key role in modulation of temperature oscillations.

It is worthwhile to note that presence of dynamic behavior stress in a significantly way the need to design a novel MILD Vortex Burner where intense, fast, controlled/stable mixing process is achieved. Stability and control of mixing process is needed to avoid operative working conditions in which dynamic behaviors can occur, behaviors that can affect combustion process efficiency.

Few works have been reported in literature concerning methane dynamic behaviors (Vanpee, 2003; Yarlagadda et al., 1990; Barbieri et al., 2005; Grey et al., 1981). Such phenomenologies are well known in case of heavier hydrocarbons with respect to methane and the kinetic responsible of such a phenomenology has been widely clarified during years. In any case the temperatures, mixture compositions and the chemistry involved in heavy hydrocarbons cool flames are meaningfully different from the ones relative to methane dynamic behavior experimentally and numerically studied in previous works. Such instabilities come out from the peculiar operative conditions that are used under MILD combustion. The high dilution levels slow down reaction rates and the modest heat release, due to oxidation reactions promoted by high pre-heating temperatures, make the shift among combustion kinetic regimes very delicate, emphasizing the competition among kinetic channels. This induces the establishment of new behaviors generally not encountered in traditional flame because the kinetics are very fast due to very high adiabatic flame temperatures that promote high temperature reactions, well known in the scientific literature (de Joannon et al.,2005-2007). In diluted conditions, the reacting system is very sensible to any external (i.e. heat exchange) or internal perturbations, so that instabilities can easily emerge.

Because of the thermo-kinetic nature of such instabilities, heat exchange to the surroundings plays a fundamental role in the establishment of such a phenomenology. Wada et al. (2009,2010) performed same numerical studies of methane oxidation under MILD operative conditions in a perfect stirred flow reactor. They found a transition from steady to unsteady conditions changing the heat transfer coefficient value.

Numerical simulations were performed in a perfect stirred flow reactor as function of the main parameters of the system, namely mixture inlet temperature and C/O feed ratio. Simulations were carried out by means of the transient Perfectly Stirred Reactor (PSR) model of Chemkin 3.7 and the detailed kinetic mechanism c1-c3. In order to value the reliability of numerical results, other kinetic mechanisms were used, as discussed later in the next section. Following indications of previous works, the modeled reactor has a volume of 100 cm3 and an internal surface area of 104 cm2. Numerical simulations were carried out at atmospheric pressure for different inlet temperatures (T_{in}) and mixtures compositions. In particular, the carbon/oxygen feed ratio (C/O) was varied from values close to zero up to 0.5. For each C/O feed ratio, the investigated inlet temperature range was 1000 -1500 K.

Adiabatic and non-adiabatic conditions were investigated. For non-adiabatic case the heat transfer coefficient was set equal to 0.02 cal/cm^2 K s. Reactor residence time and CO_2 mixture dilution level were set respectively equal to 0.5 s and 90% (by volume). The integration time considered is 5 seconds.

In agreement with previous works (de Joannon et al., 2003-2005,2007,), simulations realized for the non-adiabatic case showed the occurrence of thermo-kinetic temperature oscillations. Also the integrations performed for the adiabatic case showed the insurgence of instabilities highlighting the kinetic nature of temperature oscillations.

The characteristic temperature temporal profiles are summarized in Fig. 4.19. In particular steady combustion (a), periodic oscillations (b), damped oscillation (c) and multiple ignition (d) temperature profiles are showed in the figure.

The non-reactive profile is not reported here. For such operative conditions no temperature increment is numerically predicted within the considered integration time. The “multiple ignition” oscillations are characterized by a period longer than the flow residence time inside the reactor. For the “periodic” oscillations the frequency and amplitude remain constant within the integration time after oscillations onset, while for the “damped” oscillations the amplitude diminishes with time finally reaching a steady state value.

On the basis of such profiles, it was possible to reassume results in T_{in}-C/O maps (Figs. 4.20a, 4.20b). More specifically non-reactive, steady combustion, multiple ignition, periodic and damped oscillation areas were identified on T_{in} - C/O plane.

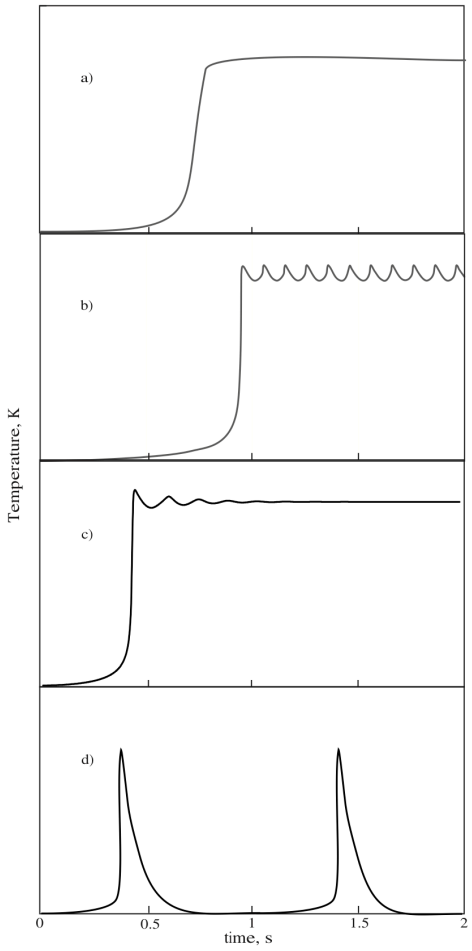

Fig. 4.19 Temporal Temperature profiles for different combustion behavior.

Fig. 4.20a is relative to the non-adiabatic case. The region relative to "non reactive" conditions extends from 1000 K up to about 1125 K for very fuel lean (C/O < 0.025) and rich mixture compositions (C/O > 0.4). Damped oscillations were detected for fuel ultra lean mixtures (0.025 < C/O < 0.04) and for T_{in} in the range (1050 K – 1125 K) and for rich conditions (0.4 < C/O < 0.5) and T_{in} comprised between 1125 and 1350 K. Multiple ignitions extends in the region comprised between the two damped oscillations areas. For C/O = 0.07 it extends from T_{in} = 1060 K to 1125 K. Increasing the C/O feed ratio, the inlet temperature range relative to "multiple ignition" shifts towards higher value. At C/O = 0.4 it is comprised between about 1125 and 1300 K.

Periodic oscillations were predicted in two different regions of the map. The former corresponds to fuel lean mixtures, namely from C/O values close to zero up to 0.2 and intermediate T_{in} (1150 -1215 K), while the latter occurs for fuel rich mixtures (0.3 < C/O < 0.4) and T_{in} higher than 1250 K. The remaining part of the map is relative to "steady combustion" conditions.

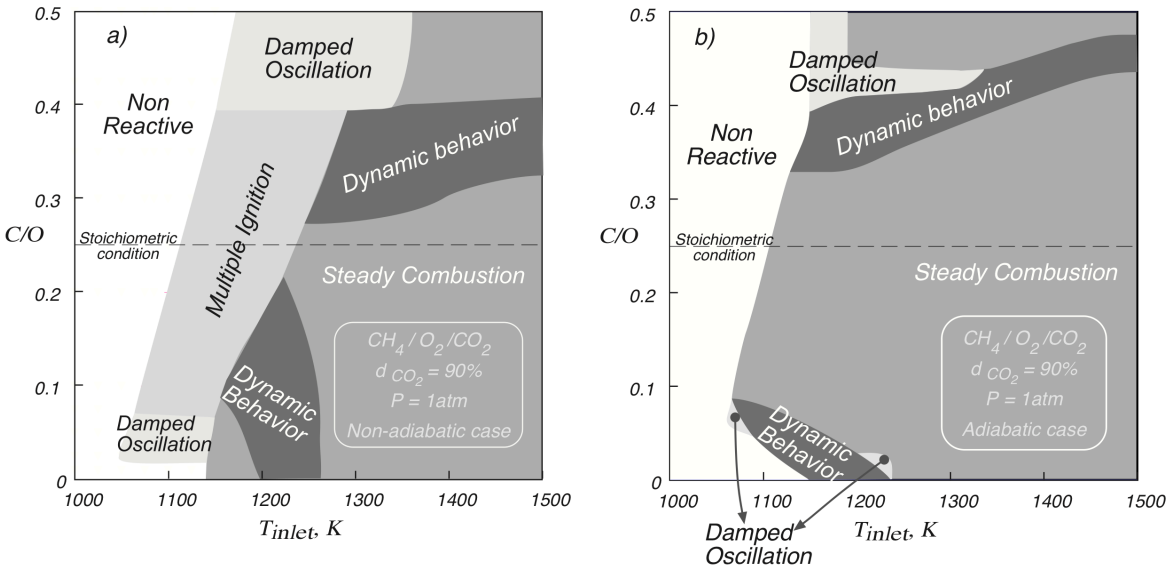

Fig. 4.20 T_{inlet}- C/O map for $CH_4/O_2/CO_2$ system in MILD Combustion conditions.

For the adiabatic case (Fig. 4.20b), the behavior map is qualitatively similar to that of non-adiabatic system. Also in such a case, "non-reactive" conditions, periodic and damped oscillations and steady state combustion areas are reported. It is worth noting that the "multiple ignition" regime is identifiable only for the non-adiabatic systems. In the adiabatic case they are replaced by steady combustion solutions. Periodic and damped oscillations areas are identified for fuel lean and fuel rich conditions. In particular they are numerically detected for C/O values close to zero up to 0.1 and low-intermediate T_{in} (1075-1215 K) and for fuel rich mixtures (0.35 < C/O < 0.45) and T_{in} higher than 1150 K. Small damped oscillations areas are positioned aside the lean periodic oscillation area, as well as for 0.4 < C/O < 0.5 and 1125 < T_{in} < 1325 K. The non-reactive area is slightly less extended that the one reported for non-adiabatic conditions, while the steady combustion region is meaningfully wider.

In order to verify the reliability of numerical results the same simulations were performed by several different kinetic detailed mechanisms (Bowman et al.,1999; Warnatz et al., 2006; Williams, 2001; Petersen et al.,2007) available in literature. They were performed in case of periodic oscillations for both fuel lean and rich mixtures for the adiabatic case. Two reference cases were considered (C/O = 0.05 and T_{in} =1100 K for lean case; C/O = 0.4 and T_{in} =1200 K for rich case). In both conditions, the most of used mechanisms were able to predict the dynamic behavior (periodic or damped oscillations) even though, mixture ignition times, oscillations frequency and amplitude detected, were slightly different with respect to c1-c3 mechanism.

Since the goal was is to investigate the chemical effects of CO_2 as diluent species on the evolution of the combustion process, the attention has been focused on the adiabatic system, where temperature oscillations are promoted by methane oxidation chemistry and not influenced by heat losses towards the surroundings that simply extends the range of operative conditions that lead to instabilities but not change the kinetics responsible of such behaviors. Nonetheless the same numerical analyses were performed for the non-adiabatic case and results (not reported), are congruent with the ones reported below for the adiabatic case.

A kinetic analysis of dynamic region was performed (for both lean and rich fuel conditions) in order to understand the kinetic responsible of temperature oscillations. Two reference cases were considered (C/O = 0.05 and T_{in} =1100 K for lean case; C/O = 0.4 and T_{in} =1200 K for rich case).For lean fuel cases, flux diagram and temperature sensitivity analyses were carried out. Such analyses suggested that the main reactions involved in the methane oxidation for the operative condition considered are:

1. $H + O_2 = OH + O$
2. $H + O_2 + M = HO_2 + M$
3. $OH + HO_2 = H_2O + O_2$
4. $O + HO_2 = OH + O_2$
5. $OH + OH = H_2O + O$
6. $CO + OH = CO_2 + H$

On the basis of such indications, the rate of production (ROP) of OH radical for the main reactions (for reaction 2, the ROP is relative to HO_2) has been considered and reported in Fig. 4.21. Also the temporal temperature profile has been reported in the figure. All the rates of production exhibit a maximum value in correspondence of T equal to 1225 K

(temperature profile inflection point). After this point, the slope of temperature profile drastically increases and temperature reaches a maximum value of about 1230 K. Afterwards, all reaction rates decrease rapidly to values close to zero.

At the temperature minimum (T equal about to 1221 K) reaction 1 is the most important, followed by reaction 5, while the reaction 3 becomes more important than reaction 2. Furthermore, the conversion of CO to CO_2 (reaction 6) is negligible.

As soon as the temperature increases, reaction 1 and 5 produce OH radicals that are destroyed by reaction 6 and 3. Reaction 2 produces HO_2 radicals that react with OH radicals producing stable compounds by means of reaction 5.

In Fig. 4.22 the heat release of main reactions, along with the temporal temperature profile, is reported as a function of time. Reactions 1 and 5 are endothermic, while reactions 2, 3, 4 and 6 are exothermic. In particular, reaction 1 is the most endothermic reaction of the system.

The trend of heat release of reactions considered is very similar. More specifically, all the heat releases show a maximum in correspondence of the temperature inflection point, for then rapidly decrease to values close to zero in the post-oxidation zone. At the inflection point, reaction 3 is the most exothermic, followed by reaction 2 and 6, that show the same heat release.

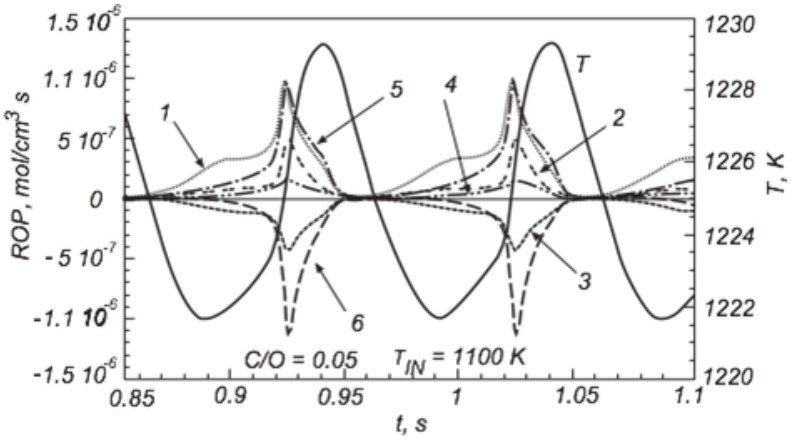

Fig. 4.21 Rate Of Production analysis and temperature profile for C/O = 0.05 and T_{in} = 1100 K.

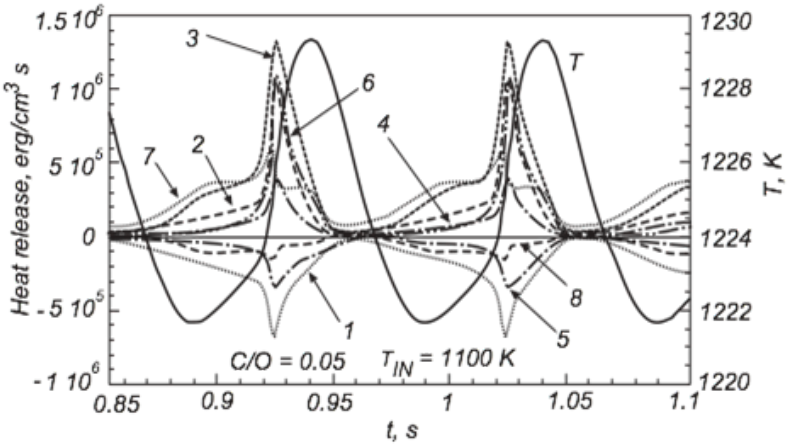

Fig. 4.22 Heat Release Rate and temperature profiles for C/O = 0.05 and T_{in} = 1100 K.

Other two reactions were reported in the figure:

7. CH3OH + M = CH3 + OH + M

8. HCO + M = H + CO + M

Reactions 7 and 8 are exothermic and endothermic, respectively. In the post-oxidation zone results show that reaction 7 is the most exothermic reaction of the system, while reaction 8 becomes more important than reaction 5.

It is well known in literature that reaction 1 starts high temperature branching reactions.

In relation to Fig. 4.22, it appears clear that for considered temperature, the heat needed for supporting reaction 1 is provided by reactions 2 and 3. In reaction 2, HO_2 radicals are formed and then destroyed in reaction 3. The heat released by reaction 2 and 3 is able to increase the working temperature of few degrees that, in the temperature oscillation range, promote high temperature branching reactions. Thus the system reactivity rapidly increases and methane is fully converted. At this point, the system goes to a "freeze state" and the incoming $CH_4/O_2/CO_2$ mixture causes a decrease of the working temperature and lower down radicals concentration to values close to zero also because of termination reactions. This mechanism is cyclically repeated and causes temperature oscillation.

Results show that the dynamic behavior is related to the competition between the branching reaction 1 and reactions 2 and 3.

As matter of fact, even though reaction 1 is faster than reaction 2, the high temperature branching reactions are limited by reaction 2 and 3. Reaction 2 consumes H radicals and O_2 limiting reaction 1, and produces HO_2 radicals that consume OH radicals through reaction 3 leading to stable species, lowering system reactivity. On the other hand, reaction

2 and 3 are the most exothermic reactions, so that they can increase system temperature and promote reaction 1. So that reaction 2 and 3 kinetically inhibit reaction 1, but thermally promote the high temperature branching reactions.

For inlet temperatures higher than the 1200 K (stable combustion), rate of production analysis and heat release rate highlighted that reaction 1 is enough fast, supported by the high temperature, that this competition does not persist and the system approaches to a single solution steady state.

For supporting the thesis that such instabilities are related to the reactions of H_2/O_2 system, numerical simulations were carried out varying the nature of diluent. In particular CH_4/O_2 systems diluted in helium, nitrogen, argon and a fictitious inert species X (with the same thermodynamic properties of CO_2) were analyzed. These simulations showed that temperature oscillations remain, independently of diluent nature. Moreover they highlighted that there is a well-defined zone of working temperature in which the dynamic behavior is established, namely whether the system working temperature is comprised between 1180 and 1280 K. Further simulations were carried out enabling heat transfer exchange of the system. They confirm that, independently of T_{in} and heat transfer coefficient values, the dynamic behavior is numerical predictable whether the working temperature falls in the above mentioned range. o highlight the role of reaction 2 and 3, such reactions were alternatively deleted from the detailed kinetic mechanism. With such modified schemes, no temperature oscillations were predicted. Numerical results suggest that oscillations are due to a delicate kinetic-heat released balance among reactions 1-2-3.

The same analysis was performed for fuel rich mixtures. Figure 4.23 is relative to a mixture with a C/O feed ratio equal to 0.4 at T_{in} = 1200 K. In the time occurring before the temperature increase, OH radicals are produced by reaction 1, 3 and 6 through CO_2 decomposition. OH radicals mainly react through reactions:

9. $OH + H_2 = H_2O + H$

10. $CH_4 + OH = CH_3 + H_2O$

When the temperature increases, reaction 1 and 5 become dominant for producing OH, while reaction 10 and 6 consumes OH radicals leading to an increase of methane dehydrogenation reactions and to an increase of CO_2 molar concentration.

Further simulations have been performed at C/O = 0.3 and 0.5, where no temperature oscillations are present. The rate of production analyses highlighted that at C/O = 0.3 the

kinetic is more similar to the one occurring at the maximum of temperature at C/O = 0.4, while for C/O = 0.5 to the one corresponding to the minimum temperature at C/O = 0.4

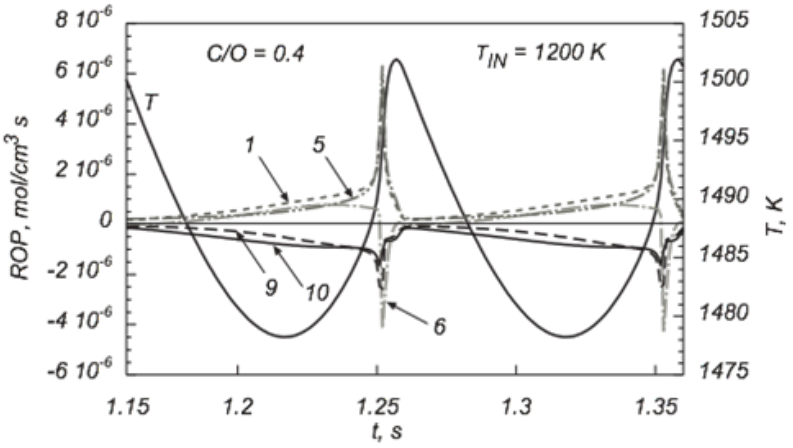

Fig. 4.23 Rate Of Production analysis and temperature profile for C/O = 0.4 and T_{in} = 1200 K.

Moreover at C/O = 0.3, the methane oxidation reactions CH_3 -> CH_2O -> HCO -> CO are very active, while at C/O = 0.5 methyl recombination reactions to ethane and C_2 species dehydrogenation reactions become important.

It is worth noting that, for rich mixture compositions, although oxygen depletion, methane is fully converted while the oxygen remains in the system. In rich conditions, the CO_2 decomposition to CO is a key reaction.

At C/O = 0.3, CO_2 decomposition frees OH radicals that can rapidly dehydrogenize methane while oxygen content is high enough to promote reaction 1 and oxidize methane. CO_2 provides for oxygen in radical form to fully consume methane.

For richer mixtures, OH radicals, produced by CO_2 decomposition, react to dehydrogenize methane to methyl radicals. In such operative conditions, they mainly recombine to ethane and C_2 products while methane oxidation routes are depressed. The depletion of O_2 implies reaction 1 is inhibited so that system reactivity is slow.

In the dynamic behavior region, the CO_2 consumes H radicals competing with reaction 1. The oxygen content and the oxidation routes are high enough to sustain reaction 1 and so high temperature branching reactions. The competition between the reverse of reaction 6 and 1 induces temperature oscillations.

Therefore in rich conditions, CO_2 decomposition compensate the oxygen depletion, but for very rich fuel mixtures, it is not sufficient to promote methane conversion because

recombination channels to C_2 compounds are very active and depress system reactivity. The kinetic competition for H radicals between reaction 1 and 6 causes the dynamic behavior.

Furthermore, it is worth noting that CO_2 decomposition reaction limits temperature increase because of its endothermic nature.

At a fixed rich C/O feed ratio, falling in the dynamic region, the higher the inlet temperature, the higher is the CO_2 decomposition rate and the recombination to C_2 species, so that they cause the end of the dynamic behavior towards the establishment to a single steady state.

In the same way earlier reported for the lean case, the diluent species was substituted with inert compounds and with the fictitious species X. In particular, temporal temperature profiles relative to a mixture with a C/O feed ratio equal to 0.4 at T_{in} = 1200 K are reported in Fig. 4.24. Numerical simulations run in the dynamic inlet conditions relatively to the system diluted in CO_2, showed that no oscillations were predictable, implying that CO_2 decomposition is responsible of the dynamic behavior for rich mixtures through the kinetic mechanism just reported.

In order to summarize, numerical simulations were performed to study the methane/ oxygen highly diluted in CO_2 combustion process in an adiabatic perfect stirred flow reactor. Results showed the occurrence of temperature oscillations and several combustion regimes. The establishment of dynamic phenomenology for hydrocarbons in model reactors has been widely recognized in literature, and they have been related to the coupling between kinetic aspects with heat exchange towards the surroundings.

The originality of this analysis is essentially due to the fact that such numerical dynamic behaviors are obtained in adiabatic conditions, so that they have to be related just to chemical kinetics. The study of such phenomenology implies a better understanding of the kinetic pathways evolving under MILD condition in presence of great amount of CO_2.

As matter of fact, under such operative conditions the modest temperature increment coupled with lower reaction rates with respect to traditional flames, caused by elevated dilution level, stresses the competition between several kinetic pathways involved in hydrocarbons oxidation. Furthermore, CO_2 could interact with fuel oxidations through decomposition reactions, altering the evolution of the combustion process.

By means of several numerical analyses, the kinetic pathways responsible of the dynamic phenomenology have been identified for both fuel lean and rich mixtures. In particular, in

the last case, the CO_2 decomposition reaction interacts with the oxidation process of methane and leads to temperature oscillations. Other results concerning the effect of CO_2 dilution on the evolution of methane MILD combustion process can be found in Chinnici et al. (2011, 2012).

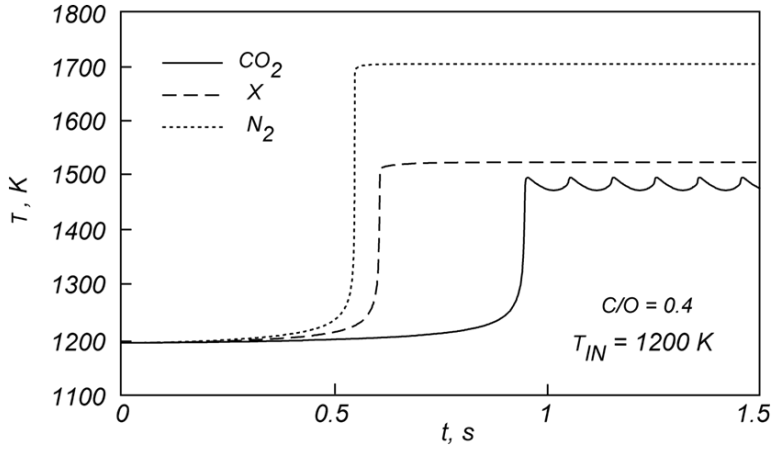

Fig. 4.24 Temporal Temperature profiles for C/O=0.4, T_{in} = 1200 K and different diluent species.

The insurgence of dynamic instabilities related to high concentration of carbon dioxide in the combustion chamber is a key issues in the development and design of a novel MILD burner configuration for eliminating oxygen and non-condensable species from CO_2 streams to be sequestered by means of a post-combustion process in MILD condition. It is well know from the literature that a MILD process need of a high quantity of recirculated hot products in the combustion chamber to be stabilized, thus, a strong and fast mixing is needed. In order to avoid the insurgence of dynamic behaviors that can decrease process efficiency and/or lead to an ineffective and not feasible post-oxidation process, a stable, well/controlled mixing process is mandatory. A variation of mixing rate (and thus of the charge composition), in fact, can lead to operative conditions subjected to temperature oscillations. Furthermore, this aspect is more complicated by long kinetic times of the post-oxidation process.

4.3.2 CFD Analysis: Preliminary Study and Geometry Definition.

As reported in the introduction, design of a novel MILD Vortex burner for a specific CO_2-stream treatment and cleaning has to address several constraints:

- long residence time of gas flow, compatible with chemical kinetic times;
- strong and fast mixing between inlet streams and recirculated fluid for combustion process stabilization;
- maximization of mixing process, for geometrical reactor optimization;
- establishment of a quasi 2D fluid-dynamic structure for easy reactor scale up/down operations.

A preliminary CFD analysis with FLUENT solver of ANSYS software was performed in order to design a novel MILD vortex burner configuration in wich a strong and well/ controlled recirculation.and dots previously reported are achieved Different parameters were investigated such as height (H/d), length (d) and exit diameter (d_{out}) of the mixing section, diameter, velocity and positions of fuel and oxygen/diluent jets.

Firstly, an analysis of the mass and energy balances was done. The nominal power of the experimental test rig is 5 KW. Considering a $CH_4/O_2/CO_2$ mixture at stoichiometric conditions, with a dilution equal to 90% and an inlet temperature system of 1273 K, the total flow rate is equal to 250 l/min (74 Nm3/min). In table 4.3 is reported the inlet jets velocity (diluent/oxygen) basing on the jet diameter and the evaluated total flow rate.

Jet diameter, cm	Velocity, m/s
0,5	102,6
0,75	45,6
1	25,6

Table. 4.3 Inlet jet velocity (diluent/oxygen)

As reference case, a diluent/oxygen jets diameter of 0,75 cm and a velocity of 45,6 m/s was used. For such a value of jet velocity, the jet Reynolds number is about 2600. Moreover, in first analysis fuel jets were not considered. For all the cases analyzed, a RANS approach with the k-epsilon model was adopted.

The reference case mesh is shown in Fig. 4.25. It is constituted by about 2.5 million of tetrahedral cells. ANSYS/Meshing was used to generated unstructured mesh. Mesh quality was checked in terms of skewness, aspect ratio, orthogonality and expansion factor. Grid

independence was checked on the basis of flow fields. The exit mixing section diameter and the width of the chamber are 2,5 cm while the base length is equal to 20 cm (square face). The jets are positioned at the centerline of the section and 2,5 cm apart the edge.

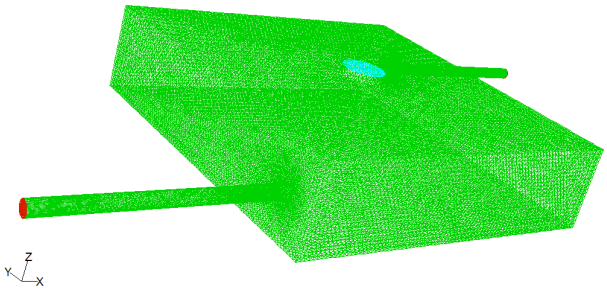

Fig. 4.25 Mesh of proposed geometry.

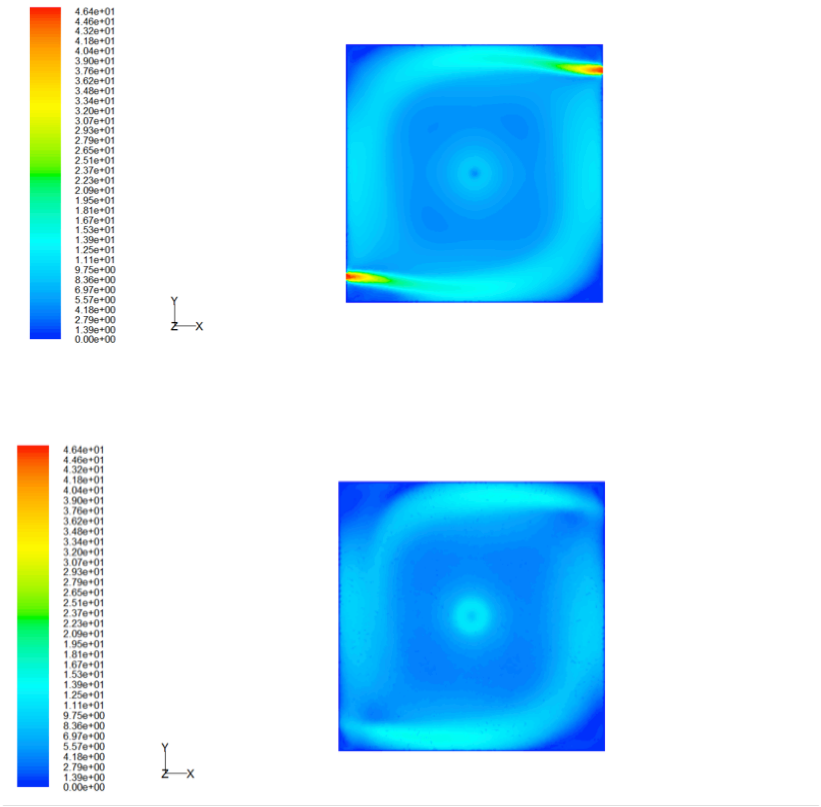

Fig. 4.26 Contours of velocity magnitude (depth =2,5 cm).

Fig. 4.26 shows the contours of velocity magnitude at the centerline and near the exit of the section (2,5 mm from the exit). The contours highlighted that a well/defined vortex

flow is established in the chamber. Furthermore,.this flow structure remains for all the depth of the chamber with a similar intensity. Different simulations were performed to understand the effect of the section depth on the flow field inside the geometry. Figs 4.27 and 4.28 show the contours of velocity magnitude at the centerline and near the exit of the section (2,5 mm from the exit) for a depth of 5 and 7,5 cm, respectively.

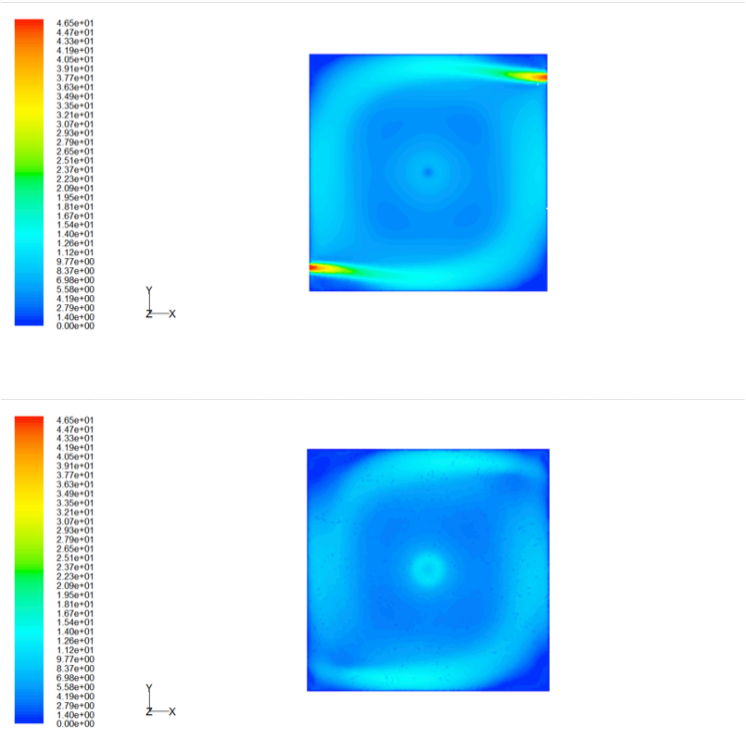

Fig. 4.27 Contours of velocity magnitude (depth =5 cm).

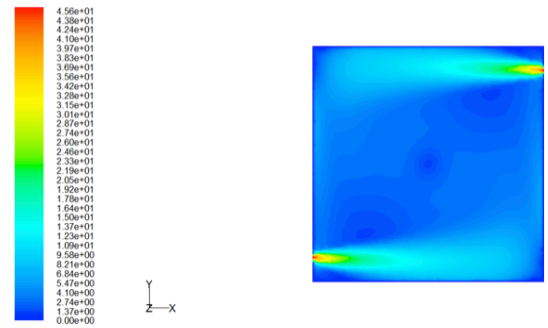

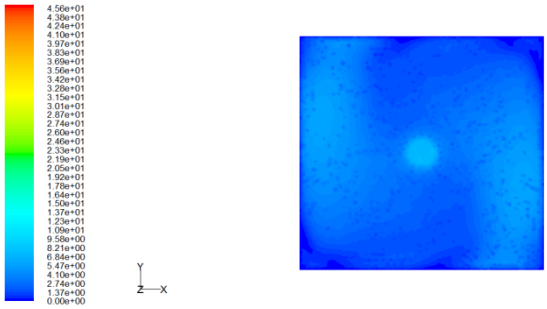

Fig. 4.28 Contours of velocity magnitude (depth =7,5 cm).

It is possible to see that for a depth of 5 cm a vortex flow structure is still present , meanwhile for a depth of 7,5 cm there is no enough recirculation, due to the higher kinetic energy losses by jets and .

Since a depth of 5 cm ensures a well/defined vortex flow structure as well as a depth of 2,5 cm, but higher residence time will be insured with respect this last case, a depth of 5cm has been chosen for the optimized geometry of the vortex burner.

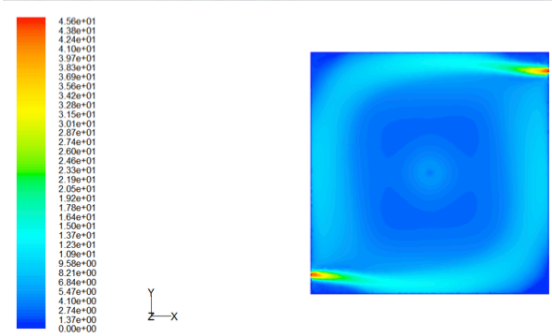

Fig. 4.29 Contours of velocity at the centerline (base =25 x 25 cm).

Fig. 4.29 shows the contours of velocity magnitude at the section centerline for a base length of 25 cm (square base) with a depth of 3 cm. It appears clear from the figure that at the center of the section there is a zone with a velocity magnitude near the zero ("dead zone") that is not visible in the reference case. Its presence is substantially due to the higher kinetic energy losses by jets (similarly to the case of depth = 7,5 cm) with respect to the reference case, just related to the fact that the distance between jet inlet and the wall is higher. Thus, also in this case a vortex flow structure is not well established. A square base was chosen since a circular base can create some problems during optical measurements and construction of the device. However, for eliminating the presence of "dead" vortex

near the corner it is possible to “cut-off” a part of such an edges, as showed in Fig. 4.30. It appears evident the benefit of such a configuration.

The effect of exit diameter on the flow field and recirculation is shown in Fig 4.31. More specifically the Fig. is referred to an exit diameter equal to 1,5 cm.

Similarly for the reference case, also for a value of exit diameter of 1,5 cm a well/defined vortex flow structure appears. However it is also possible to see that an higher flow velocity is established at the center of the section with respect to the reference case, due to the smaller exit area. High values of velocity magnitude could lead to a sensible reduction of the residence times inside the chamber. Hence, an exit diameter of 2,5 cm was chosen as reference diameter for the optimized section geometry.

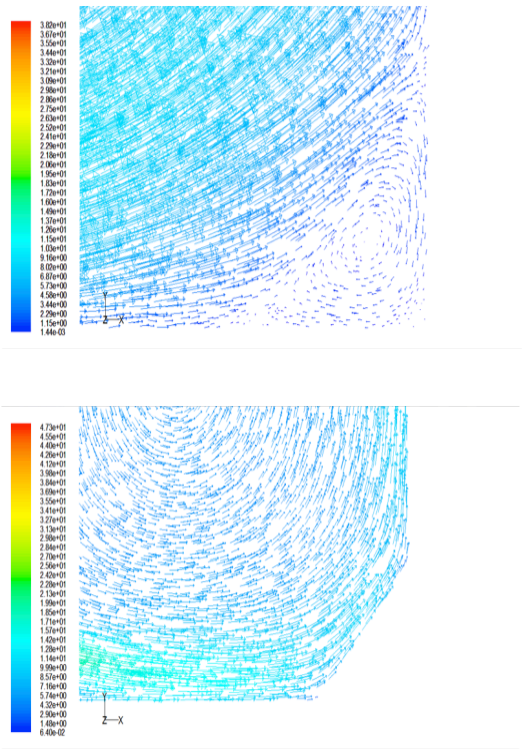

Fig. 4.30 Velocity vector for two different configurations.

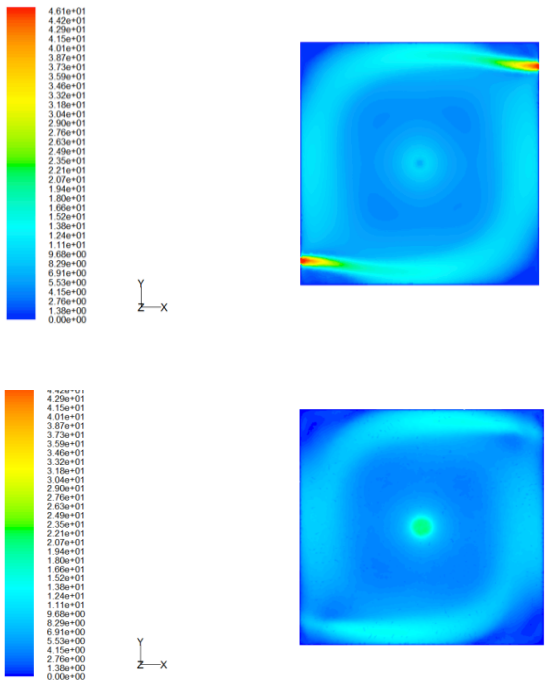

Fig. 4.31 Contours of velocity magnitude (exit diameter = 1,5 cm).

Fig. 4.32 shows the effect of fuel injections inside the mixing section (depth equal to 5 cm). For this simulation the fuel jet diameter is 0.08 cm (velocity equal to 54 m/s).

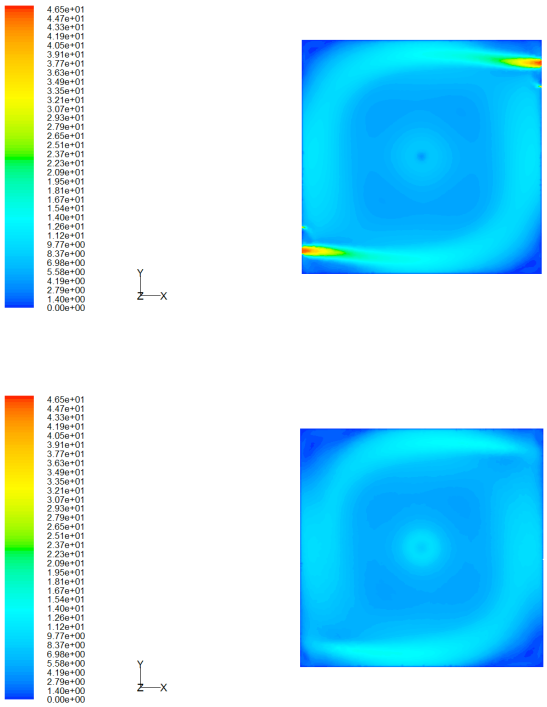

Fig. 4.32 Velocity vector for two different configurations.

It is possible to see that the presence of fuel jets does not influence in a significantly way the flow field of the mixing section. Such a results can be related to the high disproportionality of inlet flows (the ratio between primary flow rate and fuel flow rate is about 30).

Other simulations were performed for evaluating the role of diameter and positions of fuel jets. Also for such cases, flow field is not influenced by the fuel jets. Jets fuel position, instead, shows a strong influence on the mixing process of the fuel. In order to understand such effect, the methane mass fraction along the nozzle distance is reported in Fig. 4.33 for two cases analyzed (case A and B). In particular it is possible to highlight that for case A the fuel mass fraction rapidly decreases along the nozzle distance and methane is fully mixed after just 2 cm from the inlet. For case B, instead, the fuel mass fraction decreases slower with respect to case A and methane is completely mixed after 5 cm from the inlet . Such a behavior could be related to the fact that for case A fuel is directly injected into the vortex flow structure developed by the interaction of the two opposed main jets flow (oxygen/diluent), meanwhile for case B fuel is injected on the periphery of the vortex, thus, more time is needed to achieve a fully mixed state. Case A was chosen for the optimized geometry.

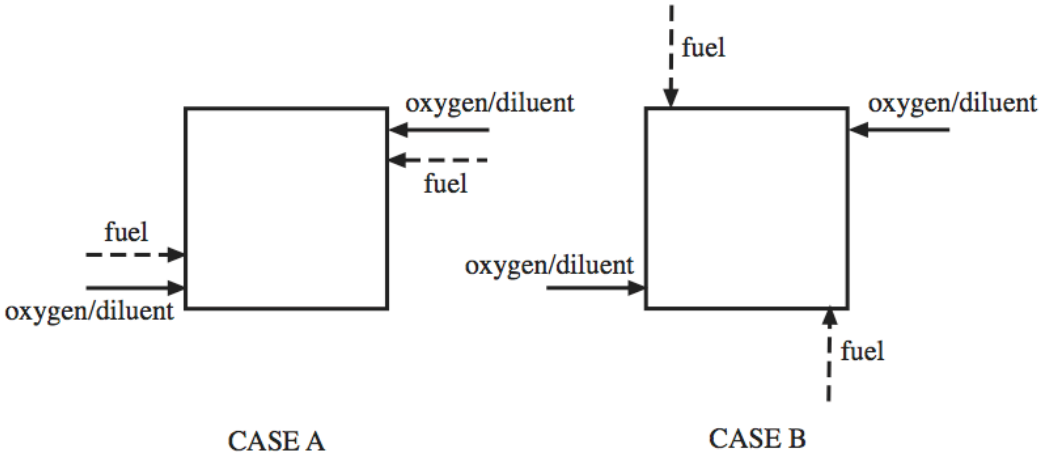

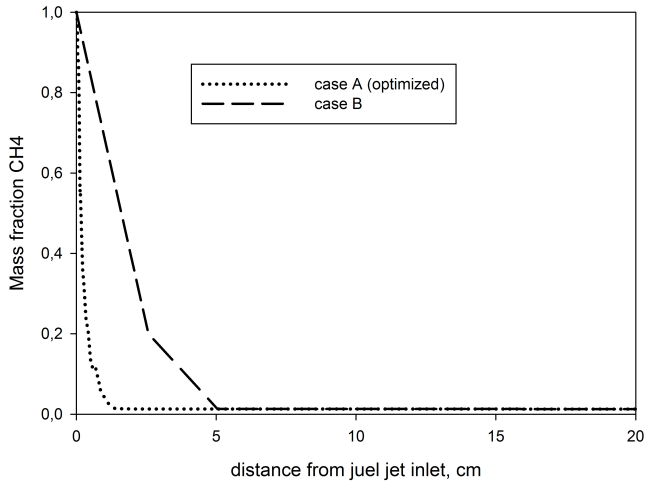

Fig. 4.33 Methane mass fraction along nozzle distance.

Further simulations were carried out in order to understand the effect of inlet velocity of main flow on the flow structure inside the chamber. In Fig. 4.34 velocity magnitude for three different inlet Reynolds number were investigated. Furthermore, velocity components for an inlet jet Reynolds number of 700 are also shown in the same figure. As can be identified in Fig. 4.34, for all cases analyzed a well/defined vortex flow structure is established inside the chamber. Such a result is very important in the context of the process in analysis since it highlights that it is possible to develop a vortex flow structure for several operative working conditions.

Defined the geometry of the experimental device, a numerical analysis were carried out to obtain a full fluid-dynamic characterization of the chamber in isothermal conditions. A detailed study of the process of cross-interference of the main jets for the establishment of a vortex structure in the reactor was performed. In particular, an analysis of the engulfment parameter (K_{tgl}), which provides a precise indication of the degree of recirculation varying the main key parameters of the process were carried out. Furthermore, Residence Time Distribution (RTD) of gas flow, intensity and extension of the vortex, varying the inlet jet Reynolds number of the main flow were obtained. Basing on such analysis the critical Reynolds number for wich a well/defined vortex structure is established in the reactor was identified. Since the objective of this study is to analyze the fluid dynamics in isothermal conditions of the process of cross-interference between the main inlet jets, for all simulations the gaseous flow is helium. In such a way it is possible to obtain the same value of Reynolds number with respect to an air flow at high temperature.

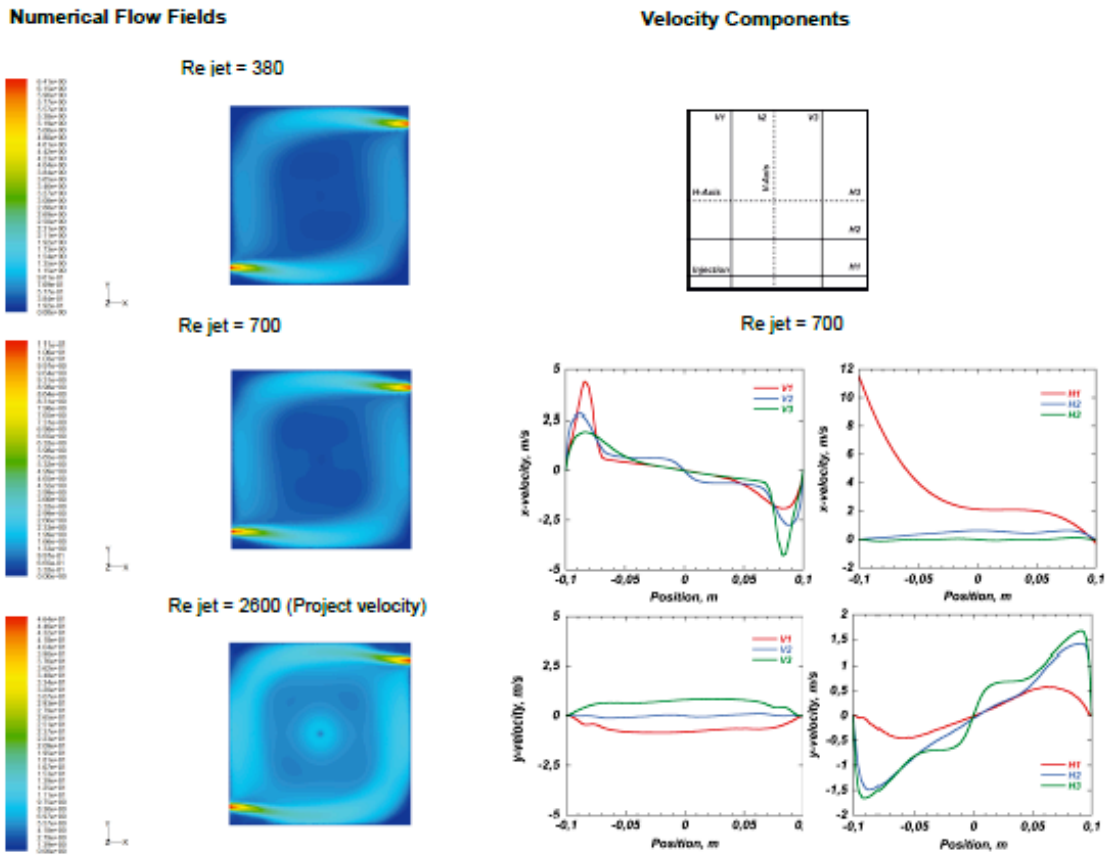

Fig. 4.34 Velocity magnitude (injection plane) for three different inlet Reynolds number.

In particular, to evaluate the degree of mixing , it was chosen to feed the two main jets with two different species but having the same chemical- physical and thermodynamic properties of helium. Finally, k epsilon RNG with swirl factor was used as turbulence model because as it will show in the paragraph of the experimental results, this model provides a better agreement between experimental data and numerical modeling with respect to the k-epsilon standard model.

In this analysis the entanglement parameter (K_{tgl}) provided similar information of the recirculation rate factor (K_v) defined in the introduction of this chapter for a MILD furnace. To define K_{tgl}, the definition of a characteristic section is needed. Fig. 4.35 highlights the section used for evaluating the K_{tgl}. It should be emphasized that this section is symmetrical with respect to the jet inlet and it provides the effective flow rate that recirculate into the chamber.

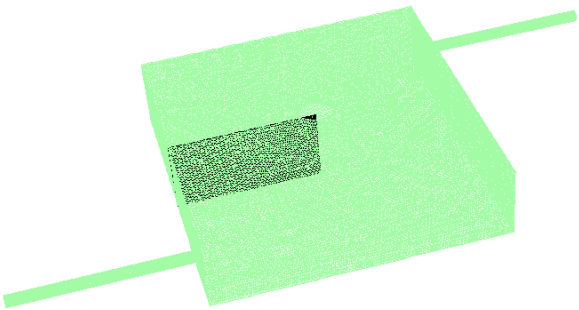

Fig. 4.35 Characteristic Section for the evaluation of K_{tgl}.

K_{tgl}.,, thus, it has been defined as:

$$K_{tgl} = \frac{\frac{1}{A}\int \rho v \, dA}{m_{0tot}} \tag{20}$$

where m_{0tot} indicates the total inlet flow rate into the reactor, A is the area of the charactersitic section (S) and v is the velocity magnitude in each cell of S. In Fig. 4.36 is reported the trend of K_{tgl} varying the inlet Reynolds number of the inlet jet from values close to 0 up to 5000. As shown in Fig. 4.36 K_{tgl} increases as Reynolds jet number increase in a range from values close to 0 up to 3000, and then reaches an asymptotic value equal to 15. For the project value of inlet Re number , K_{tgl} is 13, a value higher with respect to K_v values of a conventional MILD burner (for a MILD burner generally this value is equal to 3-4). In order to understand the presence of an asymptotic behavior, a numerical study of recirculation intensity and residence time were carried out. Relating to reactor intensity recirculation (I), this parameter was defined as the maximum value of the tangential velocity on a characteristic line. This line is set within the surface defined previously in Fig. 4.35 relatively to the plane of injection of the jets:

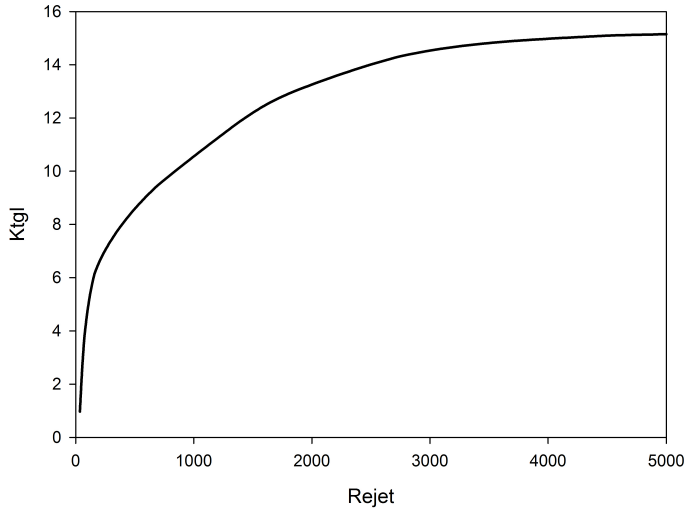

Fig. 4.36 K_{tgl} vs Rejet.

In Figs 4.37 is reported the trend of I, varying the inlet Reynolds number of the inlet jet from values close to 0 up to 5000.

It is clear from the figure that increasing Reynolds jet number lead to an increase of circulation intensity into the reactor, and such an increase is almost linear. It should be highlighted that a variation of Re on the graph refers to a variation of inlet velocity for both inlet jets, equally fed.

An assessment of RTD was performed by injecting a non-diffusive scalar tracer into the reactor and following its temporal evolution. In particular a numerical tracking pulse procedure (Liu, 2011) was performed, by wich it is possible to reconstruct the E (t) of the process, solving the field of stationary motion equation of tracer concentration:

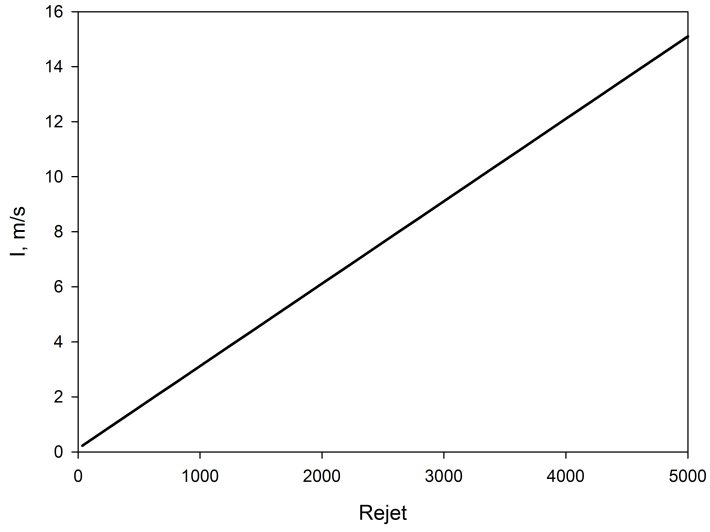

Fig. 4.37 I vs Rejet.

$$\frac{\partial c}{\partial t} + \nabla * (vc) = \nabla * (D_{eff} \nabla c) \quad (21)$$

To obtain an accurate numerical solution is necessary to choose an appropriate time step, a time step too small results in an increase of the computational effort while a too large time step would lead to an inaccurate solution. A criterion for the appropriate time step is obtained by imposing the Courant number (Courant et al., 1928), or $\Delta x * v / \Delta t$, equal to 1. Figs. 4.38 and 4.39 shows the RTD trend and the mean residence time into the reactor for several inlet jets Reynolds number. The mean residence time was calculated as(Levenspiel, 1998) as:

$$\tau_{mean} = \frac{\sum_i t_i c_i}{\sum_i c_i} \quad (22)$$

As shown in Fig. 4.40, mean residence time decreases as Re number increase. This is clear since for a closed system:

$$\tau_{mean} = \frac{V}{Q} \quad (23)$$

where V is the reactor volume and Q the total inlet volume flow rate.
From the analysis increasing the inlet flow rate Q lead to an increase of the recirculation intensity into the reactor, meanwhile the average time that a tracer particle remains into the reactor. Therefore, such an opposite behavior provides an explanation for the asymptotic trend of K_{tgl} at high Reynolds number. The evaluation of the mean residence time on the basis of RTD and a comparison with the average time calculated (V/Q) provides an indication of the active volume and the "dead volume" (Levenspiel, 1998) of the reactor. The latter is reported in % compared to the total volume of the chamber, varying inlet Reynold jets number in Fig. 4.40.

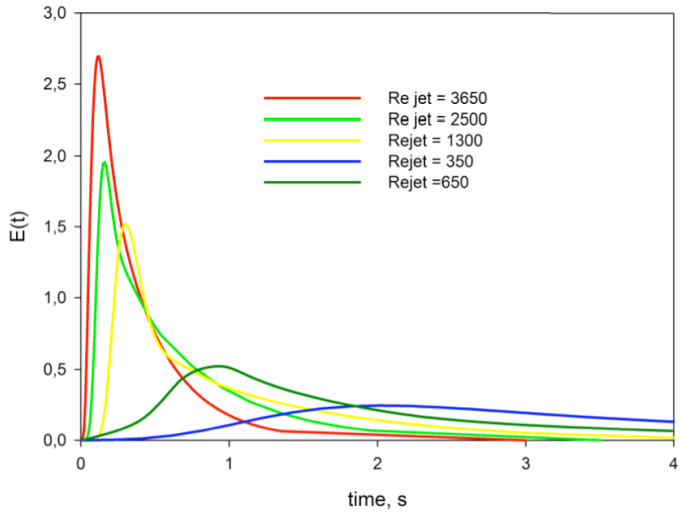

Fig. 4.38 Residence Time Distribution.

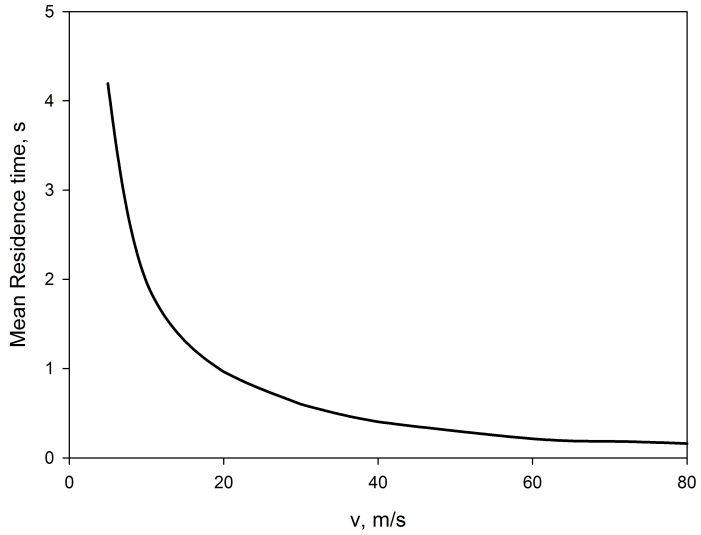

Fig. 4.39 Mean Residence Time.

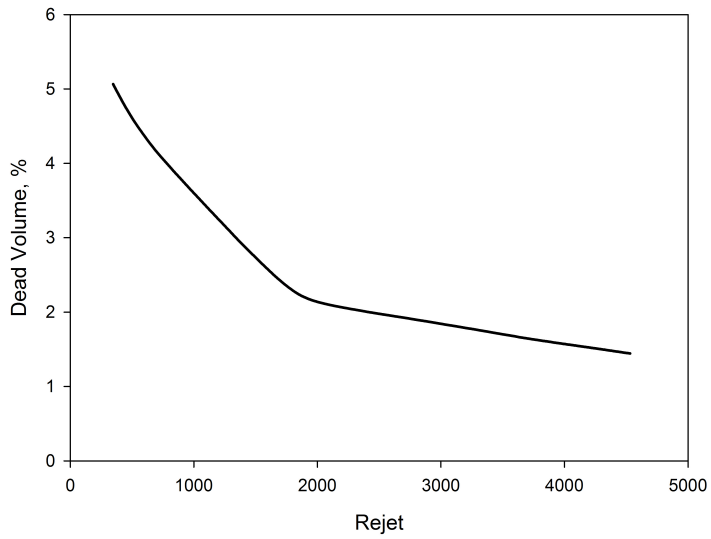

Fig. 4.40 Dead Volume %.

As shown in Fig. 4.40, % of dead volume is relatively small for all the Reynolds number analyzed. In particular, the dead volume is equal to about 5% of the total volume for Re_{jet} equal to 350 and decreases to a value of about 1% for Re_{jet} of 4500. Results suggest that establishment of a vortex structure leads to a longer reactor residence time respect to a non-cyclonic flow. Such peculiar aspect of a cyclonic flows will be further analyzed in detail in chapter 6.

The numerical RTD were also compared with the analytical equation of E (t) for a perfectly stirred reactor (CSTR). For a CSTR the equation of E (t) is the following (Levenspiel, 1998):

$$E(t) = \frac{1}{\tau_{mean}} e^{-\frac{t}{\tau_{mean}}} \qquad (24)$$

In Fig. 4.41 is reported this comparison for a Re_{jet} = 2500. From this comparison, it appears clear that for a value of Re_{jet} greater or equal to 2500, numerical RTD and analytical E (t) of a CSTR are almost coincident, except for a short delay to mixing , highlighted for the numerical case, being the latter representative of a real reactor. As reported previously, in order to evaluate the degree of mixing it was chosen to feed the two main jets with two different species but having the same chemical, physical and thermodynamic properties of helium. In such a way:

$$K_{tgl} = K_{tgl1} + K_{tgl2} \quad (25)$$

where 1 and 2 denotes the different inlet jets. Fig. 4.42 shows the ratio between K_{tgl1} and K_{tg2}. For Re_{jet} greater or equal to 2500 such a ratio is equal to one, so that similar considerations of Fig. 4.53 can be derived.

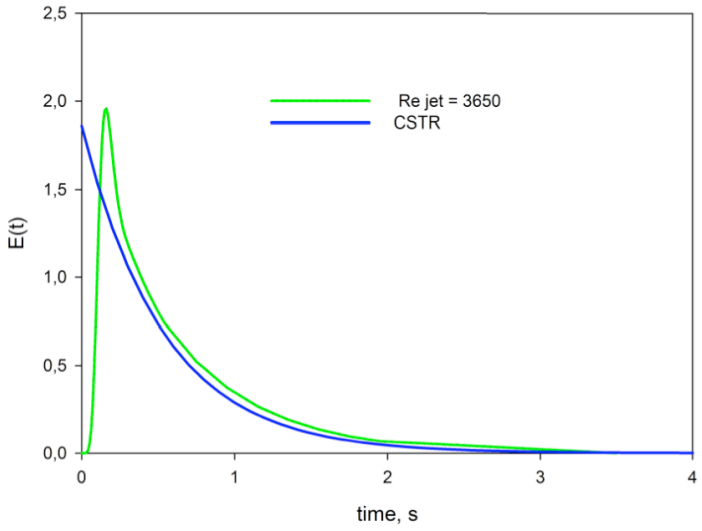

Fig. 4.41 RTD Comparison.

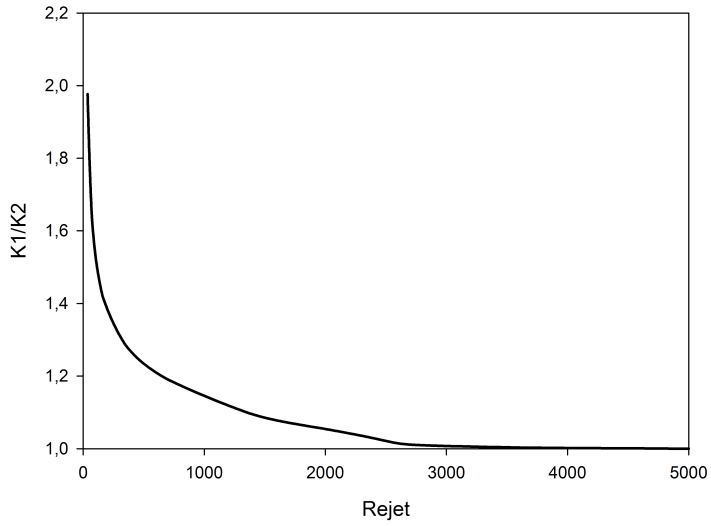

Fig. 4.42 K_{tgl1}/K_{tgl2}.

Further simulations where carried out in order to identify the critical Re_{jet} values for wich a well/defined vortex flow structure is established into the reactor. In this view, the maximum

of tangential velocity and its position respect to the wall of the reactor along the characteristic line previously descripted were followed at different height of the chamber. These trend are reported in Fig. 4.43. It is possible to highlight that for a value of Re_{jet} lower than 400, a well/defined vortex flow structure is not present, due to low inlet flow rate. In particular it can be observed that for z =2,25 cm, (i.e. near the outlet section) for such a values of Re_{jet}, magnitude of tangential velocity moves rapidly towards the exit. Furthermore, maximum of tangential velocity results extremely small. For Re_{jet} = 400, instead, such a maximum results higher respect the other cases analyzed (0.5 - 0.8 m/s) and for a value of z = 2.25 cm; the position of maximum velocity is close to the wall chamber (less than 1 cm), meaning that a vortex structure is established and this structure is extended to all the reactor size. It can be concluded therefore, that for a value of Re_{jet} = 400, a well determined recirculating flow field is established.

Further analysis were performed in order to understand the dependence of K_{tgl} respect to factors such as inlet temperature system, number of inlet jets, area of inlet and section exit. Fig. 4.44 shows the trend of K_{tgl} varying the inlet temperature system in an Arrhenius plot, holding constant the mass flow rate and the inlet jets velocity respectively. It can be highlighted that an increase of temperature, results in a reduction of recirculation degree into the reactor. Such effect is drastic when the inlet jets velocity is fixed, since Re_{jet} decreases significantly decreasing gas density. Fixing the mass flow, instead, such effect is less marked, since an increase of velocity balances the decrease of gas density.

Similar considerations can be applied varying inlet section area, fixing the inlet mass flow rate, In particular, Fig. 4.45 shows the trend of K_{tgl} for three different flow rates ($Q_1>Q_2>Q_3$), varying the inlet section area of jets.

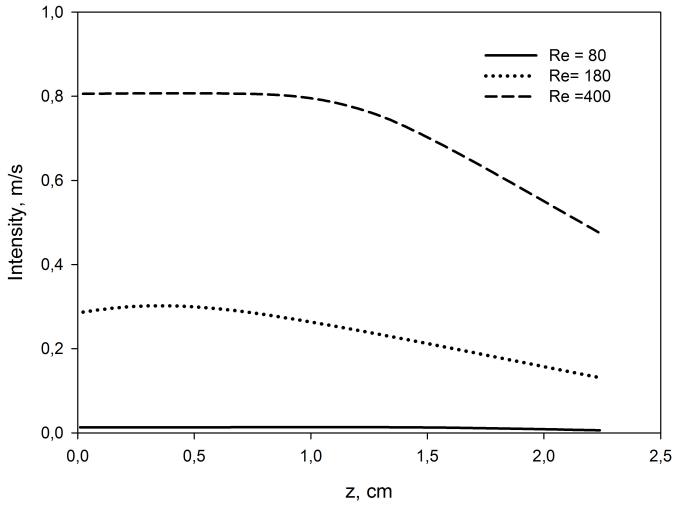

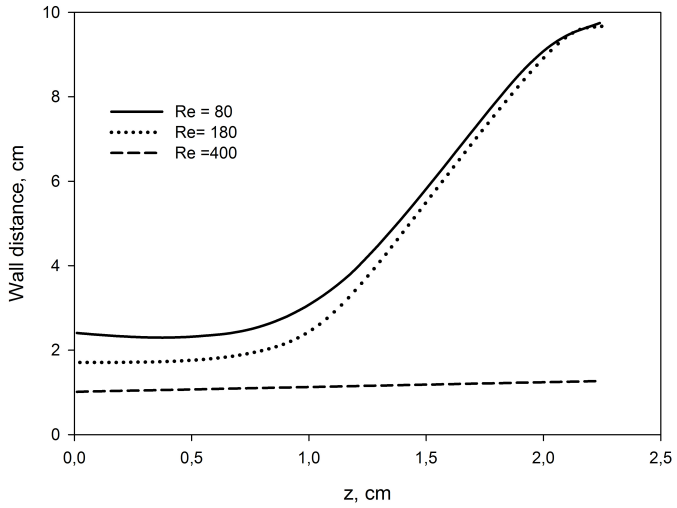

Fig. 4.43 Intensity, Intensity location at different height.

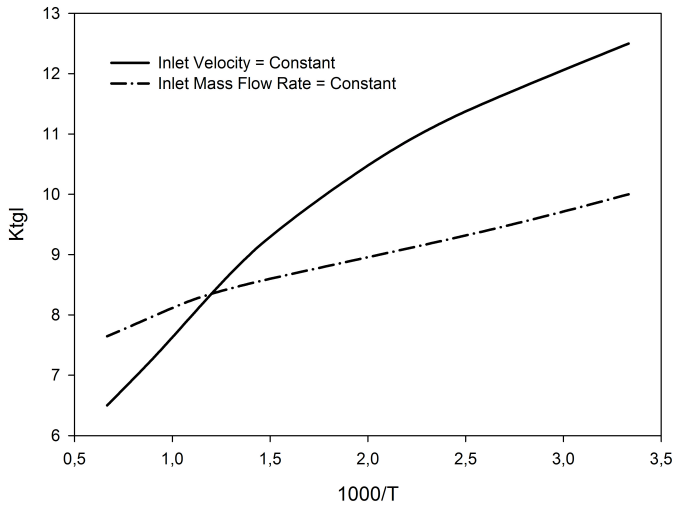

Fig. 4.44 K_{tgl} as function of temperature.

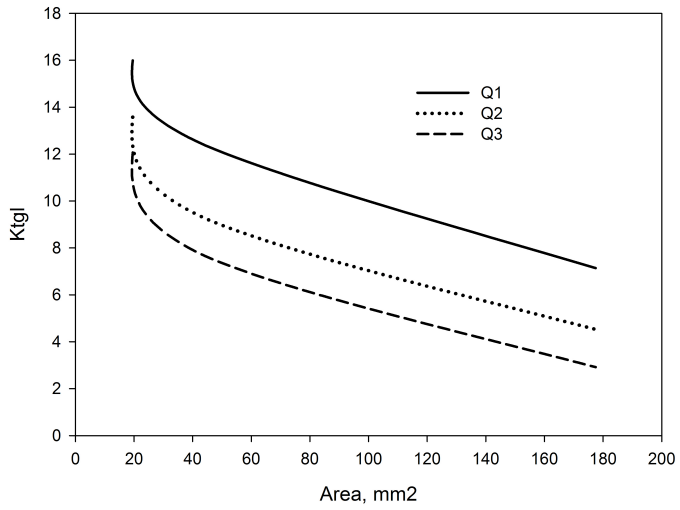

Fig. 4.45 K_{tgl} as function of inlet section area.

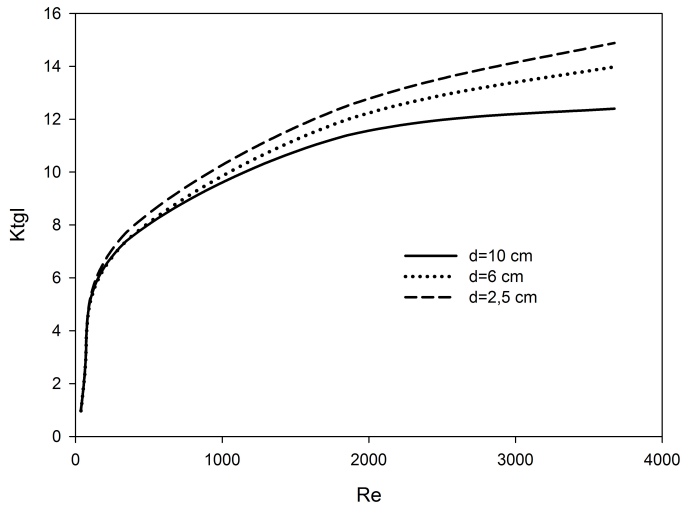

Fig. 4.46 K_{tgl} as function of outlet section area.

Decreasing the inlet section area, leads to an increase of Re_{jet} and, thus, of K_{tgl}. Fig. 4.46 reports the K_{tgl} trend as function of outlet section exit. As highlighted in this figure, K_{tgl} results a function of outlet section area for high values of Re_{jet}. In particular, K_{tgl} decreases as the outlet section area increase. This is mainly due to the fact that for high values of Re_{jet} the average magnitude of the tangential velocity increases as outlet section area decrease. For a better understanding, tangential velocity profiles along the characteristic line on the injection plane for two different values are reported in Fig. 4.47.

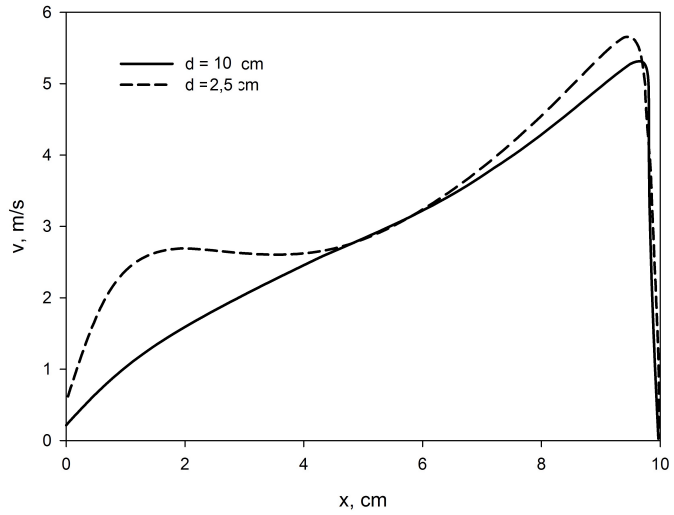

Fig. 4.47 Tangential Velocity Profiles for different outlet section area.

Finally, in Fig. 4.48 the trend of K_{tgl} for one inlet reactor configuration is reported. The trend is almost similar compared with that obtained for two inlet jets configuration, but in such case, K_{tgl} values are practically halved.

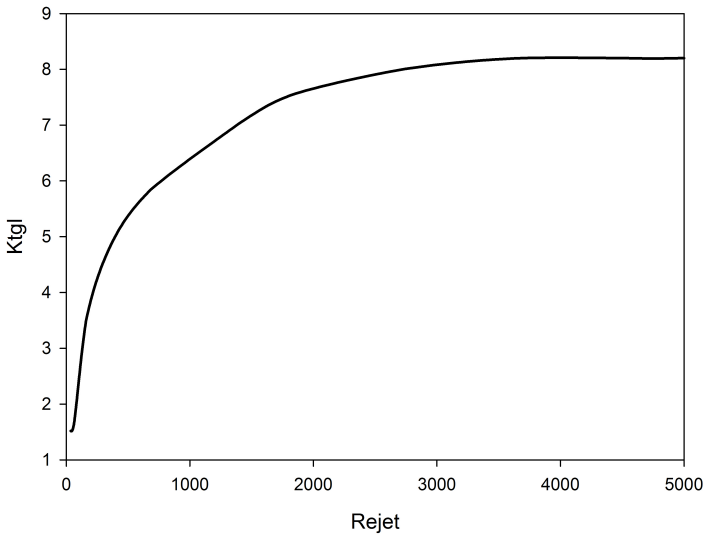

Fig. 4.48 K_{tgl} for one inlet configuration.

4.3.3 Particle Image Velocimetry

4.3.3.1 Experimental Facility and Diagnostic

As seen in the previous paragraph, a CFD Analysis was performed with the aim of designing a novel vortex chamber. configuration for MILD Combustion applications. On the basis of such analysis, a test chamber was built in order to perform an experimental characterization in isothermal conditions of fluidynamic flow fields, jets behavior and assessment of mixing degree into the chamber varying key operational parameters, such as Re_{jet}. and inlet jets number. Particle Image Velocimetry (PIV) technique was adopted to achieve these purposes. Experimental measurements were carried out in a chamber built by coupling PMMA-quartz in order to achieve a full optical access of the device and to make maintenance and cleaning operations simple. The apparatus consists of a square section (200x200 mm), in order to minimize any reflections of the laser light sheet, a height (h) of 50mm, inlet jets diameter (d_{jet}) of 7.5 mm and a section exit placed on the top side, with a diameter of 25 mm. A scketch and picture of the chamber illuminated by a thin laser light sheet are reported in Fig. 4.49.

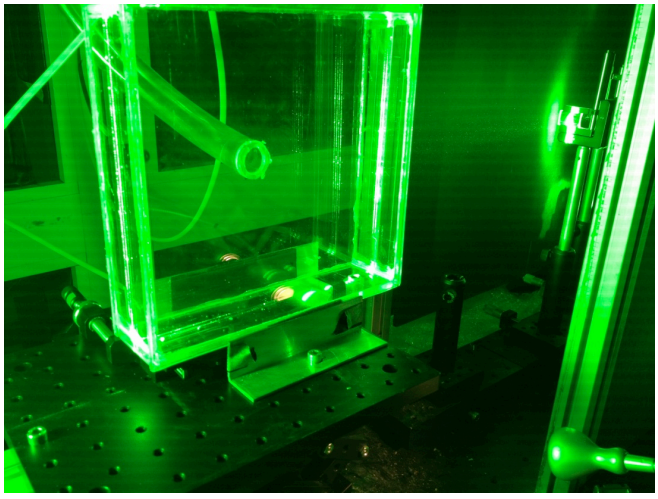

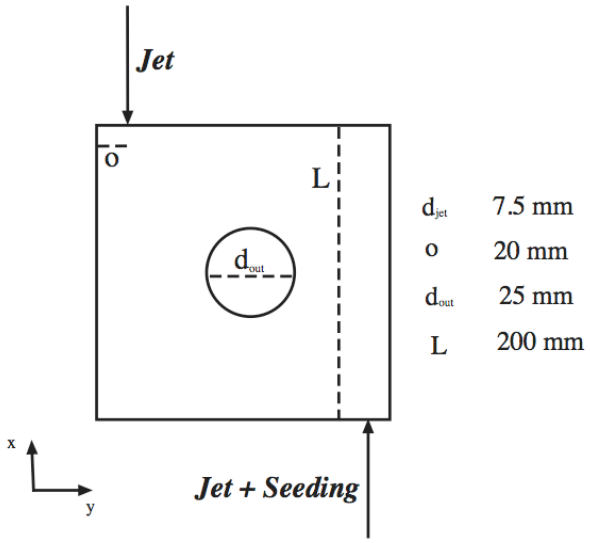

Fig. 4.49 Scketch, main geometrical characteristics of test Chamber for PIV acquisitions.

In addition to the test chamber, the experimental system is constituted by an optical detection apparatus, gas supply lines and a tracer insemination system for the flow visualization. In particular, the supply lines were made in such a way that the flow entering the test chamber was controlled and fully developed varying the inlet operating conditions. A fixed bed apparatus was used for the dispersion of the tracer particles in the gas stream.

For most experiments it is desirable that seeding particles be non-toxic, non-corrosive, non-abrasive, non-volatile and chemically inert. On the ground of these requirements, a wide variety of seeding particles is available for PIV experiments.

It is worthwhile to note, that the type of particles, for which Sc >> 1and St << 1, is the only possible choice of tracer in a gaseous system (Ottino, 1982). A particle, for instance, between 0.1 and 1 μm is sufficiently large in dimension to ensure that Brownian diffusion is low, but it is sufficiently small to immediately follow a flow.

Moreover, intensity of the scattered light, as a direct measure of particle size has always been plagued with difficulties, as detected intensity is dependent on so many other parameters of a flow system (e.g., trajectory of particle through a shaped beam/sheet, obscuration of incident and scattered light, extinction), despite some early attempts to remove the necessity of calibration (Tropea, 2011). There is also the basic difficulty that, in the Mie scattering range, the intensity is not monotonically dependent on particle size (Fig. 4.50). For the previous reasons, the inlet gaseous flow was seeded with TiO_2 particles with a mean diameter of 2 μm, that correspond to an optimum between the not-diffusing tracer

condition and an acceptable scattered light intensity. For high quality PIV records a scattering particle concentration of about 15 particles per interrogation volume is necessary (Clemens, 2002). The size of the interrogation volume depends in turn on the dimensions of the test section, but for many laboratory applications this condition corresponds to a concentration of 10^8–10^{10} m^{-3}.

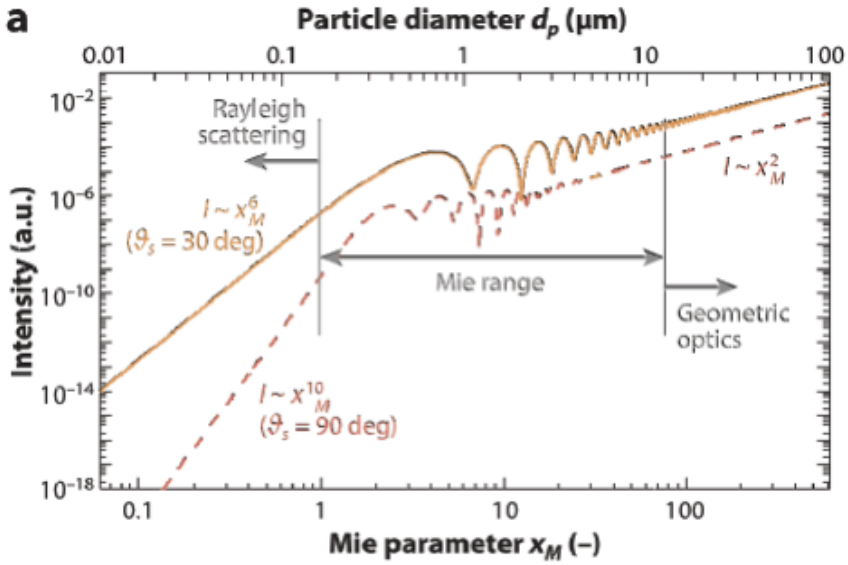

Fig. 4.50 Test Chamber for PIV acquisitions.

Suitable generators to satisfy the particle size and concentration requirements in gas flows are twin-fluid atomizers (for droplets or solid particles in liquid suspension) and fluidized beds (for solid particles). Ideally the scattering particles should be distributed uniformly in the flow, but, with large volume flow rates, requirements for globally uniform seeding may exceed the particle generation capacity. If local seeding is adopted, uniformity of seeding must be achieved in the region of investigation. In this work it has ben chosen to disperse the particles in the airflow by means of an ad-hoc realized elutriator, reported in Fig. 4.51, based on a fluidized bed device (Melling, 1997), This solution allowed for the homogeneous dispersion of particles in the airflow and for a satisfying concentration of seeders.

Fig. 4.51 Fluidized bed for seeding particles generation.

The optical characterization of the chamber is performed by recording the pattern of the light elastically scattered when a laser sheet illuminates the tracer. A Nd:YLF pulsed laser was tuned on the second harmonic wavelength (λ = 527 nm) and its beam was shaped by a set of cylindrical lenses to a sheet of constant thickness. It was varied in height by the extension of the objective field. Patterns of elastic scattered light was detected by a CMOS camera with a variable-focus telescope. Since each pulse is in a different frame, there is no directional ambiguity for the velocity vectors.

A shadow-graphic scheme has been adopted to collect images of the jets, with a proper system of lens. The pulsed laser frequency is 1000 Hz, the digital camera acquire 8-bit 1280 x 1024 pixel frames at 1000 Hz, and a BNC delay generator has been used for time base generation and synchronization. For each test condition a set of 2000 frames has been collected.

The diagnostic apparatus mainly consists of three units:

1) Laser LDY Nd:YLF double head, (λ=527 nm), maximal frequency of 10 kHz and output Energy (at 1kHz and at 527nm per laser head per pulse) of 15 mJ.

2) Camera NanoSense MkIII. Maximal resolution 1280x1024 pixels^2. Maximal frame rate= 2 kHz

3) A BNC 575 delay generator that manage the timebase generation and synchronization between the devices.

The use of a laser sheet source (Nd:YLF Laser), already available in the laboratory, allow collecting shadowgraph of the turbulent flow, and so a more detailed description of interface behavior should be achieved. n planar imaging, the laser beam is formed into a thin sheet, which can be accomplished by several different techniques (Eckbreth, 1988). The method used in this thesis is shown in Fig. 4.52, where a plano-convex cylindrical lens, that has a focal length of 500 mm, is used to focus the beam near the center of the field of view of the camera. Such long focal length lenses are used to increase the Rayleigh range, or the distance across which the beam remains focused. The larger Rayleigh range obtained from long focal length lenses permits also to have thicker sheets (in fact the final sheet thickness is 300 μm). experiments.

The particle density in the working fluid is set to give an average of 12 particle images in each 32 x 32 pixel interrogation window. Images for PIV were acquired at a rate of 1 kHz and the digitized images are cross-correlated using a recursive rectangular grid algorithm, which uses 32 x 32 pixel and then 16 x 16 pixel interrogation windows to find the mean pixel displacement. A Gaussian peak fit is used to determine the location of the cross-correlation peak to sub-pixel accuracy. Post-processing comprises a standard deviation filter to remove spurious vectors, followed by an interpolation to fill any empty locations and a Gaussian smoothing.

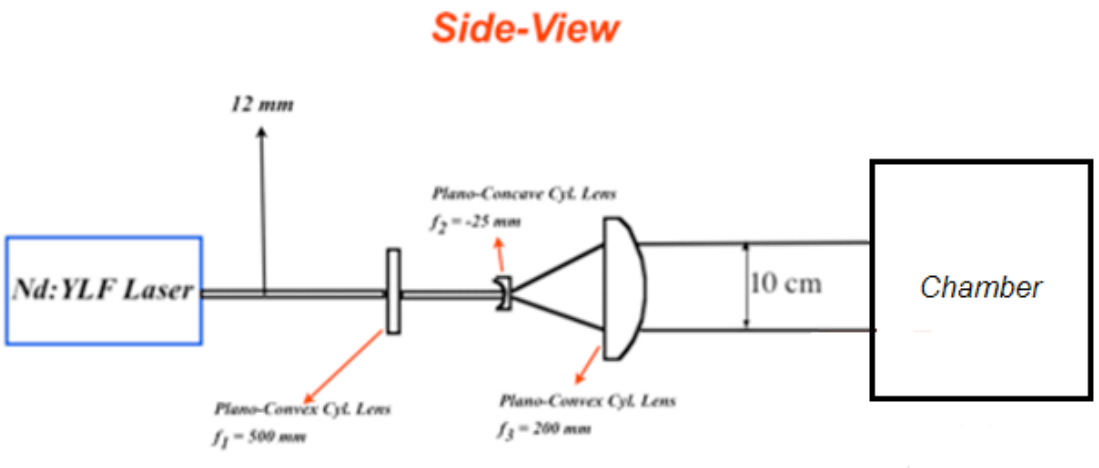

Fig. 4.52 Optical Diagnostic Apparatus.

Flow visualizations and PIV measurements have been conducted under various conditions, which differ for the inlet velocity and inlet jets number.The repeatability, or random, error is a statistical error. The uncertainty associated with the repeatability error can be assessed using the central limit theorem (Coleman, 1999).The random uncertainty of the mean velocity u_r can be calculated with:

$$u_r = \frac{1}{N}\frac{z_\alpha}{2}\frac{r_{rms}}{R} \quad (26)$$

with N the number of samples , z_α a variable related to the chosen confidence interval, r_{rms} the root mean square of the measured two-dimensional velocity in a point and R the mean two-dimensional velocity at the same location. The uncertainty of the measurement results is around 5% in the largest part of the test section for all the cases analyzed.

4.3.3.2 Test Conditions

Flow visualizations and PIV measurements were conducted on three different fields of view: 60x50 mm (near field), 110x100 mm (middle field) for the evaluation of local jet behavior and 210x200 mm (global field), for obtaining information on the flow-field developed into the chamber. Three different lenses were adopted to investigate such fields of view: 105, 60 and 28 mm respectively. All the acquisitions were carried out on the middle plane of the apparatus. For the global field investigations, it has been necessary to remove the second plano-convex lens since such a field of view resulted higher than the sheet of 100mm obtained with 28 mm lens.

Experimental campaign was conducted varying Reynolds number of jets, based on the inlet jet diameter and number of inlet jets. Operative working conditions analyses are reported in table 1. Swirl flow number was calculated based on the formula defined in Gupta (1984):

$$S = \frac{\pi D_e D_c}{4 A_i} \quad (27)$$

with A_i,the inlet area, D_e the exit chamber diameter and D_c the chamber diameter. Maximum capacity of the seeding generation system is 50 Nl/min which limits the scope of investigation to values of the Re_{jets} equal to 1500. Seeding tracer was feed in only one of

the two inlet jets. Helium at 298 K was used as working fluid in order to reproduce high-temperature conditions (i.e. similar properties of CO_2 at 1273 K).

# Jets	Re_{jet}	Swirl Number
1	450	68
2	450	34
1	650	68
2	650	34
1	1100	68
2	1100	34

Table. 4.4 Operative Working Conditions.

4.3.3.3 Global Field of View

Global field of view measurements are necessary to characterize the fluidynamic field motion into the cyclonic chamber and obtain an experimental quantification of K_{tgl}, (parameter defined previously in the paragraph of numerical results), that provides an indication of the recirculation degree into the chamber. Furthermore, data collected in this experimental campaign are considerably significant for comparing numerical results and testing several turbulence closure models for confined vortex flow applications.

Three different Re_{jet} values were investigated. In particular a value of 450 was considered first value of Re_{jet} to analyze, since numerical simulations showed that such a value is critical to establish a well/defined vortex flow field into the chamber.

A set of 2000 snapshot images were recorded for each case analyzed, then, an average image of the flow field was obtained and finally the velocity vectors.

In Fig. 4.53 shows an instantaneous flow visualization and an example of velocity vectors of mean field obtained with PIV technique, for a value of Re_{jet} equal to 650 and for two inlet jets chamber configuration. It is worthwhile to stress at this point that for such a field of view, since acquisitions have been carried out without second plano-convex lens, PIV processing has been performed only in the central part of the chamber where an uniform light sheet is present. However, measurements are significantly since a characterization of cyclonic vortex flow in terms of vortex core location, vortex dimension and vortex type (forced, combined or free vortex) can be obtained. Characterization of jets behavior and

middle field of view has been carried out by image acquisitions of 60x50 mm (near field), 110x100 mm (middle field).

It is possible to highlight that fluidynamic chamber flow structure appears complex, related to different spatial scales (jet scale and chamber scale). However, a single well/defined vortex core can be identified. Similar considerations can be applied for all the cases analyzed.

Given the characteristic line for the evaluation of the parameter K_{tgl} , Figs 4.54 and 4.55 show the trend of velocity magnitude along the characteristic line on the central-plane for two inlet jets and one inlet jet configurations, respectively. It has to be highlight that an analysis of velocity components revealed that radial component results practically negligible with respect to tangential one (difference of about one order of magntitude) for all the cases under investigation.

Typical profiles of a cyclonic chamber were identified. More specifically three regions can be highlighted:core, annular and wall regions. The core region is characterized by a forced vortex motion (solid-body rotation).

In the wall region the velocity profiles are typical of a free vortex motion and maximum of tangential velocity is placed in this zone. Annular region represents a transitional zone between core and wall regions. Tangential velocity profiles analysis revealed a more strong forced vortex behavior respect to a free vortex one for all cases analyzed. Exact location of maximum of tangential profiles respect to reactor wall, and thus, exact characterization of vortex structure type is a complex function depending on cyclone Swirl number, Re_{jet}, number and position of inlet jets (Char and Dhir, 2007). Moreover it has possible to see that the vortex structure intensity increases as well as inlet jet Reynolds number increase.

Experimental values of K_{tgl}, can be obtained by averaging the velocity magnitude values obtained for the characteristic lines and assuming that such a value is equal to the average velocity calculated on the characteristic surface. Comparison with numerical simulation shows that the maximum error that is committed in making that assumption is less than 5%.

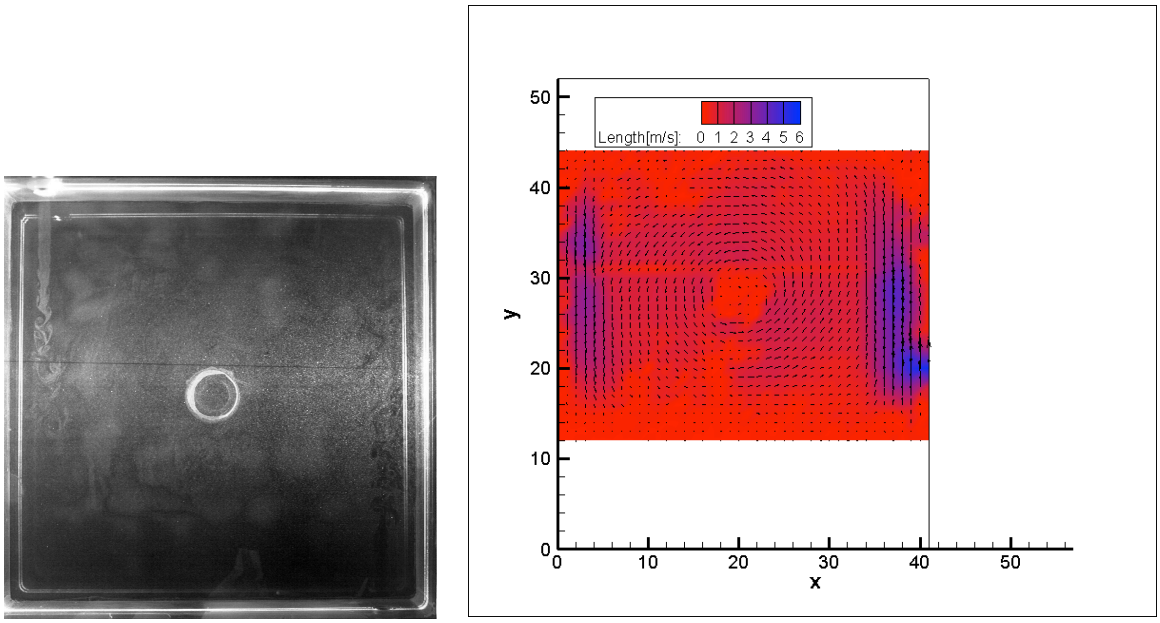

Fig. 4.53 Snapshot Re_{jet} = 650, 2 jets.

As can be seen in Fig. 4.56, the value of K_{tgl} increases almost linearly with the inlet jet Reynolds number, for the range of Re considered.

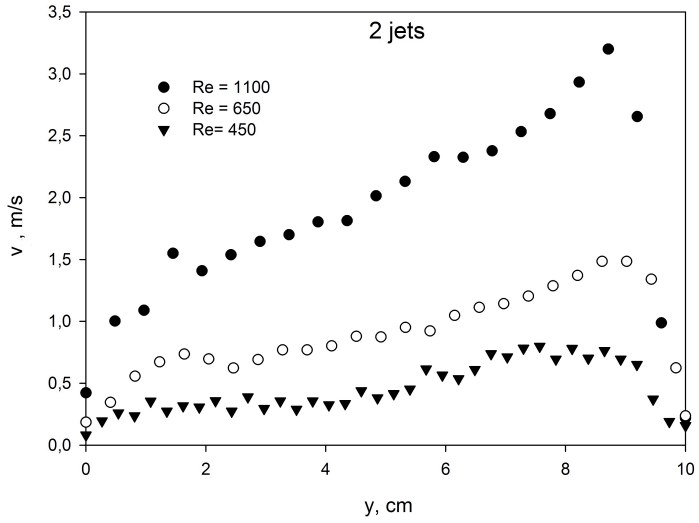

Fig. 4.54 Velocity magnitude, 2 jets.

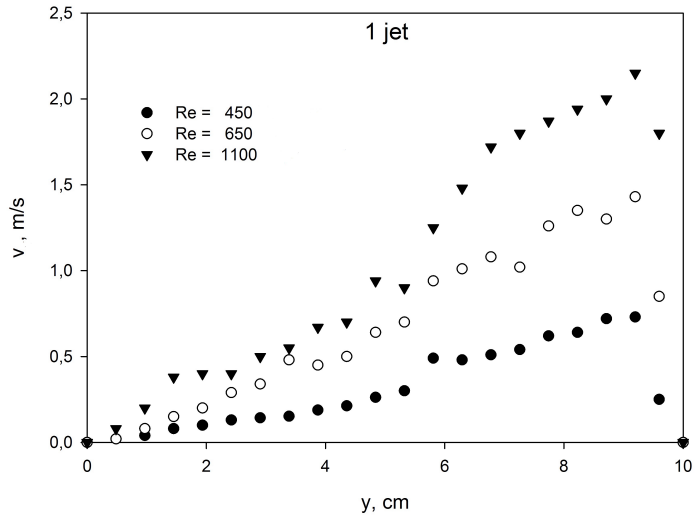

Fig. 4.55 Velocity magnitude, 1 jet.

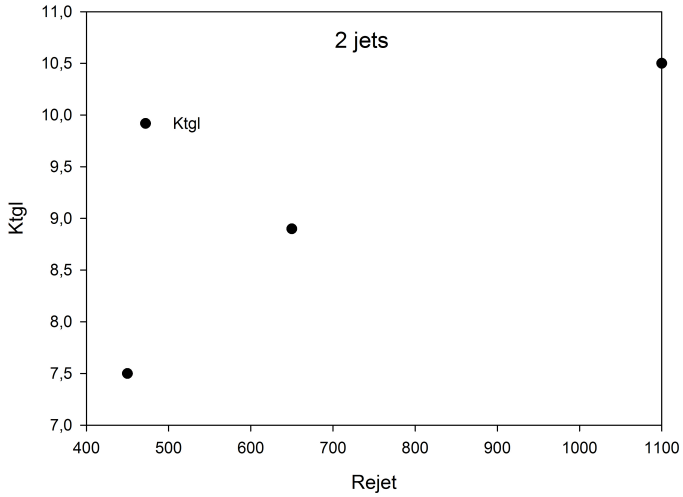

Fig. 4.56 Evaluated K_{tgl}.

4.3.3.4 Field of View 60x50 mm

With such a field of view a visualization of jet local motion, a characterization of the interface morphology, an evaluation of centerline velocity decay and spread rate and finally, an estimation of the mixing process between jet and vortex flow can be obtained. At this point , it has to be stressed that PIV campaign was principally carried out in order to evaluate the mixing process inside the chamber between the recirculated fluid and the

primary jet. Mixing process evaluation was carried out relating such a process to the engulfment process clearly defined in the next paragraph.

In Fig. 4.57 instantaneous flow visualizations of the seeded jet in the 60x50 mm field of view are reported. Different jet behavior can be identified, varying either the inlet jet Reynolds number or the number of jets, in terms of jet width and local structures.

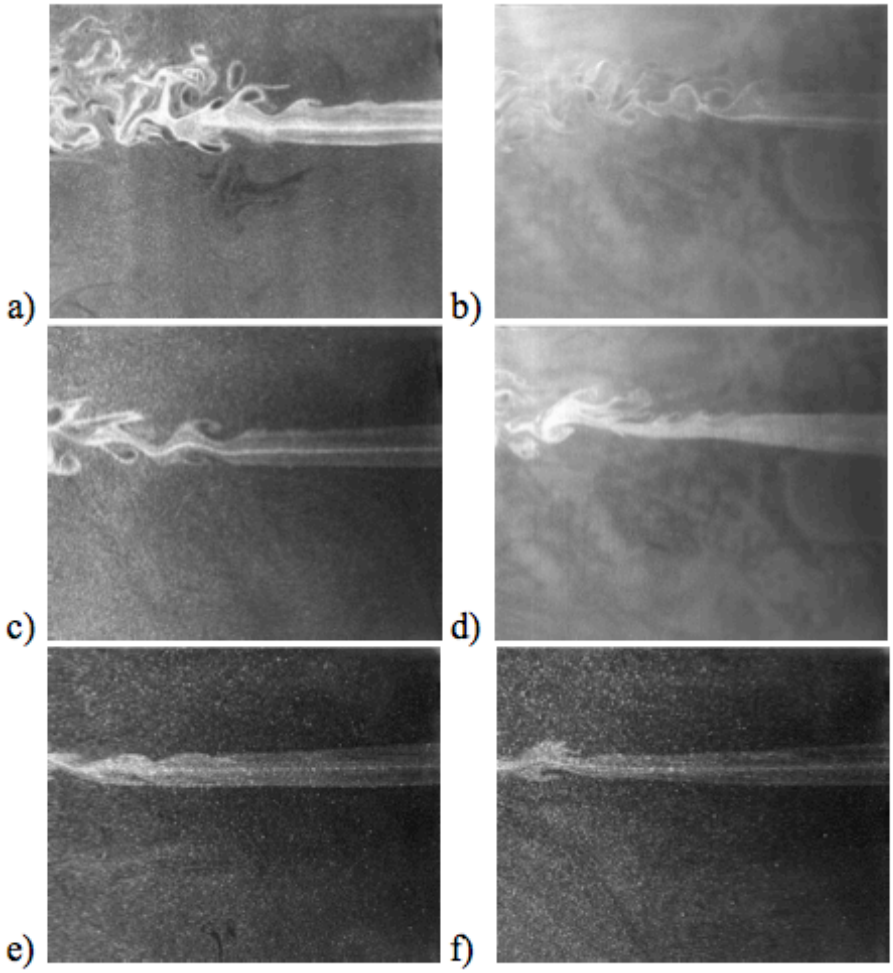

Fig. 4.57 Instantaneous flow visualizations, a) 2 jets, Rejet = 1100; b) 1 jet, Rejet = 1100; c) 2 jets, Rejet = 650; d) 1 jet, Rejet = 650; e) 2 jets, Rejet = 450; f) 1 jet, Rejet = 450.

From the images can be observed as the morphology of the interface changes dramatically from a value of Re = 400 to a value equal to 1000. At this point it should be noted that the morphology of the interface is a function not only of the inlet jet Reynolds number but also of the motion field that is established in the room. For example, considering the base chamber as characteristic length and the average value of the velocity on the characteristic

line, Reynolds number on the inlet injection plane is equal to 1300, 3000 and 5000 respectively for values of Re of the jets of 400 , 650 and 1100 and two jets configurations. A post-processing analysis 2000 image was performed for all the case analyzed. Fig. 4.58 shows velocity vectors colored by velocity magnitude related to average images obtained by post-processing analysis for two inlet jets configuration. Same analysis were performed for one inlet jet configuration but results are not shown since similar considerations can be applied.

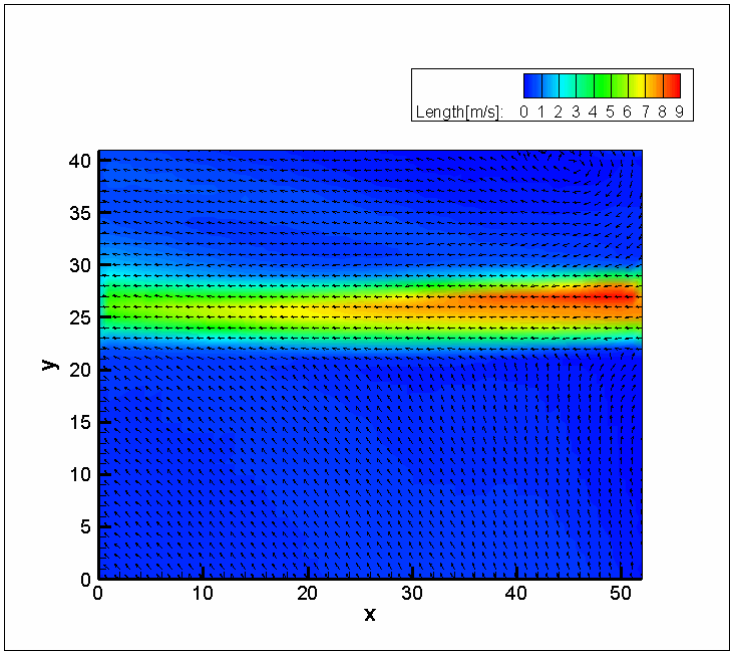

a)

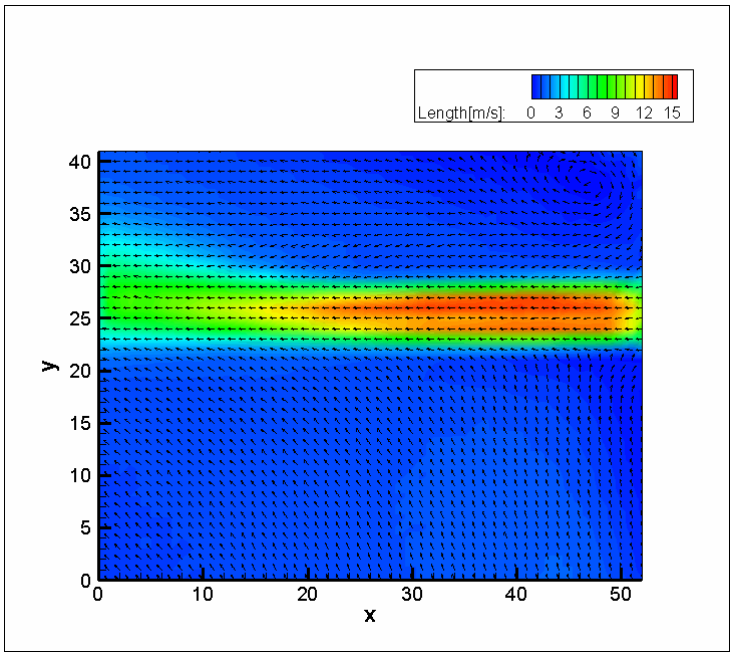

b)

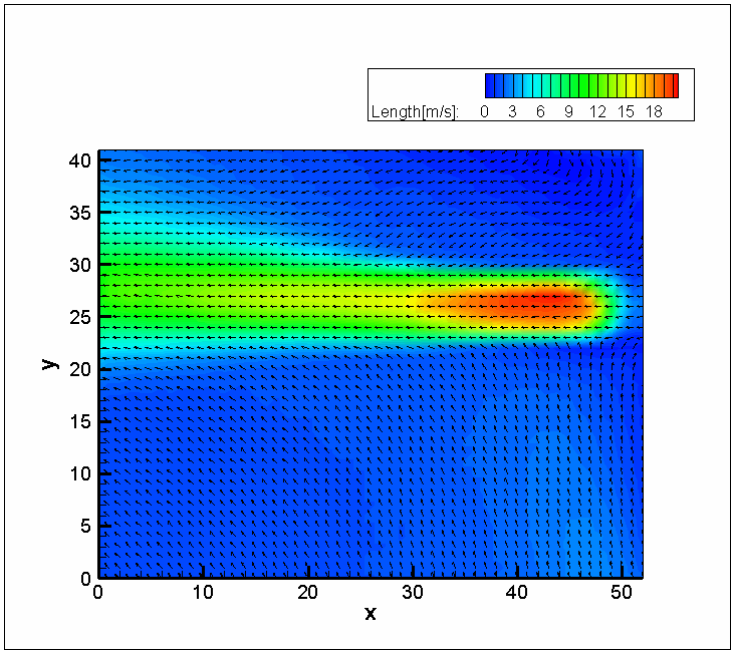

c)

Fig. 4.58 Velocity vectors colored by velocity magnitude for , a) 2 jets, Rejet = 450; b) 2 jets, Rejet = 650; c) 2 jets, Rejet = 1100.

As it is known in the literature (Iyogun and Birouk, 2009) decay centerline jet velocity and jet half-width velocity are indicators, respectively, the level of fluid quantity incorporated by the jet and jet spreading. It should be noted that half-width velocity is defined as the radial distance from the centerline of the jet, where the average velocity (v) becomes half of centerline velocity (v_0). Fig. 4.64 reports the decay of average velocity along the centerline normalized with respect to the centerline inlet velocity for the three cases in analysis. In this Fig. ordinate axis represents the distance from the nozzle normalized with respect to the inlet diameter of the jet. On the same Fig., normalized velocity decay for a free jet case (Re= 450, 1100) is also reported (Symons and Labus, 1971).

As reported in Fig. 4.59, for a value of x/d up to 2.5, normalized centerline velocity results practically close to unit, not depending on inlet jet Reynolds number value. For x/d values between 2.5 and 5 it is possible to note a fast decrease of normalized velocity for a inlet Reynold number of 1100 meanwhile for the other case this decrease is not so fast.. For x/d > 5 also for the Re =650 case is possible to note a fast decrease of centerline velocity. At x/d 8 for a Re =1100, centerline velocity is approximately 40% of the inlet jet velocity, meanwhile for Re= 450 this value is about 70% of inlet jet velocity.

Such a trend (namely decrease of penetration lenght and increase of jet velocity decay as inlet jet Reynolds number increase), is in contrast with a free jet behavior (Symons and Labus, 1971). Such a trend could be directly related to the presence of cyclonic vortex flow structure. More specifically, it is possible to note how the inlet jet velocity decay increases as the intensity of recirculation into the chamber increase. For Re = 450, centerline jet velocity profile for a free jet case is very similar with the case analyzed, except for x/d values close to 8. For higher Re number, free jet behavior is completely different with respect to analyzed jets. For Re= 1100 and x/d =8, normalized decay velocity value for a free jet is 0.8 meanwhile for a jet that interacts with a cyclonic vortex flow structure is 0.4. Such a results highlights that the interaction between cross/interfered jets and a vortex structure generated by jets theirself strongly affect the jet behavior.

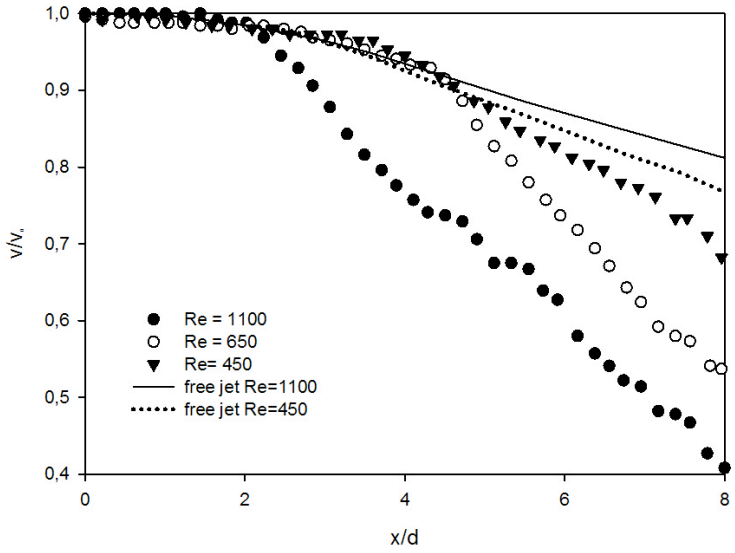

Fig. 4.59 Normalized Centerline velocity decay as function of x/d.

It is important to highlight that jets analyzed interact with a wall. The presence of a wall causes that the maximum of jet velocity is not longer located at the jet centerline, instead it moves towards the wall (Kanna and Das, 2005), so that jet velocity decay is normalized respect to the velocity maximum. For the case analyzed such a variation is related to the interaction between the recirculated flow and jet and to the presence of wall. However, it is important to note that the field of view investigated is smaller than the attachment lenght, of the jet. Analysis of maximum velocity location respect to jet centerline velocity

demonstrated that the error committed normalizing the jet velocity decay respect to the inlet centerline velocity is close to 5%. Then, considerations obtained are similar.

Fig. 4.60 reports the decay of average velocity along the centerline normalized with respect to the centerline inlet velocity for one inlet jet configuration varying jet Reynolds number. On the same Fig., normalized velocity decay for two inlet jets configurations is also reported for comparison (Symons and Labus, 1971). Fig. 4.60 highlights that number of inlet jets can significantly affect the jet velocity decay, depending on the inlet Reynolds number More specifically, it is possible to note that jet velocity decay increases as the number of jets increase. For Re=650 and1100, such effect is pronounced meanwhile for a Re=450, jet velocity decay (and thus, mixing process between primary jet and recirculated flow inside the chamber) is not significantly affected by jets number. In this case, such evidence could be mainly related to the fact that for Re = 450, recirculation intensity itself is already small for two inlet jets configuration (mean velocity is about 0.5 m/s in the reactor).

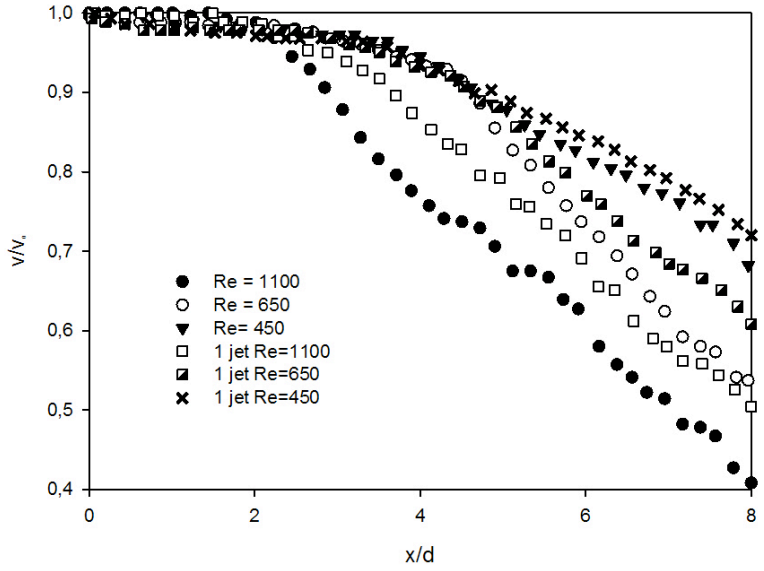

Fig. 4.60 Normalized Centerline velocity decay as function of x/d (one jet).

Experimental campaign carried out with 60x50 mm field of view showed that jet behavior significantly depends on number of inlet jets and inlet Reynolds number. Data collected highlighted that jets cross-interacting to form a cyclonic vortex structure show different characteristic behavior respect to a free jet in terms of velocity decay, jet width and fluid-dynamic structure.

4.3.3.5 Field of View 110x100 mm

With such field of view additional information of jet behavior were collected. In particular experimental campaign of two inlet jet configuration were carried out in order to estimate jet attachment lenght to the wall. The type of jet in analysis are known in the literature as “offset wall jet” (Nasr and Lai, 1998), where offset refers to the distance that exists between the wall and the centerline of the jet.

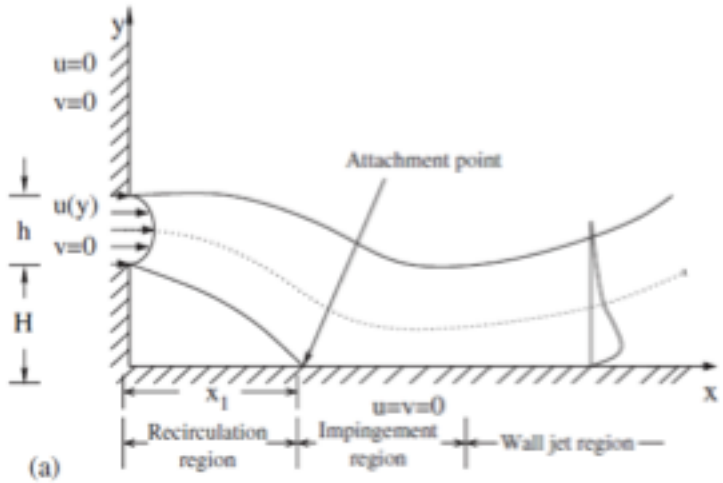

Fig. 4.61 Schematic diagram of the offset wall jet problem.

Due to the entrainment of fluid between the wall and the jet, it creates a low pressure area between the wall and the jet that pushes the jet in the direction of the wall itself and possibly the jet attaches. This effect is known as the Coanda effect . It is possible to distinguish different areas for this problem. A first zone (near field) in the proximity of the outlet section , where the jet is dominated by its initial moment and behaves as a free jet, after which it deflects and attaches to the wall . The distance between the inlet and the point of attachment is called the length of attachment . Once the jet has impacted with the wall, the jet tends to "move" along the wall (far-field) . Finally, after a certain distance, (region of impinging), the jet assumes all the characteristics of a wall-jet . For different applications it is of fundamental importance to assess the length of attachment . Kanna and Das (2005) , shows the trend of this parameter varying jet Reynolds number and the offset distance. The authors report that for a laminar jet, this length increases with jet Reynolds number, and with increasing the offset distance(Fig. 4.62).

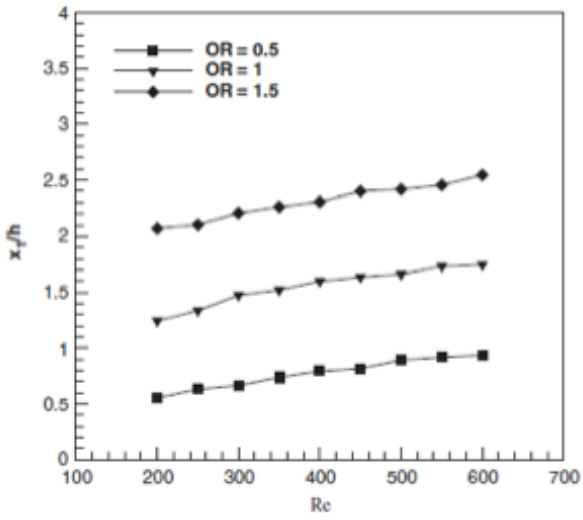

Fig. 4.62 Attachment lenght as function of Re and offset distance (Kanna and Das, 2005).

Moreover, authors report that such a parameter, and then the jet-wall interaction can be greatly influenced by the boundary conditions of the problem which is itself extremely complex. As already mentioned in the results related to the field of view of 600x500 mm, it has been observed an increase of jet deviation towards the wall with increasing Re number. In the present case, the offset value is equal to 2.

Fig. 4.63 shows jet attachment lenght as function of Re number, for two inlet jet configuration. Such a parameter is obtained by a post-processing analysis of 2000 images for each Re number considered.

It is interesting to note that for jets analyzed, the attachment lenght decreases as Re number increases. Such trend is in contrast with that reported by Kanna and Das for a laminar offset jet. This difference is due to the presence of a "recirculated" flow (formed by cross-interaction of two jets and by the particular geometry configuration) that interacts with the primary jet. Indeed, the "recirculated" flow acts pushing the jet towards the wall and this "pressure" increases as Re increase. Considering the recirculated flow as a lateral secondary flow in cross-flow with the primary jet, momentum flux ratio (J) between primary jet and lateral flow can be obtained. In particular it has been calculated that J varies from a value of 120 for Re of 450 down to 35 for a Re equal to 1100.

In conclusion, the presence of a cyclonic vortex structure generated by cross-interference of two jets involves a drastic change in the dynamics of the single jet , not only in terms of

velocity decay and spread rate (and thus in terms of mixing with the surroundings environment), but also on the interaction between jet and the wall.

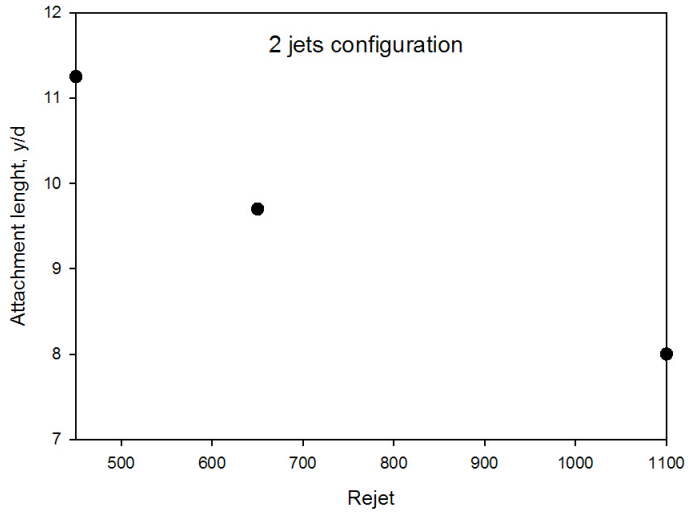

Fig. 4.63 Attachment lenght as function of Re for two jet configuration.

4.3.4 Mixing Process Evaluation

4.3.4.1 Mixing Process Evaluation: Engulfment Process definition and quantification

Recently (Philip and Marusic , 2012), it has been provided a clear view of the entrainment process, i.e. "incorporation" of fluid from the external environment of a turbulent jet to the jet itself. This process can be seen as the result of two sub-processes. In particular, the non-turbulent fluid relative to the external environment is induced and "engulfed" within the turbulent jet, through the action of large scale vortices, then it is converted into turbulent fluid through the action of the vortices at small-scale (via nibbling). So this process is the sum of processes that occur on large and small scale . In Fig. 4.64, a scheme of the engulfment process is reported (adapted from Philip and Marusic, 2012).

In this view, a cyclonic flow, generated by a cross-interference process between multiple jets can drastically complicate the overall vision of the entrainment process. For instance, fluid outside a jet may be come from the same jet, other jets or it is a mass of fluid that recirculates due to the interaction between jets. A re-definition of the entrainment process

(and its sub-processes) of a mass of fluid to be part of a jet interacting with other jets and a definition of parameters for analyzing the process of cross-interference are necessary .

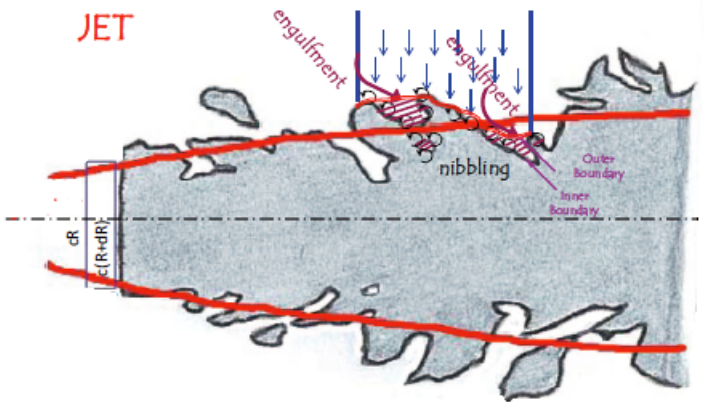

Fig. 4.64 Visualization of engulfment process, free jet case (adapted from Philip and Marusic, 2012).

A classification of the process can be obtained on the basis of different characteristic scales at which the issue is addressed. In particular, it is necessary to analyze all the steps involved characterizing the jet in its whole extent , in order to analyze all structures, from the largest to the smallest one.

Four different processes can be defined as follows:

- *Entanglement*: process that link two or more jets basing on their dynamic and drag forces, related to characteristic scale of both or all jets (problem scale);
- *Entrainment*: process that link one or more jets basing on their dynamic and drag forces, related to characteristic scale of one single jet;
- *Engulfment*: process that link one or more jets basing on their dynamic and drag forces, related to external characteristic scale of one single jet;
- *Erosion*: process that link one or more jets basing on their dynamic and drag forces, related to internal characteristic scale of one single jet.

In order to characterize the mixing process mechanism of a jet that interact with a cyclonic vortex flow, generated by a cross-interference between multiple jets, a detailed definition of parameters to quantify these processes is needed. Furthermore a quantification of such parameters by experimental and numerical point of view is necessary. It has to be stress at this point that in this thesis, attention was principally focused on the analysis and

quantification of the entanglement and engulfment processes, in order to cover all the phenomenologies that occur at large and small scale. A more general vision of all the processes involved during the cross-interference process of multiple jets, together with all the parameters that can be defined and evaluated is reported in Appendix A.2.

A clear definition of the entanglement process in terms of entanglement parameter definition and calculation has been provided in paragraph 4.4.2. In this paragraph attention is devoted to the engulfment process.

Mixing process between inlet jet and recirculated flow in the reactor is investigated on the basis of a physical process, defined in literature as engulfment. In a more general sense, the engulfment process can be defined as the radial inward flux of ambient fluid drawn into a jet and that later, it effectively "find" within jet (Han and Mungal, 2001). It appears clear that the engulfment rate controls the mixing rate of the jet fluid with the ambient fluid. To quantify such a process, and thus, the growth of a jet, the engulfment parameter (K_{glf}) can be defined as follows:

$$K_{glf} = \frac{m_t - m_0}{m_0} \tag{28}$$

Where m_0 represents the total inlet mass flow rate and m_t is the total mass flow rate of the jet along the stream-wise direction.

An example of characteristic line (SC) for the evaluation of m_t is reported in Fig.4.65.

Fig. 4.65 Visualization of the characteristic line for m_t evaluation

At this point it has to be stressed that the engulfment process can be divided in auto-engulfment (relative to a single jet) and engulfment relative to the remaining jets. In this case a measurement of the engulfment process for one single jet configuration and a comparison with the overall K_{glf} obtained for two or more inlet configurations can provided a clear vision of the degree of auto-engulfment related to a single jet.

In the experimental campaign, data about jets behavior were collected only on the centerline plane, so that no informations are available on z-direction. In such a case, m_t can be obtained under axial-symmetric hypothesis. With this consideration, m_t was defined as:

$$m_t = 2\pi \int_0^R \rho v r \, dr \tag{29}$$

Where ρ is the density of fluid and v, the average velocity of the jet at each location along the stream-wise direction. To evaluate the jet width at different location from the nozzle, a criterion for identifying the jet boundaries is necessary.

Several imaging processing procedures have been developed for jet boundary detection based on light pixel intensity and/or vorticity threshold (Westerwheel, 2012; da Silva et al., 2011). This type of procedures leads to a qualitative interface detection but are very time-consuming. Since this study is not related to a morphological detection of jet interface but it is strictly related to a quantification of "engulfed" fluid within a jet different image post-processing analysis can be applied.

In particular, in this study, jet boundaries were evaluated considering the 10% of jet centerline velocity along streamwise direction (or the maximum of jet velocity, when location of maximum not corresponds with the jet centerline) as threshold velocity value. This threshold value has been chosen for post-processing analysis since it ensures a good agreement between average value of K_{glf} calculated by light intensity analysis and velocity magnitude procedure. A 50% of the jet centerline velocity as threshold value, generally adopted in literature for the evaluation of the jet half-width, leads to an underestimation of the engulfment process. In this view, Fig. 4.66 reports a comparison of calculated K_{glf} varying treshold value and method, for 2 inlet jets configuration and Re_{jet} =1100.

For numerical simulations, axial-symmetric hypothesis is no necessary and mass flow rate of the jet at each location from the nozzle can be directly evaluated on the basis of threshold velocity criteria previously defined. Fig. 4.67 reports two examples of jet

boundary identification by means of velocity magnitude criteria for a free jet and a offset wall jet (proposed configuration), respectively.

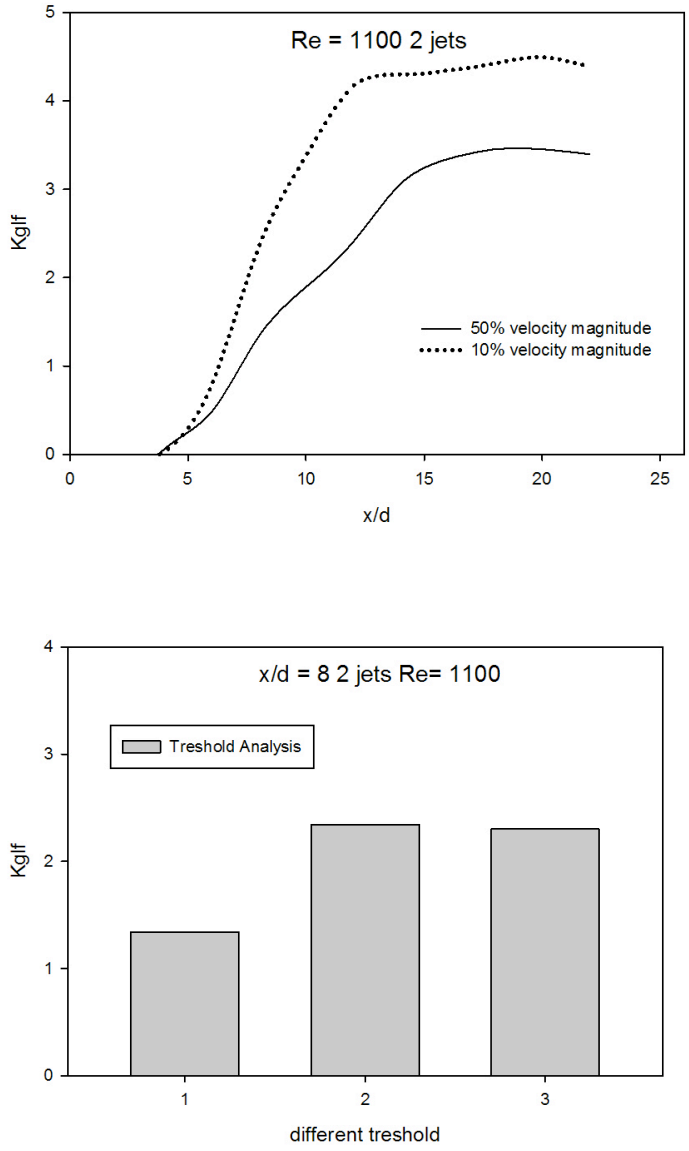

Fig. 4.66 Comparison of K_{glf} for different levels of treshold for velocity magnitude method (top), Comparison of K_{glf} for different levels of treshold for velocity magnitude method and light intensity method (bottom);1 = 50% velocity magnitude, 2= 90% light intensity 3= 10% velocity magnitude.

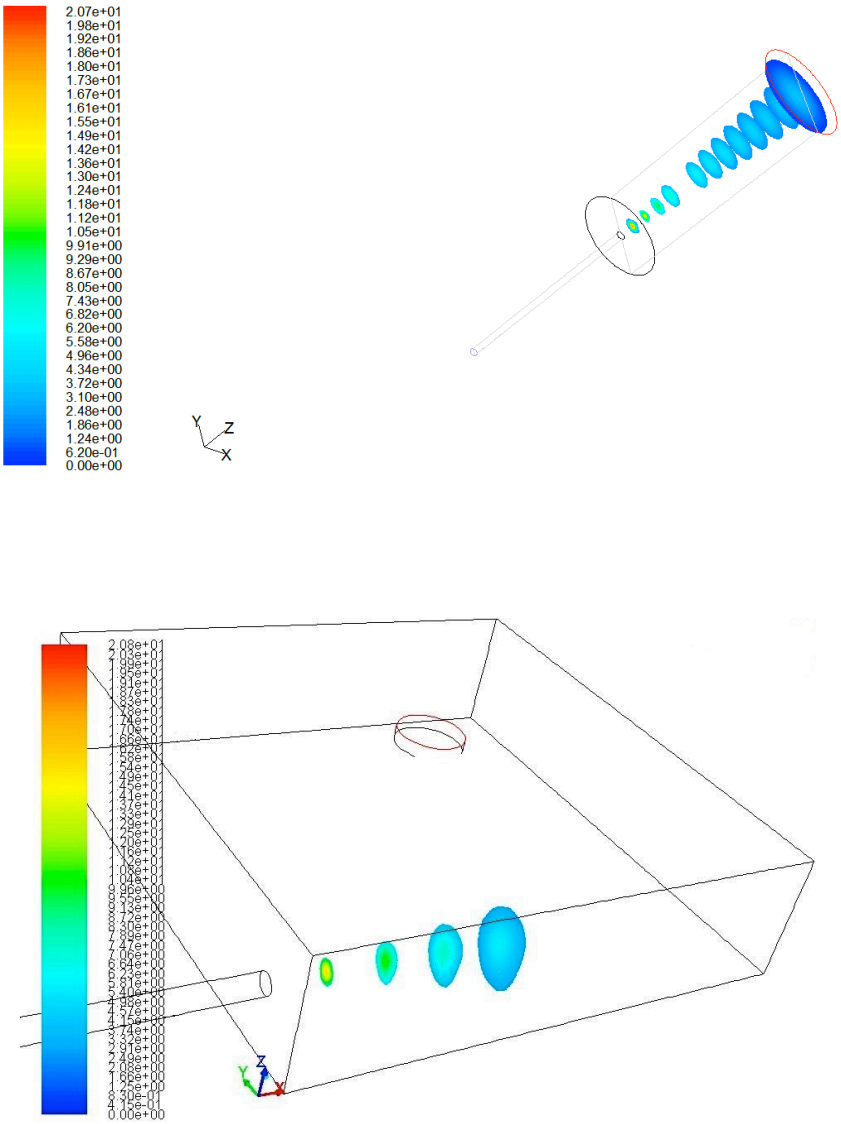

Fig. 4.67 Examples of jet boundary identification (iso-surface colored by velocity magnitude).

4.3.4.2 K_{glf}: Effect of Inlet Reynolds Number

Fig. 4.68 shows the comparison between numerical and measured engulfment ratio K_{glf} for two inlet jets configuration varying inlet Reynolds number from 450 up to 1100 and for different normalized distance (x/d_{jet}) from the nozzle. On the same Fig., K_{glf} values for a free jet case for $x/d_{jet} = 8$ are also reported. Profiles for one inlet jet configuration were not reported since similar consideration can be done. As first observation, for all the configurations analyzed, the engulfment ratio results higher than free jet values. In other

words, the engulfment process rate, and thus, the mixing process, results much faster in the configurations tested than the mixing process of a free jet with ambient fluid. Such result can be related to an increase of local vorticity for the configurations analyzed that lead to a much faster transformation of ambient fluid portions in engulfed fluid. A good agreement between numerical and measured engulfment ratios was found, except for high distance from the nozzle (x/d_{jet} = 8) where major discrepancies were highlighted. Such a discrepancy indicates that for the configurations analyzed, at a high distance from the jet nozzle, axial-symmetric hypothesis cannot be applied, due to the presence of vortex flow structure interacting with jet and of walls.

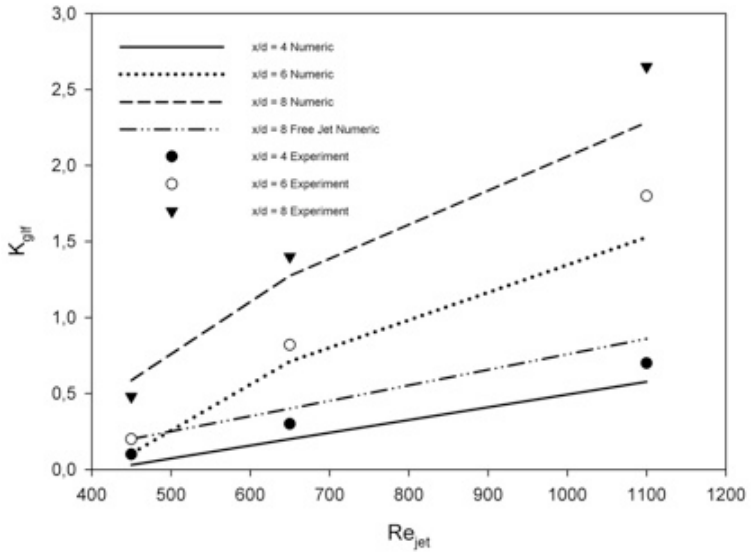

Fig. 4.68 Numerical and experimental engulfment ratio for different configurations and free jet case.

Fig. 4.69 shows the comparison between engulfment ratio K_{glf} (CFD simulations) for two inlet jets configuration and free jet case varying inlet Reynolds number from 450 up to 1100 as function of nozzle distance (x/d_{jet} up to 26).

Several considerations can be done. First of all, in the range of Re analyzed, engulfment ratio slightly depends by Re values for free jet case meanwhile is significantly affected for two jets configuration. Furthermore, engulfment ratio along reactor length is significantly different for confined case respect to engulfment ratio for the free jet case.

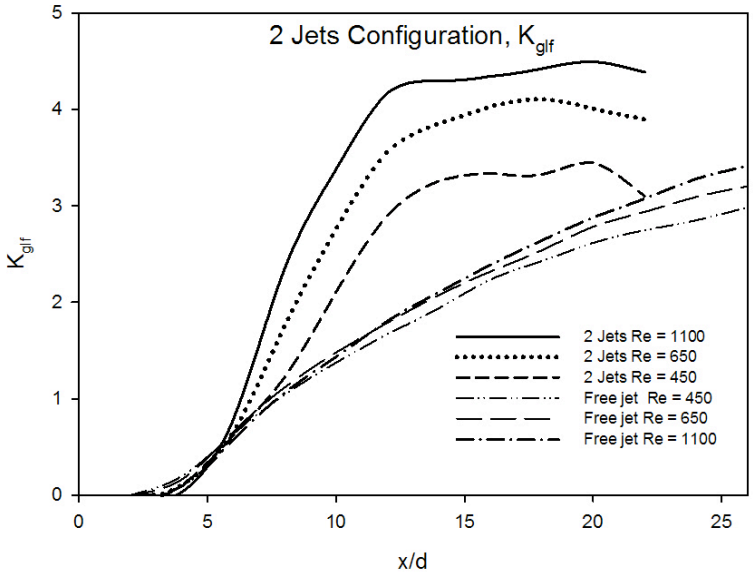

Fig. 4.69 Numerical engulfment ratio for different inlet jet Re number and free jet case.

The amount of engulfed fluid portions is much higher for all three configurations reported as compared to the free jet (in particular near jet exit). For instance, for $x/d_{jet} = 10$ and Re = 1100, K_{glf} is 1.3 for free jet and about 4 for configuration analyzed. Such result is very interesting since literature reports that engulfment process is faster for a free jet compared to an off-set wall jet and a wall jet (Iyougun and Birouk, 2009). In the configuration proposed, interaction between off-set wall jet and cyclonic vortex structure established by tangential jet inlet and/or cross-interference of multiple jet leads to an increase of engulfment rate process respect to free jet case.

It may be noted that although the engulfment ratio is higher than free jet case for all x/d_{jet} analyzed; such a parameter increases initially and then reaches an asymptotic values suggesting that the maximum engulfment ratio is limited by the confinement size. Similar considerations can be found in Arghode and Gupta (2011).

4.3.4.3 K_{glf}: Effect of Inlet Jets Number and Total Flow Rate

Fig. 4.70 shows engulfment ratio K_{glf} trend for two inlet jets configuration varying the number of tangential inlet jets up to 4, for an inlet Reynolds number equal to 1100.

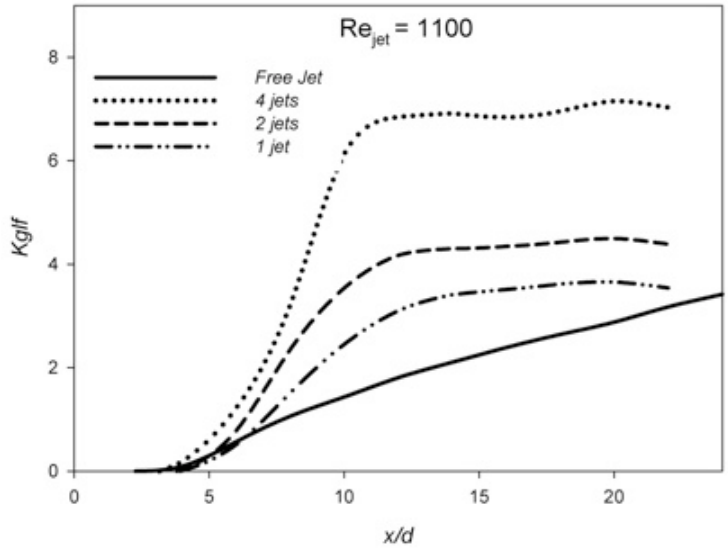

Fig. 4.70 Numerical engulfment ratio as function of inlet jets number and free jet case.

As it possible to see, Fig. reveals that engulfment ratio variation along the reactor lenght is significantly affected by inlet jets number. In particular K_{glf} increases as well as inlet jets number increase. Furthermore, analysis of reactor configurations proposed showed that for such cases K_{glf} is higher than free jet case.for the entire reactor lenght. Four inlets jet configuration reactor ensures highest K_{glf} values, and so faster mixing rate compared to other cases analyzed. For instance, for $x/d_{jet} = 10$, K_{glf} is 1.3 for free jet, 2.5 for one single inlet case, 4 for two inlets case and about 7 for four inlets case.

For configurations proposed, engulfment ratio initially increases with x/d_{jet} and then reaches an asymptotic values, showing a similar trend highlighted in Fig. 4.69. Such a behavior is related to wall confinement meanwhile Fig. shows that asymptotic value depends on the number of inlet jets (and thus, on the overall inlet mass flow rate). Similar considerations can be applied for inlet Re number = 450 and 650 (not reported). In order to better understand the effect of total inlet flow rate fed to the reactor on K_{glf} behavior, other simulations were carried out fixing total inlet flow rate and varying inlet jets number. Fig. 4.71 reports K_{glf} values along reactor lenght for a fixed inlet flow rate, varying number of inlet jets.

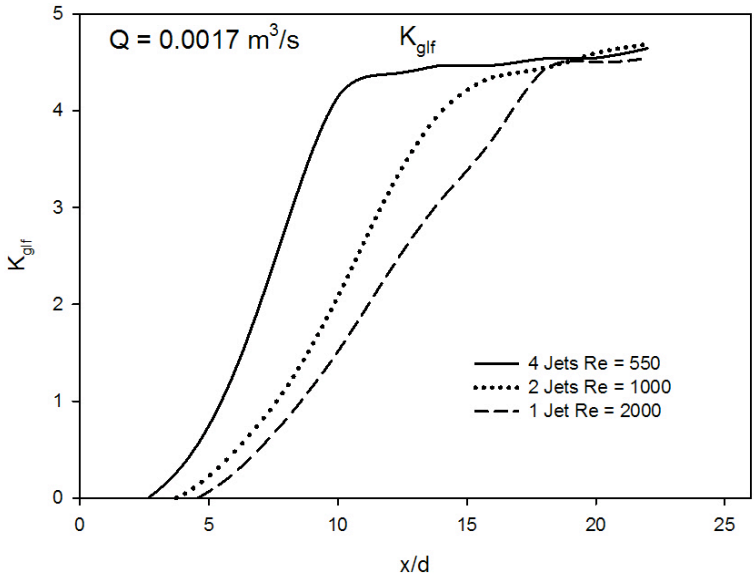

Fig. 4.71 K_{glf} *as function of inlet jets number, fixing inlet total flow rate.*

As highlighted in Fig., asymptotic value of K_{glf} is a function of total inlet flow rate fed to the reactor. In particular, fixing total flow rate, such a values is not dependent on inlet jets number. Furthermore, it is possible to note as engulfment process results faster increasing inlet jets number, also if for cases analyzed, 4 jets configuration corresponds to a smaller value of Re respect to two and one single inlet jet configurations.

Such a trend can be explained, considering that inlet jets distance decreases as number of jets increase so that cross-interference process between jets results to be more significant by increasing jets number rather than Re number, in the range of Re and jets number analyzed.

4.3.5 Comparison of PIV and CFD Analysis

As reported in chapter 2, complex flow structure of a cyclonic flow, invalidates some of the assumptions on which simple turbulence models are based. Particularly challenging for modeling are flow features that are absent in simple flows in which the models are usually tuned and validated. But, to be more concrete, the main issue here is rather the necessity of a model of turbulence that simultaneously accounts for:

1. High curvature of the average streamlines;

2. High swirl intensity and radial shear;
3. Adverse pressure gradients and recirculation zones.

Four different turbulence models were tested, three first closure models, namely standard K-ε, RNG K-ε with swirl factor and curvature correction, K-omega SST with curvature correction and one second closure model, Reynolds Stress Model (RSM). Results were compared with experimental data in order to understand wich closure models are suitable to model vortex reactor and to extend knowledge on vortex flow modeling.

Fig. 4.72 reports comparison between experimental and numerical centerline jet velocity decay for a Re = 1100 and two inlet jets reactor configuration. It is important to stress that such a Reynolds number (laminar) is related to inlet conditions, meanwhile the reactor flow field can be either associated to a low turbulence level or an high level, depending on the number of inlet jets adopted. Since, helium (low density gas) has been adopted for experimental campaign a very high Reynolds number regime (i.e., super-critical regime , $Re > 10^6$) cannot be addressed.

As it is possible to note, not all closure model tested are in agreement with experimental data. More specifically, standard K-ε gave large discrepancies between the measured and predict jet behavior, showing a faster decay and a smaller penetration lenght respect to experimental measurements. K-omega SST with curvature correction shows a better agreement respect to standard K-ε but under predicts jet decay. Finally, RNG K-ε with swirl factor and curvature correction and RSM show a very good agreement .with experimental data. The major difference between the RNG-K-ε model and standard K-ε is that the first has an additional term R_ε that compare in the ε-equation, based on the demand to damp the dissipation rate predictions by the standard model, in order to take in account the effect of elevated strain rates produced by anistropic turbulence inherited by swirling flows. This means that RNG model is more responsive to the effects of rapid strain and streamline curvature respect to standard K-ε model. Furthermore simulations were carried out taking in account the effect of swirl on turbulence in the RNG model, which enhances accuracy for vortex flows. Such a modification correlates the turbulent viscosity with the swirl number (Escue and Cui, 2010).

RSM solves transport equations for each of the terms in the Reynolds stress tensor, together with an equation for dissipation rate, so that it includes the effect of anisotropy of turbulence, wich yields it superior to model based on the Boussinesq approach when simulating highly vortex flows. However, the accuracy of RSM is limited by the closure

assumptions when modeling various terms in the exact transport equations for the Reynolds stresses. Furthermore RSM is often too unstable when used for simulation of confined vortex flows and it is computationally expensive respect to two-equations model. For instance, for the case analyzed CPU time required to solution converge with RSM is about 3.5 times higher than RNG model. For case analyzed, second order closure model does not result superior respect to a first closure model that take in account of swirl flow structure and curvature of streamlines. Similar considerations can be done, varying jet Re number. In this view all simulations were carried out with RNG K-ε with swirl factor and curvature correction. Fig. 4.73 report tangential velocity profiles comparison between RNG model and experimental measurements, varying inlet jets Re number and inlet jets number. An overall good agreement between experimental data and numerical simulations was found, for all configurations analyzed. Similar considerations can be derived for other Re_{jet} and configurations analyzed and are not reported. Other comparison between numerical and PIV data for cyclonic flow reactor configuration will be provided in chapter 6.

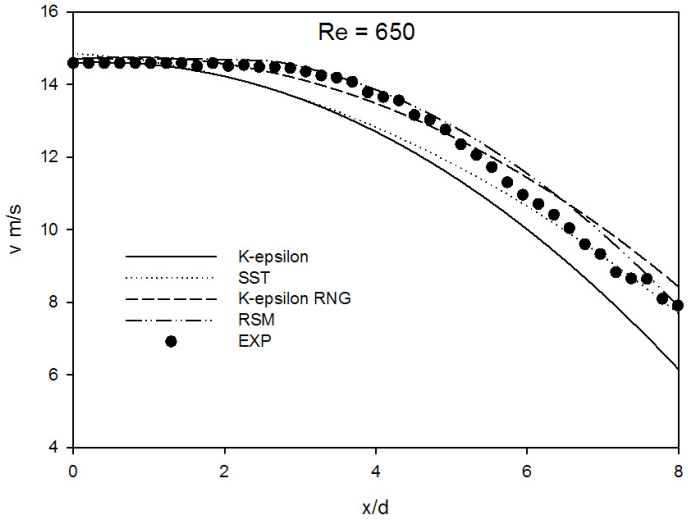

Fig. 4.72 Jet velocity decay: numerical vs experimental data.

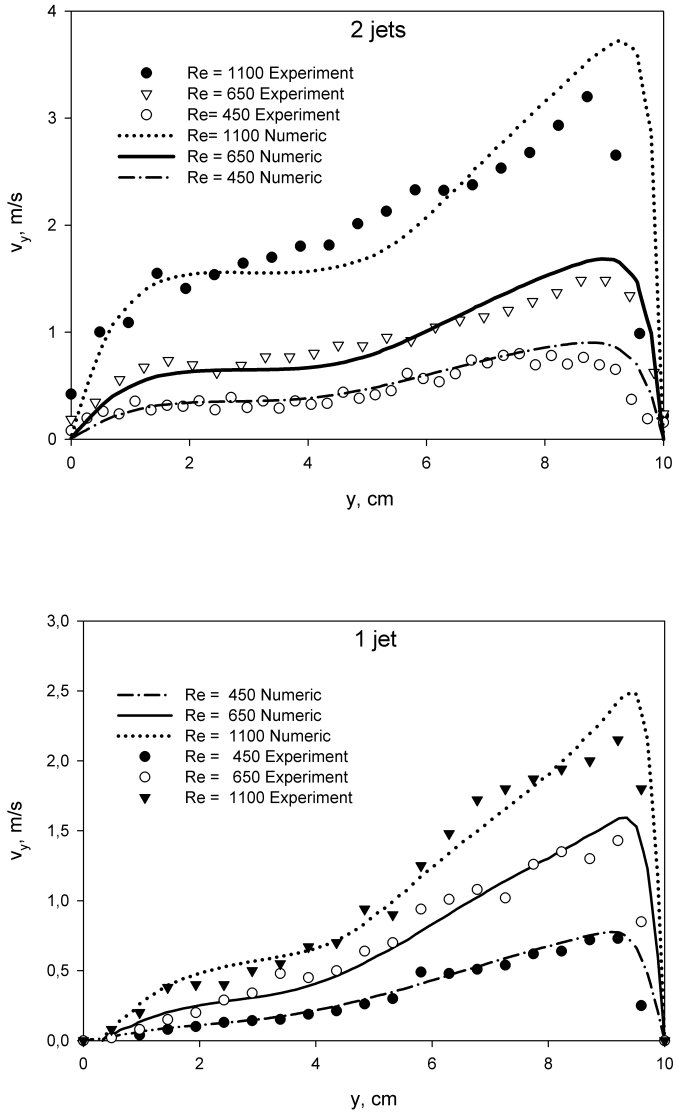

Fig. 4.73 Tangential velocity profiles: numerical vs experimental data.

4.3.6 Additional Remarks: Bi-dimensionality and Mixing

Geometrical parameters significantly affect a cyclone vortex flow structure. In this section effects of reactor shape, and dimension, type and position of inlet jets on the vortex structure and mixing process in terms of engulfment process are presented. In more details, particular attention has been devoted to reactor geometries that ensure a quasi-2D vortex structure. As reported in the introduction of the thesis , a quasi-2D vortex structure is one of the goal to address; such a structure, in fact, lead to a more easy reactor scale-up and/or

scale down. Furthermore, it results more stable respect to a complex 3D vortex structure since fluid-dynamic instabilities such as PVC are avoided. Finally, with this configuration also the mixing process results of more easy understanding.

First of all, a comparison of tangential and axial profiles for the optimized geometry is presented in Fig. 4.74 for two and one single inlet jet and a Re = 1100 at different reactor heights (centerline, +1cm and -1cm from centerline). For this configuration H/d < 1 (with H = reactor height and d = reactor diameter). Tangential velocities analysis showed that for both configurations presented, velocity profiles are quite similar at different heights, so that a quasi 2D vortex structure along the reactor can be considered. Furthermore, for one inlet configuration, tangential velocity profile is not perfectly simmetrical respect to the rotation centre because of the particular geometry. Axial profiles analysis highlighted the absence of a strong reverse (or double reverse) flow close to the vortex core; typical profiles of a vortex subjected to PVC instabilities or strong 3D effects. Configurations presented are principally characterized by a positive axial velocity related to the outlet section. As reported in chapter 2, presence of a sudden contraction results in a beneficial effects on vortex structure in terms of stabilization and absence of PVC.

As can be seen in Fig. 4.74 absence of a geometrical symmetry leads to a more unstable fluid-dynamic vortex structure for one single jet configuration. As first conclusion, thus, geometries with symmetrical inlets (i.e. two and four inlet jets) have to be preferred respect to one single inlet jet reactor configuration since result more stable.

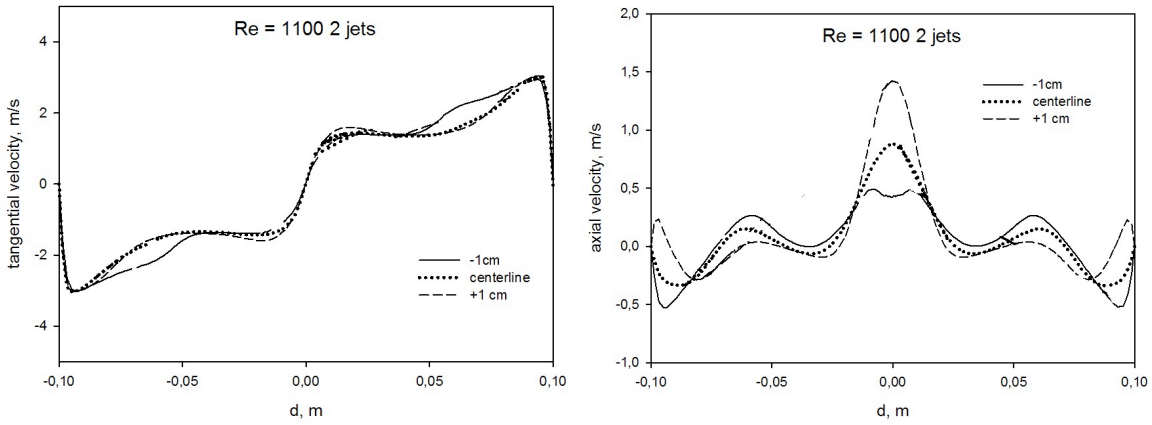

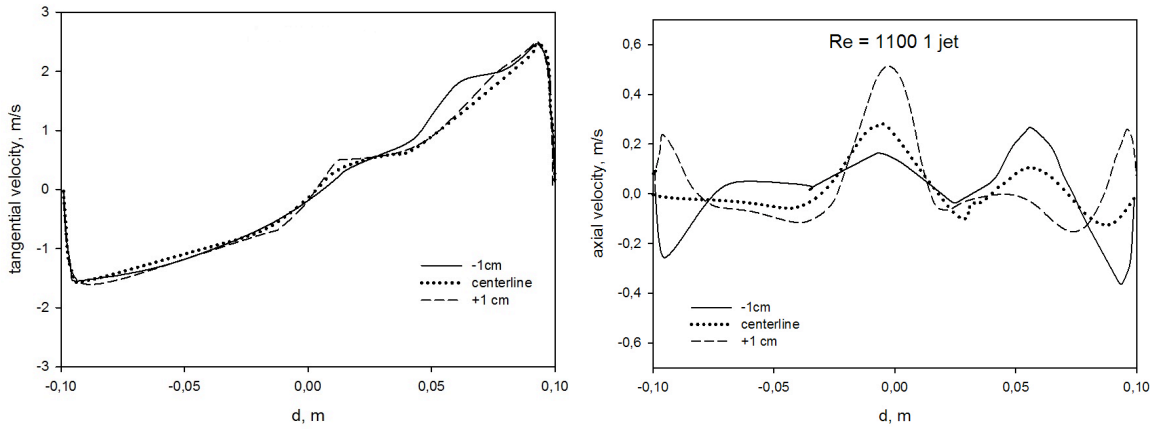

Fig. 4.74 Tangential and axial velocity profiles: two inlet jets (top) and one inlet jet (bottom).

Fig. 4.75 reports tangential and axial profiles for a wall-jet square configuration and a wall-jet cylindrical configuration, two inlet jets and Re = 1100 at different reactor heights (centerline, +1cm and 1cm from centerline). As can be seen from the Fig., no several differences with an off-set wall jet configuration can be highlighted in terms of velocity profiles.

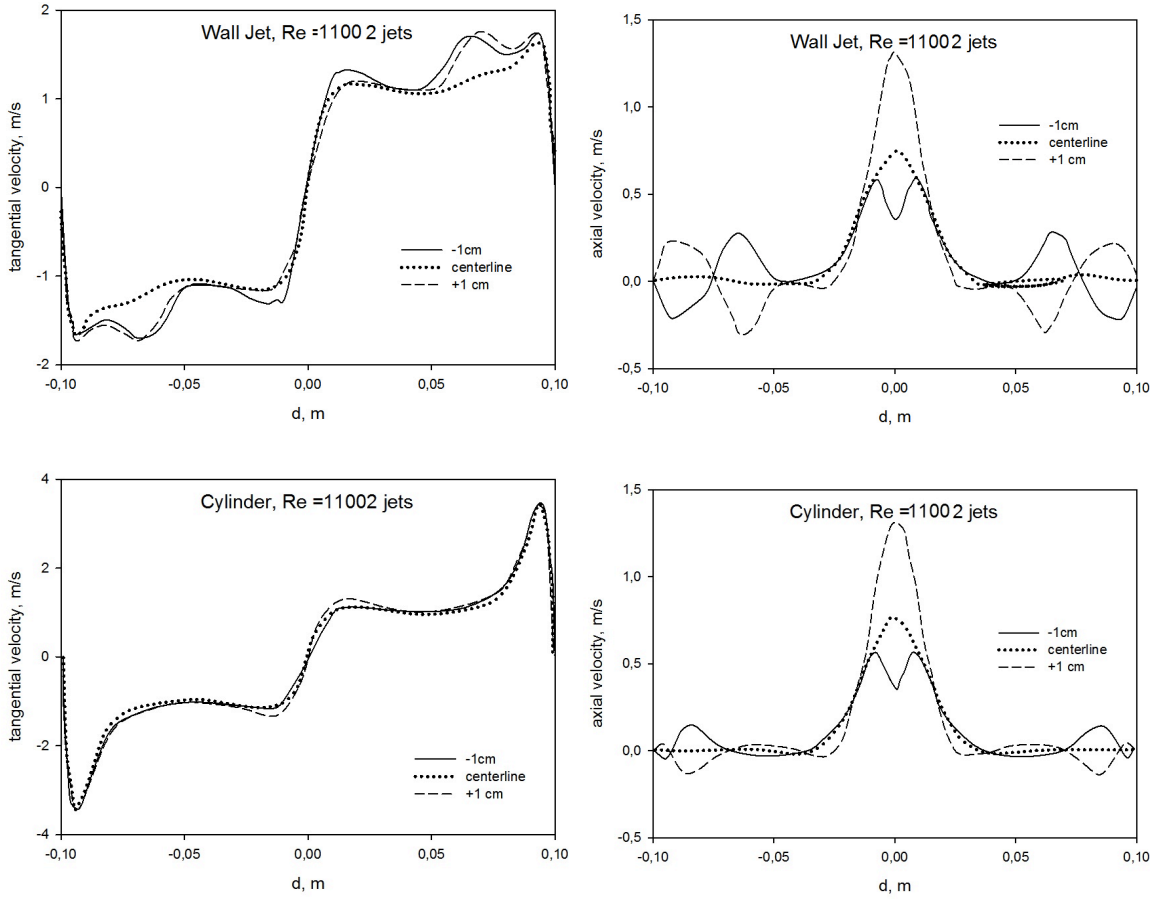

Fig. 4.75 Tangential and axial velocity profiles: wall-jet square section (top) and wall-jet cylindrical section (bottom).

Even if velocity profiles results quite similar, presence of a wall can significantly affects engulfment process and thus, mixing rate between inlet jet and the recirculated flow. In Fig. 4.76 K_{glf} is reported varying jet type and shape of the reactor section (off-set wall jet and square section, wall-jet and square section, wall-jet and cylindrical section), for two inlet jets configuration and Re = 1100.

Profiles show a similar trend characterized by a strong increase of K_{glf} with nozzle distance to arrive at a plateau for high x/d values. Fig. highlights that an off-set wall jet engulfs more fluid than a wall-jet,since presence of wall limits jet spatial evolution. No significantly differences of K_{glf} values can be higlighted varying shape of reactor section from a square to a cylindrical reactor.

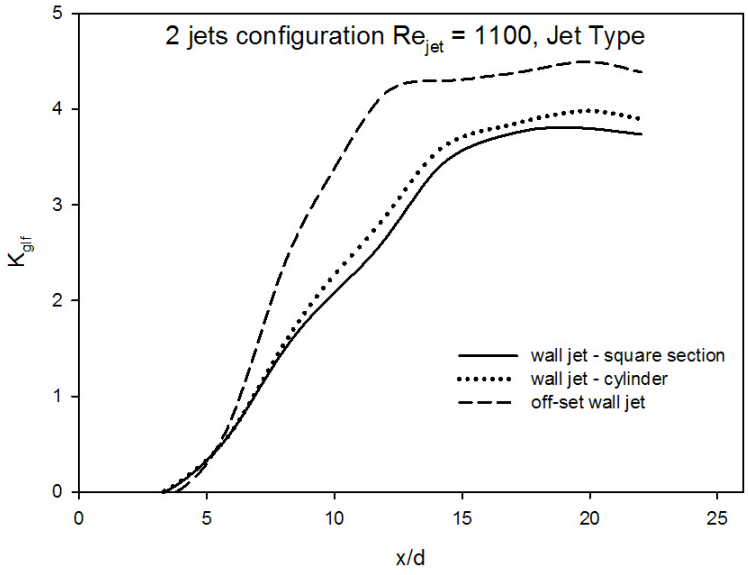

Fig. 4.76 K_{glf} as function of jet type and shape of reactor section.

Also the effect of reactor dimension (H/d) and position of inlet jets on the cyclone vortex structure have been considered. In particular, analysis of vortex structure has been carried out for a square section reactor (7*7*40 cm) with the same volume of the optimized geometry (20*20*5 cm) but with an higher H/d ratio (= 5.7). Two configurations has been tested varying jet position: two opposed inlet jets at the centerline and two opposed inlet jets at the bottom of the reactor.

Fig. 4.77 reports tangential and axial profiles for these configurations at different reactor heights (centerline, + 5cm, +15 cm, -5 cm, -15 cm from the centerline) for a Re = 1100.

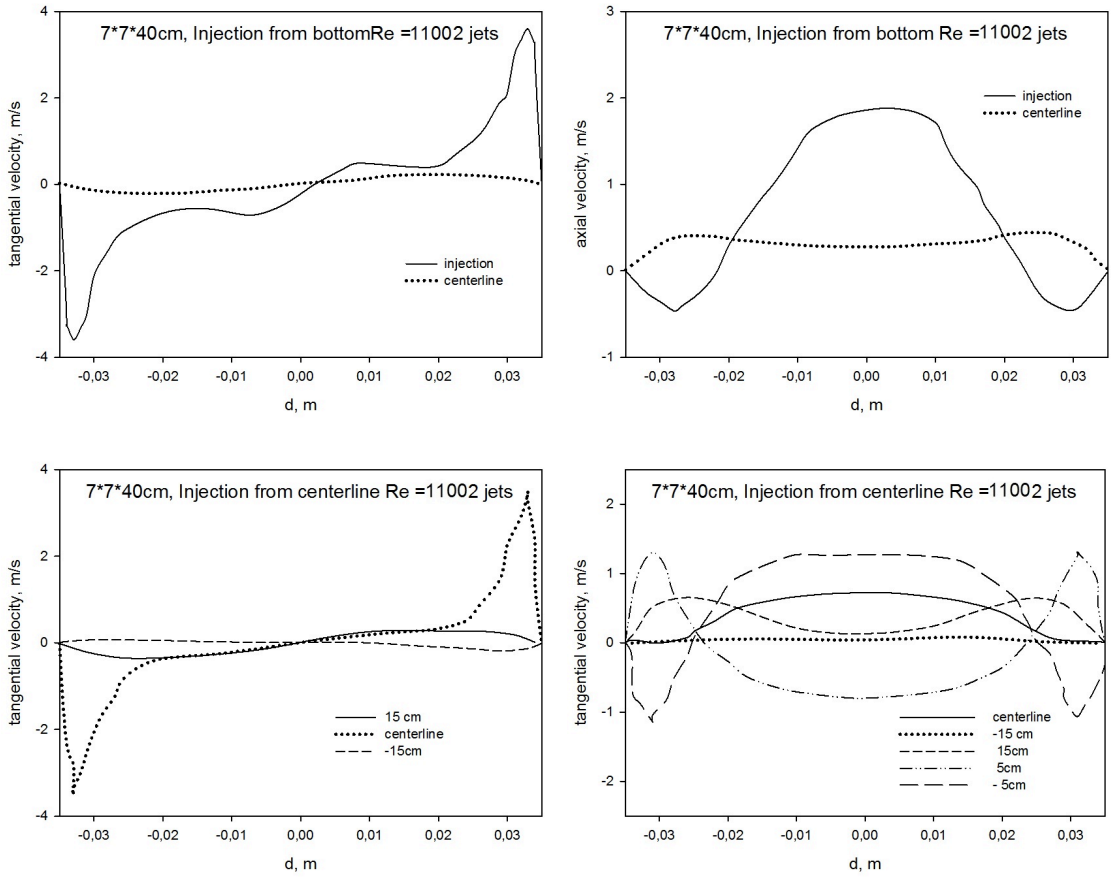

*Fig. 4.77 Tangential and axial velocity profiles: 7*7*40 cm configuration, injection from bottom (top) and injection from centerline (bottom).*

Tangential velocity profiles trend shows that for both configurations a quasi 2D fluid-dynamic structure is not present since a well-defined cyclone vortex structure is not present far from the injection plane. Furthermore, axial velocity profiles analysis lead to a different characterization of configurations tested. Geometry with injections at the bottom presents a positive flow at the vortex core and a reverse flow close to the wall at the injection plane, it presents a flat positive velocity at the centerline plane. Positioning primary jets at the centerline of such a geometry lead to a more unstable configuration respect to an injection from the bottom as reported in the Fig. In particular, for this case, a double reverse flow can be detected from axial velocity profiles.

As reported previously, presence of a quasi 2D fluid-dynamic structure can lead to a more easy scale up/down of the process (and possibility to apply the modularity concept). In this

view, analysis of cyclone vortex structure developed in a scaled geometry (7*7*3 cm) respect to reference dimensions (20*20*5 cm) has been carried out. For this configuration, outlet section has a diameter of 1 cm and inlet jet diameter is 0.3 cm. Such dimensions ensure that Swirl number is keep constant respect to optimized geometry. Two opposed inlet jets were considered. More details of this configuration will be provided in chapter 5. Fig. 4.78 reports tangential and axial velocity profile for such a geometry at different reactor height.

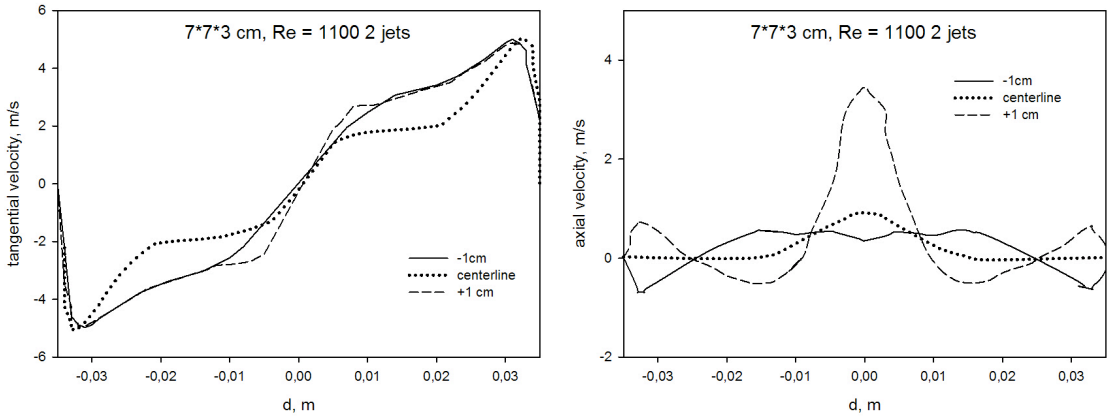

*Fig. 4.78 Tangential and axial velocity profiles: 7*7*3 cm configuration.*

As can be seen in Fig., for a fixed Re value, varying geometrical reactor dimensions and keeping H/d ratio less than 1, cyclone vortex structure appears quite similar to that observed for the optimized geometry. Increasing confinement, free vortex behavior is enhanced respect to 20*20*5 cm geometry configuration. Such analysis confirms that H/d ratio represents a critical parameter for establishing a stable quasi 2d cyclone vortex structure. Furthermore, it also attests the simplicity of scale up/down of proposed geometry.

Also the effect of inlet and outlet boundary typology on vortex structure shape has been investigated. In particular, slots (along reactor height) and inlet jets have been considered in order to asses the effect of inlet boundary on vortex structure. Furthermore, effect of presence of wall at top/bottom of the reactor has been investigated.

Fig. 4.79 reports the characterization of vortex structure for an inlet Re number = 500, a 7*7*3 cm reactor configuration, varying inlet shape (slots or jets) and considering top/bottom reactor walls as outlet boundary (outflow).

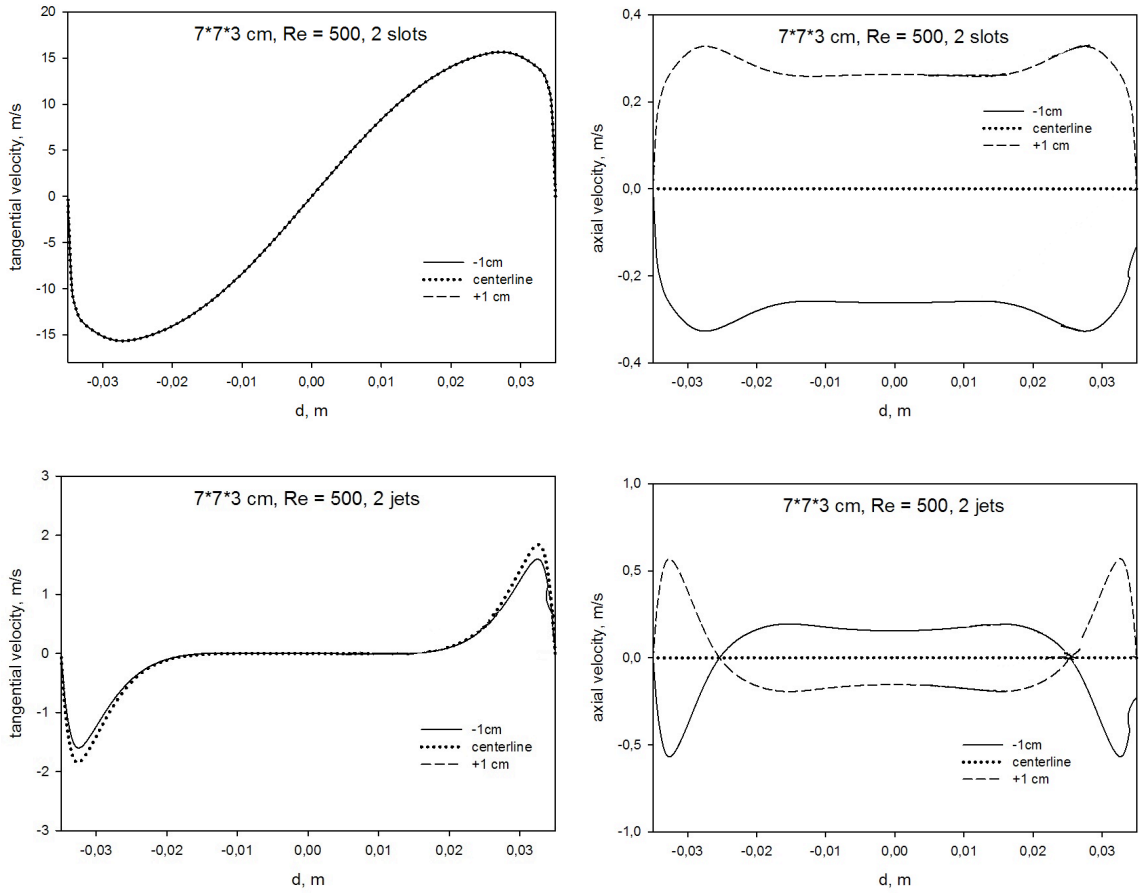

*Fig. 4.79 7*7*3 cm configuration, Re= 500, slots and inlet jets, top/bottom walls =outflow.*

As can be seen in Fig., presence of slots significantly alters the cyclonic vortex structure. First of all, respect to inlet jets and analyzing tangential velocity profiles, a more intense vortex is established in the case of slot, due to an higher inlet flow rate (for a fixed confinement) Moreover, a different vortex structure is established respect to inlet jets case (absence of a quasi zero tangential velocity at the vortex core). Analysis of axial velocity profiles, suggests that an absence of wall and a sudden contraction at the reactor top, leads to a more unstable vortex, since a quasi 2D structure cannot be established.

Fig. 4.80 shows tangential and axial velocity profiles for an inlet Re number = 500, a 7*7*3 cm reactor configuration, varying inlet shape (slots or jets) for an optimized configuration (reactor bottom = wall, reactor top = sudden contraction).

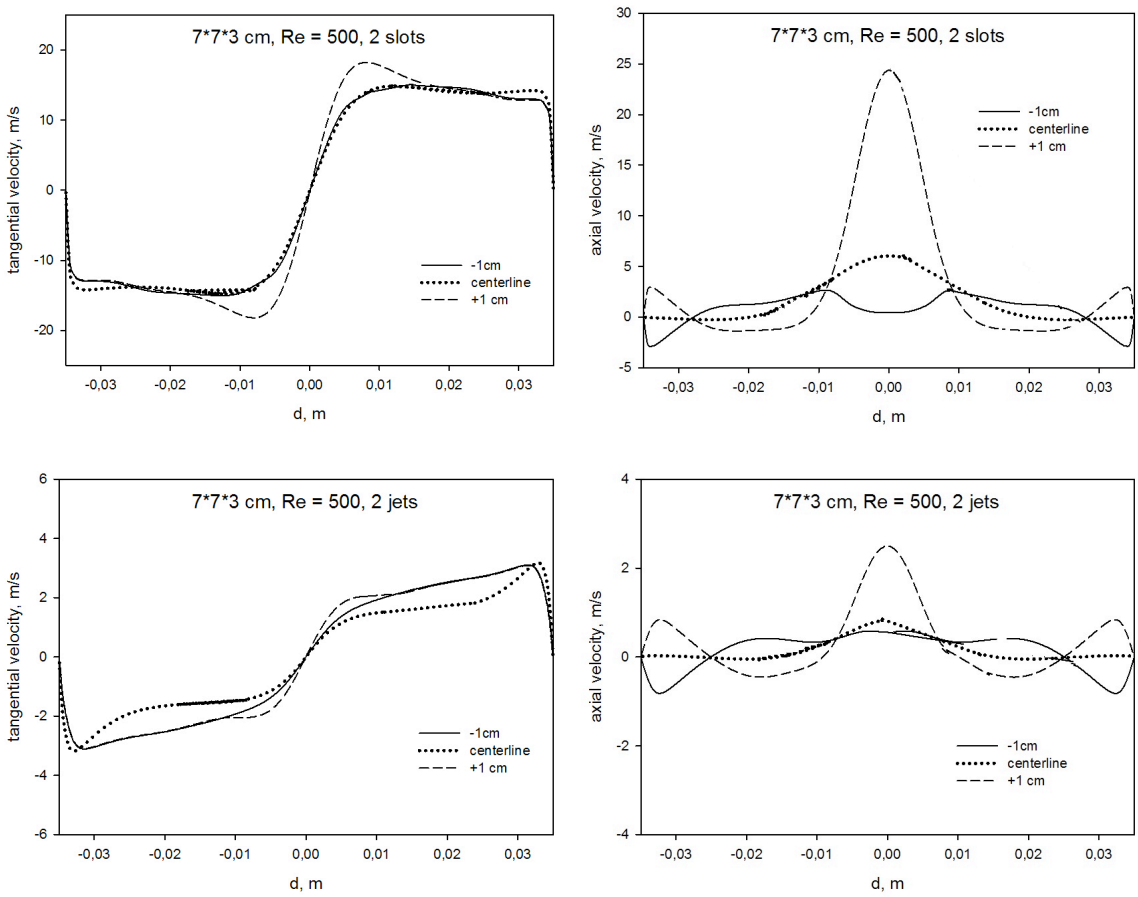

*Fig. 4.80 7*7*3 cm configuration, Re= 500, slots and inlet jets, bottom = wall, top = sudden contraction.*

Several effects can be noted. Presence of confinement and sudden contraction leads to a vortex structure in which free vortex behavior is enhanced respect to low confinement case. In fact, maximum of tangential velocity is located more close to the center of vortex core respect to low confinament case Furthermore, analysis of axial velocity profiles suggests that establishment of a stable structure (quasi 2D structure) is strictly connected with the presence of a sudden contraction. In fact, it is possible to note from Fig. 4.80 that presence of high confinement leads to a more stable cyclonic vortex structure.

Also in this case, a more intense vortex is established for slots case respect to inlet jets case.

Fig. 4.81 reports tangential and axial velocity profiles along reactor height (centerline, +19 cm, -19 cm from centerline), 7*7*40 cm reactor configuration with two inlet slots and Re= 1100. Simulations have been performed in order to asses the effect of inlet slots in geometries characterized by an high H/d ratio (= 5.7).

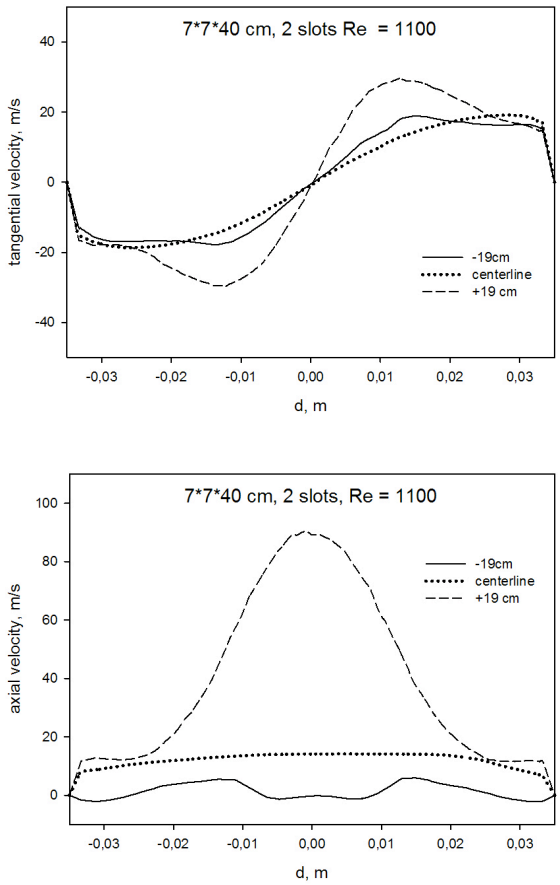

*Fig. 4.81 7*7*40 cm configuration, Re= 1100, slots and inlet jets, bottom = wall, top = sudden contraction.*

Results confirm that presence of slots lead to a more strong vortex structure. In this case, maximum of tangential velocity results higher than inlet velocity of a factor 1.5. Furthermore, also in this case, H/d ratio bigger than 1 leads to an unstable configuration (from analysis of axial profiles), so that effect of H/d ratio results more important respect to inlet type in stabilizing vortex flow.

Finally Fig.4.82 reports tangential and axial velocity profiles along reactor height (centerline, +1 cm, -1 cm from centerline), 7*7*3 cm reactor configuration with two inlet slots and Re= 500. Simulations have been performed in order to asses the effect of inlet and outlet location. More specifically top of the Fig. is related to a configuration with three inlets, two opposed inlets slot (v_{lat}) and one single jet located at the bottom of the reactor configuration (v_{bottom}= 2 v_{lat}), meanwhile bottom of the Fig is related to a reactor configuration with two inlet slots and two opposed outlet sections.

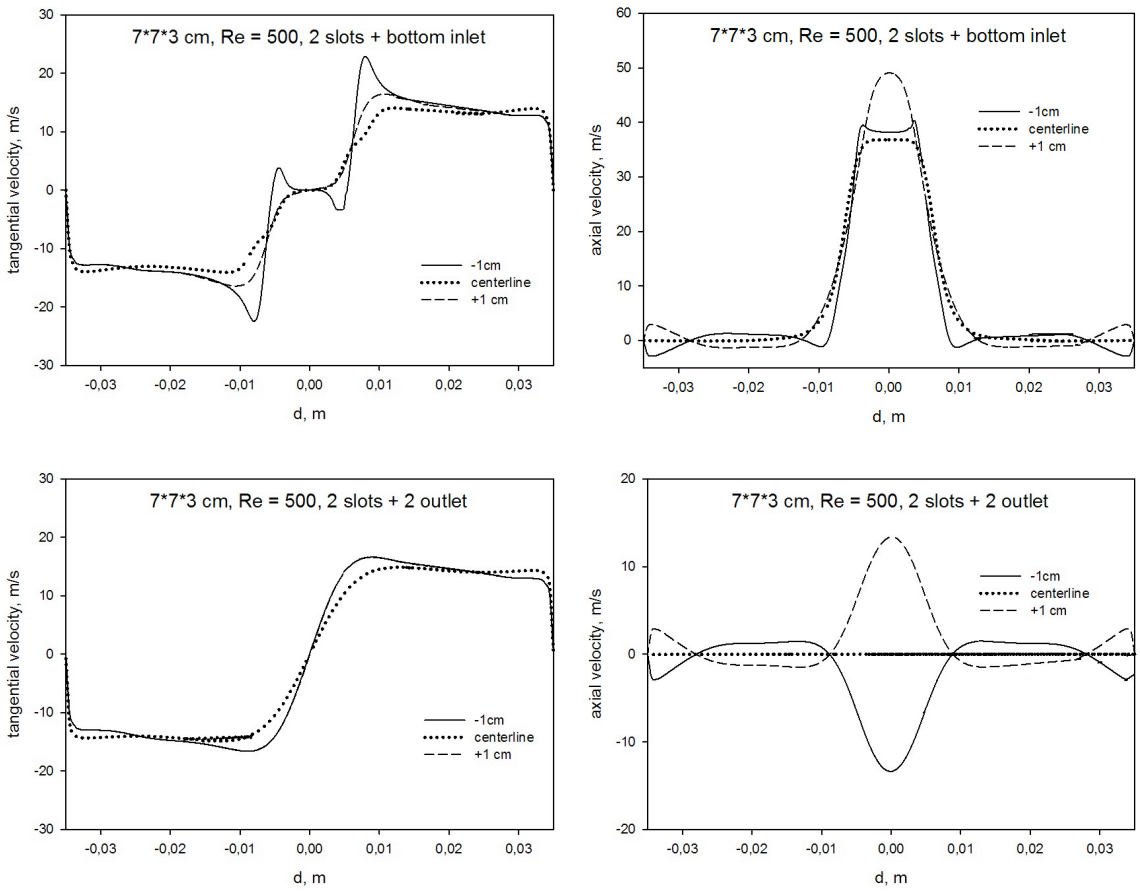

*Fig. 4.82 7*7*3 cm configuration, Re= 500, top) slots + bottom inlet jet, bottom) 2 slots+ 2 outlet (sudden contractions).*

inlets, two opposed inlets slot (v_{lat}) and one single jet located at the bottom of the reactor configuration (v_{bottom}= 2 v_{lat}), meanwhile bottom of the Fig is related to a reactor configuration with two inlet slots and two opposed outlet sections.

It is worthwhile to note that the presence of an additional inlet at the bottom reactor lead to a stable cyclonic vortex structure, even if a counter-rotative vortex near vortex core can be seen. Presence of two opposed outlet sections creates a strong variation of fluid-dynamic structure; in particular analysis of axial velocity suggests that a complex 3D vortex is established adding a second outlet section to optimized configuration. Similar considerations can be obtained from similar configurations with jets as inlet boundary.

Summarizing, in this section several reactor configurations have been analyzed. Geometrical parameters investigated are:

- shape of the reactor section;
- H/d ratio;
- position of inlet jets;

- number of inlet jets
- type of inlet boundary (slots or jets);
- confinement effect;
- reactor dimension.

Results showed that such a parameters can significantly affect vortex fluid-dynamic structure in terms of vortex intensity, vortex shape, vortex stabilization (2D/3D vortex structures) and mixing process between inlet flow and recirculated fluid.

4.3.7 Reactive CFD

In this section reactive CFD of process in analysis is proposed and analyzed. Kinetic analysis suggested that post-oxidation process can be effectively established. Reactive CFD analysis has been carried out with the aim to further understand the process and to asses the effect of vortex structure (turbulence) on the post MILD-oxidation process for CO_2-cleaning.

Modeling MILD Combustion shows several issues that have been highlighted in the introduction of this chapter. Reactive process has been analyzed by a RANS appraoch. Mesh adopted was the same for isothermal case (3.5 million of tetrahedral cells) All the equations has been discretized adopting a 2^{nd} order scheme. SIMPLE algorithm has been chosen for pressure-velocity coupling. K-epsilon RNG with swirl and curvature effect has been adopted for turbulence closure. The discrete ordinate (DO) is chosen for the radiation model. For all the simulations, inlet turbulence intensity was set to 5% with a turbulence lenght scale equal to 0.007 times hydraulic diameter of inlet jets. Reactor walls were considered as isothermal walls. Such a choice concerning the wall boundary has been adopted since simulations have been performed with the aim to reproduce the system constructed and reported in Appendix A.3 and to obtain significant information. DRM19 (http://www.me.berkeley.edu/drm/), a reduced kinetic mechanism of 84 reactions and 19 species, has been chosen as kinetic mechanism. Such a mechanism is largely used in literature for methane combustion processes under MILD Combustion conditions. Eddy Dissipation Concept (EDC) has been chosen for describing kinetic-turbulence interaction. Moreover, key parameters of EDC has been modified according to Aminian (Aminian et al., 2012), for a better prediction of peculiar characteristics of a MILD process. For all the

simulations, convergence has been obtained when at the same time all residuals resulted less then 10^{-6} and calculated temperature at outlet section did not vary more than 1K at the at the next iterative step. In this view, a monitoring point has been defined at the centre of outlet section in order to evaluate molar fraction values of key species (CH_4, O_2, CO, CO_2, H_2, H_2O) as well as outlet temperature. Simulations have been performed, basing on results obtained with kinetic analysis. varying equivalence ratio $\phi = (C/O_{mix})/(C/O_{stoich})$, inlet temperature system (T_{in}) (thus, varying mean residence time and K_{tgl}), for a fixed residual oxygen mole fraction of 5%.

For each simulation, temperature of inlet fuel streams was set equal to 500 K. Fig. 4.83 shows contours at injection (middle) reactor plane of reactor temperature and oxygen mole fraction, for an inlet temperature system (main flow, O_2/CO_2) of 1250 K, entanglement parameter (K_{tgl}) equal to 13 and equivalence ratio of 1.02. For this case, calculated mean residence time is approximately 0.5 s. Such a condition is representative of the feasible region, highlighted by kinetic analysis and reported in the section 4.3.3.1.

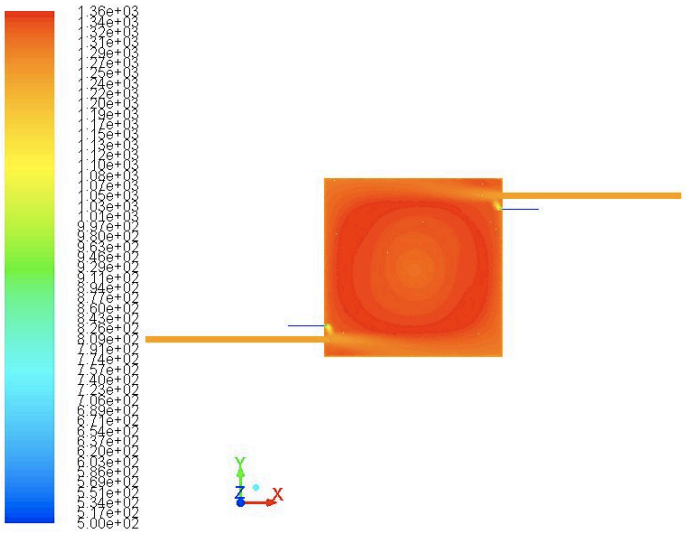

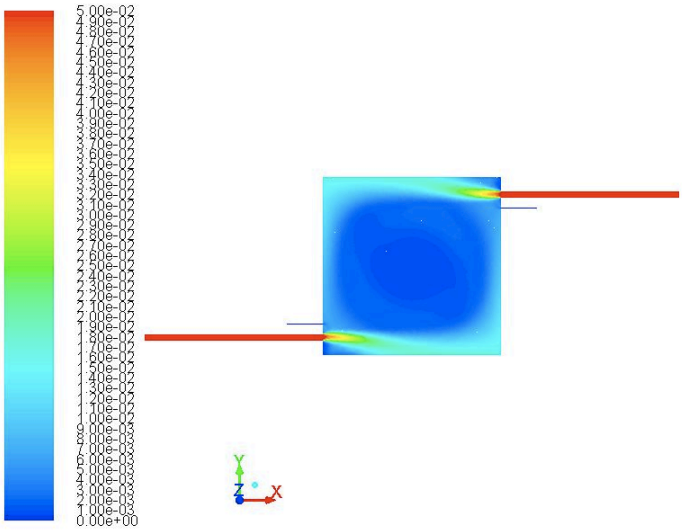

Fig. 4.83 Contours of temperature and oxygen mole fraction, T_{in} = 1250 K, ϕ =1.02, O_2 = 5%.

It is possible to note that maximum temperature increase (ΔT) respect to inlet temperature system is approximately 110 K. Such a small "jump" of temperature is typical of a MILD Combustion process, related to low oxygen environment in which reaction take place. Oxygen fraction shows a maximum at the vortex boundary, for then, decrease to values close to zero at the vortex core. In order to further understand process evolution, Fig. 4.84 reports temperature and oxygen profiles along two characteristic lines placed at the middle plane: centerline (located at the middle of the reactor) and injection line (located at centerline of inlet jet).

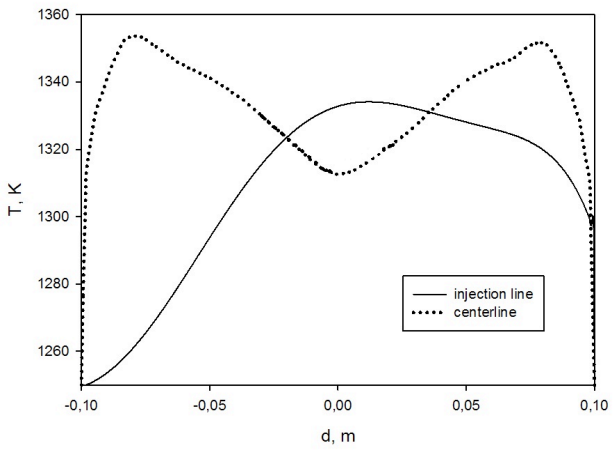

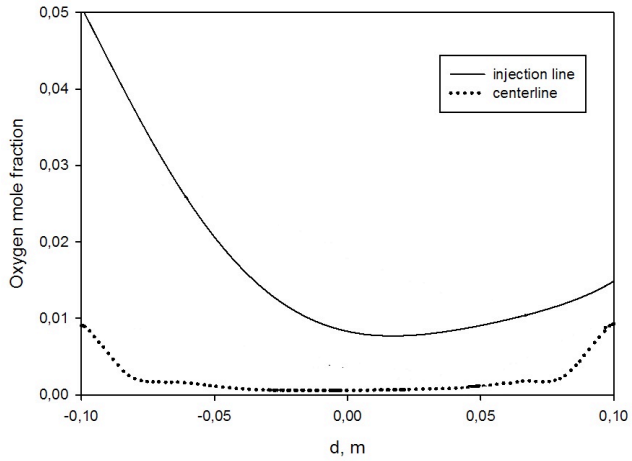

Fig. 4.84 Temperature and oxygen mole fraction profiles along two characteristic lines

Analysis of centerline profiles highlighted that maximum of reactor temperature is located close to maximum of tangential velocity, suggesting that reaction principally proceeds along vortex boundary. Moving from vortex boundary to vortex core, temperature rapidly decreases reaching a minimum (1310 K), highlighting that in such a zone oxygen and fuel are completely converted.

Tab 4.5 reports mole fraction of key species (in ppm) evaluated at the monitoring point, varying equivalence ratio. Also the target values are reported. It is worthwhile to note that, according to kinetic analysis, post-oxidation MILD process of CO_2-exhaust stream for non-condensable reactive species reduction is effectively feasible only for equivalence ratio values close to stoichiometric one. For all the simulations performed, net production of CO_2 (g/s) resulted positive.

Species	ϕ =1	ϕ =1.02	ϕ =1.04	ϕ =1.12	ϕ =1.2	Target
O_2	920	8	4	2	1	10
CO	22	30	72	9800	12420	1000
H_2	30	35	80	142	300	100
CH_4	/	/	/	/	/	/

Tab. 4.5Mole fraction of key species (ppm) at monitoring point, T_{in} = 1250 K, O_2 = 5%, varying ϕ .

4.4 - Summary of the main findings

The effective feasibility of a CO_2-exhaust stream cleaning process from non-condensable reactive species has been explored by means of kinetic analysis in ideal chemical reactors with Chemkin package. Such analysis highlighted that such a process can effectively take place under MILD Combustion conditions. Furthermore, this process is characterized by higher chemical times respect to conventional combustion processes and high quantity of CO_2 as diluent species in the combustor can lead dynamic behavior appearance in terms of temperature oscillations. Fast and stable mixing is necessary to stabilize the process, relating to long chemical times and high disproporzionality between primary jet (oxygen/ diluent) and fuel (small quantity of fuel is needed).

Design of a novel Vortex MILD burner has been proposed to address this peculiar post-oxidation process. Cyclonic flow configuration reactor has been chosen since ensures high residence time and mixing rate respect to non-vortex flow structure. Configuration proposed, based on cross-interference of jet with a tangential inlet for generating the vortex flow, showed residence times compatible with MILD post-oxidation process. Furthermore, optimized geometry is compact ($H/d_{reactor} < 1$). Such peculiar characteristic is critical since fluid-dynamic instability connected with a vortex flow (i.e. PVC) can be avoided and reactor scale-up results very easy (modularity). Reactor has a square section with multiple inlet off-set wall-jets; it has been found that such a geometry ensures a faster mixing process respect to other geometry type.

During analysis, particular attention has been paid to a quantification of mixing rate enhancement in the cyclone device. Isothermal PIV measurements have been performed in order to obtain information on jet decay and to characterize vortex flow structure in the reactor. Several turbulence closure models has been tested. Of these, RNG K-ε model and RSM reproduced accurately the experimental findings in terms of jet velocity decay and tangential velocity profiles.

Mixing rate between primary jets and recirculated flow has been investigated in terms of engulfment process. More specifically, a parametric analysis of the mixing process has been performed varying the main process parameters, namely inlet jet Reynolds number and jets number. Results highlighted that for all the reactor configurations considered, the mixing process is strongly enhanced as compared with a free jet, chosen as reference case.

Finally, several reactor configurations have been analyzed, varying geometrical reactor parameters in order to assess the effect of such a parameters on vortex structure and mixing process. Main purpose was to find configurations that ensure stable, quasi 2D fluidynamic vortex structures. Parameters investigated have been:

-shape of the reactor section;

- H/d ratio;

- position of inlet jets;

-number of inlet jets

- type of inlet boundary (slots or jets);

- confinement effect;

- reactor dimension;

- outlet and inlet location.

Results showed that such a parameters can significantly affect vortex fluid-dynamic structure in terms of vortex intensity, vortex shape, vortex stabilization (2D/3D vortex structures) and mixing process between inlet flow and recirculated fluid.

A part of the research activity has been devoted to the pratical construction of MILD Vortex Burner. Flowsheet and pictures of this apparatus during construction operations are available in Appendix A.3.

Chapter 5

MILD Vortex Burner: Large Eddy Simulation and Applications to Lean Premixed Combustion

5.1 - Introduction

Large Eddy Simulation is an important tool generally adopted for characterizing fluid-dynamic flow structures in terms of characteristic frequency, presence of temporal/periodic instabilities of the flow and for understanding stabilization mechanism of combustion processes.

This chapter presents isothermal LES results of vortex burner configuration proposed and analyzed in details in chapter 4. Respect to chapter 4, vortex flow configuration is also analyzed in view of coupling MILD Combustion with Lean Premixed Combustion (LPC) concept, wich plays an important role in several industrial applications (i.e. gas turbine applications). Strong and fast mixing of primary flow with the hot products is necessary for stabilizing lean and ultra-lean mixture in MILD conditions and represents the critical point for successful application of this concept to LPC. Furthermore, residence times need to be compatible with kinetic times of process. Ultra-lean and ultra-diluted conditions can sensibly affect kinetic times respect to conventional combustion process.

LES has been adopted to analyze temporal evolution of engulfment process. Characteristic frequencies, temporal oscillations of engulfment ratio have been studied as function of inlet Re number and number of inlet jets. Characteristic flow structures have been correlated to enhancement mixing phenomena highlighted in chapter 4.

Furthermore, temporal analysis of vortex flow structure has been investigated in order to add informations collected in chapter 4.

5.2 - Lean Premixed Combustion

5.2.1 General Concepts

Lean combustion is employed in nearly all combustion technology sectors, including gas turbines, boilers, furnaces, and internal combustion (IC) engines. This wide range of applications attempts to take advantage of the fact that combustion processes operating under fuel lean conditions can have very low emissions and very high efficiency.

This section highlights only general aspects of Lean combustion process, focusing the attention to gas turbine applications and relevant issues. An extensive review of Lean combustion process can be found in Dunn-Rankin (2008).

In premixed combustion, fuel and oxidizer are mixed at the molecular level prior to ignition. Combustion occurs as a flame front propagating into the unburnt reactants. Premixed flames propagate in a mixture of fuel and air due to heat conducted from the burned hot products to fresh cold reactants. Premixed combustion often occurs in a thin reaction zone separating reactants and products. Turbulent premixed flames are particularly complicated due to very strong coupling of the flame with the small-scale structure of turbulence (Peters, 2000).

Premixed combustion is much more difficult to model than non-premixed combustion. The reason for this is that premixed combustion usually occurs as a thin, propagating flame that is stretched and contorted by turbulence. For subsonic flows, the overall rate of propagation of the flame is determined by both the laminar flame speed and the turbulent eddies. The laminar flame speed is determined by the rate that species and heat diffuse upstream into the reactants and burn. To capture the laminar flame speed, the internal flame structure would need to be resolved, as well as the detailed chemical kinetics and molecular diffusion processes. Since practical laminar flame thicknesses are of the order of millimeters or smaller, resolution requirements are usually unaffordable in terms of computer storage. The effect of turbulence is to wrinkle and stretch the propagating laminar flame sheet, increasing the sheet area and, in turn, the effective flame speed. The large turbulent eddies tend to wrinkle and corrugate the flame sheet, whilst the small turbulent eddies, if they are smaller than the laminar flame thickness, may penetrate the flame sheet and modify the laminar flame structure.

In premixed flames, the fuel and oxidizer are intimately mixed before they enter the combustion device. Reaction then takes place in a combustion zone that separates unburnt reactants and burnt combustion products.

Lean fuel premixing combustion (LPC) is considered to be one of the most promising technologies for emission reduction in gas turbine combustion systems. LPC is used widely in many applications, including gas turbines, boilers, furnaces, and internal combustion engines. This wide range of applications all attempt to use the advantage that combustion processes operating under fuel lean conditions can have very low emissions and very high efficiency. Pollutant emissions are reduced because flame temperatures are typically low, reducing thermal NO_x formation.

In addition, for hydrocarbon combustion, when lean combustion is accomplished with excess air, complete burnout of fuel generally results, reducing hydrocarbon and carbon monoxide emissions. Unfortunately, achieving these improvements and meeting the demands of practical combustion systems is complicated by low reaction rates, extinction, instabilities, mild heat release, and sensitivity to mixing, making robust and reliable systems difficult to design (Lieuwen, 2005). Recent research (Valeria-Medina et al., 2009, Valeria-Medina, 2009, Syred, 2006) has focused on the use of this technology for the improvement of the combustion process, adding passive and active mechanisms of suppression for the reduction of combustion related instabilities and/or development of new design for Lean Premixed Combustion systems.

Thermo-acoustic instabilities and oscillations constitute a key issue in many fields of combustion application such as aerospace propulsion systems and gas turbines operating in Lean Premixed Combustion (LPC) regime (Candel, 2002).

It is well recognized in literature that such phenomenon results from the resonant coupling mechanisms of fluid dynamic, unsteady heat release and acoustic properties of the combustion chamber (Merk, 1956; Lieuwen, 2003; Culick, 2006), which may lead to large oscillations of the flow, inducing many undesirable effects. These instabilities may, in fact, cause flashback, flame blow-off, increase heat fluxes to the system wall and drive vibrations in mechanical components with consequent structural damages (Fritsche, 2005).

Among the different types of instabilities that can affect a combustor, the ones arising from acoustic and fluid dynamic phenomena will be briefly reviewed.

In the presence of upstream and boundary ductworks, which impose certain acoustic characteristics to the flow, self-excited oscillations may arise in realistic combustors, which

cause a strongly-pulsating flow and vortex formation (Lieuwen, 2005). Acoustic instabilities are characterized by the propagation of acoustic waves in the combustion chamber. Oscillations arise and their frequency is determined by the chamber geometry. Thus, if noise is present inside the chamber, certain frequencies can be selected and amplified by the combustion system. In a combustion chamber, acoustic energy is mainly generated due to variations of the heat release rate: an unsteady source of heat behaves like a source of sound.Acoustic waves are thus generated and propagate upstream and downstream of the flame location. These waves are then reflected at the inlet and outlet sections of the combustion chamber. The reflected acoustic waves travel back to the flame, increasing their perturbations and affecting again the instantaneous heat release. Therefore a coupling between the acoustic field where chemical reactions occur and the heat release process arises. According to the Rayleigh criterion (Rayleigh,1896), the acoustic oscillations will amplify themselves when the fluctuations in heat release and acoustic pressure at the flame location are in phase with each other. Another criterion for the system to develop combustion instabilities is that the acoustic energy received from the fluctuating heat release is larger than the energy lost both at the boundaries of the chamber and from the viscous dissipation (Gupta, 1984; Borghesi et. al, 2009; Schmitt et al., 2007). The physical mechanisms of the flame response to these acoustic perturbations are strongly dependent on the nature of the flame: partially premixed flames are very sensitive to equivalence ratio fluctuations. In fully premixed flames heat release rate fluctuations are linked to variations in the flame surface area. The pressure fluctuation can be driven by either the oscillation in the flow (Dowling, 1999)or the displacement of the flame anchoring point (Biagioli et al.,2009).

The other types of instabilities that can occur in a combustion chamber are developed by fluid dynamic phenomena. They lead to combustion fluctuating periodically inside the combustion chamber. These instabilities are called hydrodynamic instabilities and appear due to the establishment of certain flow patterns.

The development of a vortex shedding can be a source of instabilities (Kulsheimer and Buchner, 2002). In this context, acoustic and fluid dynamic instabilities can be strongly coupled mechanisms in turbulent, premixed combustion systems. The formation of vortices have thus been identified as a mechanism driving the combustion instabilities (Schmitt et al. 2007).

In cyclone vortex chamber, precessing vortex core (PVC) is the main fluid-dynamic instabilities that can be occur. PVC can be also responsible for large fluctuations in the velocity and mixing fields. If these fluctuations become coupled with acoustic frequencies of the combustion chamber, combustion-induced oscillations and high pressure pulsations could arise. Fig. 5.1 summarizes the interactions between the different mechanisms leading to instability in gas turbine combustion.

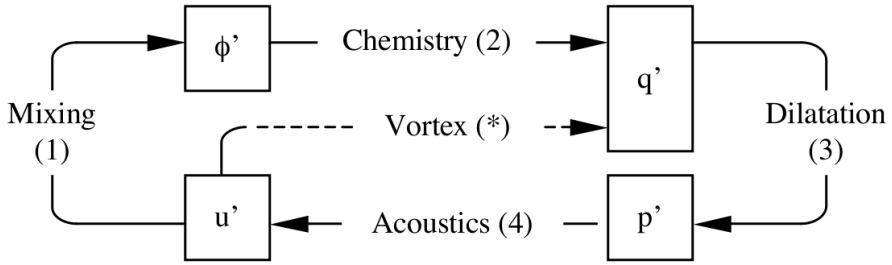

Fig. 5.1 Links between different quantities in typical gas turbine combustion instabilities (adapted from Candel, 2002).

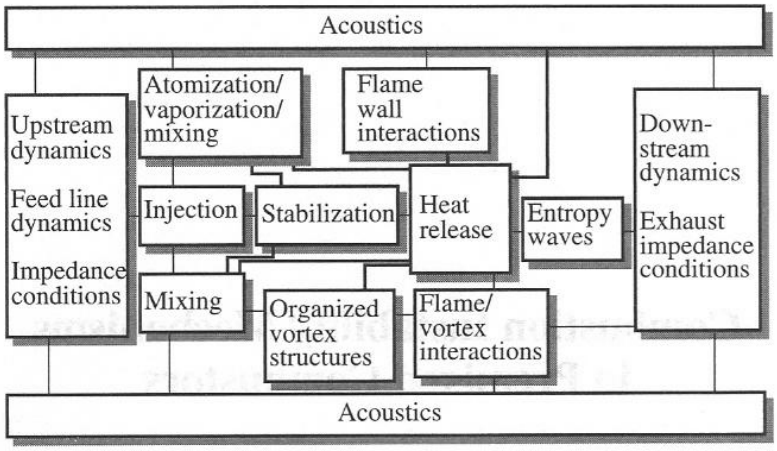

Fig. 5.2 Main factors affecting combustion instabilities (adapted from Candel, 2002).

There are numerous complex physical processes that affect combustion instability, and they depend highly on the system geometry and operating conditions. Some of the main factors that take part in the process of generating the instability in a system are shown in

Fig. 5.2. All of them are interrelated in a very complicated manner, though they can be classified into either system geometry or operating condition factors.

5.2.2 MILD and LPC: Identification of the problem

As reported previously, Lean Premixed Combustion concept can achieve the best compromise between pollutant emissions and efficiency in several fields of combustion application (i.e. gas turbine) (Lieuwen et al., 2001; Foglesong et al., 1999). Under fuel lean conditions, in fact, flame temperature is typically low, reducing thermal NOx formation. Furthermore, complete burnout of fuel is achieved when leaning is accomplished with excess air.

Unfortunately, this type of combustion increases the flame receptivity to external perturbations thereby promoting the onset of large amplitude pressure oscillations (Seo, 2003). For instance, operating near lean flammability limits, strong unsteady fluctuations of heat release may be appear, due to non-uniform mixing of the inlet flows into combustor chamber, so that the occurrence of thermo-acoustic instabilities phenomenon is stressed (Fric, 1993; Wang-Ping et al., 1996) Combustion stabilization of lean and ultra-lean mixture, thus, remains a key issue for both conventional and alternative LPGT based on internal recirculation concept, since it has been recognized that the use of mixture close to the lean flammability limits can lead to combustion driven oscillations problems.

Different strategies have been developed over the past twenty years to resolve the dilemma between stable and complete combustion versus ultra-low NOx emissions in LPC regime for gas turbine applications. Recently, MILD Combustion concept (Cavaliere and de Joannon, 2004; de Joannon et al., 2007), which is based on the principle of high temperature air combustion has been proposed as effective strategy to simultaneously reduce pollutants emissions and suppress combustion instabilities, experienced with Lean Premixed Combustion. Coupling MILD and LPC concepts, absence of thermo-acoustic instabilities could be achieved in gas turbines, since the combustion process would be characterized by uniform heat release, typical of MILD processes. Furthermore, it has shown that reaction of lean to ultra-lean mixtures supported by high-temperature burned gases could be very advantageous in extending the limit of operating range to leaner side where ultra-low NOx emissions are achieved while maintaining complete combustion (Arghode and Gupta, 2011; Aida et al., 2005). Several works have been shown that MILD provide significant improvement in gas turbine combustor performance in terms of

combustion stability, efficiency and pollutant emissions (Arghode et al., 2012; Khalil et al. 2013; Khalil and Gupta, 2011). An extensively review of MILD concept application to LPC can be found in Cavaliere et al. (2008).

This type of process need to take place in gas turbines configurations where internal recirculation is significantly enhanced respect to conventional design to yield a high level of mixing and subsequent heating of the fresh air-fuel mixture by means of the recirculated hot products. Strong and fast mixing of primary flow with the hot products is necessary for stabilizing lean and ultra-lean mixture in MILD conditions and represents the critical point for successful application of this concept to LP concept. Furthermore, mixing times have to be comparable with characteristics chemical kinetic times of a MILD process, which are very different with respect to conventional combustion systems (de Joannon et al., 2012; Picarelli, 2011) to ensure the realization of the combustion process.

Furthermore, it has been highlighted that thermo-acoustic instabilities derived by coupling mechanism of unsteady heat release, fluid-dynamic instabilities and acoustic phenomena. Stable flow structures establishment in design of novel combustion chamber configurations are necessary in order to avoid the occurrence of fluid-dynamic instabilities that can lead to thermo-acoustic instabilities phenomena into the combustor.

In this context, a novel geometrical configuration of combustion chamber based on vortex flow design analyzed in chapter 4 is proposed below, with the aim to realize a very fast mixing between primary and recirculated flow. Mixing between inlet jets and environment is studied in terms of engulfment process, defined in chapter 4. The effects of jet Reynolds number and jets number on the mixing process are presented. Cyclone vortex chamber ratio ($H/d_{chamber}$) is such that vortex structure result stable (quasi-2D structure) and fluid-dynamic instabilities such as PVC can be avoided.

5.3 - Results and Discussions

5.3.1 Kinetic Analysis

This small section reports numerical analysis for studying the evolution of methane ignition process in diluted, preheated and lean conditions with the aim to evaluate characteristic kinetic times of such a mixtures that are needed for dimensioning novel

combustion chamber in the context of MILD-LP coupling concept. Methane has been chosen as fuel for all simulations, performed by means of PLUG application of Chemkin 3.7 software. c1-c3 mechanism has been adopted for numerical simulations. Such results are adapted from Picarelli (2011), Picarelli et al. (2011) and de Joannon et al (2012)

A complete review of autoignition process of conventional and alternative fuel under MILD Combustion conditions can be found in Picarelli (2011).

Fig 5.3 shows the auto-ignition time (τ_{ign})versus $\alpha = 1000/T_{in}$ for three carbon/oxygen C/O, 0.1, 0.2 and 0.3, for methane/oxygen system diluted at 85% in nitrogen. ratio.

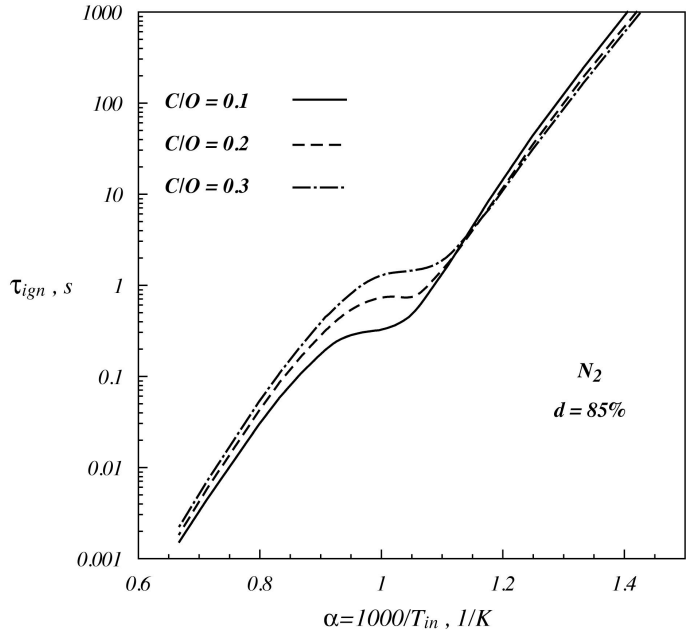

Fig. 5.3 - Auto-ignition delay time computed for three C/O ratio.

All the profiles show a similar trend, already highlighted in chapter 4. For inlet temperature lower than 850 K, the ignition delay is almost independent on carbon to oxygen ratio, while at temperature higher than 850 K the richer the mixture, the longer the auto-ignition time is. In addition, it is worth noting than the temperature ranges where an NTC (negative temperature coefficient) behavior can be observed, in all the three considered cases, shift toward lower temperature values with increasing C/O feed ratio. At temperature above NTC regions ones differences among τ_{ign} values become more relevant. NTC has been reported in de Joannon et al. (2012). Analysis suggests that lean working conditions lead to a faster ignition process in the temperature range of interest for LP applications respect to autoignition times evaluated in chapter 4..

Furthermore, effect of pressure and dilution level on the autoignition process of methane in MILD combustion conditions have been analyzed.

Fig 5.4 shows the auto-ignition delay times as a function of parameter α (=1000/T_{in}) for a methane-oxygen system diluted in nitrogen up to 85 %. The mixture composition (C/O) has been fixed equal to 0.2 varying pressure from 0.5 up to 50 atm. In general, the auto-ignition delay time decreases as the system pressure increases and it is less sensitive to pressure variation for high-pressure values.

Finally, Fig 5.5 shows auto-ignition delay time versus parameter α for several values of dilution degree while the pressure is fixed to 1 atm and the C/O feed ratio is 0.2. Solid-line represents auto-ignition delay times for a system diluted at 85 %, while dotted and dotted-dashed lines show respectively characteristic times for mixtures diluted up to 90 and 95% in nitrogen.

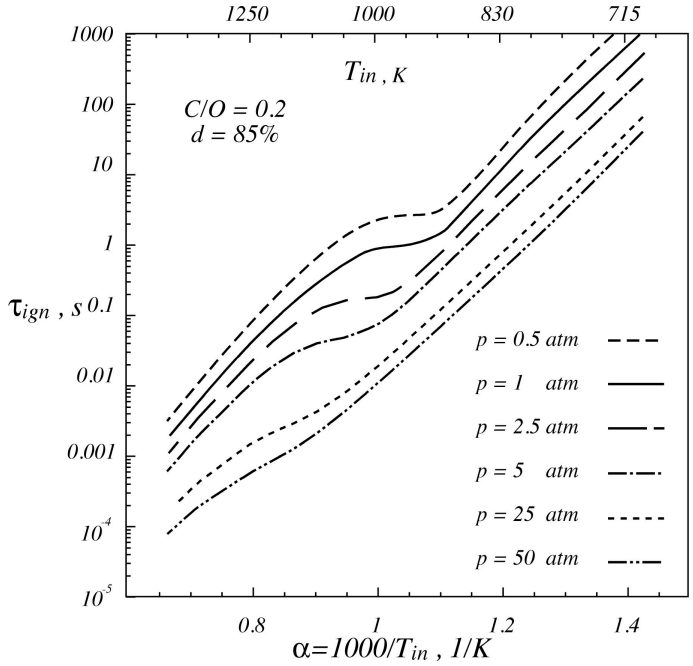

Fig. 5.4 - Comparison among auto-ignition delay times at different pressure.

General trend shows that auto-ignition time increases as mixture dilution degree increases. It is worth noting that the effect of mixture dilution level variation on auto-ignition times is similar to the one relative to system pressure variations since modifying the mixture dilution degree means varying reactants partial pressure.

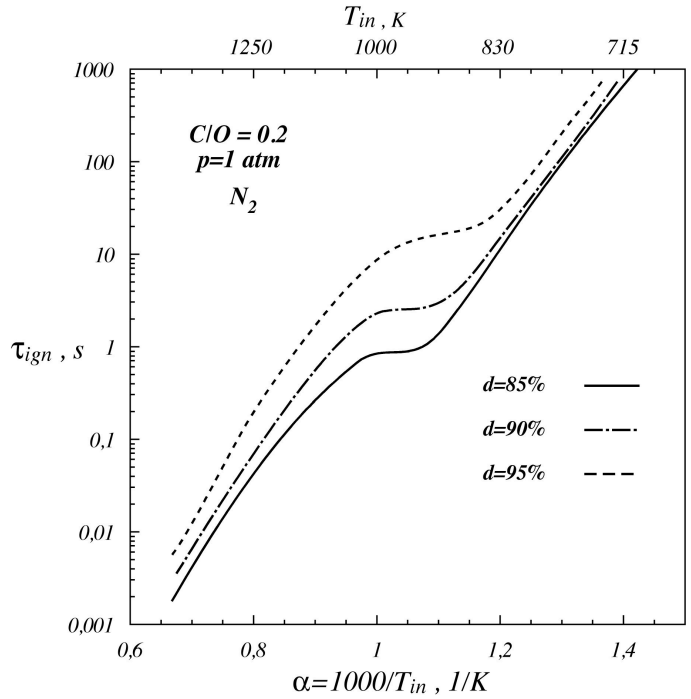

Fig. 5.5 - Comparison among auto-ignition delay times for different dilution degree

Summarizing, such a kinetic analysis highlighted that for typical MILD-LP working conditions (inlet temperature, carbon/oxygen ratio, pressure, dilution), methane autoignition process is faster respect to a MILD Combustion process for CO_2-exhaust streams cleaning reported in chapter 4.

5.3.2 Geometry definition

As reported previously, calculated kinetic times for a MILD-LP process result to be smaller than that evaluated for a MILD-CO_2-cleaning process. As highlighted in chapter 4, reactor residence time need to be compatible with kinetic times in order that combustion process can takes place. In this view, analysis of cyclone vortex structure has been carried out in a reduced-size geometry (7*7*3 cm) respect to configuration reported in chapter 4 for MILD-CO_2-cleaning process analysis (20*20*5 cm). Mixing process quantification, identification of vortex topology, reveal of fluid-dynamic instabilities related to a cyclonic vortex structure are the key aspects of this LES investigation.

The outlet section has a diameter of 1 cm and inlet jet diameter is 0.3 cm. In such a way, geometrical Swirl number is keep constant respect to standard configuration (20*20*5 cm)

Offset distance between inlet jet and wall is keep equal to 2. As well as for the geometry adopted in chapter 4, also for this configuration, H/d ratio is < 1, condition that ensures a stabilization (quasi-2D structure) of the vortex structure. Furthermore, with these dimensions, reactor mean residence time results compatible with calculated autoignition times. It is worthwhile to note that a reduced-size geometry is helpful for LES investigations in order to save simulation costs since such a approach is very CPU time-consuming.
Number of inlet jets has been varied from one up to 4. In order to obtain a more easy meshing procedure, a square section has been chosen for inlet and outlet reactor sections.

5.3.3 Large Eddy Simulation

5.3.3.1 Set-up

The governing equations for the problem to be investigated here, are the conservation equations of mass and momentum for an incompressible Newtonian Fluid in their instantaneous, local form:

$$\frac{\partial \bar{u}_i}{\partial x_i} = 0$$

$$\frac{\partial \bar{u}_i}{\partial t} + \bar{u}_j \frac{\partial \bar{u}_i}{\partial x_j} = -\frac{1}{\rho}\frac{\partial \bar{p}}{\partial x_i} + \frac{\partial}{\partial x_j}\left(\nu \frac{\partial \bar{u}_i}{\partial x_j}\right) - \frac{\partial \tau_{ij}}{\partial x_j}$$

where the over-bar denotes the filtering operator, ϱ and ν are the helium density and kinematic viscosity, respectively, p the pressure and τ_{ij} the components of the SGS stress tensor:

$$\tau_{ij} = \overline{u_i u_j} - \bar{u}_i \bar{u}_j$$

To filter the governing equations, a low-pass box filter in the physical space (Poinsot and Veynante, 2005) was used having a width,Δ , equal to the cubic root of the grid cell volume (i.e., equal to the characteristic length of the grid cell).
The LES filtering process filters out the turbulent structures whose scales are smaller than the filter width so that the resulting equations govern the dynamics of the large-scale

structures. However, due to the non-linear nature of the conservation equations, the filtering operation gives rise to unknown terms that have to be modeled at the sub-grid scale (SGS) level (Poinsot and Veynante, 2005). The unknown term arising from the filtering operation applied to the momentum equation and the energy equation is the SGS stress tensor. The closure of the SGS stress tensor was achieved with the dynamic Smagorinsky–Lilly eddy viscosity model (Lilly, 1992). The model coefficient was dynamically calculated during the LES computations using the information about the local instantaneous flow conditions provided by the smallest scales of the resolved (known) field. This allowed the resulting SGS turbulent viscosity to respond properly to the flow structures, thus grasping the transition from initially laminar flow to turbulent flow. In other words, SGS stresses is computed via the SGS turbulent viscosity ν_{SGS} and the filtered rate of strain $\bar{S}_{ij} = (\frac{\partial \bar{u}_i}{\partial x_j} + \frac{\partial \bar{u}_j}{\partial x_i}) / 2$:

$$\tau_{ij} - \frac{1}{3}\tau_{kk}\delta_{ij} = -2\nu_{SGS}\bar{S}_{ij}$$

with:

$$\nu_{SGS} = L_{SGS}^2 \bar{S}$$

where $\bar{S} = (2\bar{S}_{ij}\bar{S}_{ij})^{1/2}$ is the characteristic filtered rate of strain and $L_{SGS} = \min(\kappa d, C_s V_c^{1/3})$ is the SGS mixing length, with κ the von Karman constant, d the distance to the closest wall, V_c the volume of the computational cell and C_s the Smagorinsky coefficient. C_s is computed at each time step adopting the dynamic Smagorsky-Lilly version (Germano et al., 1991; Lilly, 1992), with a test-filter (whose width is twice the grid size) and clipped to the range (0; 0.23) to avoid numerical instabilities. The upper bound of this range aims at preventing the appearance of extremely high C_s values which, on the one hand, are not physical and, on the other hand, can lead to high spatial variations of C_s and destabilize the solver. The imposed maximum value for C_s ($C_{s,max}$) should be high enough to allow the description of all types of flow, but the particular value imposed is different in each CFD code, showing that there is no widely-accepted value for $C_{s,max}$. Here, $C_{s,max}$=0.23 is used, which is the default value in Ansys Fluent 14.

The computational domain has been created with the Gambit software. Meshing procedure is a critical point for LES investigations. A coarse grid can lead to unrealistic flow fields meanwhile a finer mesh can result extremely CPU-time consuming. The choice of a right filter (Δ) is associated with the grid size and it is an another key point that need to be faced adopting LES approach. Several authors suggested guidelines for an optimal mesh procedure. In particular, the quality of any LES computation mostly relies on the percentage of the resolved turbulent kinetic energy. According to Pope's criterion (Pope, 2004), a good LES should be able to resolve at least 80% of the turbulent kinetic energy. Furthermore, Gaitonde (2008) provided a set of guidelines for an a priori determination of a non-uniform grid resolution for LES. Here, it has been highlighted that two turbulence references scale need to take in account for a good mesh realization: integral scale ($L_{RM} = \frac{k^{3/2}}{\varepsilon}$) and micro Taylor scale. Analysis of energy spectrum on a one-dimensional model energy spectrum for isotropic turbulence revealed that while the integral scales is positioned at the top limit of the inertial range, the Taylor scale is located almost two decades lower, at more or less optimum position that can be well suited for defining a grid size for this flow. Such an observation has been provided to be extendable to non-homogenous turbulence, so that Taylor scale would be the ideal parameter to define the grid resolution for LES computations. Taylor micro-scale (λ) is a combination of the turbulent energy lenght-scale and the Kolmogorov scale ($\eta = (\frac{\upsilon^3}{\varepsilon})^{1/4}$) as $\lambda \sim L_{RM}^{1/3}\eta^{2/3} = (10\frac{k\upsilon}{\varepsilon})^{1/2}$. Consequently, an LES based on the Taylor micro-scale would become over-resolved at high Re number; and a bound on the filter scale such as $\Delta = \max(\lambda, L_{RM}/10)$ could be recommended. For this study, grid size has been chosen according to such a criteria. Integral lenght scale has been easily obtained from RANS simulations. In this view, an example of L_{RM} contours obtained from RANS simulation with a RSM closure is reported in Fig. 5.6. Generated meshes are constituted by a number of hexahedral cells in the range of (2.5-3.5) millions. ANSYS/Meshing was used to generated a non-uniform structured mesh. With criteria adopted cell lenght varied in the range 0.25-1 mm. Furthermore, an adaptive grid procedure has been adopted during calculation activities, refining the grid in the zones with higher velocity gradients.

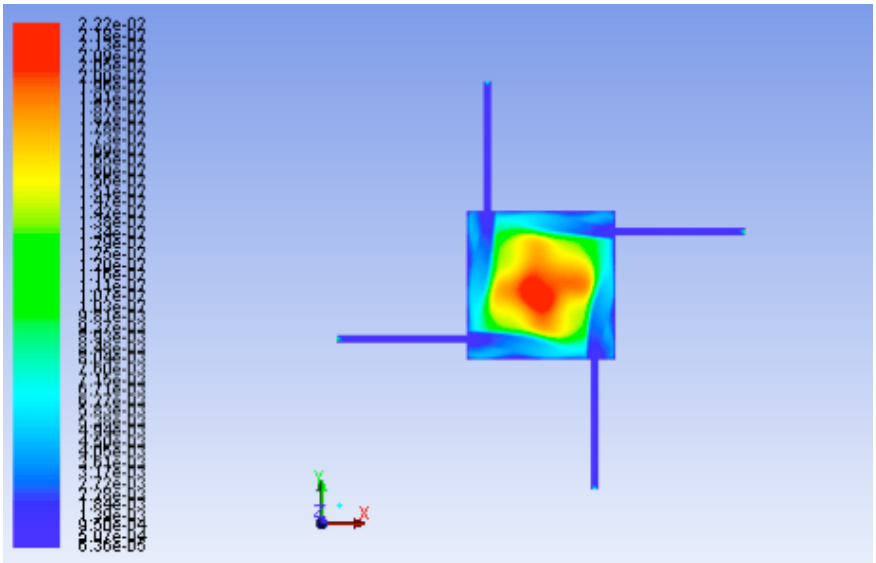

Fig. 5.6 Integral lenght-scale contours from a RANS simulation (in meter)

Pope's criterion was verified for all the grids generated at the stage of full-developed flow. To this end, the percentage of the resolved turbulent kinetic energy η, was calculated as:

$$\eta = \frac{k_{res}}{k_{tot}} = \frac{k_{tot} - k_{sgs}}{k_{tot}} = 1 - \frac{k_{sgs}}{k_{tot}}$$

where k_{res} is the resolved turbulent kinetic energy, k_{sgs} the modeled (sub-grid scale) turbulent kinetic energy and k_{tot} the total turbulent kinetic energy (which is the summation of k_{res} and k_{sgs}). k_{res} has been calculated as:

$$k_{res} = \frac{1}{2}(u'^2 + v'^2 + w'^2)$$

where u', v' and w' are the velocity fluctuations in x,y and z directions, respectively.Such a values have been extracted from statistics. Total simulation time has been set equal to four time the mean reactor residence time (τ). Such a value ensures the achievement of a statistical independence for all the variables. Statistic analysis have been carried out not considering the first 2τ. The sgs turbulent kinetic energy k_{sgs} was estimated from the expression (Sagaut, 2000):

$$k_{sgs} = \frac{1}{(C_S \Delta)^2} v^2_{sgs}$$

where υ_{sgs} is the sgs turbulent viscosity given by the dynamic Smagorinsky–Lilly model (Lilly, 1992), C_S the dimensionless coefficient of that model and Δ the filter length. The average value of η for all the simulations is approximately 90%

All the simulations have been initialized with a flow-field obtained from a converged RANS with a RSM closure. Outlet section has been modeled as pressure outlet boundary;
Since LES is an unsteady model, the velocity profile imposed at the inlet of the domain must be time-dependent. In this study, Vortex Method (VM) (Sergent, 2002; Mathey et al., 2006) has been adopted. It consists in generating and transporting randomly in the inlet plane a given number (here: 200) of 2D-vortices whose intensity and size depends on the local value of k and the turbulence dissipation rate. Other settings at the inlet boundary are equal to those adopted in RANS simulations.
For the spatial discretization of the model equations, second order bounded central schemes were chosen. The time integration was performed using the second order implicit Crank-Nicholson scheme. The Semi-Implicit Method for Pressure-Linked Equations (SIMPLE) modified for unsteady simulations (Patankar and Spalding, 1972) was used to implement the pressure-correction equation.
Parallel computations were performed by means of the segregated pressure-based solver of the ANSYSs Fluent. The solution for each time step required around 30 iterations to converge with the residual of each equation smaller than $1.0e^{-4}$. For each LES investigation, 8 logic processors of a double processor, esa-core machine (Mac-Pro) with 12 logic processors for each processor were used. CPU. Simulation time step has been chosen in order that the Courant number was less then 1 for each iteration. A simulation required about 3 weeks for converging, due to the long residence times connected with the flows under investigation, the small time step adopted and the total simulation time (4τ) needed for obtaining a statistical independence of all the variables. Five cases have been carried out in order to explain several results obtained in chapter 4 and to clarify different aspects of cylonic vortex flow aerodynamic. Details of cases analyzed are reported in Table 5.1. Reactor average Re number (based on the average reactor velocity magnitude and reactor diameter) varies from 8000 (case a) up to 22000 (case c).

Case	N° jets	Inlet velocity m/s	Inlet Re number	Mean residence time, s	Time step, s	Total N° time step
a	1	60	1670	0,27	0,0002	6000
b	2	60	1670	0,136	0,0001	6000
c	4	60	1670	0,068	0,00005	6000
d	2	30	840	0,27	0,0002	6000
e	4	15	420	0,27	0,0002	6000

Tab. 5.1 Details of LES cases

5.3.3.2 Time Averaged Flow

In this section mean axial and tangential velocity profiles along reactor height obtained by LES calculations are reported and analyzed. First of all, a comparison between velocity components profiles obtained from RANS calculation with a RSM closure and LES is reported in Fig. 5.7. In particular, Fig refers to a 4 inlet jets configuration and a inlet Re number of 1670 (case c). Results show a overall good agreement of velocity components profiles obtained by RSM and LES calculations. LES profiles showed higher velocity magnitude and a more marked free vortex behavior respect to RSM calculations. Similar considerations can be done for the other cases analyzed. In this view, Fig. 5.8 reports tangential and axial profiles for cases a,b and e. It is worthwhile to note that for such a cases a vortex structure with a strong free vortex behavior is established with respect to the cyclonic vortex structure highlighted and analyzed in chapter 4 for a 20*20*5 cm reactor configuration. Such a difference can be principally due to an higher confinement level in such a case. Summarizing, increasing the reactor confinement level a free vortex behavior is emphasized

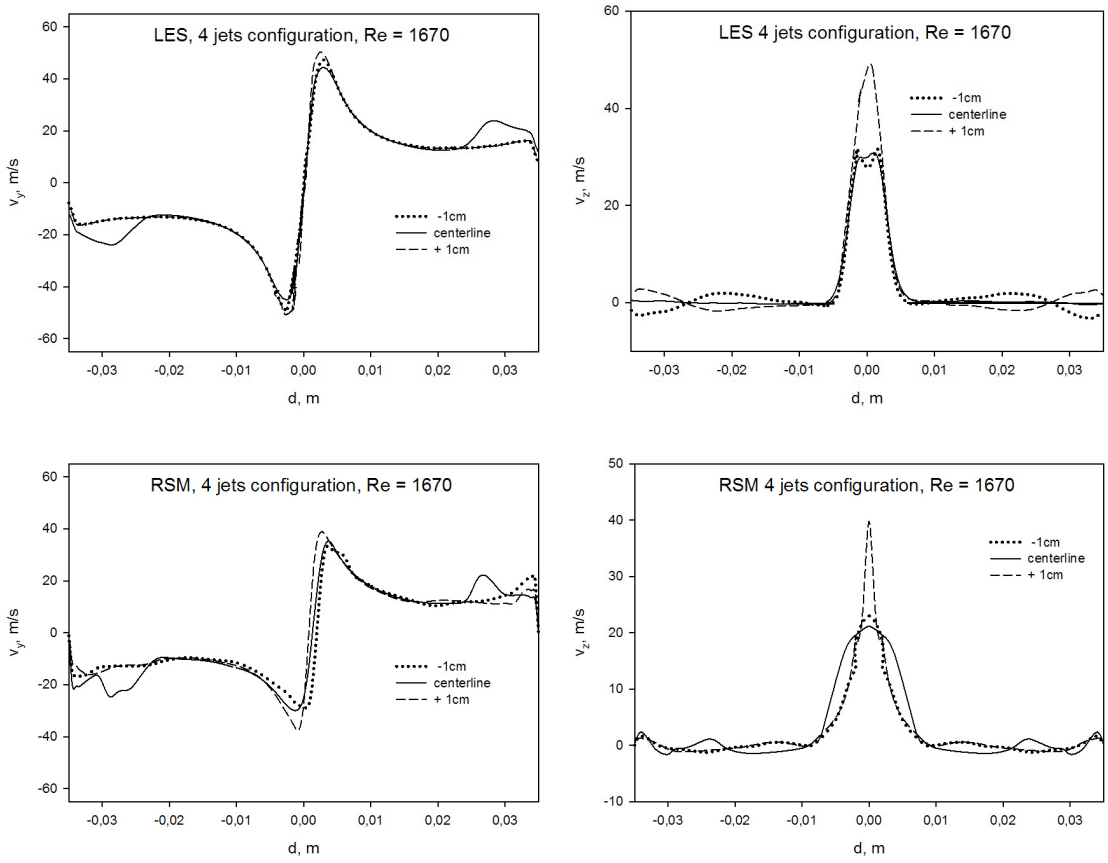

Fig. 5.7 Comparison between mean velocity profiles computed by LES and RSM

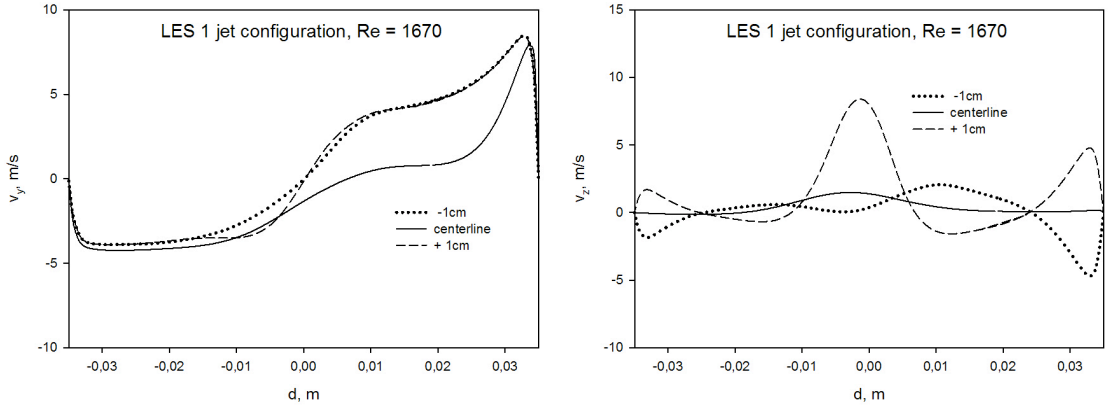

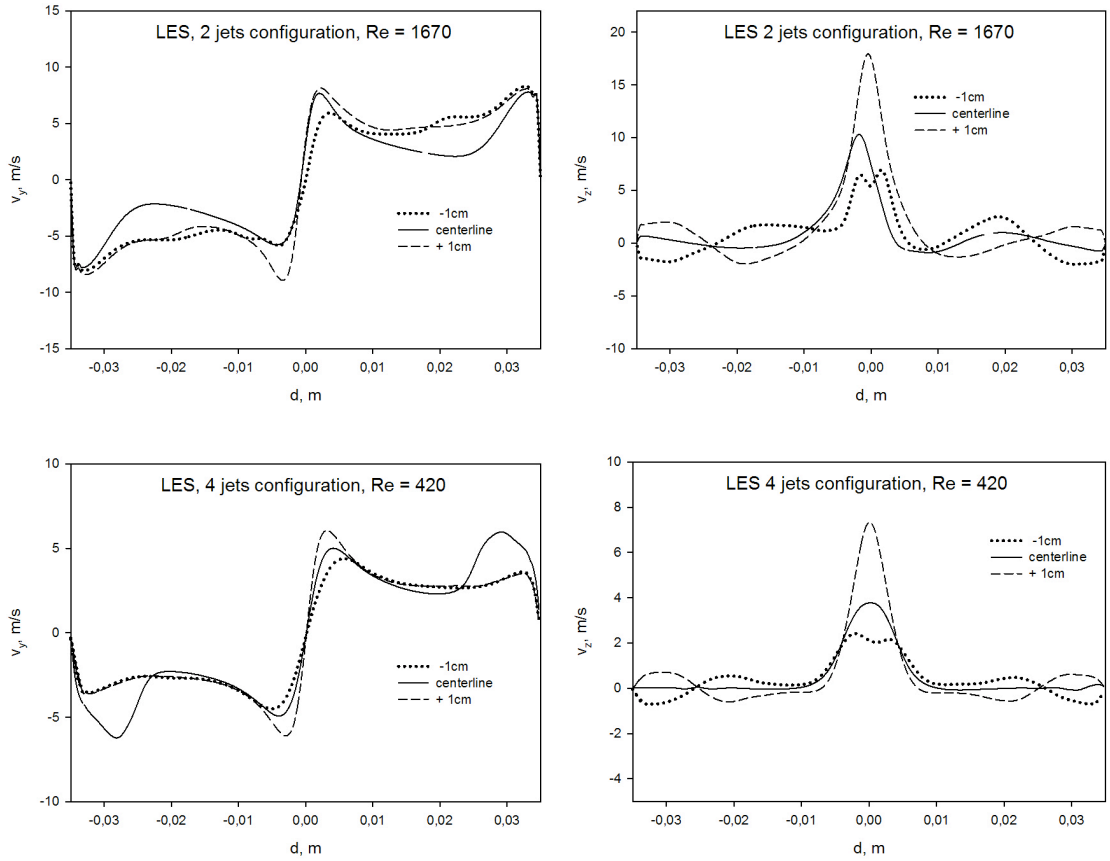

Fig. 5.8 Tangential and axial mean velocity profiles case a, b and e (from top to bottom)

5.3.3.3 Coherent structure identification

As reported in chapter 3, in this study vortex structure identification has been obtained by means of Q-criterion isosurfaces visualization. As pointed out in this chapter, such a method reveal a vortex structure in a flow by highlighting the flow regions where the vorticity prevails over the strain rate. Q-criterion has been chosen for this study because of all the Eulerian coherent structure criteria (ECC) developed, it displays the most clear coherent vortices (Dubief and Delcayre, 2011). As well as all for the other ECC, such a criteria requires a user-defined threshold to indicate the regions where a structure exists. In addition, the boundaries of the structure depend on the selected threshold, lending subjectivity to the definition of the size or boundary of the structure (Green et al., 2007). Recently, other approach (Lagrangian criterion) such as the direct Lyapunov exponent (DLE) method (Haller 2001) have been adopted for obtaining a structure that is "objective" (frame-independent). However, such a approach results more time-consuming

respect the use of an Eulerian criteria and in several cases does not add significant informations to the vortex structure topology.

In Fig. 5.9 instantaneous Q-criterion iso-surfaces (reactor top view) taken at a random time step are shown as level sets of 0.1-1-10% maximum value of Q, for a two inlet jets configuration and inlet Re number = 1670.

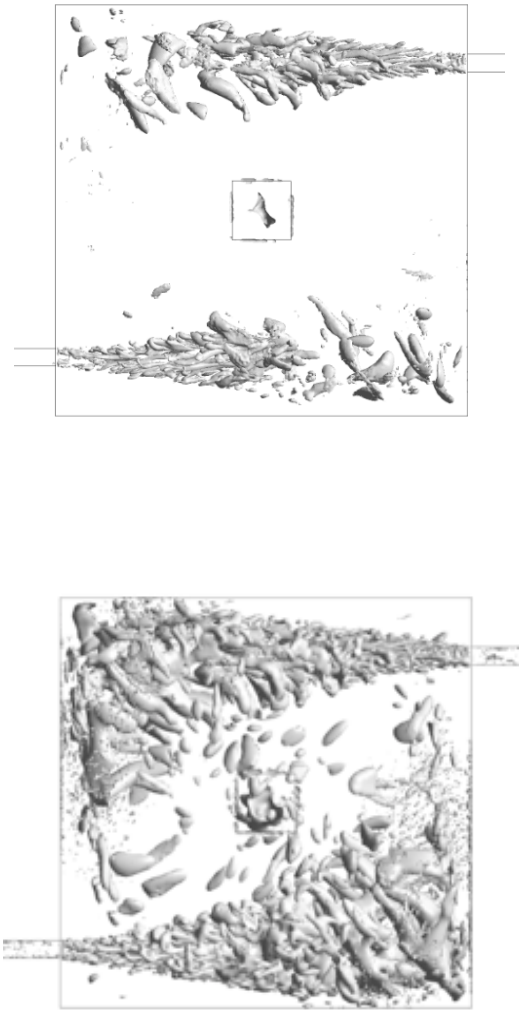

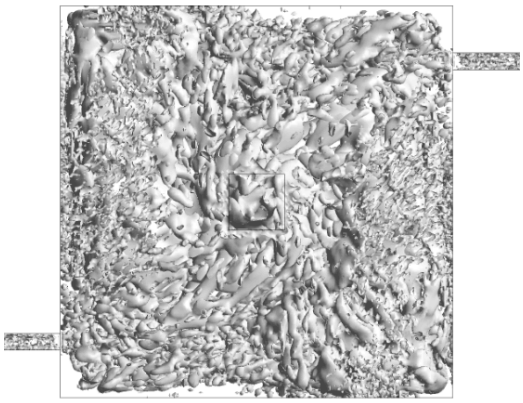

Fig. 5.9 Coherent structures highlighted adopting different Q-threshold values; from top to bottom 10% Q_{max}, 1% Q_{max} and 0.1% Q_{max}

It is worthwhile to note the use of different Q-treshold values can give different representation of the flow. In particular the density of structures isolated by the Q criterion decreases as the threshold increases. The theory behind the eduction method offers no strong basis to support any one plot in Fig. 5.9 against the others as a representative picture of coherent vortices. A selection can be made on vorticity since the first impact of a vortex on turbulent quantities is to create vorticity fluctuations. As can be seen from Fig. 5.9 a too large threshold could hide structures which contribute greatly to high vorticity fluctuations. In addition, a too small level of Q suggests that the impact of most isolated structures on the dynamic of flow is covered by large scale structures.

In order to minimize the weight of subjectivity on the choice of the threshold, a conditional sampling technique (Dubief and Delcayre, 2011) is needed since it appears to provide a valuable hint through the threshold Q which gives the highest level of vorticity fluctuations. Following suggestions of other authors (Dubief and Delcayre, 2011; Green et al., 2007), a level sets of 1 % maximum value of Q criterion is adopted in this work.

In Fig. 5.10 the instantaneous Q-criterion structures are shown as level sets of 1 % maximum value varying inlet jets number from one up to 4 and fixing inlet Re number equal to 1670 and 420 (case a, b, c and e).

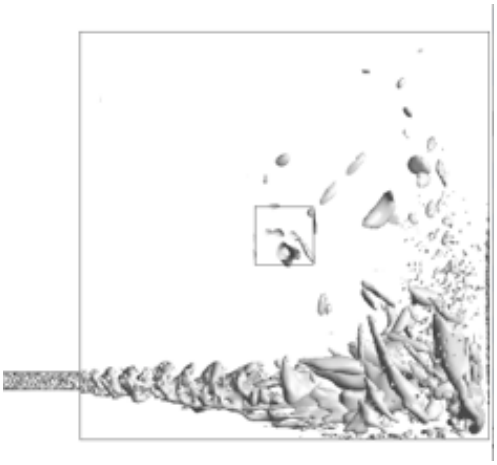

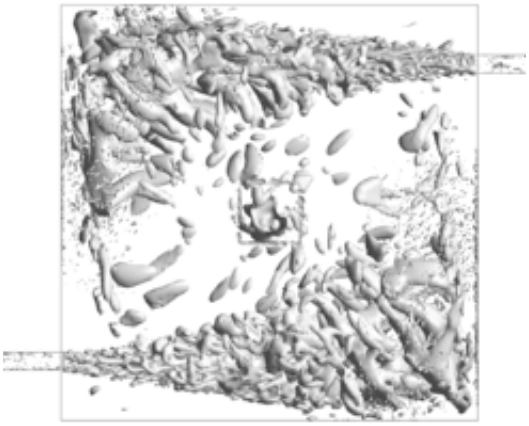

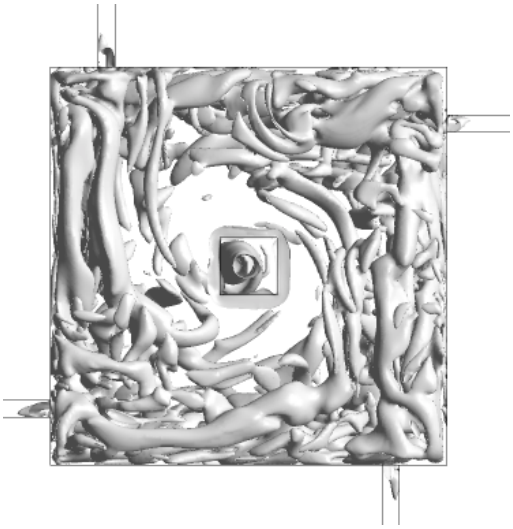

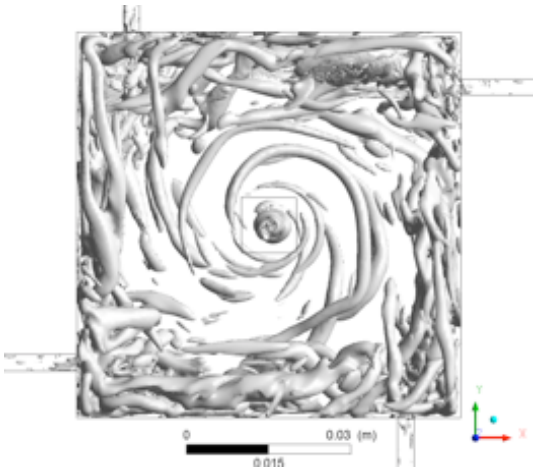

Fig. 5.10 Coherent structures highlighted adopting a level set of 1% Q_{max} for different reactor configurations

The topology of the flow given by Q-criterion isosurfaces is different varying reactor configuration. As it possible to observe in Fig., typical fluid-dynamic structures related to a jet growth can be highlighted for one single and two inlet jets reactor configuration. In particular layered structures which are vorticity sheets associated with vortices can be detected. Such a structures are more marked for two inlet jets configuration respect to one single jet case. For a 4 inlet jets configuration a different structure is present for both the inlet Re number considered. More specifically, in addition to the expected layered structures, "tubular" vortices have been distinguished. The presence of such a "vorticity tubes" can be attributed to an high level of vorticity detected respect to other configuratons analyzed, which extend for almost the entire of the reactor and it is not longer linked to the jet growth. In this view, Fig. 5.11 reports the instantaneous Q-criterion structures for all the case analyzed previously by setting as treshold 1% maximum of Q referred to 4 inlet jets case ($Q_{treshold}$= 1% $Q_{max4inletjets}$ = $5e^5$ s^{-2}).

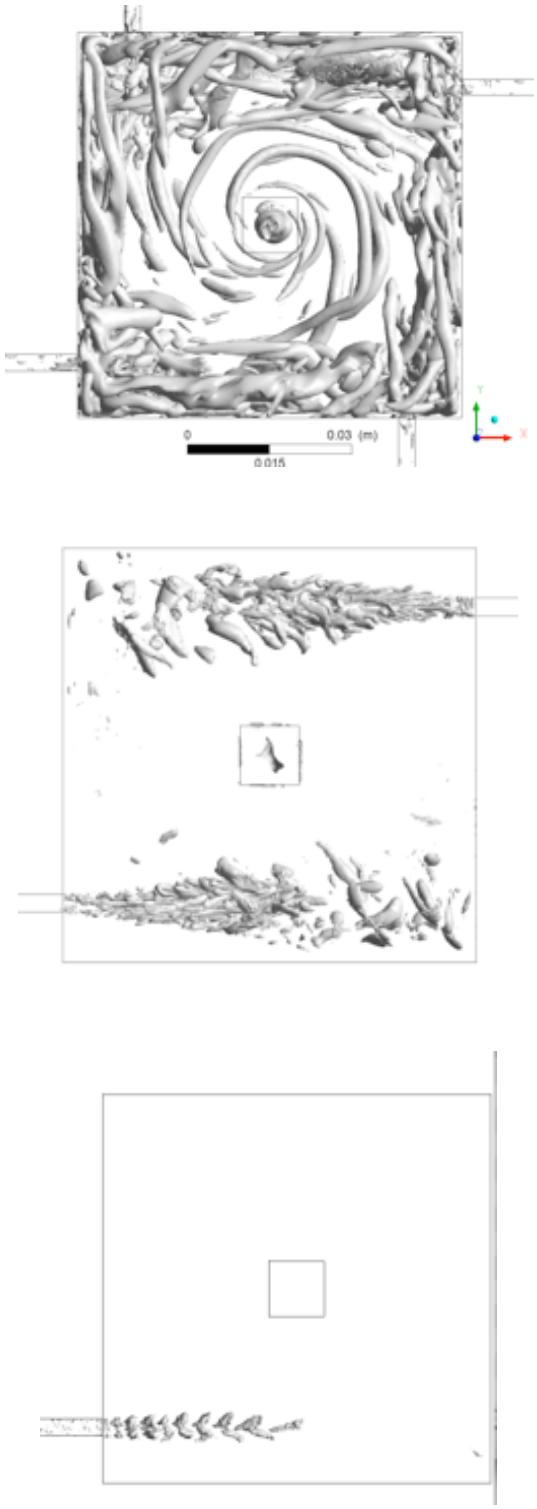

Fig. 5.11 Coherent structures highlighted adopting a level set of 1% $Q_{max4inletjets}$ *(*$5e^{5}$ s^{-2}*) for different reactor configurations*

It is worthwhile to note that for a fixed inlet Re number, local vorticity increases by increasing the number of inlet jets. It can be deduced, thus, that the mixing process rate enhancement obtained by increasing inlet jets number and highlighted in chapter 4 by

engulfment parameter analysis is directly related to an increase of local vorticity into the reactor and to the presence of “vorticity structures” that extend to almost all of the reactor.

5.3.3.4 Precessing Vortex Core Analysis

As reported in chapter 3, Precessing Vortex Core (PVC) is the main fluid-dynamic instability connected with a cyclonic vortex flow. The PVC is a quasi-periodic motion (low-frequency) of the core of the main vortex along axis rotation (cyclone’s geometrical center). Such a peculiar instability is principally associated with a cylonic flow characterized by a strong 3D structure (strong reverse/double reverse axial flow).

PVC strongly influences the flow phenomena in cyclones; the quasi-periodic fluctuations induced by the PVC might lead to large-amplitude pressure fluctuations, and hence mechanical failure.

Several methods have been suggested in order to reveal PVC in a cyclonic vortex flow by root means square (rms) of velocity components and/or pressure field analysis.

Experimental studies of cyclonic flow reveal the strong impact of vortex core precession on the level of the velocity fluctuations (Derksen and Van den Akker, 2007). Near the center, typically 80% of the kinetic energy of the fluctuations is contained in coherent fluctuations located close to the center of a cyclone, which might be attributed to the PVC Near the center, rms values are much. higher than close to the wall. This very likely can be attributed to the PVC, as the rms profiles reflect some features of the gradients. in the average velocity profiles. Vortex-core precession can be also visualized by means of pressure field analysis in a horizontal plane of the reactor. The core of the vortex is generally associated with the point of least pressure (Gupta and Kumar, 2007). In this study, both approaches have been adopted in order to reveal presence/absence of fluid-dynamic instabilities for the vortex reactor configurations proposed.

Fig. 5.12 shows rms of velocity components along the characteristic line for 4 inlet jets case (Re_{jet} =1670) at different reactor height (centerline, +1 cm, -1cm from the centerline). rms velocity values were derived from the measured velocity time series.

As it is possible to observe that for all the three velocity components, maximum of rms is located at the outer boundary of the vortex. Furthermore, rms velocity values in the core

region results much lower than that calculated at the outer boundary, suggesting that PVC is absent for such a configuration.

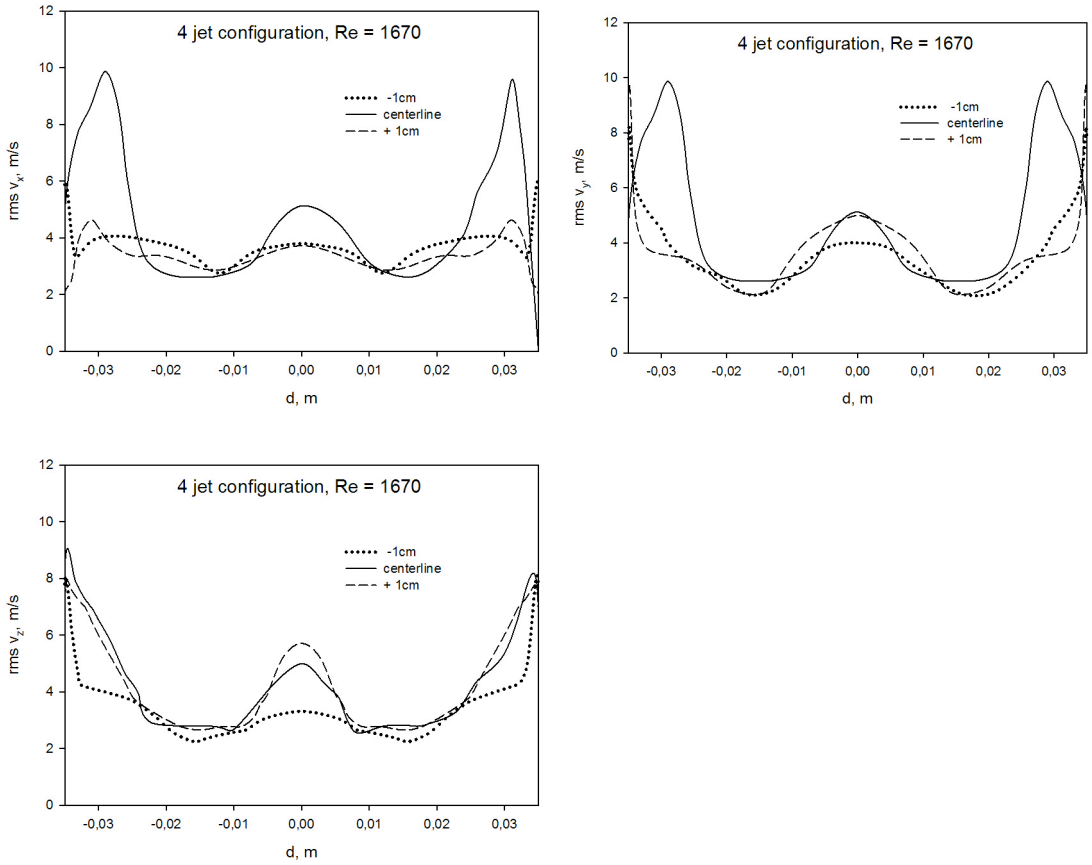

Fig. 5.12 Rms velocity components for 4 jets configuration, Re= 1670

Similar considerations can be derived from the analysis of rms of velocity components for one single and two inlet jets configuration. In this view, Fig. 5.13 shows rms of tangential and axial velocity components along the characteristic line for one single and two inlet jets case (Re_{jet} =1670) at different reactor height (centerline, +1 cm, -1cm from the centerline). It is worthwhile to note that also for such a configurations maximum of rms is located at the vortex boundary suggesting the absence of PVC. However for one single inlet jet case different considerations can be derived respect to 2 and 4 inlet jets configurations. First of all, absence of a symmetrical geometry leads to a non-symmetric rms profiles with maximum of velocity fluctuations shifted more close to the jet region. Furthermore, a comparison between magnitude of mean velocity and rms reveals a stronger temporal fluctuations of the velocity components respect to symmetrical configurations, where smoother fluctuations have been detected. Such an aspect is critical for the mixing process and it will be analyzed in details in the next section.

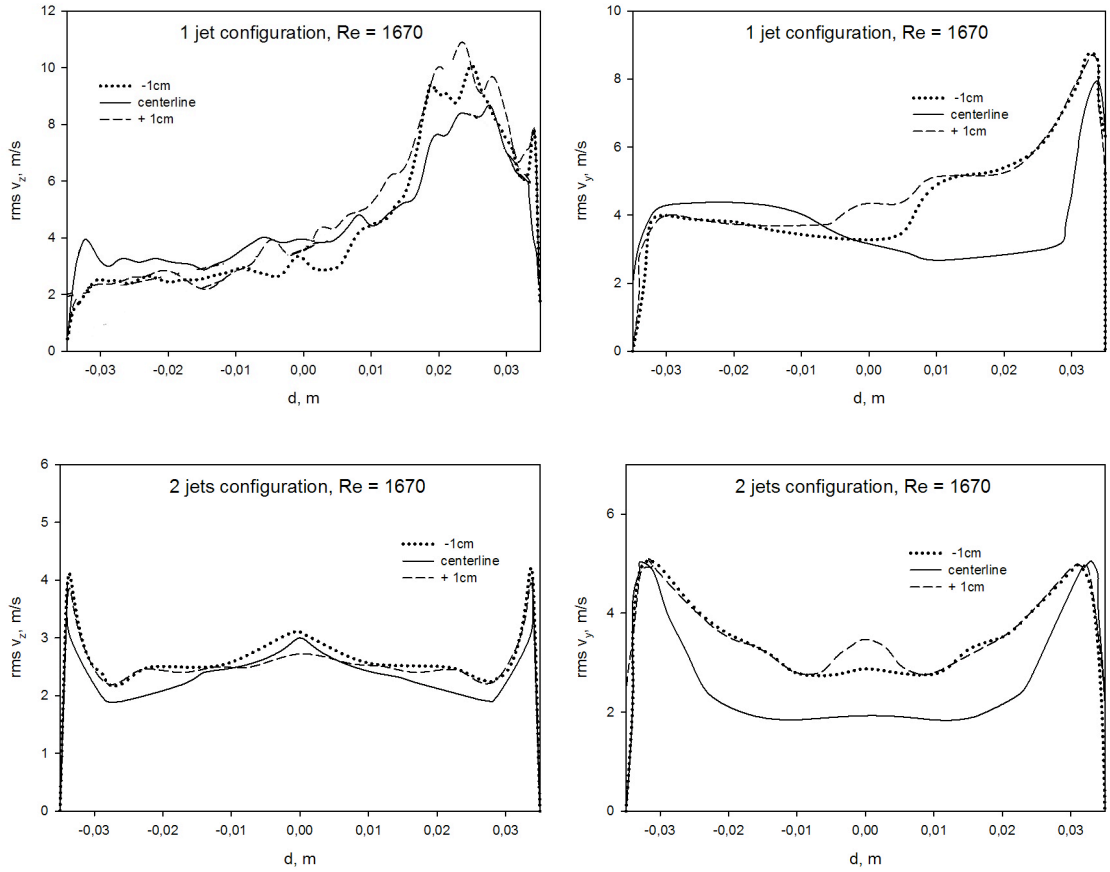

Fig. 5.13 Rms of axial (left) and tangential (right) velocity for one and two jets configuration, Re= 1670

In Fig. 5.14, a visualization of vortex core at several time step is reported for the 4 inlet jets case. Vortex core is highlighted by means of pressure iso-surface (pressure minimum).The time spacing between the subsequent images is 0.025s. It is worthwhile to note that for all the time step, the vortex core coincides with the reactor axis rotation and a quasi-periodic precession motion of the vortex core is absent.

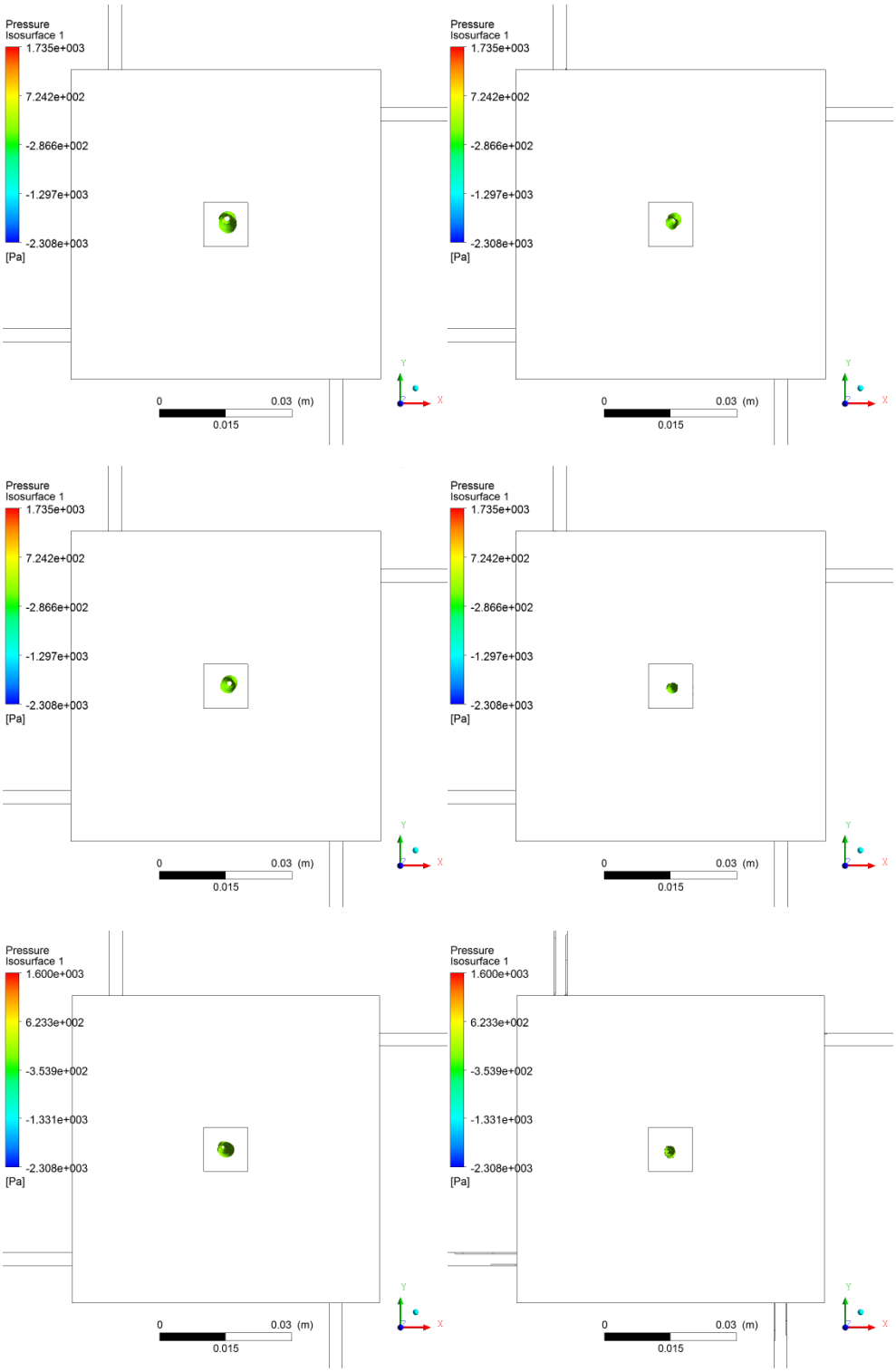

Fig. 5.14 Istantaneous visualization of vortex core location for different time step

In order to better highlight such an aspect in Fig. 5.15 the average vortex-core position throughout the cyclone.obtained from a temporal average procedure of time series is reported. From this Fig. appears clear that the vortex core overlaps the reactor axis rotation, revealing that PVC phenomena is absent

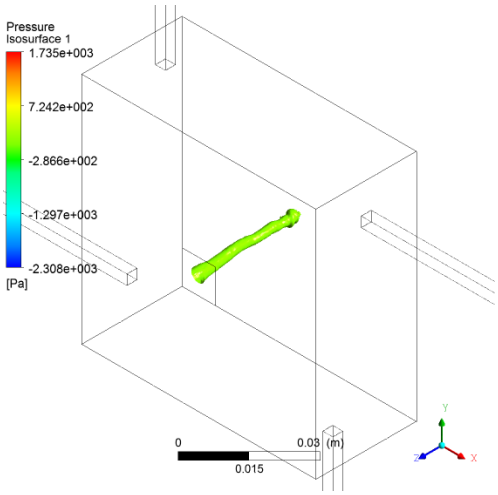

Fig. 5.15 Average vortex core position (4jets Re= 1670)

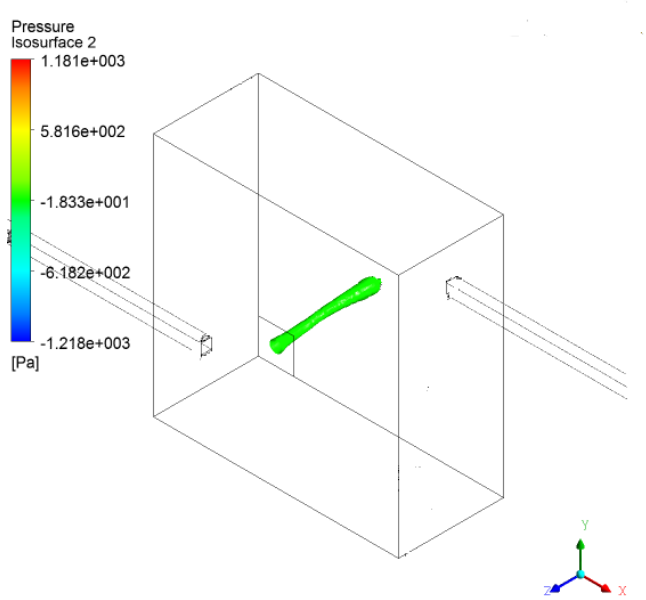

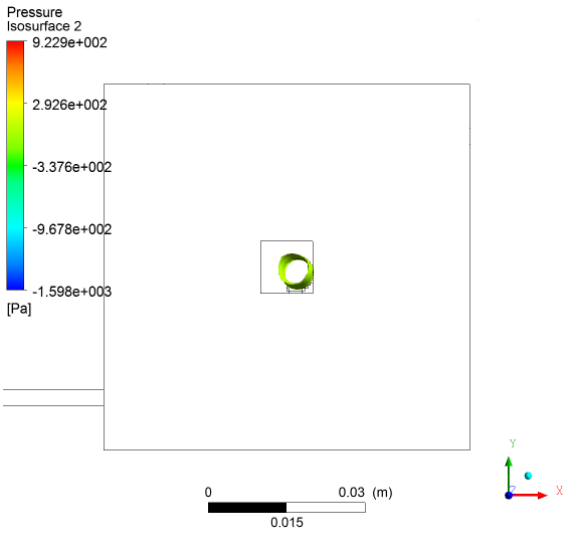

Fig. 5.16 Average vortex core position for one and two inlet jets configuration

Fig. 5.16 shows the average vortex-core position throughout the cyclone.for one an two inlet jets configurations. As it is possible to note also for such a configurations, PVC phenomena is not present. Respect to two and four inlet jets cases, for one single inlet configuration, the average vortex core position is not coincident with the reactor's centre . Such an aspect is principally related to an absence of geometrical symmetry that lead to a non-symmetric vortex structure with a marked 3D behavior.

5.3.3.5 Engulfment Ratio: Time series and Frequency Spectra

In this section the time series of the engulfment ratio (K_{glf}) for cases analyzed and their corresponding spectra obtained by frequency analysis are reported and analyzed. Such a study is meaningful since key informations about the temporal evolution of the mixing process between recirculated and inlet fluid at the reactor can be derived. In other words, the effect of jets number and inlet Re number on the stabilization of the mixing process in a cyclonic flow can be analyzed.

First of all, K_{glf} as function of the nozzle distance (x/d_{jet}) for a 2 inlet jets reactor configuration (Re_{jet} = 1100) obtained by RANS calculations is shown in Fig. 5.17. Also the K_{glf} trend for a 20*20*5 cm reactor configuration and for a free jet case are reported for comparison.

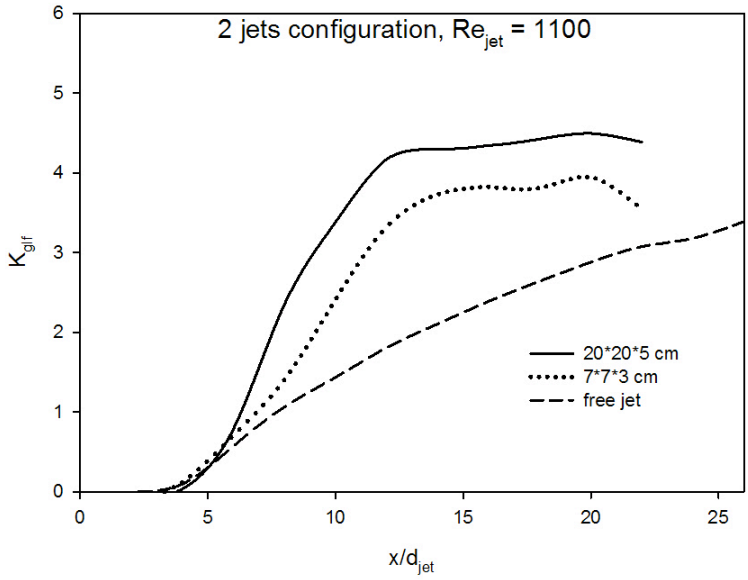

Fig. 5.17 Effect of confinement level on the engulfment ratio

It is worthwhile to note that K_{glf} shows a similar trend for both confinement levels, increasing as the distance from the nozzle increase for then reach an asymptotic value at high nozzle distance. Such an asymptotic value is higher for a low level of confinement, since jet growth results less sensitive to the presence of a wall and, thus, more fluid (recirculated) is "available" for the engulfment process. However, also for high level of confinement (7*7*3 cm reactor configuration), the mixing process is strongly enhanced with respect to a free jet case and similar considerations highlighted in chapter 4 can be applied.

Fig. 5.18 reports time series of the engulfment ratio (K_{glf}) for several cases analyzed (a, b, c and e), at a distance from the nozzle (x/d_{jet}) equal to 12 (and considering jet centerline). Engulfment ratio (K_{glf}) has been calculated with the same procedure adopted for RANS calculations but considering the istantaneous value of velocity magnitude. On the Fig. also the K_{gl} value obtained by RANS calculations is reported for comparison. f

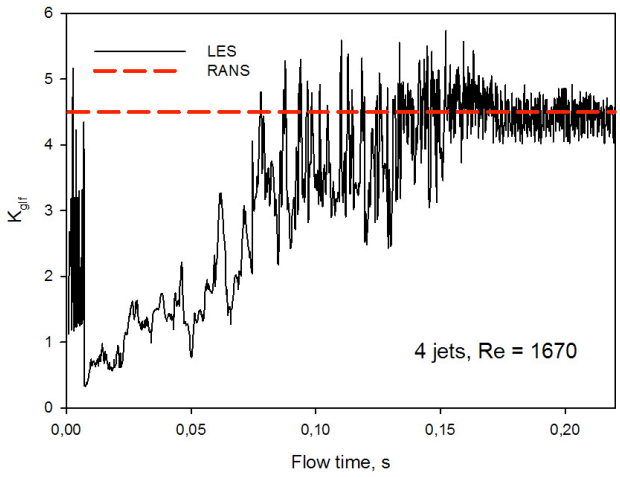
LES
RANS
4 jets, Re = 1670
K_{gif}
Flow time, s
0
1
2
3
4
5
6
0,00
0,05
0,10
0,15
0,20

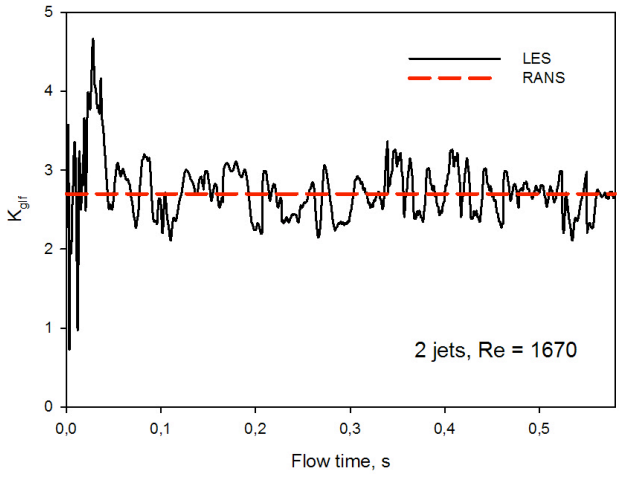
LES
RANS
2 jets, Re = 1670
K_{gif}
Flow time, s
0
1
2
3
4
5
0,0
0,1
0,2
0,3
0,4
0,5

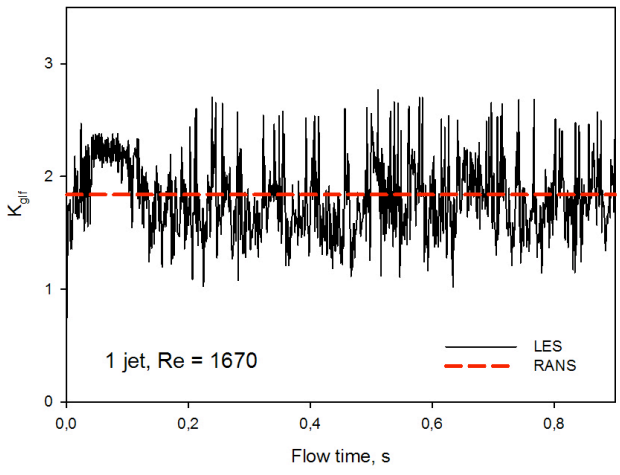
LES
RANS
1 jet, Re = 1670
K_{gif}
Flow time, s
0
1
2
3
0,0
0,2
0,4
0,6
0,8

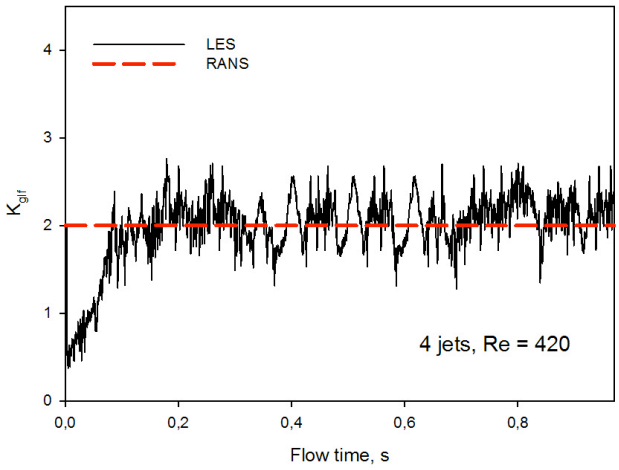

Fig. 5.18 Time series of the engulfment ratio for several cases analyzed

It is worthwhile to note that time series of engulfment ratio is significantly affect by number of inlet jets and inlet Re number. For all the simulations, K_{glf} after an induction time (that is a function of the simulation itself), starts to oscillate around its mean value. Oscillations magnitude reflects some peculiar characteristics of the mixing process. High/ irregular oscillations are related to an unstable and not/well controlled mixing meanwhile small quasi-regular oscillations of K_{glf} reveal a stable and well/controlled mixing.

First of all, as well as highlighted in chapter 4, increasing inlet jets number leads to an increase of K_{glf} (and thus, of the mixing process rate). Furthermore, such a parameter also affects mixing process stabilization. In particular, for a fixed inlet Re number, an asymmetrical geometry (such as one single inlet jet case) leads to an unstable mixing meanwhile symmetrical geometries are characterized by a well/controlled mixing process. For instance, the maximum variation of K_{glf} respect to the average value (obtained with RANS) for 4 inlet jets configuration and Re=1670 is about 8%, meanwhile is 30% for one single inlet case. Such a result can be principally attributed to an high values of rms of velocity magnitude (velocity fluctuations) detected for one single inlet case respect to the other cases analyzed. Secondary, for a fixed inlet flow rate, it is possible to note that for the nozzle distance considered, the average value of K_{glf} results similar not depending on the number of inlet jets adopted. However, also in this case, a symmetrical configuration lead to a stable mixing respect to the asymmetrical one. Same analysis has been carried out also at different nozzle distances; similar considerations can be obtained. From flow time analysis, it appears clear that for the cases analyzed the rate of mixing process is different.

For example, the evaluated K_{glf} time series varies in the range 0;0.22 s for 4 inlet jets case and Re_{jet} = 1670 meanwhile it is comprised in the range 0;1 s for one single inlet jet configuration (Re_{jet} = 1670). In this view, a frequency analysis of the K_{glf} time series has been carried out in order to obtain informations about the characteristic frequency (Power Spectral Density) of the mixing process, varying the key parameters. In particular, a Blackman filter has been adopted in order to transform the signal input.

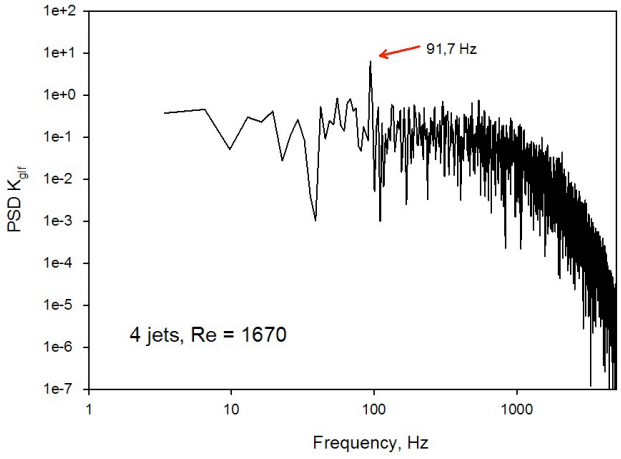

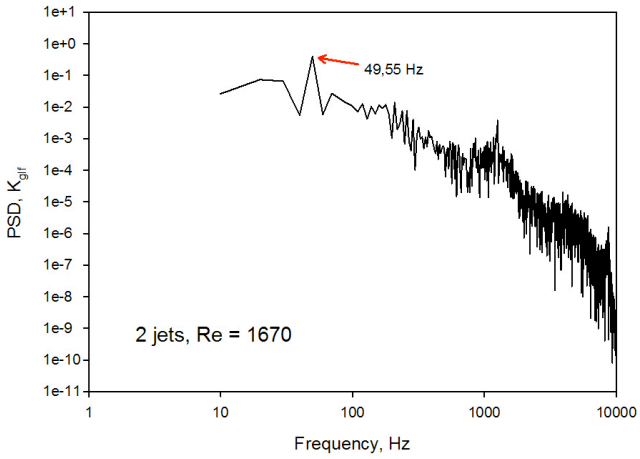

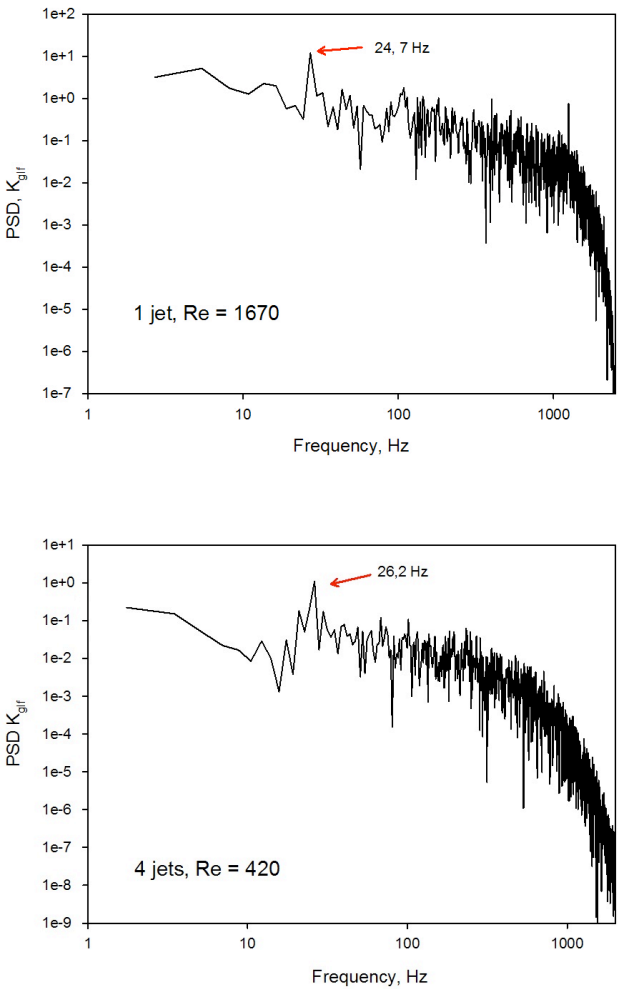

Fig. 5.19 PSD of the engulfment ratio for several cases analyzed

Characteristic frequencies of K_{glf} time series evaluated by Fourier analysis result a function of the total inlet flow rate. First of all, it is worthwhile to note that for a fixed inlet Re number, the characteristic frequency increases by increasing the inlet jets number approximately in a linear way with the total flow rate. For instance, increasing the total flow rate from a value Q (1 jet case) up to 4Q, the characteristic frequency K_{glf} varies from 24,7 Hz up to 91,7 Hz. At the contrary, fixing the total inlet low rate and varying the number of inlet jets, the evaluated characteristic frequency appears similar, suggesting that the mixing process rate is governed by vortex intensity, and thus, by the total inlet flow rate.

5.3.3.6 Frequency spectra of velocity time series

During LES calculations, the instantaneous velocity magnitude and its components have been recorded at several monitoring points in the reactor for all the cases analyzed. After, a Fourier analysis of these time series has been performed in order to collect informations about the characteristic frequencies of the flow. In this way, further informations about vortex stabilization and the topology of the established vortex can be obtained. Fig. 5.20 shows the location of the monitoring points defined in this study.

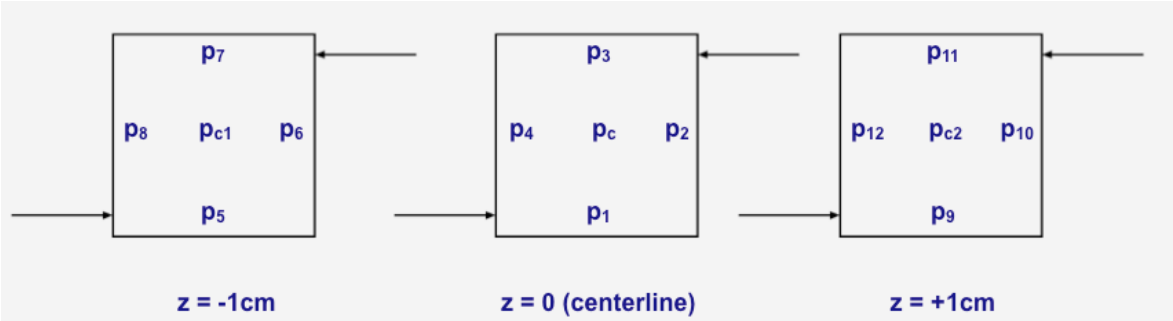

Fig. 5.20 Location of monitoring points

Fig. 5.21 shows the frequency spectra of velocity time series for a 4 inlet jets configuration (Re_{jet} = 1670) at several monitoring points. Also the calculated characteristic frequency is reported.

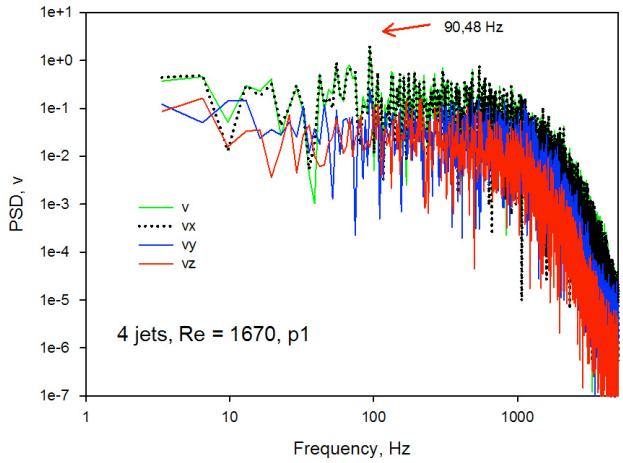

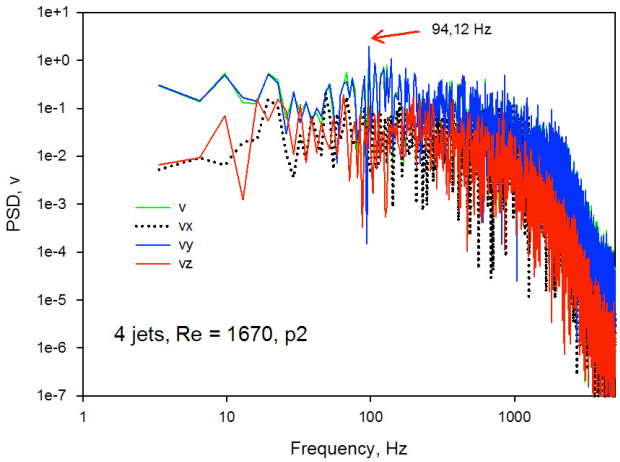
94,12 Hz
PSD, v
Frequency, Hz
v
vx
vy
vz
4 jets, Re = 1670, p2
1e+1
1e+0
1e-1
1e-2
1e-3
1e-4
1e-5
1e-6
1e-7
1
10
100
1000

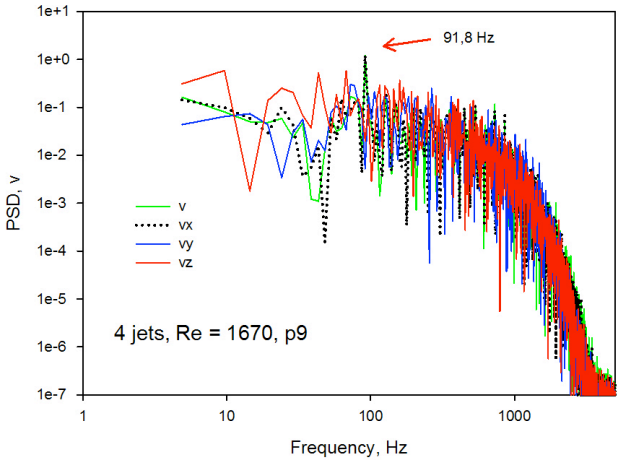
91,8 Hz
PSD, v
Frequency, Hz
v
vx
vy
vz
4 jets, Re = 1670, p9
1e+1
1e+0
1e-1
1e-2
1e-3
1e-4
1e-5
1e-6
1e-7
1
10
100
1000

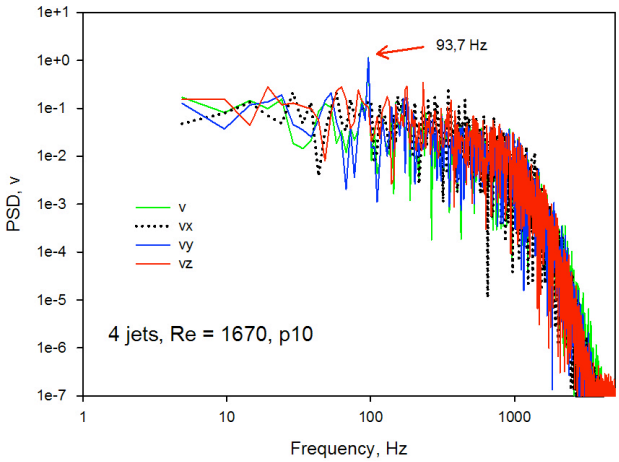
93,7 Hz
PSD, v
Frequency, Hz
v
vx
vy
vz
4 jets, Re = 1670, p10
1e+1
1e+0
1e-1
1e-2
1e-3
1e-4
1e-5
1e-6
1e-7
1
10
100
1000

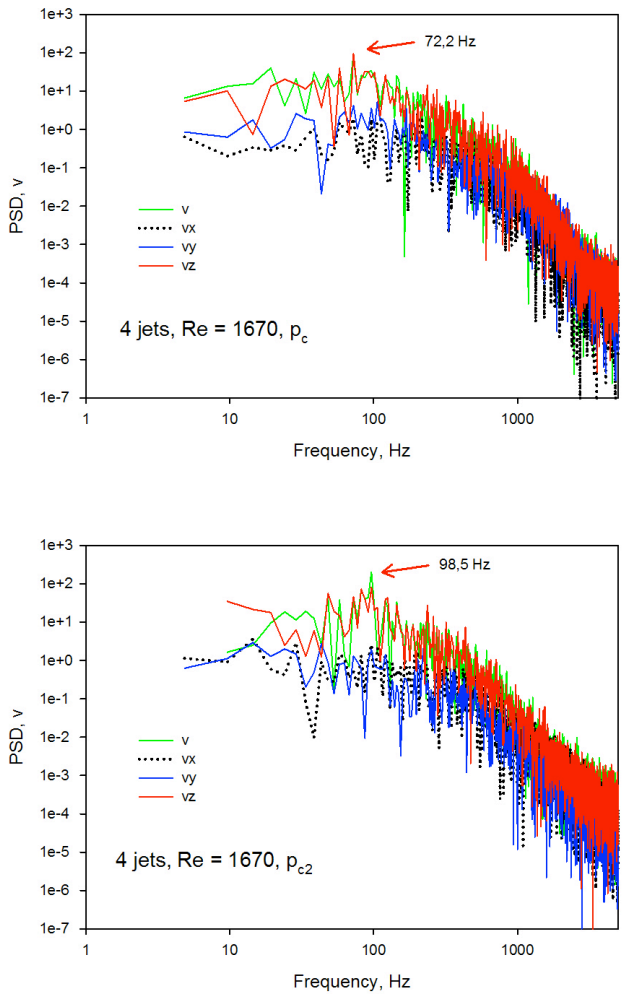

Fig. 5.22 Frequency spectra of velocity time series and its components at several monitoring points; 4 inlet jets case Re_{jet} = 1670

Several considerations can be done. First of all, it is worthwhile to note that the use of a symmetrical configuration leads to a stable/quasi 2D cyclonic vortex structure for what concerning the spatial and temporal vortex evolution. In fact, a similar characteristic frequency (approximately 90 Hz) has been found at the monitoring points located at the vortex boundary, not varying along the reactor height. Such a result highlights that a similar fluid-dynamic structure is established at the vortex boundary on both the temporal and spatial scales.

At the contrary, the characteristic frequency varies moving from the outer boundary of the vortex to the centre, suggesting that a cyclonic structure is a complex structure governed by different spatial and temporal scales. Moreover, it is also possible to note that at the vortex boundary the structure is principally “driven” by the tangential velocity components

(velocity magnitude and tangential velocity signals resulted similar and higher respect the other one analyzed), meanwhile at the vortex core the main components is the axial component. Finally, a comparison between the engulfment ratio spectra and velocity spectra highlighted a similar characteristic frequency for a fixed monitoring point. Such a result can be attributed to the fact that the engulfment ratio and the mixing process are strictly connected with the istantaneous velocity fluctuations, the local value of vorticity and the topology of the established fluid-dynamic structure.

Fig. 5.23 shows the frequency spectra of velocity time series for a 4 inlet jets configuration (Re_{jet} = 420) at several monitoring points. Also the calculated characteristic frequency is reported.

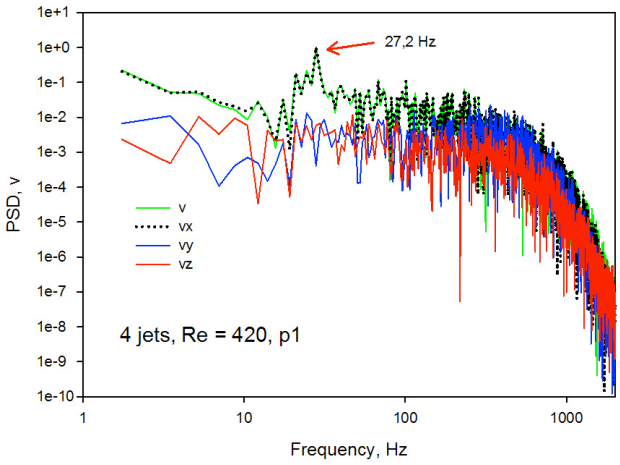

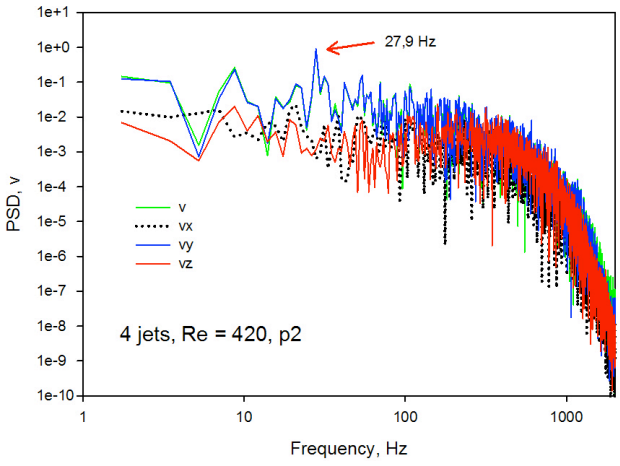

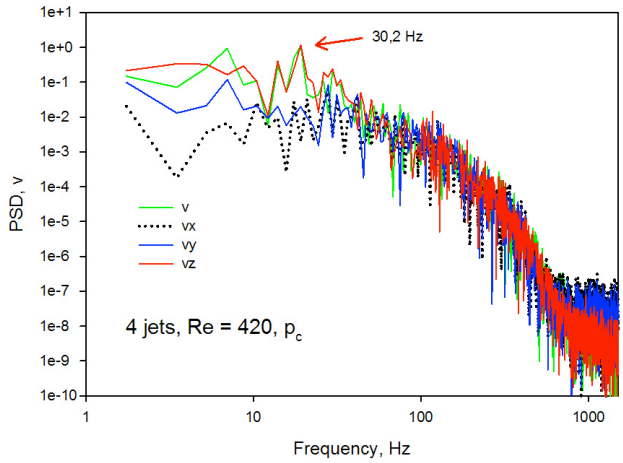

Fig. 5.23 Frequency spectra of velocity time series and its components at several monitoring points; 4 inlet jets case Re_{jet} = 420

Similar considerations can be provided for a Re_{jet} = 420 and 4 inlet jets. A strong, stable vortex structure is established with a characteristic frequency of approximately 27 Hz. Such a frequency does not change along the vortex boundary and the reactor height, suggesting once again that the H/d reactor ratio is a critical parameter for establishing a well/defined, stable vortex structure. All the proposed configurations are characterized by a H/d reactor ratio < . It is also worthwhile to note that as well as highlighted in the previous section, the evaluated characteristic frequency results a function of the total inlet flow rate. Also in this case, the main velocity component at the vortex boundary is the tangential velocity meanwhile at the vortex core is the axial velocity. Frequency analysis of 2 inlet jets case, varying inlet Re number shown similar results and it has not been reported. Finally, frequency analysis of velocity time series for one single inlet jet reactor configuration is reported in Fig. 5.24.

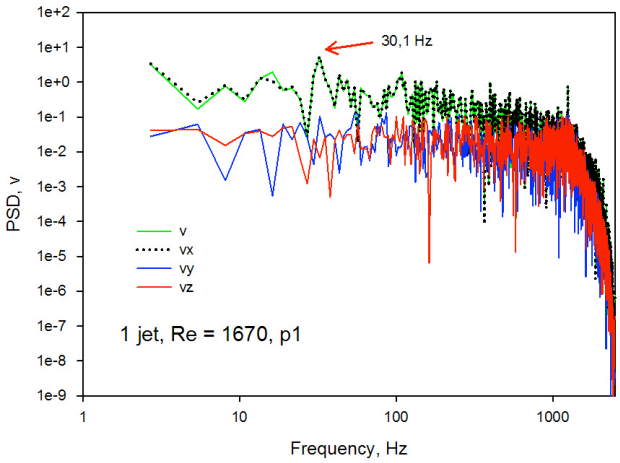
30,1 Hz
v
vx
vy
vz
1 jet, Re = 1670, p1
PSD, v
Frequency, Hz

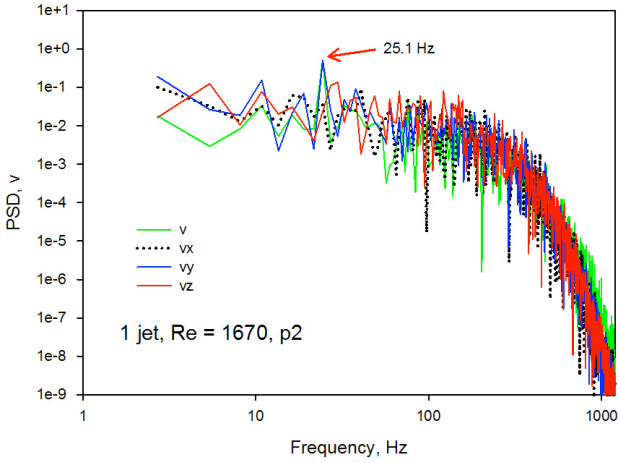
25.1 Hz
v
vx
vy
vz
1 jet, Re = 1670, p2
PSD, v
Frequency, Hz

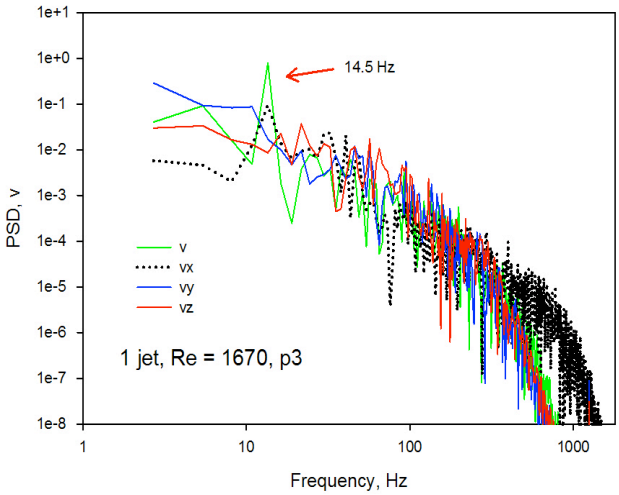
14.5 Hz
v
vx
vy
vz
1 jet, Re = 1670, p3
PSD, v
Frequency, Hz

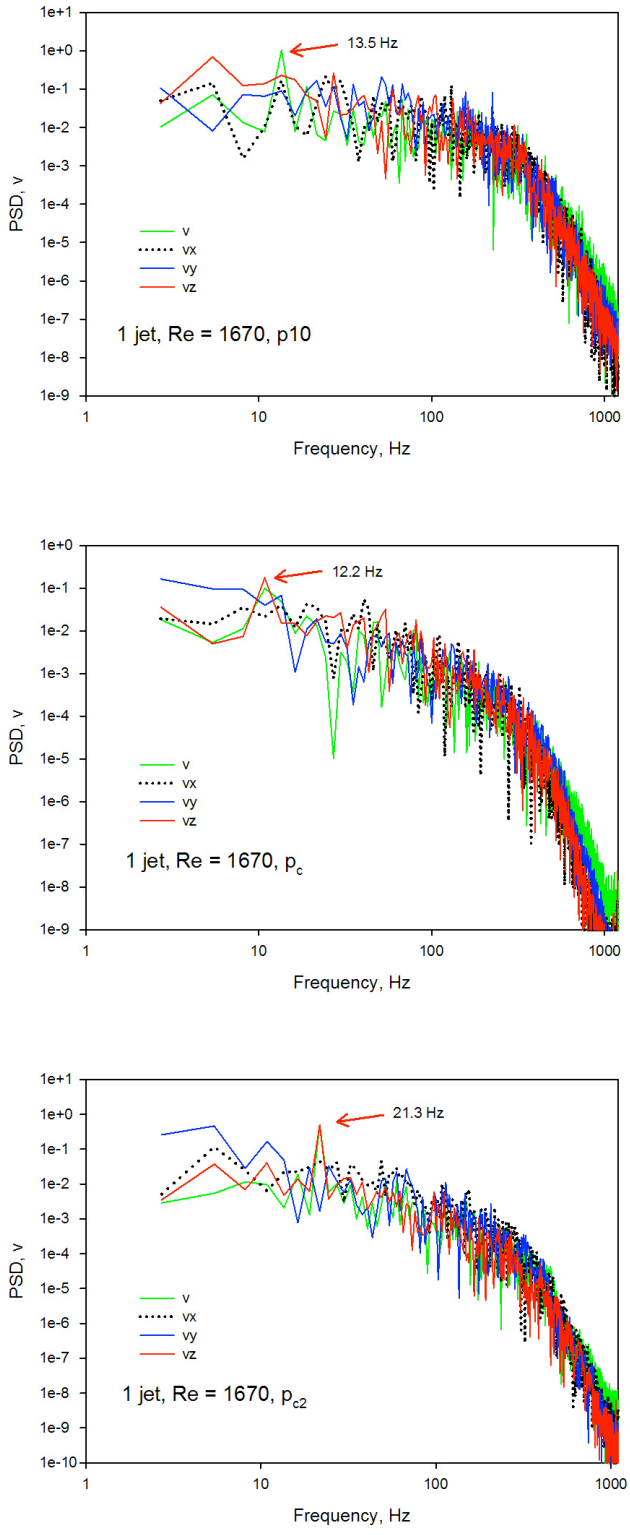

Fig. 5.24 Frequency spectra of velocity time series and its components at several monitoring points; 1 inlet jet case Re_{jet} = 1670

Different considerations can be derived with respect to the symmetrical configurations analyzed. For one single inlet jet case, different characteristic frequencies have been

detected along vortex boundary, revealing the establishment of a non/stable vortex structure. For example, the characteristic frequency is about 30 Hz at the monitoring point p1, meanwhile it is 14.5 Hz at p3. Moreover, frequency varies with the reactor height. For instance, the characteristic frequency at p10 (same location of p1 at a different reactor height), is 13.5 Hz, about one half of that obtained at p1. Frequency analysis of velocity time series recorded at monitoring points located at the vortex core, confirmed that a cyclonic vortex structure is a complex structure that evolves on different temporal and spatial scales. In conclusion, such a study suggests that a non-symmetrical configurations have to be avoided in order to obtain a stable vortex structure. In this way, also a strong, well/controlled mixing process can be achieved.

5.4 - Summary of the main findings

Kinetic analysis showed that the methane ignition process in diluted, preheated and lean conditions is significantly different respect to conventional working conditions. Reactor residence times for the geometrical configurations proposed and analyzed in this chapter resulted compatible with chemical kinetic times, so that they can be adopted for MILD-LP applications. Concerning to the mixing process, results highlighted that a strong, fast and stable mixing between recirculated and inlet fluid can be achieved with the proposed geometries. For a fixed inlet Re number, mixing process between inlet and recirculated fluid is enhanced by increasing number of inlet jets due to a strong increase of vorticity into the reactor. Temporal analysis of engulfment parameter (K_{glf}) revealed that mixing process between inlet and recirculated fluid is strongly affected by reactor configuration. A well/controlled mixing is obtained for 2 and 4 inlet jets configurations meanwhile an unstable mixing, characterized by high amplitude/non-regular oscillations of K_{glf} is obtained for one single jet configuration.

Furthermore, pertaining to the presence of fluid-dynamic instabilities such as PVC, LES results showed that the appearance of instabilities in a cyclonic vortex flow can be avoided by adopting very compact cyclonic chamber (H/d ratio < 1). In particular, Precessing Vortex Core phenomena is affected by reactor configuration in terms of outlet location and reactor dimension. PVC is a phenomena associated to high values of root mean square (rms) of velocity components at vortex core and a precession of vortex core (identified by

location of pressure minimum) along the axis rotation. For all configurations analyzed, characterized by H/d ratio <1 and a sudden contraction as outlet section, PVC phenomena, connected to a strong 3D cyclonic vortex structure, is avoided. This result reveals a well-established vortex stabilization for all the configurations investigated.

Characterization of vortex flow has been performed by means of coherent structures visualization. Such a analysis revealed that a fluid-dyanmic vortex structure is significantly affected by reactor configuration. Typical fluid-dynamic structures associated with jet growth can be highlighted for one single and 2 inlets reactor configurations meanwhile a vorticity "tube" structure can be highlighted for 4 inlet jets reactor configuration. Coherent structures visualization revealed a strong increase of vorticity into the reactor for 4 inlet jets case respect to other geometries considered.

Finally, in this chapter a frequency analysis has been performed in order to characterize a vortex structure. Such a analysis revealed a more marked 3D vortex behavior for one single inlet reactor configuration (due to a non-symmetrical structure) respect to 2 and 4 inlet jets configurations characterized by a well/defined quasi 2D fluid-dynamic structure. Analysis has been carried out at different monitoring points along reactor height and at several distances from vortex centre. Frequency analysis showed that a cyclonic flow is characterized by a complex structure. In fact, for a fixed configuration, Swirl and inlet Reynolds number, different frequencies of velocity components have been obtained varying location of monitoring point, suggesting that a vortex structure connected to a cyclonic flow evolves on several spatial and temporal scales. For a fixed monitoring point, similar frequencies of engulfment parameter (K_{glf}) and velocity magnitude has been detected, highlighting that such a parameter is strongly associated with velocity magnitude and its fluctuations and local vorticity. Furthermore, such a frequency results a function of total flow rate. For all the configurations analyzed, frequency analysis suggested that velocity associated with stream-wise jet direction is the main velocity component at the vortex boundary meanwhile axial velocity is the principal component at the vortex core.

In conclusion, proposed reactor configurations, based on a cross-interference of opposed multiple jets in order to create a stable and intense cyclonic vortex flow are characterized by: absence of fluid-dynamic instabilities, presence of a strong, fast and stable mixing, together with residence times compatible with kinetic times. Such a peculiar characteristics make these novel reactor configurations useful for MILD-LP combustion applications and superior in terms of efficiency with respect to the conventional technologies.

Chapter 6

Novel Solar Vortex Gasifier

6.1 - Introduction

In this chapter the main results obtained during my visiting research period at CET of University of Adelaide are presented and discussed. More specifically, this chapter presents the design and modeling of a novel SolarVortex Gasifier for applications in the energy sector.

First of all, an brief state of the art of Solar Gasification processes,and the identification of the problem is reported. Then, the results will be presented by dividing them into paragraphs according to the different aspects of the process investigated. Thus, the first session is related to CFD analysis, carried out in order to define a novel reactor geometry.

Second session reports particle residence time distribution evaluation as function of main critical parameters, namely geometrical factors, total inlet flow rate and particle diameter.

During CFD analysis, particular attention was devoted to understand the effect of geometrical parameters on the cyclone vortex structure developed into the chamber, in terms of vortex core dimension and vortex shape.

6.2 - Solar Gasification

6.2.1 General Concepts

Gasification is a process that, under addition of a gasification agent, usually steam, converts any carbon-containing material, such as coal, petroleum, coke, biomass or waste into a synthesis gas (syngas) composed primarily of CO and hydrogen. This endothermic reaction takes place at temperatures above approximately 1000 K.

Recently, gasification has gained in importance as an environmentally-friendly disposal and conversion technology of residues from heavy crude oil processing. Conventional gasification is also used in integrated gasification combined cycle (IGCC) plants fired with

low or negative-valued feedstocks for clean and efficient electricity production (Rezaiyan and Cheremisinoff, 2005)

In conventional gasification the energy required to heat the reactants and to run the chemical reaction is either produced by partial oxidation of the feedstock (auto-thermal gasifiers) or provided externally (allothermal gasifiers). Auto-thermal gasification has the advantage that any losses associated with the heat transfer are avoided and the construction of the gasifier is simplified. Furthermore, the temperature can be adjusted quickly and accurately by regulation of the amount of oxygen injected. On the other hand, allothermic gasification usually results in higher-quality syngas, because the products are not contaminated by combustion byproducts. Gasification reactors are divided into three groups depending on how the solid fuel is brought into contact with the gasification agent: fixed/moving bed, fluidized bed or entrained flow. The type of reactor influences the residence time, reactor temperature and pressure, and certain characteristics of the produced gas. For this reason each reactor type is suited for a specific type, rank, and size distribution of solid feedstock.

Fixed/moving bed gasifiers contain a bed of lump fuel supported by a grate and maintained at a constant height. The feedstock is fed from the top end and flows countercurrent to the rising gas stream. A single particle moving through the bed passes different zones including drying and preheating, devolatilization, gasification, oxidation, and ash removal. Fixed bed gasification systems are simple, reliable and offer high efficiency with respect to feedstock and energy consumption. Outlet gas temperature are in the range 425–650 ○C, feedstock size is between 6 and 50 mm. As a consequence of the moderate temperatures the product gas contains around 10% hydrocarbons, mostly CH_4. A typical example of a commercial fixed bed gasifier can be found in (Lurgi, 1970). Fluidized bed gasifiers accept feedstock as grains with a size in the range 6 to 10 mm. The solid feedstock is suspended on upward-blowing jets of the gasification agent. The result is turbulent mixing of gas and solids. The tumbling action, much like a bubbling fluid, provides more effective chemical reactions and heat transfer. Reactors of this type are characterized by outlet gas temperatures in the range 900 to 1050 °C, a high specific gasification rate and product uniformity. A typical example of the fluidized bed technology can be found in Bogner and Wintrup,.1984).

Entrained-flow gasifiers are operated with pulverized feedstock with generally particles of less than 100 μm. The solid feedstock is entrained with the gasifying agent to react in a

concurrent flow having the form of a high temperature flame. The principal advantages of this process are the ability to handle practically any coal as feedstock and to produce a clean, tar-free and low-in-methane synthesis gas. Entrained-flow reactors require relatively high flow rates leading to small residence times. In order to obtain full conversion of the coke, entrained flow reactors operate at very high temperatures (above 1400 ○C) and require, therefore, a comparably high oxidant supply. Devolatilization products are released in the high temperature region and thus further cracked and oxidized. This technology has bee selected for the majority of commercial IGCC plants. The two best-known types of entrained-flow gasifiers are the top-fired coal- water-slurry feed gasifier, as used in (Schlinger. 1984) and the dry coal feed side-fired gasifier (Vogt et al.,1981).

Solar thermochemistry refers to a number of process technologies that harness concentrated solar energy by absorbing sunlight in an endothermic chemical reaction occurring at high temperatures. The products of these chemical reactions are usually called solar fuels or solar energy carriers, as they carry solar energy in an amount equal to the reaction's enthalpy change. Overviews on the different technologies envisaged and on processes that were experimentally demonstrated are given in (Kodama, 2003; Fletcher, 2001; Steinfield and Palumbo, 2001). Of all these processes upgrading and decarbonization of fossil fuels results of particular interest for several applications.

The processes involved in upgrading and decarbonization of fossil fuels can be grouped into three categories: (a) solar thermal cracking of hydrocarbons, in which solid carbon and hydrogen is produced, (b) solar reforming, in which a gaseous hydrocarbon is reacted to a H_2-CO mixture (syngas) in a steam or CO_2 atmosphere, and (c) solar steam-or CO_2-gasification of solid carbonaceous materials (von Zedtwitz et al., 2001). High temperature solar pyrolysis of coal and biomass was already reported in 1983 byW. H. Beattieand et al and Antal et al., respectively. The solar pyrolysis of oil shale and the recovery of the volatile product was reported by Berber and Fletcher (1988). Lately, research focused on thermal splitting of methane into hydrogen and carbon black. Successful lab-scale experiments were reported by Abanades and Flamant.(2006), Dahl et al. (2004), Hirsch and Steinfield (2004). The solar reforming of methane was reported among others by (Dahl et al., 2001; Kodhama et al., 2004; Buck et al.,1991).

Solar thermal gasification is gaining attention due to its ability to provide an alternative and cleaner pathway to process carbonaceous materials often derived from fossil fuel refinement processes. As stated by Z'Graggen and Steinfeld (2008); Trommer and

Steinfeld (2006), the advantages of using solar energy to drive the endothermic gasification process are numerous and include upgraded calorific value of the carbonaceous feedstock, higher H_2 to CO ratio in the product syngas compared with the syngas derived in conventional auto-thermal gasification, reduced pollutants discharge due to the lack of combustion, and the elimination of oxygen input.

A review of literature (Steinfield 2005; Piatkowski et al. 2011) suggests that as well as for conventional gasification, there all existing solar gasification reactors can be categorized into one of the three groups; packed bed, fluidized bed and entrained. Each group has its characteristic residence time and operating temperature.

Packed bed solar gasification reactors generally have the longest residence time and the lowest operating temperature out of the three groups. The gasification agent, usually steam or CO_2, is passed through a packed bed of reactant materials either from above or below (Piatowski 2011; Taylor et al. 1981). Packed bed solar gasification reactors cannot be scaled up easily because the timely removal of hot ash and the addition of new bed are materials very difficult to achieve for large scale systems (Taylor et al. 1981).

The residence time and operating temperature of fluidized bed solar gasification reactors are typically between that of packed bed and entrained flow. In fluidized beds, feedstock particles are semi-suspended in turbulent motion by the gasification agent until they are fully reacted or reach a small enough size to be entrained and carried out of the bed by the gasification agent. The distribution of temperature within fluidized beds is highly uniform due to the enhanced heat and mass transfer rates of turbulent mixing. The operating temperature is usually kept below 980 °C for coal and 900 °C for biomass materials to prevent ash fusion (Basu 2010). An example of fluidized bed solar gasification reactor is the internally circulating fluidized bed solar gasification reactor developed by Kodama et al. (2008). Experimental runs showed that the buildup of ash inside the fluidized bed is detrimental to the reactor's energy conversion efficiency. An ash removal system needs to be implemented before the reactor can be scaled up.

Entrained flow solar gasification reactors operate at elevated temperatures, usually above 1500K, to compensate for their relatively short residence time (Z'Graggen 2008). The feedstock particles need to be very fine so they could be entrained and fully react within the reactor cavity. Vortex flow is employed in all entrained flow solar gasification reactors because it provides the longest path for particles, maximizes the residence time and increase the solar irradiation absorption area by keeping the particles near the wall. Hence,

sometimes entrained flow solar gasification reactors are referred to as vortex flow solar gasification reactors or solar vortex gasifier (SVG). One major benefit of entrained flow solar gasification over packed bed and fluidized bed is the timely removal of hot ash and waste materials by the intense vortex flow. Entrained flow reactors could be easily scaled up from a laboratory prototype without implementing a specific hot waste disposal system. Therefore, the entrained flow configuration is the most promising of the three mentioned.

The research group led by Steinfeld at the Swiss Institute of Technology Zurich (ETH) has been developing directly irradiated entrained vortex flow solar chemical reactors for the gasification of carbonaceous materials, methane decomposition and coproduction of Zn and syngas. Their 5kW reactors generally consist of a quartz window, a compact parabolic concentrator (CPC), an aperture and a cylindrical cavity which efficiently captures the concentrated solar radiation entering through the aperture. Particles are injected into the reactor through tangential inlets to obtain a vortex flow structure in the reactor. The cylindrical cavity also helps establishing a stable continuous vortex flow to entrain particles and directly expose them to solar radiation. Particles absorb the concentrated solar radiation and react within the cylinder. Fig. 6.1 shows the reactor used by Steinfeld's research group for the solar gasification of petroleum coke and water slurries.

Using the reactor in Fig. 6.1, Z'Graggen et al. (2006, 2012) successfully demonstrated

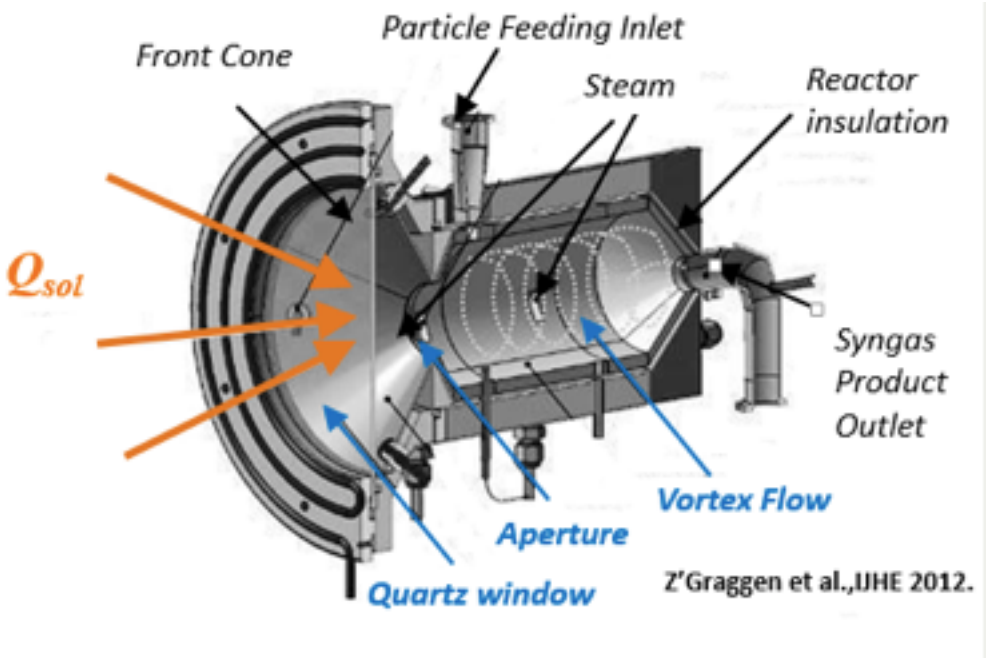

Fig. 6.1 -Schematic diagram of the solar vortex gasifier developed by Steinfeld's group.

the steam gasification of petroleum coke powder, coke-water slurry and liquefied vacuum residue. Dry coke powder showed the highest solar to chemical energy conversion efficiency. From the experimental data, a model of the 5kW laboratory scale reactor was developed, and validated. The model found that tube shaped cavity performs better than the commonly used barrel shaped cavity because more particles are exposed to the high flux solar radiation. The same model also predicted that large scale vortex flow solar gasification reactors would be more efficient than the laboratory scale one due to improved insulation (Z'Graggen, 2008 PhD Thesis).

6.2.2 Development of a Novel Solar Vortex Gasifier: Identification of the problem

While there are many benefits to vortex flow solar gasification, it is still not ready for large scale pilot studies because of two key issues. In details, literature highlights that keeping the window clean from particle deposition and short residence time of particles into the reactor are the main challenges to be solved for a strong development of this technology for large scale applications (Steinfield 2005; Ozalp et al., 2013). Such issues significantly affect chemical conversion of particles, reactor efficiency and can lead to a failure of the system.

The reactor window is a critical part of solar gasification technology. More specifically, it is used to control the atmosphere in the gasifier and prevent the egress of particles from it. The window in directly irradiated solar chemical reactors often suffers from the overheating due to the decreased transparency caused by particle deposition, leading to a reduction in the solar power absorption and potential failure due to overheating.

Trial tests (Kodama et al. 2008; Kogan & Kogan 2002; Hirsch & Steinfeld 2004) conducted using directly irradiated solar chemical reactors have shown that particle deposition on the window poses a great challenge to the continuous operation of these reactors.

Hirsch and Steinfeld (2004) designed, fabricated a 5kW prototype directly irradiated vortex flow methane decomposition reactor. Carbon black particles were seeded in the methane flow to enhance heat absorption and transfer. During their experimental runs, they experienced difficulties keeping the reactant/product particles off the window, particularly

when the reactor was placed vertically. To combat the problem of window deposition, carbon black particles were only seeded intermittently, and some optimization experiments had to be ended before steady state. Hirsch and Steinfeld (2004) attributed the severe deposition on the window in the vertical position to buoyancy effects.

Currently, tangential purging gas nozzles are added between the window and the compact parabolic concentrator (CPC) to prevent particles from going through the aperture and reaching the window (Kogan and Kogan, 2002; Hirsch and Steinfield, 2004; Krishna and Ozalp, 2013). The introduction of purging gas dilutes the products and decreases the energy conversion efficiency because a portion of the incoming solar energy is absorbed by the purging gas to raise its temperature to the reactor's operating temperature. Adding purging gas nozzles is a passive post design solution to the problem of particle deposition on the reactor window. Furthermore, purging gas nozzle locations are strongly connected with the fluid-dynamic flow structure established into the cavity and the operative working conditions adopted (Yu et al, 2012). An alternative and better approach would be eliminating the particle deposition on the window through the manipulation of the reactor cavity's flow field which depends on its geometrical parameters.

The second issue that needs to be addressed is the short residence time within the vortex flow solar gasification reactor cavity. Reactor performance can be assessed through parameters such as solar to chemical energy conversion efficiency and conversion extent for a certain reactant. Both parameters rely on residence time. To put simply, longer residence time allows more reactant particles to complete their reactions.

The solar vortex gasifier developed by Steinfeld's research group at ETH achieved a peak solar to chemical conversion efficiency of 26% using coke and water slurry mixtures during the experimental runs at PSI's solar furnace (Piatowski et al. 2011). The mentioned efficiency shows that the solar vortex gasifier is much more efficient than the other continuously fed solar chemical reactors which typically have energy conversion efficiencies in the range of 8 to 16% (Kodama et al. 2008; Taylor et al. 1983; Hirsch and Steinfeld 2004; Z'Graggen et al. 2006).

In order to increase the effectiveness of solar gasification reactors, there needs to be a strategy to increase the energy conversion efficiency and solid fuel conversion extent. One possibility is to increase residence time of particles in the reactor chamber so that they have enough time for complete conversion (Ozalp et al.,2012-2013). This issue can be addressed by manipulating reactor geometrical parameters.

Furthermore, it is desirable for the particle's size would be a direct function of its residence time within the reactor. It is well known in literature that the time for a complete conversion of a particle depends on particle size and gasification reactions affect particle's size. (Vicente et al., 2003). As reaction proceeds a particle gradually becomes smaller. The particle's size is also related to the fuel properties. For example, coal and biomass feeds to a gasifier show very different properties especially for which concerning particle size distribution (Wilk and Hofbauer,2013; Ocampo et al.,2003; Kruesi et al, 2014).

It maybe undesirable for smaller particles to spend too long in the reactor while the bigger particles too short. If there is a strong correlation between particle size and residence time, particles regardless of their sizes would just have enough time to completely react within the reactor.

In this view, a novel design of a solar vortex gasifier is proposed in order to develop an efficiently and flexible reactor in which at the same time the window appears clear without the use of auxiliary purge gas, high residence time of solid particle can be obtained and residence time distribution of particle results a function of particle's size. To address this scope, CFD Analysis has been performed in order to evaluate the effects of changing key parameters, namely geometrical factors, total flow rate and particle size, on window state, mean residence time and the residence time distribution of solid particle.

6.3 - Results and Discussions

6.3.1 Geometry Definition

The proposed geometry is shown in Figure 2. As can be seen in Figure 2, the geometry resembles a cyclone gas solid separator. There are 4 tangential injection inlets at the bottom in order to create a strong vortex flow within the cavity. The outlet is positioned up the top near the aperture. The exact location of the outlet is an investigated variable. The outlet and inlet areas are arranged such that velocities of flow entering the cavity and exiting the cavity are the same.

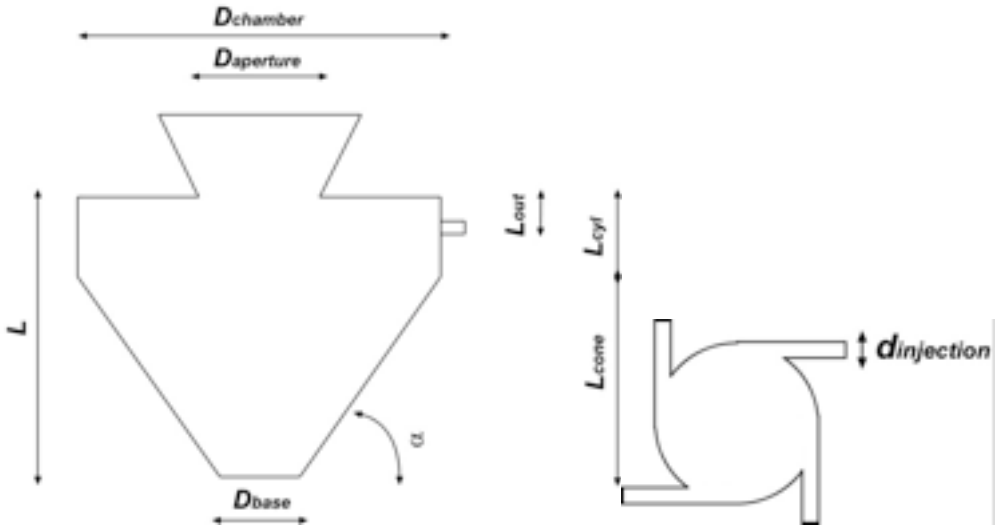

Fig. 6.2 -Proposed geometry frontal view (left) and top view (right)

The dimensions of the proposed geometry are calculated theoretically and taken out of literature. For a feasibility study of industrial scale solar vortex gasification, the power input into the proposed geometry was set to be 1 MW. Using an average solar radiation flux of 2.5MW/m2, the aperture diameter was calculated to be 40 cm. The diameter of the cone base (D_{base}) is 10 times that of the inlet cross sectional area. More specifically, D_{base} is 30cm, meanwhile $d_{injection}$ is 3 cm.

The conversion extent within the reactor is assumed to be 100%, and the energy conversion efficiency 56% (Z'Graggen, 2008 PhD Thesis). From the two mentioned idealized assumptions, the amount of carbon gasified per second and the required steam flow rate were calculated. The resultant inlet velocity was calculated to be 20m/s.

The proposed geometry differs from the common solar vortex gasifiers developed by Steinfeld's group in two ways; the shape of the reactor cavity is a combination of a cone and cylinder, and reactants are fed in from the bottom and exit up from the top. The addition of the cone is to enhance the recirculation and capture of particles in the bottom part of the cavity. Therefore, the cone angle is a critical operating parameter. Sensitivity analysis was carried out varying the cone angle, the ratio of aperture to reactor, reactor length and outlet position to obtain a first optimized geometry which prevents the deposition of particles on the window. Using this geometry, flow rates and particle size effects on the residence time were investigated.

6.3.2 Numerical Procedure

Design of a solar vortex gasifier is a complex problem that involve heat transfer, chemistry and fluid-dynamic modeling of fluid and solid phase. Due to the complex nature of the vortex flow solar gasification, the current paper only focuses on the fluid dynamics aspect of the proposed vortex flow solar gasification reactor. Reaction kinetics and heat transfer would investigated in subsequent papers.

A commercial finite volume based tool, Ansys 14.0 is employed in the simulations. These simulations involve fluid flow, turbulent species transport and particle tracking. The proposed three-dimensional geometry is first built with Gambit and a non uniform unstructured grid is generated with ANSYS 14 Workbench. Mesh independence and mesh quality were checked to ensure the suitability of the mesh. The total number of elements for all the configurations tested are approximately 2 million. Fig. 6.3 reports an example of mesh used during analysis.

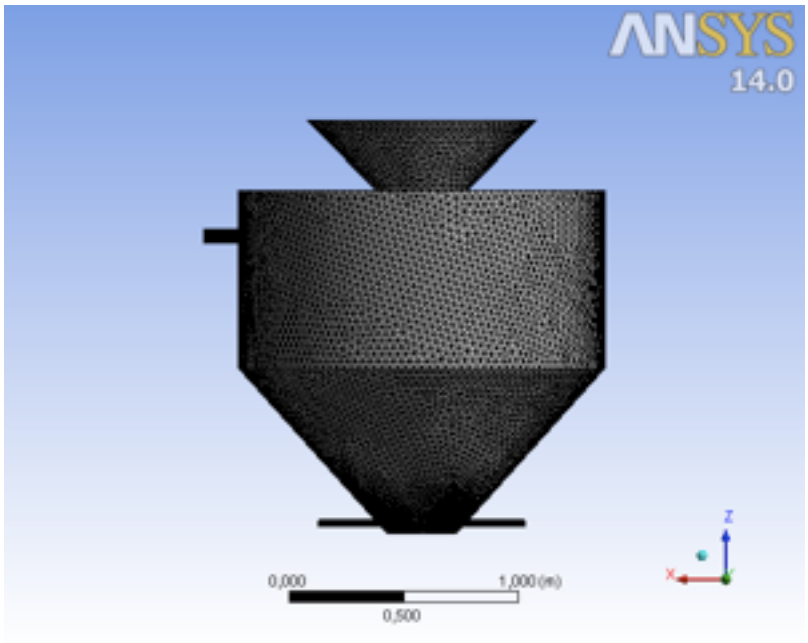

Fig. 6.3 -Example of mesh adopted during analysis.

Since chemistry is not considered in the simulations and the gasification process is significant at elevated temperatures, steam at 1000K has been chosen to represent the fluid phase and the transport properties i.e. density and viscosity.

To model the vortex flow structure correctly, several factors were taken into account, namely the high curvature of the average streamlines, high swirl intensity and radial shear and adverse pressure gradients in recirculation zones. These three features make the turbulence in a vortex flow highly anistropic (Cortes and Gil, 2007). First order closure turbulence models could be very weak to predict the vortex flow realistically (Cortes and Gil, 2007). Second order closure models i.e. Reynolds Stress Model are often adopted in literature to obtain a more realistic prediction of the flow (Cortes and Gil 2007). However, second order closure models generally require more CPU-time compared with first order closure turbulence models. Furthermore, solution convergence is more difficult to obtain.

In literature, K-epsilon RNG with swirl factor and curvature correction was found to be a reliable first closure model to predict vortex flow behavior in a confined chamber. Several papers adopting this approach for modeling a solar vortex reactor can be found in literature (Ozalp and Jaya Krishna, 2010; Jaya Krishna and Ozalp, 2013; Ozalp and Kanjirakat, 2010).

Therefore, this model is implemented in the current study. As stated previously, to simplify the modeling and ensure accuracy, chemical reactions, heat transfer and gas-particle interaction are not considered in the current simulation. The steady state equations pertaining to the present analysis consist only of momentum, continuity, K and epsilon and are reported below:

Continuity Equation:

$$\frac{\partial(\rho u_i)}{\partial x_i} = 0$$

Momentum Equation:

$$\frac{\partial\left(\rho u_i u_j\right)}{\partial x_j} = \frac{\partial P_{eff}}{\partial x_i} + \frac{\partial}{\partial x_j}\left[\mu_{eff}\left(\frac{\partial u_i}{\partial x_j} + \frac{\partial u_j}{\partial x_i}\right)\right] - \rho g_i$$

K – equation:

$$\frac{\partial(\rho k u_i)}{\partial x_i} = \frac{\partial}{\partial x_j}\left(\left(\mu + \frac{\mu_i}{\sigma_k}\right)\frac{\partial k}{\partial x_j}\right) + G_k - \rho\varepsilon$$

ε – equation:

$$\frac{\partial(\rho \varepsilon u_i)}{\partial x_i} = \frac{\partial}{\partial x_i}\left(\left(\mu + \frac{\mu_i}{\sigma_k}\right)\frac{\partial k}{\partial x_j}\right) + C_{1\varepsilon}\frac{\varepsilon}{k}G_k - C_{2\varepsilon}\rho\frac{\varepsilon^2}{k} - R_\varepsilon$$

Where

$\mu_{eff} = \mu + \mu_t$

$\mu_t = \rho C_\mu \frac{k^2}{\varepsilon}$

$P_{eff} = P + \frac{2}{3}\rho k$

$C_\mu = 0.0845$

$C_{1\varepsilon} = 1.42$

$C_{2\varepsilon} = 1.68$

$C_{3\varepsilon} = \tanh\left|\frac{u_3}{\sqrt{u_1^2 + u_2^2}}\right|$

$G_k = \mu_t S_{ij} \frac{\partial u_i}{\partial x_j}$

$R_\varepsilon = \frac{C_\mu \rho \eta^3 \left(1 - {}^{\eta}/_{\eta_0}\right)}{1 + \beta\eta^3} \frac{\varepsilon^2}{k}$

$\eta = \frac{Sk}{\varepsilon},\ S = \left(2S_{ij}S_{ij}\right)^{1/2},\ \eta_0 = 4.38,$

$\beta = 0.012,\ \sigma_k = 0.7179,\ \sigma_\varepsilon = 0.7179$

$S_{ij} = \frac{\frac{\partial u_i}{\partial x_j} + \frac{\partial u_j}{\partial x_i}}{2}$

Discrete Phase Model (DPM) was implemented to evaluate the particle trajectories through the fluid phase, so that their residence time and behavior can be investigated.A Lagrangian framework is expected to be accurate for entrained flow gasification where particle volume fractions are dilute, on the order of 1-4 %, contrary to fluidized bed gasifiers, where the volume fraction of the dispersed phase is high enough to make particle-particle interactions significant (Kumar and Ghoniem, 2012).

With this approach, the motion of a particle is calculated by integrating the force balance on the particle in the Lagrangian reference frame. For particles much heavier than the fluid ($\rho_p / \rho >> 1$), Elghobashi and Truesdell (1992) have shown that the only significant forces are Stokes drag and buoyancy and that Basset force can be neglected being an order of magnitude smaller. In this study, particle trajectory is calculated as:

$$\frac{du_{p,i}}{dt} = F_D(u_i - u_{p,i}) + \frac{g_i(\rho_p - \rho)}{\rho_p}$$

Where F_D is:

$$F_D = \left(\frac{18\mu}{\rho_p d_p^2}\right)\frac{C_D Re_{p,i}}{24}$$

And the Reynolds number is:

$$Re_{p.i} = \frac{\rho_p d_p |u_{p,i} - u|}{\mu}$$

To save on computational resources, one way coupling approach was used for the discrete phase, so that discrete phase does not affect the fluid-dynamics of the fluid phase. 5000 carbon spherical particles with the density 2000 kg/m^3 were injected from the inlets of the reactor. The dispersion of particles due to turbulence in the continuous fluid phase was predicted using stochastic tracking model, in the discrete random walk, the fluctuating velocity components are sampled assuming the Gaussian probability distribution. Mono sized particle injection varying particle diameter from 1 micron up to 1000 micron were carried out to evaluate the effects of particle's size on particle residence time distribution in the reactor. In particular, the residence time of each particle is recorded at the reactor outlet as each particle exits from the reactor and the residence time distribution was obtained by plotting the histogram of time of the number of particles that leave the reactor at each time interval. Reactor walls have been considered as a reflect boundary.

The governing equations are solved using the finite volume method. SIMPLE algorithm has been employed for pressure-velocity coupling. All the equations are discretized using the second order upwind scheme. Simulation is considered converged when all the residuals arrive at 10^{-6}.

6.3.3 Test Cases

As reported previously, K-epsilon RNG with swirl factor and curvature correction is implemented in the current study for modeling vortex. As highlighted in chapter 4, such a first closure turbulence model is able to predict peculiar behaviors of a vortex flow .

In the context of solar vortex gasifier, few relevant experimental data are available, data needed to test and validate different closure model. Recently (Ozalp et al., 2013) reports significantly PIV data of their solar cyclone reactor under non reactive conditions for several working conditions. Tangential and axial velocity profiles together with vortices contours along reactor height are available.

In this view, Ozalp's reactor has been modeled testing four different turbulence models, three first closure models, namely standard K-ε, RNG K-ε with swirl factor and curvature correction, K-omega SST with curvature correction and one second closure model, Reynolds Stress Model (RSM). Results were compared with experimental data in order to understand wich closure models are suitable to model solar vortex reactor.

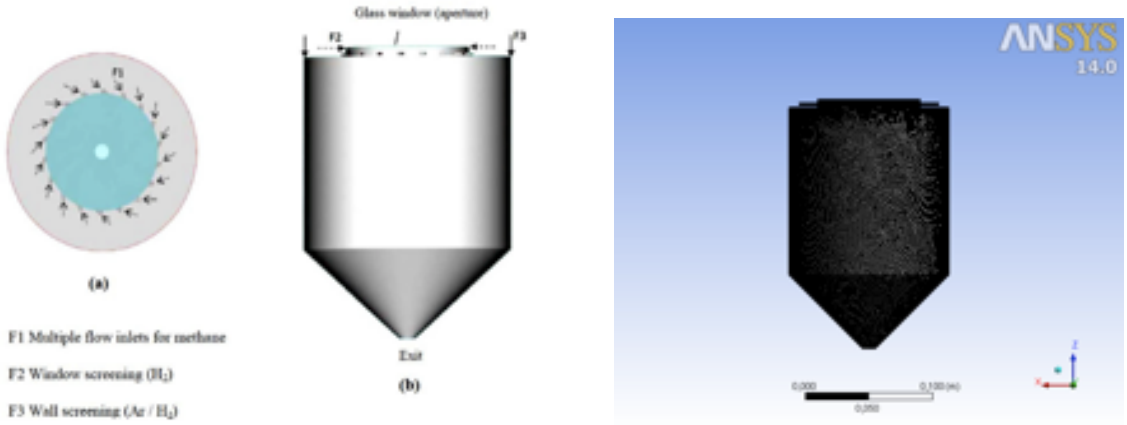

Mesh	
Nodes	1585717
Elements	3283031

F1	10 l/min
F2	1 l/min
F3	10 l/min

Fig. 6.4 -Scheme of Ozalp's group reactor with mesh and standard operative working conditions (100% CFD settings) details.

Fig. 6.5 reports comparison between experimental and calculated tangential velocity profiles at z= 0mm, varying turbulence closure models and total inlet flow rate.

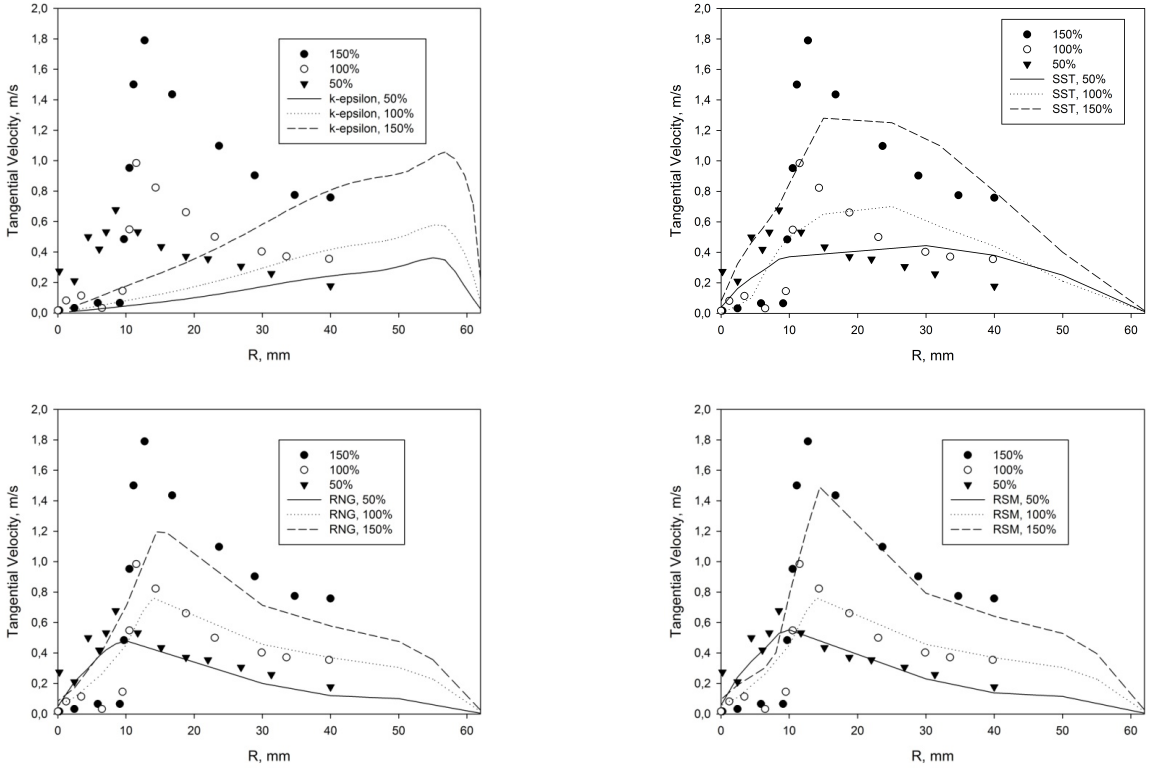

Fig. 6.5 -Experimental and calculated tangential profiles of Ozalp's reactor with different closure models.

It is worthwhile to note that not all closure model tested are in agreement with experimental data. More specifically, standard K-ε gave large discrepancies between the measured and calculated velocity profiles, predicting a forced vortex instead of a combined one. Such unusual behavior is well documented in literature (Cortes and Gil, 2007).

K-omega SST with curvature correction, RNG K-ε with swirl factor and curvature correction and RSM show a good agreement with experimental data. In particular, of first closure models tested, RNG K-ε shows the best agreement with experimental data. RSM (second closure model) results more accurately of RNG K-ε but at the same time is very CPU-time consuming, so that RNG K-ε has been chosen for the current study.

It is worthwhile to note that not all closure model tested are in agreement with experimental data. More specifically, standard K-ε gave large discrepancies between the measured and calculated velocity profiles, predicting a forced vortex instead of a combined one. Such unusual behavior is well documented in literature (Cortes and Gil, 2007).

K-omega SST with curvature correction, RNG K-ε with swirl factor and curvature correction and RSM show a good agreement with experimental data. In particular, of first

closure models tested, RNG K-ε shows the best agreement with experimental data. RSM (second closure model) results more accurately of RNG K-ε but at the same time is very CPU-time consuming, so that RNG K-ε has been chosen for the current study. Other test cases for closure models comparison concerning cyclonic reactor configurations (not solar applications) are reported in Appendix A.4.

Particle tracking procedure adopted in this study has been tested based on results of Steinfield's group reactor (Hirsch and Steinfield, 2004). Mesh adopted and simulation details are reported in Fig. 6.6.

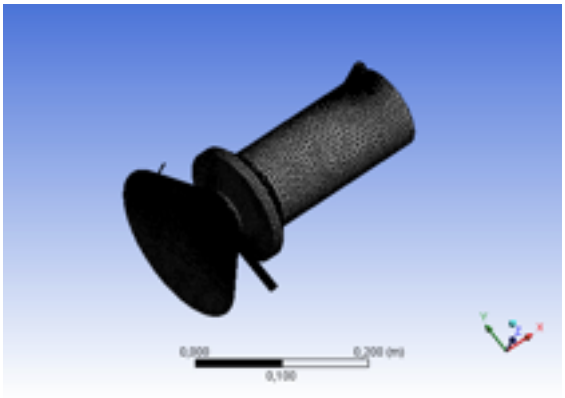

Space Time, V/ Q, s	*Total Flow Rate, l/ min*	*Evaluated Mean Residence Time, s*	*Numerical Mean Residence Time*
4.95	*19*	*7.3*	*8.1*

Fig. 6.6 -Geometry of Steinfield reactor and simulation details.

Hirsch and Steinfield carried out experiments for methane decomposition in their vortex flow solar reactor, observing a mean residence time of 7.3 s. Adopting numerical procedure previously descripted, mean reactor residence time,,particle residence time distribution and particle pathlines have been obtained. Carbon particles with a diameter of 1 micron were used in this analysis in order to obtain an ideal tracer behavior. A good agreement between experimental and evaluated mean residence time was found. Fig. 6.7 reports evaluated particle residence time distrubution and particle pathlines inside the reactor.

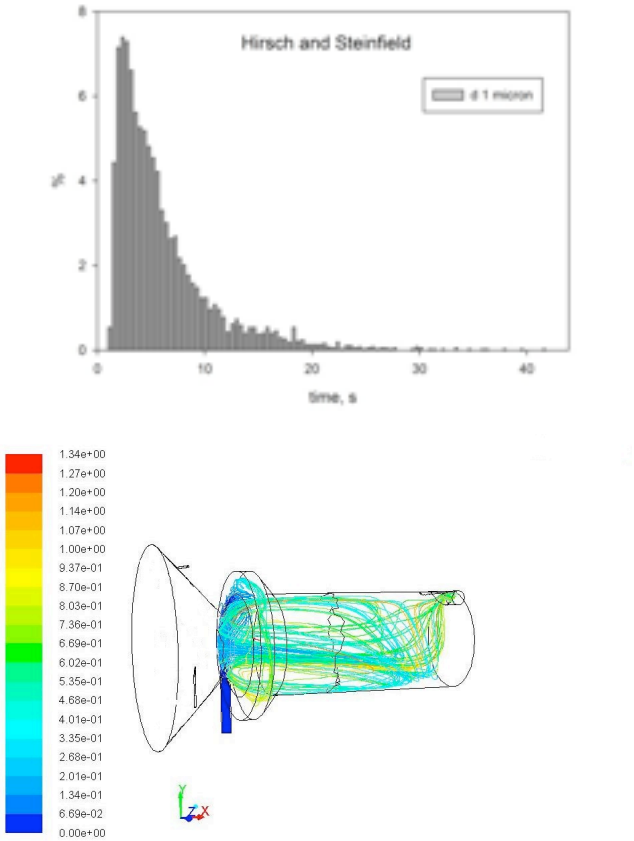

Fig. 6.7 -Particle residence time distribution and calculated pathlines released from main inlet (methane).

6.3.4 CFD Analysis:Particle Tracking

As reported previously, a sensitivity analysis was carried with varied key geometrical reactor parameters in order to select an optimized geometry which prevents the deposition of particles on the window without the use of auxiliary seal gas inlets. In order to address this aim, a criterion to assess particle deposition on the quartz window needs to be selected. The Discrete Phase Model can provide a measure of total concentration of particles in a cell, thus providing an estimation of particle density in a particular region of the reactor (Krishna and Ozalp, 2013). However, in this study, a quantification of particle concentration on the reactor window was not performed because this study focuses only on whether changing geometrical parameters can prevent particle and not their effectiveness. For this study, the particle deposition on the window can be sufficiently described with two

states, clear and not clear. The window is considered clear if no particle trajectories are present into the CPC cavity and not clear otherwise.

Fig. 6.8 shows the particle tracking analysis for two different geometrical configurations, in particular, the effect of varying cone angles on the window state. In Fig. 6.8, the particles tracked are of 1 micron which effectively makes them flow tracers, and all geometrical parameters other than the cone angle are fixed. For cases analyzed, reactor lenght is fixed to 1.5 m and $D_{chamber}/D_{Aperture}$ is equal to 3.

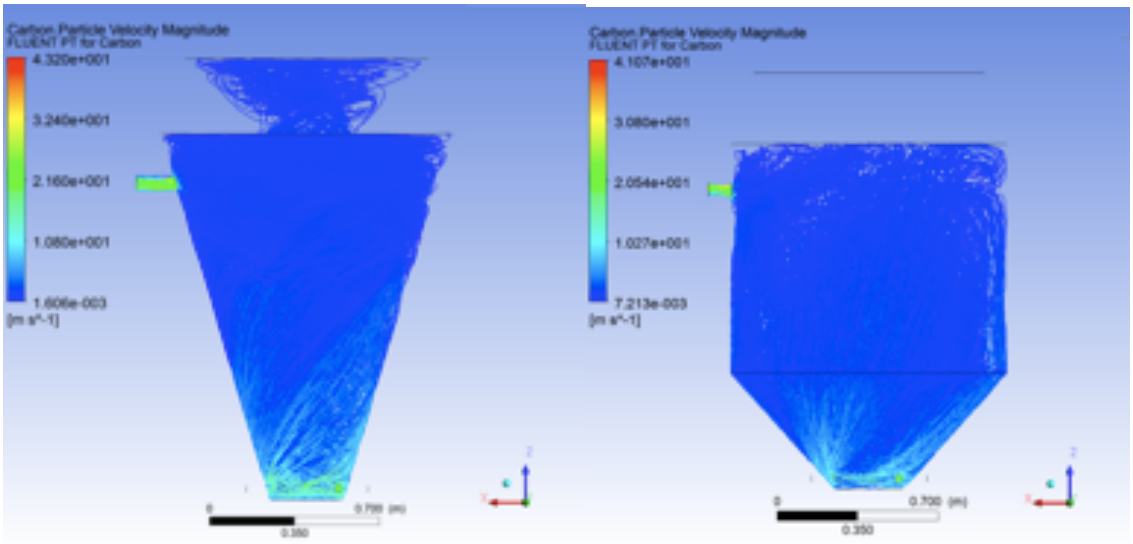

Fig. 6.8 -Particle tracking analysis for two different configurations: left) cone angle = 75 degrees and right) cone angle = 50 degrees

It can be seen that cone angle is critical in preventing particle deposition. In the 75 degrees cone angle configuration, the trajectories of the particles are present inside the CPC and thus, the window is not clear. Meanwhile, the second configuration with a cone angle of 50 degrees successfully prevented entry of particles into the CPC cavity and the deposition of particles on the window.

In order to better understand the effects of cone angle, an analysis of the velocity profiles inside the reactor has been performed. Tangential and axial velocity profiles along the reactor's length were analyzed. The locations for the velocity profiles are reported in table 6.1 and visualized in Fig. 6.9..

Line No.	Axial Location from bottom (m)
0	0.1

1	0.2
2	0.75 (half of the reactor)
3	1.3
4	1.5
5	0.1
6	0.2
7	0.75 (half of the reactor)
8	1.3
9	1.5

Tab. 6.1 -Lines Axial location for velocity profiles analysis

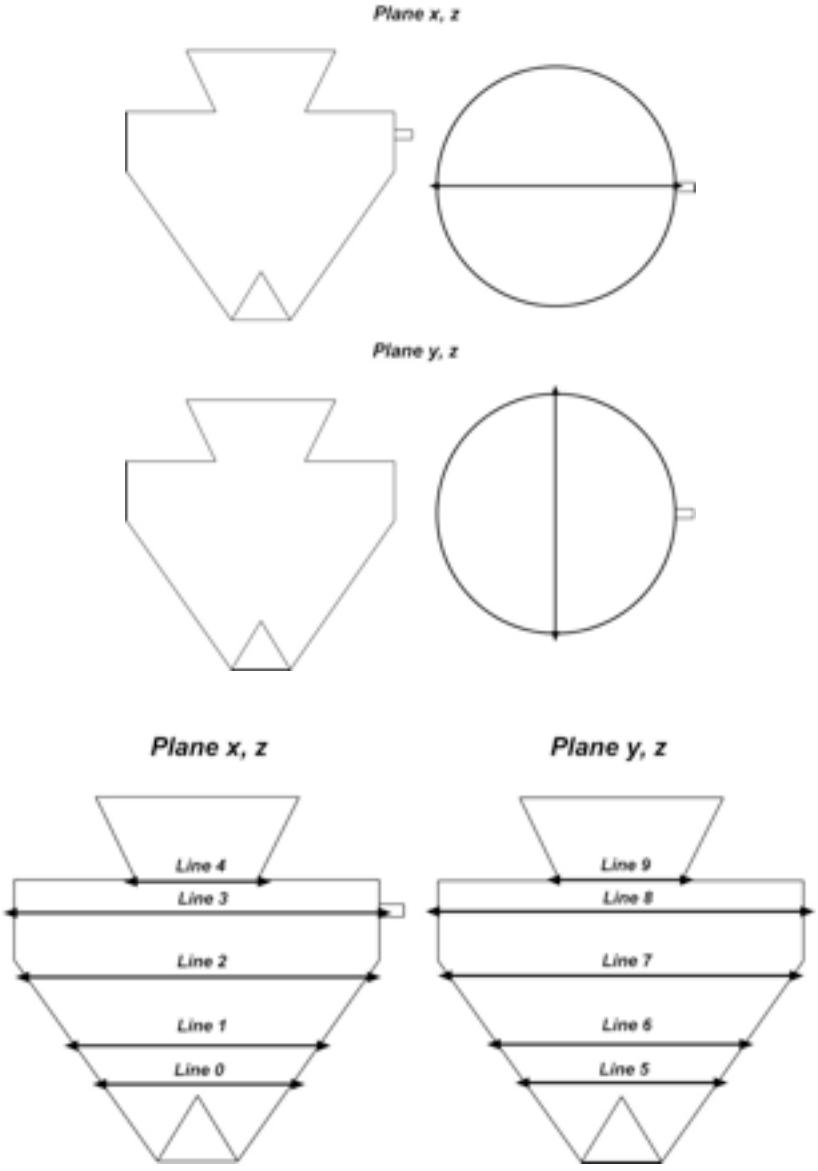

Fig. 6.9 -Visualization of lines location for velocity profiles analysis

The tangential and axial velocity profiles obtained at different axial locations for the two cone angle configurations are displayed in Fig. 6.10.

WINDOW NOT CLEAR

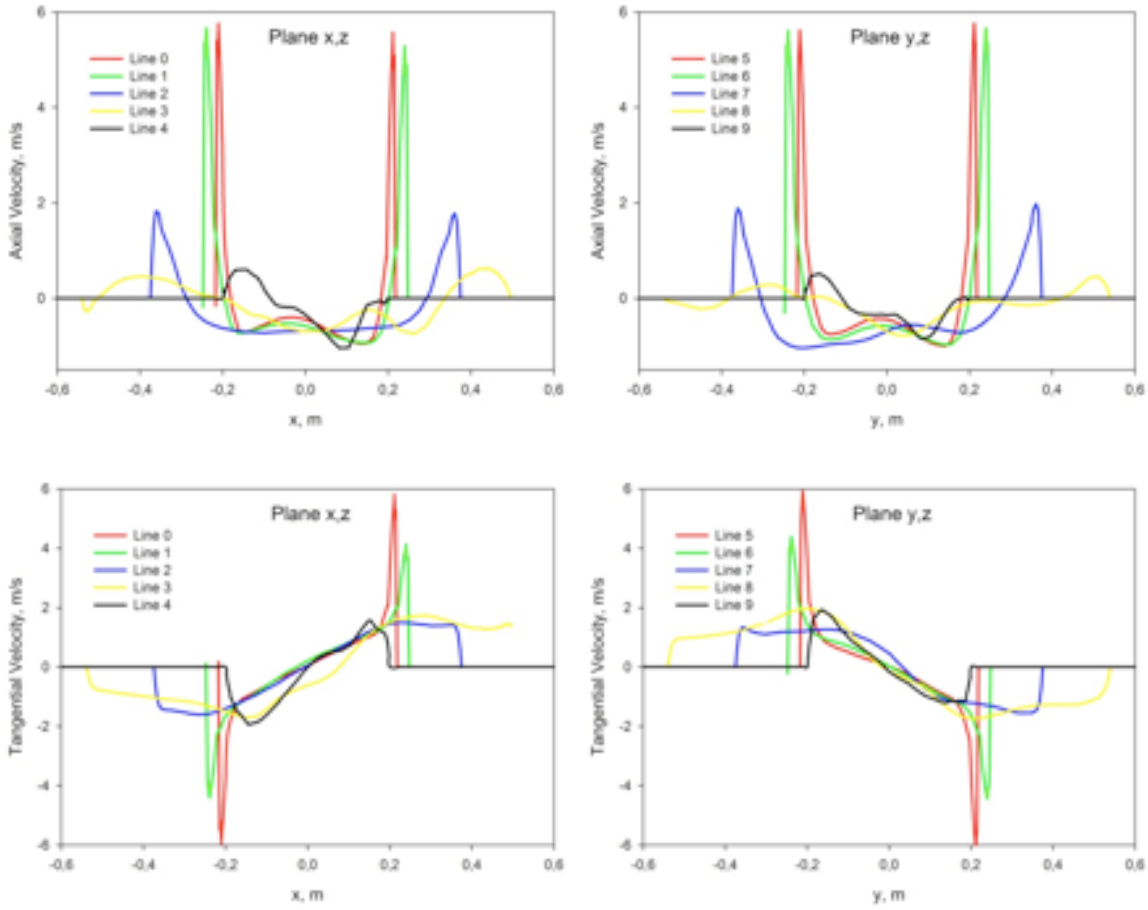

WINDOW CLEAR

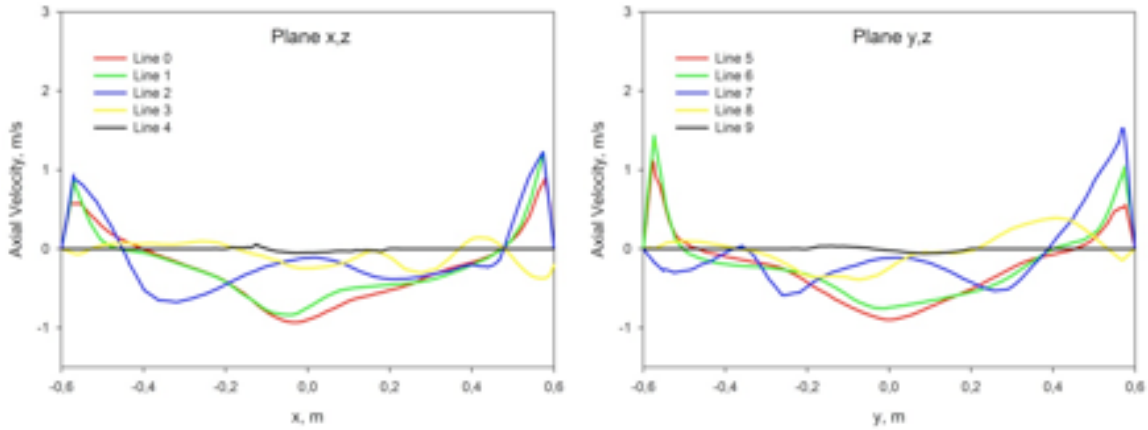

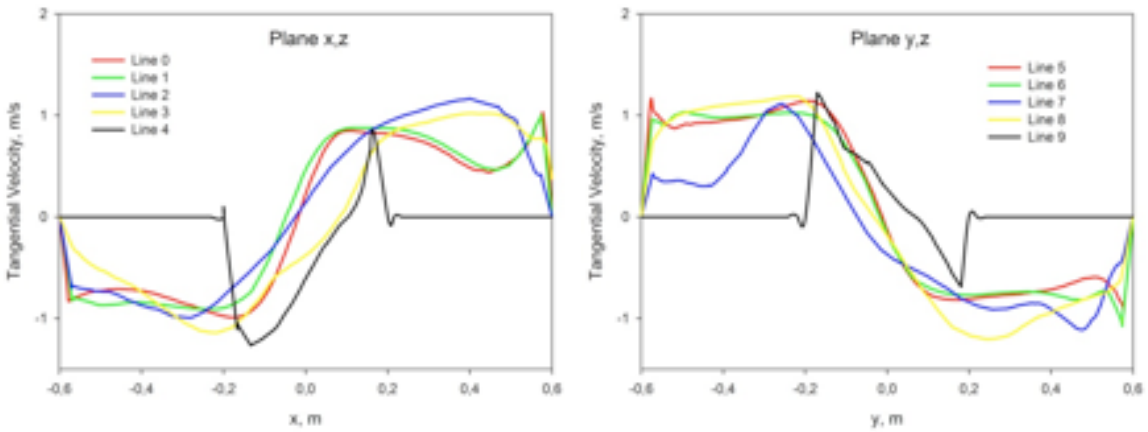

Fig. 6.10 -Axial and tangential velocity profiles taken at the axial locations mentioned in table 6.1 for two geometrical configurations; cone angle of 75 degrees (top) and cone angle of 50 degrees (bottom).

First of all, for both configurations, a well-defined vortex flow can be observed from the tangential velocity profiles. The peak tangential velocity is close to the wall for most part of the reactor cavity for both geometrical configurations. At the lower part of the reactor, a forced vortex is observed, and at the upper part, a combined vortex is seen. Increasing the cone angle leads to an increase in the magnitude of tangential velocity which reflects an increase in vortex intensity. Examining the axial velocity profiles reveals the reversed flow in the core region of the vortex for both configurations. Higher magnitudes of axial velocity can be observed along the reactor for the not clear window case with respect to the clear case. This implies that the reverse flow is stronger for the not clear case. The main difference between the two geometrical configurations is the axial velocity profile at the aperture plane. More specifically, for the clear case, the axial velocity profile is almost flat and quasi-zero, meanwhile for the dirty case, recirculation is observed in the proximity of the aperture. Furthermore, vortex core dimension results different for the two case analyzed. Vortex core can be higlighted following maximum of tangential velocity profiles along reactor height. For not clear case, vortex core appears smaller respect to clear case vortex, in particular it results smaller than aperture diameter at reactor top (i.e lines 3 and 8).

To achieve a better understanding of the flow structure and the connection between cone angle and particle deposition on the window, the front view of the iso-static pressure (relative) surface for quasi zero pressure value is visualized and shown in Figure 6.11.

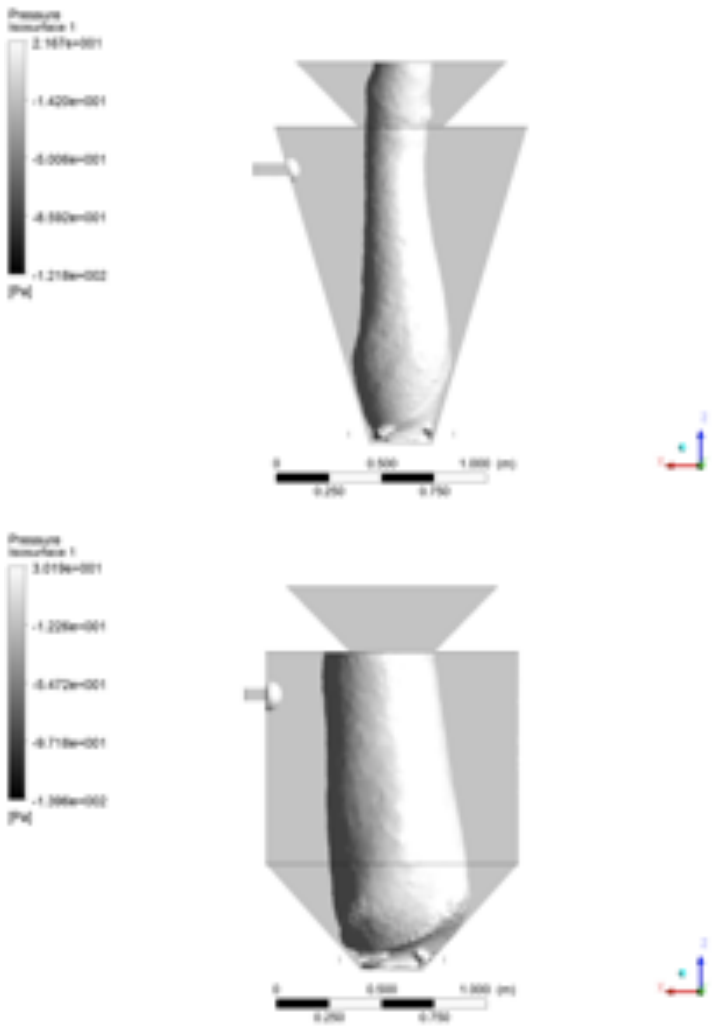

Fig. 6.11 -Iso-pressure surface for approximately zero pressure

The use of iso-pressure surface highlights the vortex core structure and dimensions. In particular, pressure threshold for surface visualization has been chosen in such a way that surface boundary fitted with maximum of tangential velocity profiles location along reactor height. As reported previously, it is worthwhile to note that in a cyclone chamber, vortex core dimension can be highlighted by maximum of tangential velocity profiles location (Wang, PhD Thesis, 2004) and vortex core can be associated with the point of least pressure (Derksen and Van den Akker, 2000; Gil and Cortes, 2007).

As can be seen in Fig. 6.11, the cone angle affects the vortex core dimensions which subsequently affect the particle deposition on the window. For the not clear case, the dimensions of the vortex core are smaller than the aperture diameter so the particles that orbit in the vicinity of the core are more likely to enter the CPC cavity through the gap

between the vortex core and aperture, supported by pressure gradient that exists between outer vortex boundary and CPC.

In the clear state case, all of the aperture is covered by the low pressure core so that particles that orbit outside of the core also orbit outside of the aperture and hence, are unlikely to enter the CPC cavity. Fig 6.10 shows that reverse flow is established at the edge of the aperture, and at the center of the aperture, a near zero velocity flow is present. This means that for the not clear case, a flat zero axial velocity only exists in the center of the low pressure core and not at the aperture edge. Small pressure gradients are desirable as they prevent large fluctuations in velocity profiles.

From Fig. 6.11, it is obvious that cone angle affect the swirling features and the dimensions of the vortex core significantly. The same CFD analysis was performed on the other key geometrical parameters, namely the reactor length and the diameter ratio of reactor cavity to aperture. Table 6.2 reports the characteristics of the geometries tested and the state of the quartz window.

In order to relate the geometrical parameters to the vortex structure, swirl number analysis was performed. The swirl number is calculated as follows (Gupta, 1984):

$$S = \frac{\int_0^{2R} v_{ax}\, v_{tg} r dA}{R \int_0^{2R} v_{ax}^2 dA}$$

Where v_{ax} is the axial velocity component, v_{tg} is tangential, and R is the characteristic dimension which is a geometrical parameter.

$$S_{bottom} = \frac{\int_0^{2R} v_{ax}\, v_{tg} r dA}{R_{bottom} \int_0^{2R} v_{ax}^2 dA}$$

$$S_{top} = \frac{\int_0^{2R} v_{ax}\, v_{tg} r dA}{R_{top} \int_0^{2R} v_{ax}^2 dA}$$

The geometries analyzed were divided into two parts; the conical bottom part and the cylindrical top part. Swirl number was calculated at lines 3 and 0 which represent the two parts respectively. In Table 6.2, the calculated swirl numbers at the top and bottom parts of the cavity, their ratio and the value of R at different heights are also reported. Particle tracking results for several geometries investigated are reported in Fig. 6.12.

WINDOW NOT CLEAR

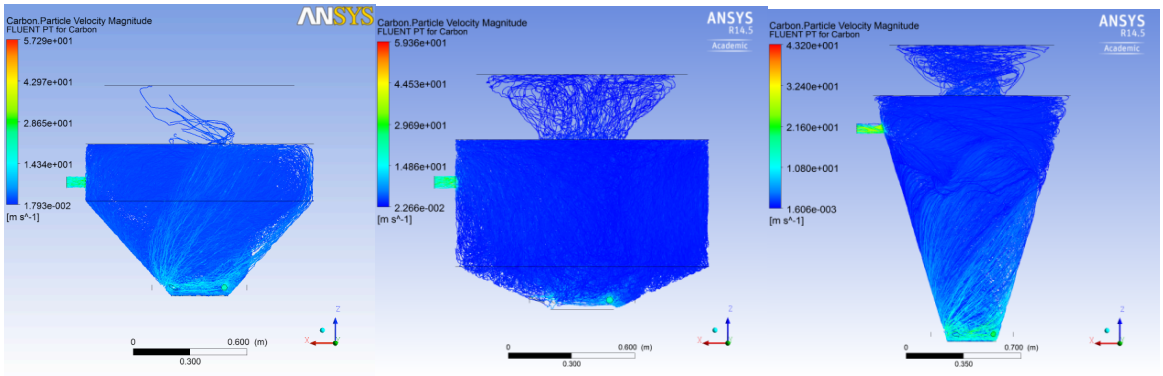

WINDOW CLEAR

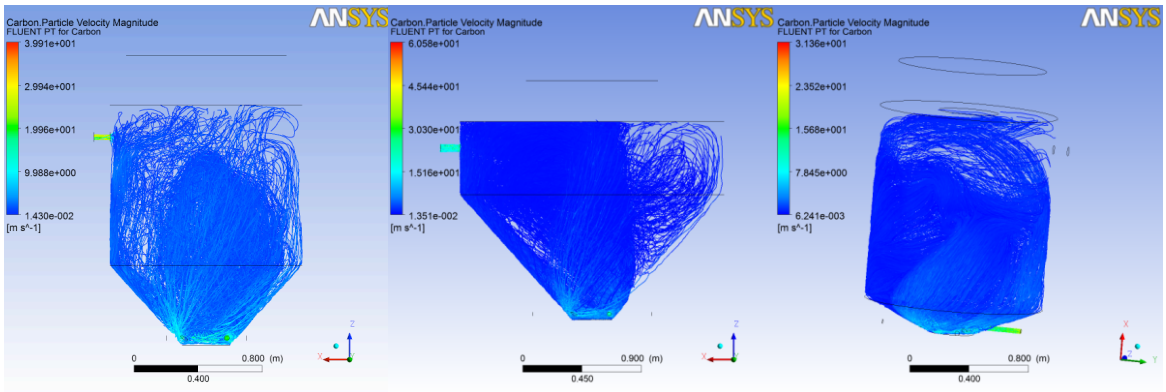

Fig. 6.12 -Particle tracking results for several geometries tested

The values reported in this table reinforce the concept that fluid dynamics structure plays an important role in keeping particles from depositing on the window. In particular, the swirl number ratio shows the existence of a critical value for the occurrence of particle deposition. For a swirl number ratio of less than 5, the analyzed geometrical configurations kept the window clean. In the configurations where the diameter ratio of chamber to aperture or the length is overly big, vortex flow cannot established for the entirety of the reactor, and axial flow carries particles through the aperture.

Angle, °	*$D_{chamber}/D_{aperture}$*	*L*	*Swirl number Bottom*	*Swirl number Top*	***Swirl Number Ratio***	*R_{bottom}*	*R_{top}*	*Window State*
75	*3*	*1.5*	*1.05*	*0,17*	***6.1***	*0.217*	*0.6*	*Not Clear*
50	*3*	*1.5*	*0.75*	*0,2*	***3.75***	*0.353*	*0.6*	*Clear*

25	3	1.5	0.25	0,1	**2.5**	0.6	0.6	Clear
60	3	1.5	0.85	0.15	**5.5**	0.263	0.6	Not Clear
50	1	1.5	1.05	0,17	**6.2**	0.217	0.6	Not Clear
50	3	1.5	0.75	0,2	**3.75**	0.353	0.6	Clear
50	4	1.5	0.6	0,114	**5.4**	0.353	0.8	Not Clear
50	5	1.5	0.56	0.093	**6.1**	0.353	1	Not Clear
50	3	0.8	1.33	0,22	**6.04**	0.6	0.6	Not Clear
50	3	2.5	0.48	0,06	**8**	0.353	0.6	Not Clear

Table 6.2: Table of results for swirl number analysis and window state

Moreover, it can be concluded that for any clear window configuration, there must be a vortex flow and the dimensions of the vortex core must be sufficiently large to cover the whole aperture.

In order to emphasizes the role of vortex core dimension on quartz window state, several simulations were carried out varying dimension of the aperture, fixing a geometry. In particular simulations were performed in an optimized geometry with a reactor cavity of 1.5 meters of length, diameter ratio of 3 and cone angle of 50 degrees, varying aperture diameter dimension (10, 20, 40, 60 and 100 cm). For case analyzed, vortex dimension at line 3 is approximately 50 cm, so that $d_{vortex}/d_{aperture}$ varies from 0.5 up to 5. Swirl number ratio between bottom (inlet) and top (outlet) is 3.75.

Fig. 6.13 reports quartz window state as function of Stokes number and $d_{vortex}/d_{aperture}$ ratio. In this case Stokes number has been calculated referring to mean velocity magnitude in the reactor and reactor diameter as characteristic lenght scale.

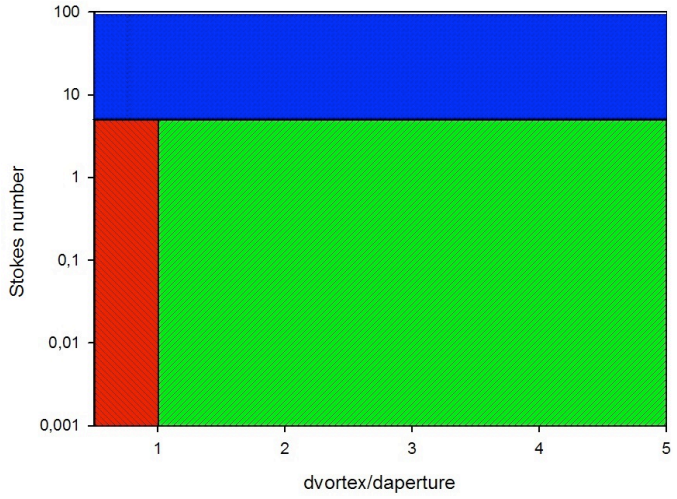

Fig. 6.13 -Window state as function of Stokes number and $d_{vortex}/d_{aperture}$ ratio (Swirl ratio = 3.75)

Fig. highlights that particle deposition on quartz window only occurs for small particles, meanwhile for Stokes number > 5 window appears clear not depending on d_{vortex} /$d_{aperture}$ ratio (blue zone of the map). Effect of vortex structure and particle diameter will be explained in the next paragraph. Furthermore, it will possible to note that for Stokes number < 5, d_{vortex} /$d_{aperture}$ ratio plays a key role in keeping clear quartz window. In particular, window appears clear for all cases for which d_{vortex} is bigger than $d_{aperture}$ (green zone of the map); for other cases window is not clear (red zone of the map).

It is worthwhile to note that d_{vortex} /$d_{aperture}$ ratio on the map were calculated considering a swirl ratio equal to 3.75. Variation from clear to not clear window state condition (d_{vortex} / $d_{aperture}$ approximately equal to 1) will be a function of Swirl number ratio since such a parameter affects vortex structure and vortex core dimension. For existing solar vortex gasifier configurations, considered as test cases (Hirsch and Steinfield, 2004; Ozalp et al., 2013), Swirl number ratio (evaluated between inlet and outlet) is approximately 1 meanwhile d_{vortex} /$d_{aperture}$ results less than 1. Such a value of d_{vortex} /$d_{aperture}$ suggests why auxiliary inlet seal gas is needed for keeping clear window state in such a configurations.

6.3.5 RTD: Effect of geometry, particle diameter and total flow rate

In order to understand the effect of particle size, geometrical parameters and total flow rate on the residence time distribution of particles, all the simulations were performed in an optimized geometry with a reactor cavity of 1.5 meters of length, diameter ratio of 3, varying cone angle from 25 to 50 degrees.

The residence time distribution is obtained through ANSYS 14 Fluent and shown in a histogram of the percentage of particles leaving the cavity at specified time intervals. The mean residence time is calculated using the histogram.

In this study, space time (Levenspiel 1974) is compared with the calculated mean residence time of particles and is defined as the ratio of the total volume of the reactor to the volumetric flow rate entering the cavity. The variation of particle residence time with respect to space time is important to gauge the effect of the vortex flow on residence time.

Figure 6.14 shows the residence time distribution histograms of a mono-dispersed particles injection, varying particle diameter from 1 up to 1000 micron, in a reactor with a fixed cone angle of 40 degrees.

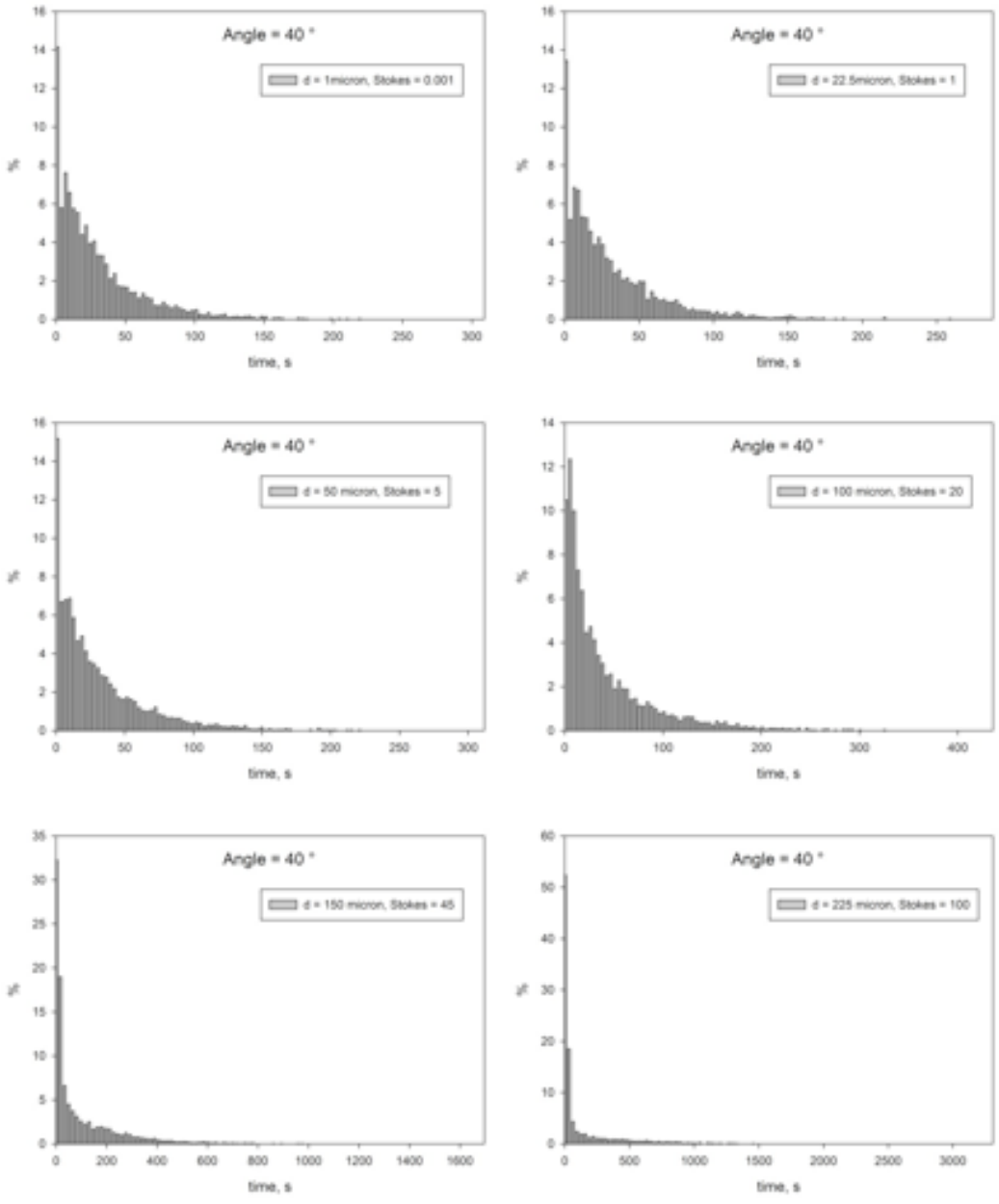

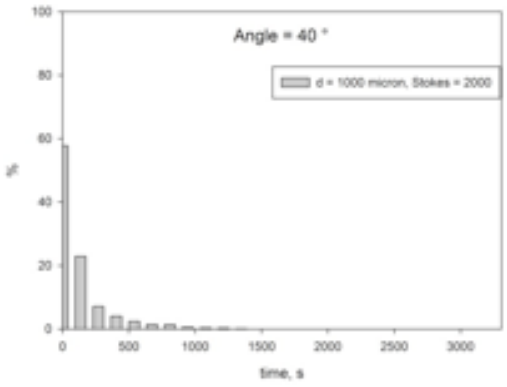

Fig. 6.14 -Particle Residence time distribution as function of particle diameter

Mean residence times obtained from respective histograms are summarized in Figure 6.15, meanwhile a comparison between reactor space time and particle mean residence time is reported in Table 6.3.

Space Time, V/Q	*Stokes Number*	*Particle Diameter, micron*	*Evaluated Mean Residence Time, s*	*%*
26.92	*0.001*	*1*	*30,19*	*12,1*
26.92	*1*	*22.5*	*30,97*	*15,1*
26.92	*5*	*50*	*31,1*	*15,5*
26.92	*20*	*100*	*41,33*	*53*
26.92	*45*	*150*	*94,19*	*250*
26.92	*100*	*225*	*124*	*360*
26.92	*500*	*500*	*263,26*	*877*
26.92	*2000*	*1000*	*464*	*1623*

Tab. 6.3 -Comparison between space time and evaluated mean residence time as function of particle diameter

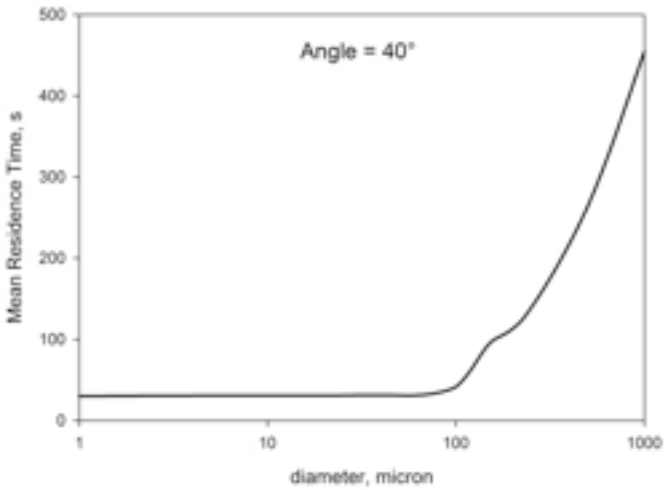

Fig.. 6.15 -Mean residence time distribution as a function of particle size ranging from 1 micron to 1000 microns

As we can see from Fig. 6.15, for the proposed configuration, the particle mean residence time is a strong function of particle size. Referring to the table, tracer like particles such as 1 micron particles show a longer residence time with respect to space time. This is due to the presence of swirl flow (Ozalp 2013). Particles with stokes numbers of greater than 1 show a higher residence time with respect to the smaller particles, and this deviation increases with stokes number. For particles of 1000 microns, the residence time can be increased by 1 or 2 of order of magnitude with respect to the small particles. It is worthwhile to note that Stokes number has been calculated respect to inlet flow velocity and inlet diameter, so that a strong variation of calculated residence time is noticeable starting from Stokes close to 20. Generally, such a strong deviation is observed for a Stokes number > 1 (e.g. St = 5), conditions for which a particle can not be consider like a tracer. Considering reactor diameter and mean velocity magnitude in the reactor for evaluating Stokes number, it can be found that also for analyzed case a strong deviation appears for Stokes =5. Furthermore, from table 6.3, calculated mean residence time appears very high for big particles (e.g. 464 s for a particle of 1000 micron), that could be longer that time need for a complete particle conversion. In this view, it is needed to stress that calculations have been carried out under non reactive condtions and assuming mono-disperse particle injection only in order to assess effect of key parameters on residence time distribution. It is well know that under gasification conditions, particle diameter is not constant but diminishes with the progress of reactive process. Moreover, time for a

complete particle conversion is also a function of several parameters, such as gasification temperature, particle diameter and particle nature. In this view, calculated mean residence time values can be also consistent from a quantitative point of view with respect to time required for a complete conversion. For example, Ozalp et al. (2013) reported a mean residence time up to 185 s, depending on working operative conditions of their solar vortex reactor for particle diameter of 1 micron.

In order to visualize the effect of particle size, 2 different sized mono particles were tracked in the reactor cavity. Their pathlines are shown in Figure 6.16. Big particles were observed in the inner region and small particles were found near the wall. At the bottom, all the particles are directed to the wall by the tangential inlet flow. The small particles follow the preferential path of the gas flow that is located close to the wall where the peak tangential velocity occurs, and cannot enter the vortex core region. The big particles instead deviate from the streamlines of the flow, decelerating because of their higher inertia and move back into the center due to the cone geometry and gravity. In the center, there exists a reverse flow so that the particles need to spend more time in the vortex core before redirecting up and escaping.

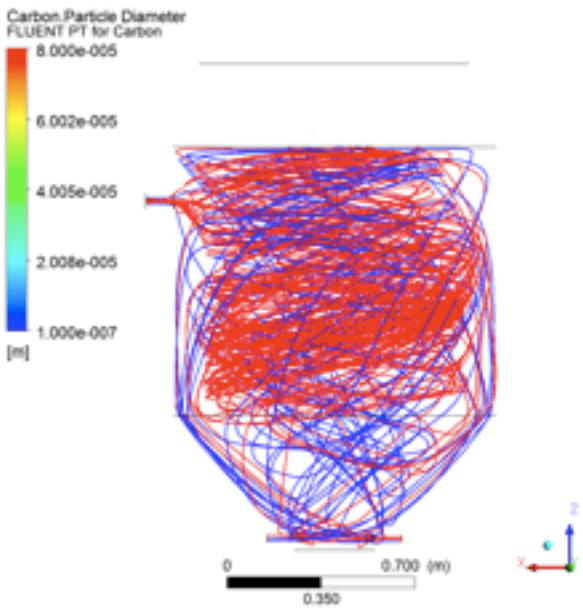

Fig.. 6.16 Particle trajectories visualization for 2 different particle sizes; 100 microns (red) and 1 micron (blue)

In Figure 6.17, the effect of cone angle on mean residence time is reported. Fig. highlights that increasing the cone angle, the mean residence time increase. This effect is more pronounced for big particles. Table 6.2 reports the swirl number at the bottom for the three configurations tested. The swirl number increases as the cone angle is increased. Hence, a stronger vortex extends the mean residence time. Furthermore, for the proposed geometry, increasing the cone angle also leads to a stronger reverse flow in the core region that explains why cone angle affects big particles' residence more than small particles. Fig. 6.18 investigates the effect of total flow rate on residence time for small tracer like particles with a stokes number of 0.001. It can be seen that decreasing the flow rate has the effect of increasing the residence time. This is obvious since total flow rate is directly involved the calculation of space time which predicts the mean residence time of the gas flow. Examples of calculated particle RTD, varying total flow rate and fixing St =0.001 are reported in Fig. 6.19.

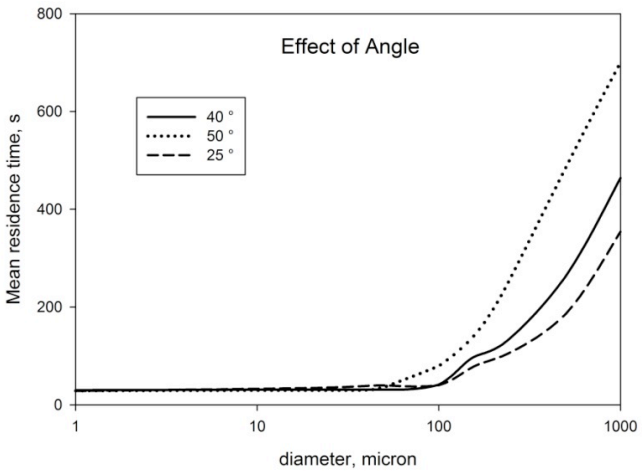

Cone Angle, °	*Swirl Number Bottom*
25	*0.28*
40	*0.48*
50	*0.75*

Fig.. 6.17 Mean residence time as a function of cone angle and particle size

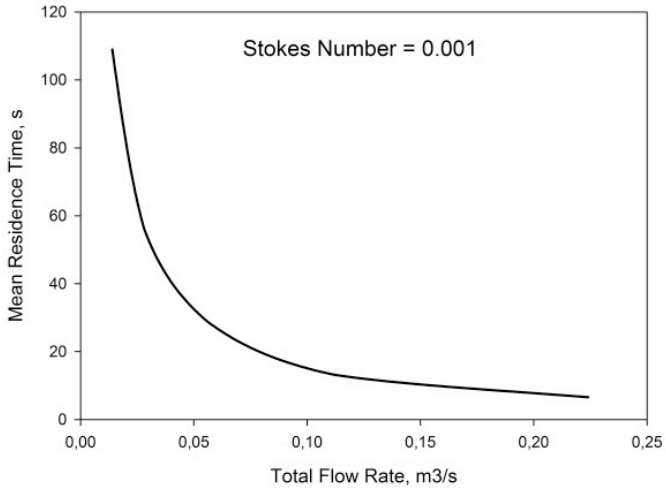

Fig. 6.18 Mean residence time as a function of total flow rate for a Stokes number of 0.001

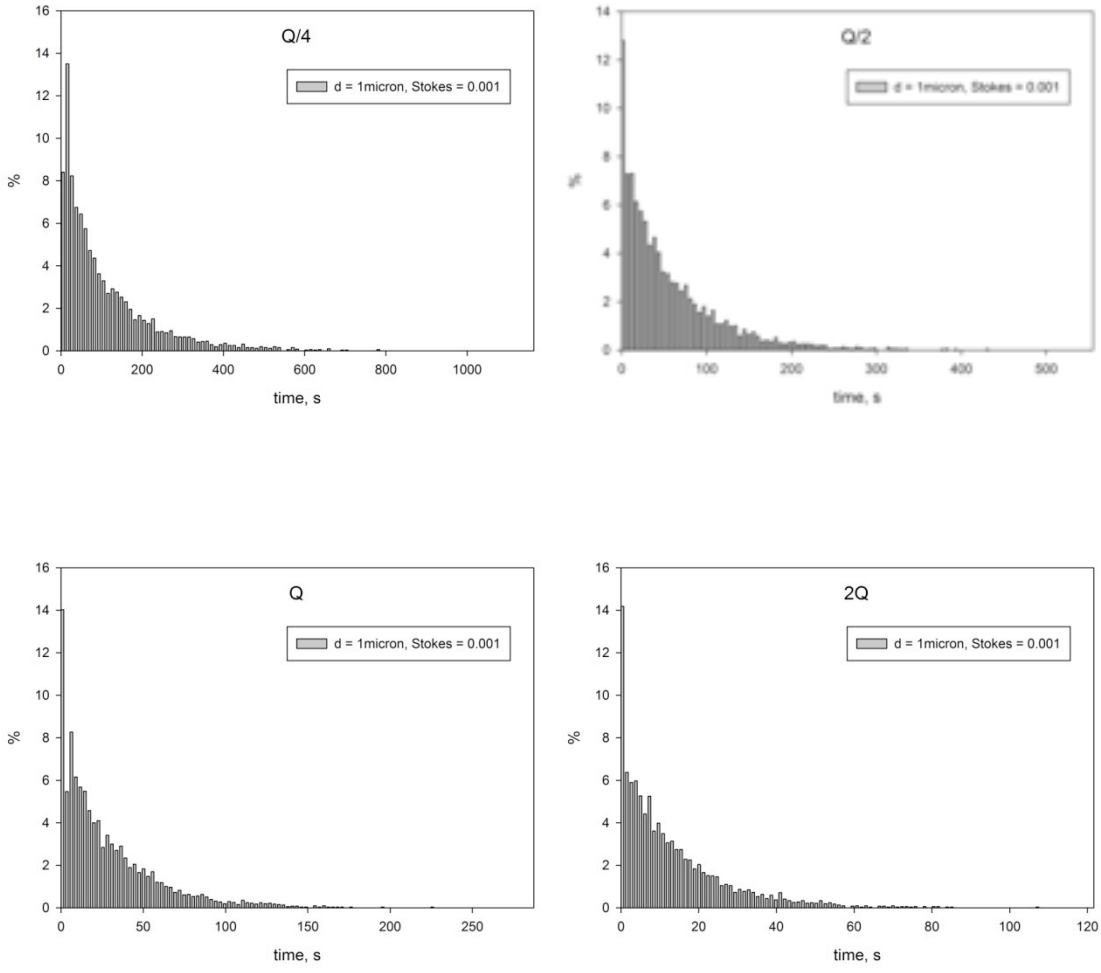

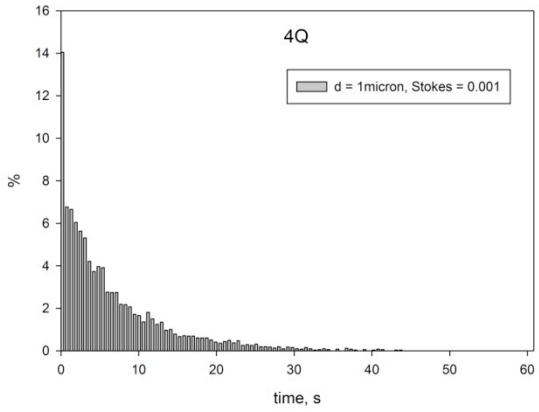

Fig. 6.19 -Particle Residence time distribution as function of total inlet flow rate (St =0.001)

In order to understand the effect of total flow rate on big particles' residence time, Fig. 6.20 reports the variation of the mean residence time with the respect to space time for particles of 75 microns. In this case, it is possible to see that increasing the flow rate is helpful to maximize the difference between mean residence time and space time. For low flow rates, the intensity of the vortex flow is insufficient to significantly cause a big variation in the mean residence time of small and big particles. Meanwhile, increasing the total flow rates leads to the establishment of a stronger vortex, with high benefits on the maximization of residence time of big particles. Increasing flow rate, Stokes number decreases fixing a particle's size. This can explain why for very high flow rates the variation between calculated residence time and space time reach a plateau. Increasing the flow rate up to the maximum flow rate investigated is not good because for the given particle diameter, it is possible to reach stokes numbers so that particles behave like flow tracers and exit the reactor in very short residence time following the gas.

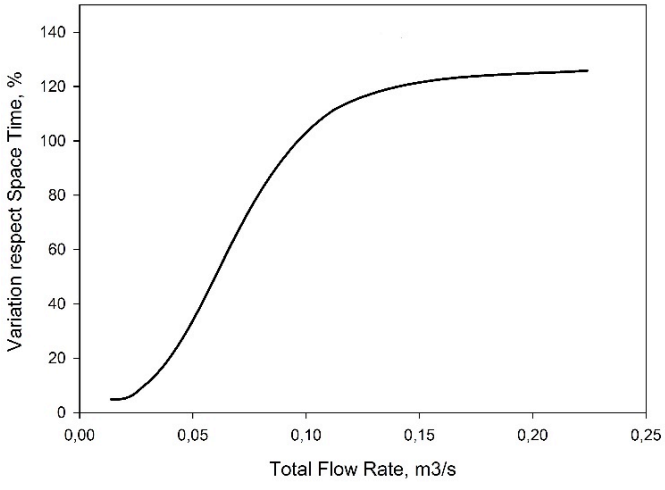

Fig. 6.20 Variation with respect to space time as a function of total flow rate for particle size of 75 micron and cone angle of 50 degrees

6.4 - Summary of the main findings

This study proposed a new novel solar vortex gasifier configuration for obtaining an efficient and flexible reactor configuration for this type of technology. Through CFD techniques, the effects of geometrical parameters on particle deposition have been investigated. Analysis highlighted that geometry configuration significantly affect the window state and the fluid-dynamic structure established in the cavity. Analysis suggests that a large vortex core dimensions (bigger than aperture diameter), connected to the vortex intensity and geometrical parameters, are necessary to prevent particle deposition. Also the effects of particle's size, cone angle and total flow rate have been investigated.

Results showed that the particle deposition on the window can be minimized and the variation in residence time of big and small particles can be maximized with the proposed novel design of vortex flow solar gasification reactor.

Chapter 7

Conclusions

7.1 - Overview of the PhD work

The present PhD work was conducted in order to further our understanding of cyclonic flows aerodynamic for energy system applications. In this view, three different processes in which such a peculiar flow can be applied have been proposed and investigated, namely, MILD Combustion for CO_2-cleaning, MILD Combustion for LP applications and Solar Thermal Gasification. All of these processes, need of several conditions to take place, such as fast and strong mixing between fresh mixture and recirculated fluid into combustion chamber, absence of fluidynamic instabilities and long residence time. Cylonic flows have been used to achieve these need. In this view, both experimental and numerical approach have been adopted in this work. More specifically, cyclonic vortex structure has been investigated by means of CFD analysis with both RANS and LES approach and by Particle Image Velocimetry technique.

In the literature review presented in Chapter 2, a main aspects of cyclonic flows requiring further investigations were identified. Not depending on the specific field of application, in this work, key input parameters that affect a cyclonic vortex structure have been selected and investigated. Cyclonic flow has been characterized on the basis of several output parameters, namely residence time, mixing process, fluid-dynamic instabilities, vortex topology and modularity aspects. Each of this output parameter presents different subcategories that have been explored. For example, topology is related to vortex behavior (free/forced/combined), structure type (2D, 3D), vortex intensity and vortex core dimension. It is worthwhile to note that a single input parameter can affect several output parameters of vortex structure since they are strictly interconnected.

Fig. 7.1 reports a schematic diagram of the PhD work, highlighting all the input and output parameters identified and analyzed in this study. Correlation between input and output parameters reported in the Fig., quantification of inlet parameters effects on output

parameters and connection between the different output parameters have been the key aspects investigated in this work.

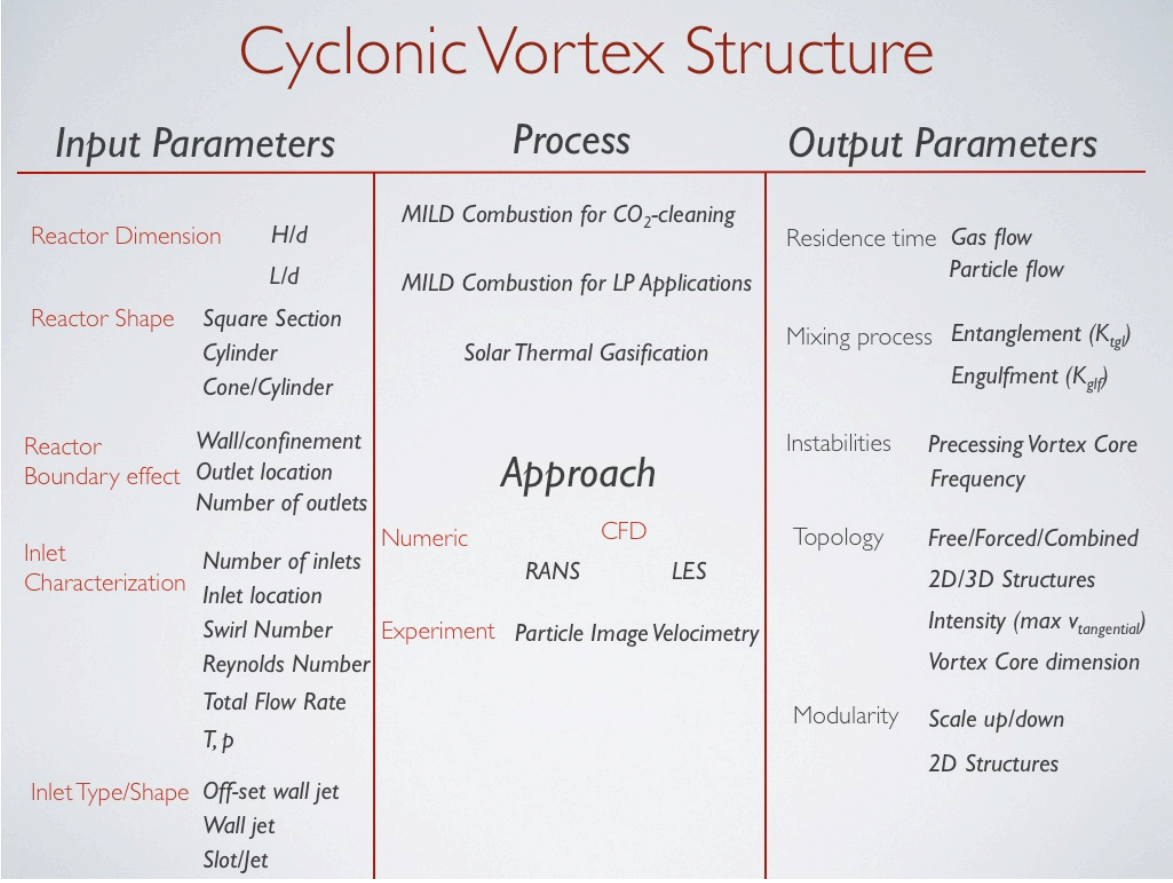

Fig. 7.1 Overview of the PhD work

The first work (Chapter 4) analysed the cyclonic vortex flows application to MILD Combustion processes devoted to non-condensable reactive specie removal from CO_2-exhaust streams to be sequestered, while the second work (Chapter 5) is aimed by identified novel reactor configurations for MILD-LP processes.

The last work (Chapter 6) represented a novel design investigation of a Solar Vortex-Enhanced Gasifier in order to improve and develop such a technology.

In the following a summary of main results obtained in this PhD work is reported, organized by chapter.

Chapter 4 highlighted that:

- CO_2-exhaust stream cleaning process from non-condensable reactive species by means of a MILD Combustion process is effectively feasible ;
- Kinetic analysis showed higher chemical times respect to conventional combustion processes. Furthermore high quantity of CO_2 as diluent species can lead to dynamic behavior appearance in terms of temperature oscillations;
- All the configurations analyzed are based on a cross-interference of jets, tangentially located for generating the vortex flow. Calculated mean reactor residence time are longer compared with the reactor space time due to the establishment of strong recirculation zones (peculiar characteristic of a cyclonic flow) and are compatible with evaluated kinetic times;
- A vortex reactor configuration with $H/d_{reactor} < 1$ and a sudden contraction ensures the establishment of a stable cyclonic vortex flow (quasi 2D structure) meanwhile configurations with $H/d_{reactor} > 1$ and low confinement levels lead to an unstable vortex;
- Reactor shape and inlet type are a critical parameters for the mixing process between inlet and recirculated fluid; a square reactor section and an off-set wall jet as inlet condition ensures a maximization of the mixing process respect to other configurations analyzed;
- Fixing an inlet jet Re number, mixing process increases by increasing number of inlet jets. Moreover, mixing process is strongly enhanced for all the configurations analyzed as compared with a free jet, chosen as reference case, due to an increase of the local vorticity;
- Increasing the inlet jet Re number, mixing process in terms of engulfment process increases;
- For all the configurations analyzed, engulfment parameter reaches an asymptotic values due to the presence of reactor walls (confinement). For a fixed configuration, such a value is a function of the confinement level and the total inlet flow rate;
- Intensity and type of vortex is a function of $H/d_{reactor}$ ratio, inlet Re and Swirl number, type of inlet boundary and confinement level. Vortex intensity increases by decreasing $H/d_{reactor}$ ratio, by adopting slots as inlet boundary instead of jets and by increasing level of confinement, inlet Re number and total flow rate. A combined vortex has been highlighted for all the configurations analyzed. A more marked free vortex behavior has been observed by increasing total flow rate (adopting slots for example) for a fixed confinement and by increasing reactor confinement level. For a fixed Swirl and Re

number, mixing process is enhanced for a combined vortex with a marked forced behavior;

- PIV technique is an efficient method in order to obtain information on jet decay and to characterize vortex flow structure in the reactor. Several turbulence closure models has been tested with obtained experimental data. Of these, RNG K-ε model with swirl and curvature correction and RSM reproduced accurately the experimental findings in terms of jet velocity decay and tangential velocity profiles;
- Inlet and outlet boundary are critical parameters affecting vortex structure. Presence of one single inlet and/or multiple outlet sections lead to an unstable and/or non-symmetrical vortex configuration;
- For a fixed configuration, the establishment of a stable structure is principally a function of the inlet jet Re number. The critical Re number can be evaluated by analyzing vortex intensity and vortex dimension;
- Entanglement factor is a function of inlet jet Re number, total flow rate, temperature and confinement level (outlet section dimension). Entaglement increases by increasing inlet Re number, total flow rate and it decreases by increasing inlet temperature and outlet section dimension;
- For all the configurations analyzed, entanglement parameter reaches an asymptotic values at high Re number because of a balance between short mean reactor residence time and high vortex intensity.

Chapter 5 highlighted that:

- Large Eddy Simulation is an efficient tool for cyclonic vortex flows investigation. In particular a space-temporal analysis of fluid-dynamic structures connected to such a peculiar flow can be performed by means of LES approach;
- For a fixed inlet jet Re number, mixing process between inlet and recirculated fluid is enhanced by increasing number of inlet jets due to a strong increase of vorticity into the reactor;
- Fluid-dyanmic structure is affected by reactor configuration. Typical fluid-dynamic structures associated with jet growth can be highlighted for one single and 2 inlets reactor configurations meanwhile a vorticity “tube” structure can be highlighted for 4 inlet jets reactor configuration;

- Temporal analysis of engulfment parameter (K_{glf}) revealed that mixing process between inlet and recirculated fluid is strongly affected by reactor configuration. A well/controlled mixing is obtained for 2 and 4 inlet jets configurations meanwhile an unstable mixing, characterized by high amplitude/non-regular oscillations of K_{glf} is obtained for one single jet configuration;
- Frequency analysis is a needful tool for cyclonic vortex structure characterization. Such a analysis revealed a more marked 3D behavior for one single inlet reactor configuration (due to a non-symmetrical structure) respect to 2 and 4 inlet jets configurations characterized by a well/defined quasi 2D fluid-dynamic structure. Analysis has been carried out at different monitoring points along reactor height and at several distances from vortex centre;
- Frequency analysis showed that a cyclonic flow is characterized by a complex structure. In fact, for a fixed configuration, Swirl and inlet Reynolds number, different frequencies of velocity components have been obtained varying location of monitoring point, suggesting that a vortex structure connected to a cyclonic flow evolves on several spatial and temporal scales;
- For a fixed monitoring point, similar frequencies of the engulfment parameter (K_{glf}) and velocity magnitude have been detected, highlighting that such a parameter is strongly associated with velocity magnitude, its fluctuations and local vorticity. Furthermore, such a frequency results a function of total flow rate;
- For all the configurations analyzed, frequency analysis suggests that the velocity component associated with the stream-wise jet direction is the main velocity component at the vortex boundary meanwhile the axial velocity is the principal component at the vortex core;
- Precessing Vortex Core phenomena is affected by reactor configuration in terms of outlet location and reactor dimension. PVC is a phenomena associated to high values of root mean square of velocity components at vortex core and a precession of vortex core (identified by location of pressure minimum) along the axis rotation. For all configurations analyzed, characterized by H/d ratio <1 and a sudden contraction as outlet section, PVC phenomena, connected to a strong 3D cyclonic vortex structure, is avoided. This result reveals a well-established vortex stabilization for all the configurations investigated.

Chapter 6 highlighted that:

- Geometrical parameters significantly affect the window state and the fluid-dynamic structure established in the cavity of SVG;
- Window state appears clear for Stokes number >5 and for large vortex core dimensions. In particular a vortex core bigger than aperture diameter is necessary to prevent particle deposition;
- Vortex core dimension is a function of Swirl number ratio between inlet and outlet section. Large vortex core dimension is achieved for a Swirl number ratio close to 1;
- Residence time distribution (RTD) of particles strongly depends on geometrical parameters, particle size and total flow rate. The novel SVG configuration proposed (constituted by a cylinder/cone) ensures at the same time longer particles residence time respect to conventional SVG configurations and a maximization of residence time variation of big and small particles. In particular, due to the reactor configuration, small particles can only move outside the vortex boundary, meanwhile big particles are principally present in the vortex region characterized by an axial reverse flow;
- For big particles, effect of cone angle is a critical parameter on RTD. In particular, RTD of particles increases by increasing reactor cone angle;
- Not depending on particle size, mean particle residence time results bigger than reactor space time due to the establishment of a strong vortex structure into the reactor;
- For Stokes number < 1, mean particle residence time increases by decreasing total flow rate. For a fixed particle size and a Stokes number > 1, variation of mean residence time respect to the reactor space time increases by increasing total flow rate due to a stronger vortex intensity. For a very high flow rate such a variation decreases since Stokes number values <1 can be reached.

7.2 - Guidelines for further studies

In this section, few topics for further investigations are suggested.

In chapter 4, a novel MILD Vortex burner configuration for non-condensable/reactive species from CO_2-exhaust streams has been proposed and analyzed. This research activity has been concluded with the practical construction of a laboratory scale apparatus (some pictures of the reactor are reported in Appendix). Experimental campaign of the reactive

process will provide further informations on the effective feasibility of the process and its applicability range in terms of operative working parameters. Finally, with such a device, not full understanding aspects of combustion stabilization and turbulence/chemistry interaction under MILD Combustion conditions could be analyzed and clarified.

In chapter 5, dynamics of the hydrodynamic structures (i.e. their rotation or precession) connected to a cyclonic flow have been characterized by means of an incompressible non-reactive LES investigation for MILD-LP combustion applications. The use of a compressible formulation of Navier Stokes equations can be helpful to clarify the possible acoustic/fluid-dynamic instabilities interactions into the vortex reactor. Furthermore, a reactive LES investigation could add key informations to the MILD process evolution in terms of stabilization. It is worthwhile to note that such a approach could be limited by CPU power since a LES simulation with a semi-detailed kinetic mechanism (i.e DRM19, adopted for RANS simulations) requires an high computational cost. Finally, LES analysis could be performed varying pressure system (simulations have been carried out at atmospheric pressure) in order to asses the effect of high pressure on cyclonic vortex structure characterization.

In chapter 6 design of a novel Solar Vortex Gasifier has been performed by means of a non-reactive RANS approach. In this study, an isothermal LES investigation could be helpuf in order to reveal more information on the interaction between the cyclonic flow aerodynamic and the window state.

Appendix

A.1 Numerical Approach and Post-Processing Methods

A.1.1 Reynolds Averaged Navier-Stokes Models

All fluid motions (laminar or turbulent) are governed by a set of dynamical equations namely the continuity, momentum and the energy equation (Navier Stokes equations),

$$\frac{\partial \rho}{\partial t} + \frac{\partial}{\partial x_i}(\rho u_i) = 0 \tag{30}$$

$$\frac{\partial}{\partial t}(\rho u_i) + \frac{\partial}{\partial x_j}(\rho u_i u_j) = -\frac{\partial p}{\partial x_i} + \frac{\partial \tau_{ij}}{\partial x_j} \tag{31}$$

$$\frac{\partial}{\partial t}(\rho E) + \frac{\partial}{\partial x_i}(\rho H u_i) = \frac{\partial}{\partial x_i}(\tau_{ij} u_j - q_i) \tag{32}$$

$u_i(x,t)$ represents the i-th component of the fluid velocity at a point in space x and time t, $p(x, t)$ is the static pressure, $\tau_{ij}(x, t)$ are the viscous stresses, $\varrho x, t)$ is the fluid density, E and H are the total energy and total enthalpy per unit mass, q_i is the heat flux which is proportional to the temperature gradient:

$$q_i = -k\frac{\partial T}{\partial x_i} \tag{33}$$

with k is the thermal conductivity. For incompressible fluid motion, the viscous stresses can be defined as:

$$\tau_{ij} = 2\mu(s_{ij} - \frac{1}{3}s_{kk}\delta_{ij}) \tag{34}$$

si_j is the instantaneous strain rate tensor given by:

$$s_{ij} = \frac{1}{2}\left(\frac{\partial u_i}{\partial x_j} + \frac{\partial u_j}{\partial x_i}\right) \tag{35}$$

For incompressible flows the Navier-Stokes can be simplified to the following form:

$$\frac{\partial}{\partial x_i}(u_i) = 0 \tag{36}$$

$$\frac{\partial}{\partial t}(u_i) + u_j \frac{\partial}{\partial x_j}(u_i) = -\frac{1}{\rho}\frac{\partial p}{\partial x_i} + \nu \frac{\partial^2 u_i}{\partial x_j \partial x_j} \tag{37}$$

The four main numerical procedures for solving the Navier-Stokes equations are the direct numerical simulation (DNS), the large eddy simulation (LES), the detached eddy simulation (DES) and the Reynolds-Averaged Navier-Stokes (RANS) approach. The most accurate approach is DNS where the whole range of spatial and temporal scales of turbulence are resolved. Since all the spatial scales, from the smallest dissipative Kolmogorov scales (l_η) up to the energy containing integral length scales (l), are needed to be resolved by the computational mesh, the number of points required in one direction is of the order,

$$N = \frac{l}{l_\eta} \tag{38}$$

The number of points required for a resolved DNS in three dimensions can be estimated as,

$$N = \left(\frac{l}{l_\eta}\right)^3 \sim \left(\frac{ul}{\nu}\right)^{\frac{9}{4}} = \mathrm{Re}^{\frac{9}{4}} \tag{39}$$

The number of grid points required for fully resolved DNS is enormously large, especially for high Reynolds number flows, and hence DNS is restricted to relatively low Reynolds number flows. DNS is generally used as a research tool for analyzing the mechanics of turbulence, such as turbulence production, energy cascade, energy dissipation, noise production, drag reduction.

When the flow is turbulent, it is convenient to analyze the flow in two parts, a mean (time-averaged) component and a fluctuating component (Jayaraju, S.T., 2009):

$$
\begin{aligned}
U_i &= \bar{U}_i + u_i' \\
P_i &= \bar{P} + p' \\
T_{ij} &= \bar{T}_{ij} + \tau_{ij}'
\end{aligned}
\tag{40}
$$

Over line is a shorthand for the time average and in case of RANS, $\bar{\bar{U}}_i \equiv \bar{U}_i$ and $\bar{u}_i' = 0$ .The above technique of decomposing is referred to as Reynolds Decomposition. Inserting this decomposition into the instantaneous equations and time averaging results in the Reynolds averaged Navier-Stokes equations (RANS):

$$
\frac{\partial}{\partial x_i}(\bar{U}_j) = 0 \tag{41}
$$

$$
\frac{\partial}{\partial t}(\bar{U}_i) + \bar{U}_j \frac{\partial}{\partial x_j}(\bar{U}_i) = -\frac{1}{\rho}\frac{\partial \bar{P}}{\partial x_i} + \nu \frac{\partial^2 \bar{U}_i}{\partial x_j \partial x_j} - \frac{\partial}{\partial x_j}(\bar{u}_i \bar{u}_j) \tag{42}
$$

$\bar{u}_i \bar{u}_j$ represents the correlation between fluctuating velocities and is called the Reynolds stress tensor. All the effects of turbulent fluid motion on the mean flow are lumped into this single term by the process of averaging. This will enable great savings in terms of computational requirements. On the other hand, the process of averaging generates six new unknown variables. Now, in total there are ten unknowns (3-velocity, 1-pressure, 6-Reynolds stresses) and only four equations (1-continuity, 3 components of momentum equation). Hence, we need six equations to close this problem. This is referred to as the Closure problem. Based on the way we close the Reynolds stress tensor, there are two main categories, namely the eddy viscosity models and the Reynolds stress model.

The Reynolds stress tensor resulting from time averaging of the Navier- Stokes equations is closed by replacing it with an eddy viscosity multiplied by velocity gradients. This is referred to as the Boussinesq assumption.:

$$
\bar{u}_i' \bar{u}_j' = -\nu_t \left(\frac{\partial \bar{U}_i}{\partial x_j} + \frac{\partial \bar{U}_j}{\partial x_i} \right) \tag{43}
$$

where ν_t is the turbulent (eddy) kinematic viscosity. The last equation can be rewritten as:

$$\overline{u_i'u_j'} = -\nu_t\left(\frac{\partial \bar{U}_i}{\partial x_j} + \frac{\partial \bar{U}_j}{\partial x_i}\right) + \frac{2}{3}\rho\delta_{ij}k \tag{44}$$

where δ_{ij} is the Kronecker delta, δ_{ij} is equal to one if i = j and zero if i and j are different.

k is the turbulent kinetic energy given by:

$$k = \frac{1}{2}\overline{u_i'u_i'} \tag{45}$$

the eddy viscosity is treated as a scalar quantity and is determined using a turbulent velocity scale v and a length scale l, based on the dimensional analysis.There are different types of eddy viscosity models (EVM) based on the way we close the eddy viscosity. Algebraic or zero equation EVM's normally use a geometric relation to compute the eddy viscosity. In one equation EVM's, one turbulence quantity is solved and a second turbulent quantity is obtained from algebraic expression. These two quantities are used to describe the eddy viscosity. In two equation EVM models the two turbulent quantities are solved to describe the eddy viscosity. In the Reynolds stress models (RSM), an equation is solved for each Reynolds stress component as well as one length scale determining equation. However, RSM's are computationally much more demanding when compared to EVM's.

A.1.1.1 Standard k-epsilon turbulence model

The k-epsilon turbulence model uses the gradient diffusion hypothesis to relate the Reynolds stresses to the mean velocity gradients and the turbulent viscosity. The turbulent viscosity is modeled as the product of a turbulent velocity and length scale. In k-epsilon the turbulent velocity scale is computed from the turbulent kinetic energy, which is provided from the solution of its transport equation. The turbulent length scale is estimated from the turbulent kinetic energy and its dissipation rate. The dissipation rate of the turbulent kinetic energy is provided from the solution of its transport equation.

The k-epsilon ε model introduces two new variables into the system of equations. The momentum equation is then:

$$\frac{\partial}{\partial t}(\rho u_i) + \frac{\partial}{\partial x_j}(\rho u_i u_j) = \frac{\partial p'}{\partial x_i} + \frac{\partial}{\partial x_j}\left(\mu_{eff}\frac{\partial u_i}{\partial x_j}\right) \tag{46}$$

where μ_{eff} is the effective viscosity accounting for turbulence:

(47) $$\mu_{eff} = \mu + \mu_t$$

where μ_t is the turbulent viscosity. The k-epsilon model assumes that the turbulence viscosity is linked to the turbulence kinetic energy and dissipation via the relation:

(48) $$\mu_t = \rho c_\mu \frac{k^2}{\varepsilon}$$

The values for k-epsilon come directly from the differential transport equations for the turbulent kinetic energy and the turbulence dissipation rate (Jones and Launder, 1972). For a steady flow:

(49) $$\frac{\partial}{\partial x_j}(\rho u k) = \frac{\partial}{\partial x_j}[(\mu + \frac{\mu_t}{\sigma_k})\frac{\partial k}{\partial x_j}) + P_K - \rho\varepsilon$$

(50) $$\frac{\partial}{\partial x_j}(\rho u \varepsilon) = \frac{\partial}{\partial x_j}[(\frac{\mu_t}{\sigma_\varepsilon}\frac{\partial k}{\partial x_j}) + \frac{\varepsilon}{k}(c_{\varepsilon 1}P_k - c_{\varepsilon 2}\rho\varepsilon_k)$$

The production term has the form:

(51) $$P_k = \mu_t \{2[((\frac{\partial u}{\partial x})^2 + (\frac{\partial v}{\partial y})^2 + (\frac{\partial w}{\partial z})^2\ ] + ((\frac{\partial u}{\partial y}) + (\frac{\partial v}{\partial x}))^2 + ((\frac{\partial u}{\partial z}) + (\frac{\partial w}{\partial x}))^2 + ((\frac{\partial w}{\partial y}) + (\frac{\partial v}{\partial z}))^2\ \}$$

The costant of the k-epsilon are reported below (Jones and Launder, 1972):
$c_\mu = 0.09$, $c_{\varepsilon 1} = 1.44$, $c_{\varepsilon 2} = 1.92$, $\sigma_k = 1.0$, $\sigma_\varepsilon = 1$

The RANS equations have the same form as the laminar equations provided the molecular viscosity, μ, is replaced by the effective viscosity. The most important difference is that two new partial differential equations need to be solved. As the time scales encountered with the turbulence are much shorter than those connected with the mean flow, the k-epsilon equations are much stiffer than the laminar equations. The profiles of the turbulent kinetic energy and its dissipation are typically much more peaked near the wall than the mean velocity profile. These peaks are difficult to capture. Therefore a finer grid for the turbulence quantities has to be applied near the wall than for the mean flow.

Boundary conditions are needed for the model equations. However, at solid walls there may be significant differences. In k-epsilon it is appropriate to set k = 0 at the wall but the dissipation is not zero there; instead one can use the conditions:

$$\frac{\partial \varepsilon}{\partial n} = 0 \tag{52}$$

where n is the coordinate normal to the wall. When this is done, it is necessary to modify the model itself near the wall. A number of modifications at low Reynolds numbers for the k–epsilon model have been proposed (Patel et al, 1985; Wilcox, 2002). At high Reynolds numbers, the viscous sublayer of a boundary layer is so thin that it is difficult to use enough grid points to resolve it. This problem can be avoided by using wall functions. The wall function is relying on the existence of a logarithmic region in the velocity profile. The log-law of the wall was used for the wall treatment (Launder and Spalding, 1974):

$$u^+ = \frac{1}{k}\ln(y^+) + C \tag{53}$$

where $\varkappa$ is the evaluated Von Karman constant 0.38 and C = 4.1 is the integration constant depending on the wall roughness (Osterlund et al., 2000). y^+ is the dimensionless distance from the wall:

$$y^+ = \frac{u_t y}{v} \tag{54}$$

where u_t is the friction velocity.

A.1.1.2 Reynold Stress Models

Eddy viscosity models have significant deficiencies. In three-dimensional flows, the Reynolds stress and the strain rate may not be related in such a simple way. This means that the eddy viscosity may no longer be a scalar. Anisotropic models based on using k-epsilon equations were proposed (Craft et al., 1995).

The most complex models in common use are Reynolds stress models which are based on dynamic equations for the Reynolds stress tensor itself. The exact transport equation for the Reynolds-stress tensor $u_i u_j$ is obtained from the momentum equation by multiplying the instantaneous component u_i equation by the fluctuation velocity u'_i , adding the two and then time-averaging the result. The result can be written for constant-density flows neglecting body forces after some rearrangement as:

$$c_{ij} = -P_{ij} - D_{ij} + \theta_{ij} - \varepsilon_{ij} \quad (55)$$

Here P_{ij} is the production of $u'_i u'_j$; ϕ_{ij} is the pressure-strain term,which promotes isotropy of turbulence; ϱ_{ij} is the dissipation (i.e. transformation of mechanical energy into heat in the small-scale turbulence) of $u'_i u'_j$. D_{ij} is the convection and diffusion of $u'_i u'_j$. The pressure-strain term, which is an important term since its contribution is significant, is modeled. The pressure-strain correlation ϕ_{ij} was split into two components that were given as:

$$\theta_{ij,1} = -c_1 \frac{\varepsilon}{k}(\overline{u}_i \overline{u}_j - \frac{2}{3}\delta_{ij}k)\,\mathrm{c} \quad (56)$$

$$\theta_{ij,2} = -c_2 \frac{\varepsilon}{k}(P_{ij} - \frac{2}{3}\delta_{ij}P_k) \quad (57)$$

the constant for ϕ_{ij} are: $c_1 = 1.8, c_2 = .0.6$.

In three dimensions, this model requires the solution of seven partial differential equations in addition to the equations for the mean flow. These equations are solved in a manner similar to that for the k-epsilon equations and even more care is required in their solution.

There is no doubt that the Reynolds stress model has greater potential to represent turbulent flow phenomena more correctly than the k–epsilon model. Excellent results have been obtained (Ferziger and Perin, 1999) for some flows in which the k–epsilon types of models are known to perform badly; however, in some flows their performance is not better at all (e.g., swirling flows, flows with strong curvature and with separation from curved surfaces, etc.).

A.1.1.3 Large Eddy Simulation and Smagorinsky Model

Eddy viscosity models have significant deficiencies. In three-dimensional flows, the Reynolds stress and the strain rate may not be related in such a simple way. This means that the eddy viscosity may no longer be a scalar. Anisotropic models based on using k-epsilon equations were proposed (Craft et al., 1995).

The large eddy simulation technique was developed based on an implication from Kolmogorov's theory of self-similarity that the large eddies of the flow are dependent on the geometry while the smaller scales are more universal. Hence, the big three-dimensional

eddies which are dictated by the geometry and boundary conditions of the flow involved are directly calculated (resolved) whereas the small eddies which tend to be more isotropic are modeled.

Large eddy simulation (LES) treats the large eddies more exactly than the small ones. In LES, the large scales in space are calculated directly as illustrated in Fig. A.1. The LES technique is based on a separation between large and small scales. A grid size first has to be determined. Those scales that are of a characteristic size greater than the grid size are called large or resolved scales, and others are called small or sub-grid scales. The sub-grid scales are included by way of a model called the sub-grid model (Shalaby, 2007). An elaborate explanation on LES can be found in several text books (Sagaut, 2002; Pope, 2000).

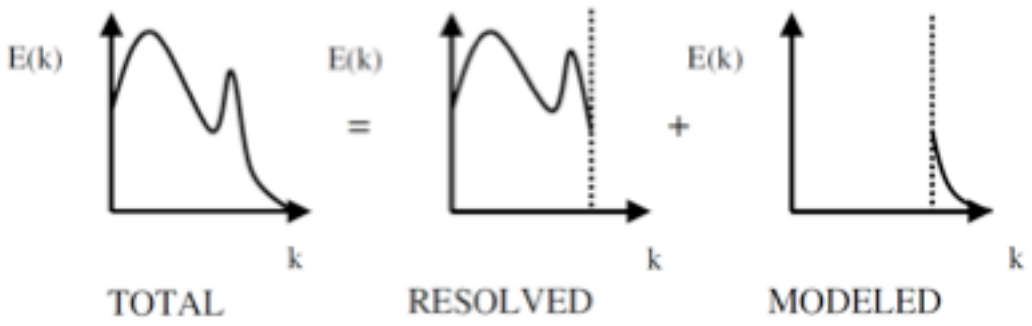

Fig. A.1 - Decomposition of the energy spectrum.

In case of RANS, the instantaneous continuity and momentum equations are time averaged to obtain a steady form of the averaged equations. In case of LES, instead of time-averaging, the instantaneous time-dependent equations are filtered. Filtering is a method that separates the resolvable scales from the sub-grid scales. Filtering can be performed in either wave number space or the physical space. The filter cut-off should lie somewhere in the inertial range of the spectrum.

In finite volume methods, box filters are always used because the finite volume discretization itself implicitly provides the filtering operation. One of the earliest volume average box filters is (Deardorff, 1973):

$$\hat{\phi}(X,t) = \frac{1}{\Delta^3} \int_{x-0.5\Delta x}^{x-0.5\Delta x} \int_{y-0.5\Delta x}^{y-0.5\Delta x} \int_{z-0.5\Delta x}^{z-0.5\Delta x} \phi(\xi,t) d\xi d\eta d\zeta \tag{58}$$

$$\phi = \hat{\phi} + \phi^s$$

In the above equation, ϕ denotes the resolvable scale filtered variable and ϕ^s denotes the sub-grid scale fluctuation. Δ is the filter width given by $\Delta = (\Delta x \Delta y \Delta z)^{1/3}$. A generalized filter (Leonard,1974) as a convolution integral is given by:

$$\hat{\phi}(X,t) = \iiint G(X-,\Delta)\phi(\xi,t) d^3\xi \tag{59}$$

G is the filter function that determines the scale of resolved eddies. The filter function is normalized by requiring that,

$$\iiint G(X-,\Delta) d^3\xi = 1 \tag{60}$$

The filter function in terms of the volume average box filter can be written as:

$$G(X-\xi,\Delta) = \begin{cases} \frac{1}{\Delta^3}, |x-\xi| < x/2 \\ 0, otherwise \end{cases} \tag{61}$$

Finally, the decomposition of the flow into a filtered part and a sub-grid part looks like,

$$\begin{aligned} U_i &= \hat{U}_i + u_i^s \\ P &= \hat{P} + p^s \\ T_{ij} &= \hat{T}_{ij} + \tau_{ij}^s \end{aligned} \tag{62}$$

The hat operator ^. in the above equations represents the filtering operation as opposed to the time-averaging in case of RANS. Moreover, contrary to RANS, where the average of fluctuations is zero, in LES, $\hat{\hat{U}}_i \neq \hat{U}_i$ and $\hat{u}^s \neq 0$ .Further details on the filtering methods can be found in (Davidson, 2000; Lacor, 2007).

Inserting the above decomposition into the instantaneous equations results in the following filtered Navier-Stokes equations,

$$\frac{\partial \hat{U}_i}{\partial x_j} = 0$$

(63)

$$\frac{\partial \hat{U}_i}{\partial t} + \hat{U}_j \frac{\partial \hat{U}_i}{\partial x_j} = -\frac{1}{\rho}\frac{\partial \hat{P}}{\partial x_i} + \nu \frac{\partial^2 \hat{U}_i}{\partial x_i \partial x_i} - \frac{\partial \tau_{ij}^{sgs}}{\partial x_j}$$

where τ_{sgs} are the sub-grid scale stresses. From the energy cascade theory, it is know that t the energy transfer occurs from the bigger scales to the smaller scales. Hence, the main purpose of an SGS model is to represent the energy sink. The representation of the energy cascade is an average process. However, locally and instantaneously the transfer of energy can be much larger or much smaller than the average. Moreover, there is also the phenomenon of energy backscatter in the opposite direction (Piomelli et al.,1996). Ideally SGS models should actually account for all these phenomena. However, if the grid scale is much finer than the dominant scales of the flow, even a crude SGS model will result in good predictions of the behavior of the dominant scales.

One of the simplest SGS model is the Smagorinsky model [161]. The unknown sub-grid-scale stresses are modeled employing the Boussinesq assumption as in the case of RANS. The sub-grid-scale stress are related to the eddy viscosity as follows,

$$\tau_{ij} - \frac{1}{3}\tau_{kk}\delta_{ij} = -\nu_t\left(\frac{\partial \hat{U}_i}{\partial x_j} + \frac{\partial \hat{U}_j}{\partial x_i}\right) \quad (64)$$

The eddy-viscosity is modeled as:

$$\nu_t = L_s^2\sqrt{2\hat{S}_{ij}\hat{S}_{ij}} \quad (65)$$

where L_s is the length-scale for the sub-grid scale and is given by $C_sV^{1/3}$, where V is the computational cell volume. It is interesting to note that the length scale is now the filter width rather than the distance to the closest wall as in RANS. C_s is a constant which is taken to be 0.17. The only disadvantage of the Smagorinsky model is the constant C_s, which is not really a constant, but is flow dependent. It is found to vary between 0.065 and 0.3 (Leonard, 1974; Jones et al., 1995). In the dynamic version (Germano et al.,1991), C_s is dynamically computed based on the information provided by the resolved scales of motion. The specification of L_s as $C_sV^{1/3}$ is not justifiable in the viscous wall region as it incorrectly

leads to a non- zero turbulent shear-stress at the wall. In order to rectify this a Van Driest damping function to specify the length scale is needed (Moin and Keen, 1982) as:

$$L = C_s V^{\frac{1}{3}} \left[1 - \exp\left(\frac{y^+}{A^+} \right) \right] \tag{66}$$

where $y^+ = u_\tau \, d/\nu$ is the non-dimensional distance from wall, u_τ is the wall shear stress velocity, d is the distance to the nearest wall and A=25 is the Van Driest constant. The above-described SGS model is the standard version. As pointed out at the beginning of the chapter the LES simulations in the present thesis are performed employing the Fluent flow solver of ANSYS software. The Smagorinsky model implemented in Fluent deviates slightly from the standard version defined before

In Fluent the length-scale for the sub-grid scale is computed as min ($\varkappa d, C_s V^{1/3}$). $\varkappa$ is the von Karman constant (typically a value of 0.41 is used), d is the distance to the closest wall. $\varkappa d$ is indeed one of the first mixing length models in the literature to handle the turbulent viscosity (Prandtl, 1925). Van Driest damping is basically an improved version of Prandtl's mixing length model. Both the Prandtl and the Van Driest model are algebraic and from the zero-equation models category.

Furthermore the constant C_s in Fluent is taken to be 0.1 instead of 0.17 as was originally proposed. The value of 0.17 for C_s was originally derived for homogeneous isotropic turbulence in the inertial subrange. However, this value was found to cause excessive damping of large-scale fluctuations in transitional flows near solid boundaries, and has to be reduced in such regions. A C_s value of around 0.1 has been found to yield the best results for a wide range of flows, and is the default value in Fluent.

In particular in this thesis the implementation of a dynamic SGS model is adopted (Germano et al.,1991). In the dynamic Smagorinsky-Lilly model the Smagorinsky model constant C_s is dynamically computed based on the information provided by the resolved scales of motion. The dynamic procedure thus obviates the need for users to specify the model constant C_s in advance. The Smagorinsky model constant is dynamically computed instead of given as an input to the solver, but clipped to zero or 0.23 if the calculated model constant is outside this range to avoid numerical instabilities (Elsayed and Lacor, 2011). The second advantage of the dynamic Smagorinsky-Lilly model over the Smagorinsky model is the treatment near the wall. In the dynamic Smagorinsky-Lilly model, a damping

function for the eddy viscosity near the wall is not required, since the model constant goes to zero in the laminar region just near the wall.

A.1.1.4 Dispersed phase Motion Modeling

Euler-Lagrange method for dispersed phase motion modeling is an helpful tool in the development and optimization of cyclonic apparatus. In this thesis modeling of a disperse phase in a fluid flow was carried out with the dual purpose of obtaining Residence Time distribution (RTD) of both continuos and dispersed phase inside the system in analysis by means of particle pathlines tracking.

With the approach adopted the continuous phase flow is treated in an Eulerian manner while the disperse phase flow is treated in a Lagrangian manner. In the Eulerian approach the flow variables are a function of space and time, thus are represented as fields. In the Lagrangian approach instead individual particles are considered and the position and velocity of each particle is a function of time only. Therefore, in the Euler-Lagrange approach mass and momentum conservation equations are solved for the continuous phase. For the disperse phase, the position and velocity of each particle is obtained from Newton's second law. This requires the interpolation of the continuous phase velocity from the Eulerian grid to the local particle position. For flows involving a small number of dispersed particles it is possible to solve a set of Lagrangian equations for every element. However, if the number of particles is large, a statistical approach is more practical. Hence, discrete particle trajectories are calculated. Each calculated particle represents a large number of physical particles of the same physical properties, which is characterized by the particle flow rate $\dot{N}_p$ along each calculated particle trajectory.

The Euler-Lagrange method can be classified with respect to the kind of coupling between the phases. The simplest approach is one-way coupling approach. In a one-way coupled system the particle mass loading respectively volume-loading is assumed to be small enough so that any effects which the presence of the dispersed phase may have on the continuous phase can be neglected. Thus, only the local velocity of the continuous phase has a direct impact on the particle motion. If the effects of the particles on the carrier fluid can not be ignored two-way coupling is required. Additionally, four-way coupling takes into account the particle-particle collision effects due to higher void fraction of the dispersed phase and due to turbulence modification by the particles

A.1.1.5 Spectral Analysis

In this thesis spectral analysis is used to obtain information about the frequencies contained in a data set, to analyze the spectral components shared by several signals or to determine the transfer function of a system.

Classical spectra analysis generally uses fast Fourier transform (FFT) which is a common tool in practical applications. Actually, efficient computational algorithms are available and allow the implementation of FFT methods on signal processing. However, fast Fourier methods induce various difficulties, in part due to the assumptions made to improve the numerical efficiency. These difficulties affect the results by finite-length effects: a signal cannot be known during a infinite time. These effects may be attenuated by windowing the signal. Another problem with Fourier transform spectral analysis relates to the compromise between the frequency resolution and statistical stability. The shorter is the sampling time, lower is the frequency resolution. Hence, statistical stability of the results may be achieved only by averaging a large number of periodograms.

The fast Fourier transform (FFT) is a recursive algorithm for evaluating the discrete Fourier transform and its inverse. Suppose that a physical process is represented by time function, h(t). The function is sampled at N times, tk = kΔt where k = 0; 1; 2;… ;N - 1. From these N measurements, hk, N complex amplitudes, Hn, are determined which satisfy the N equations:

$$H_n = \sum_{k=0}^{N-1} h_k e^{ik\frac{2\pi n}{N}} \tag{67}$$

The sampled function then has the discrete Fourier expansion:

$$h_k = \frac{1}{N}\sum_{n=0}^{N-1} H_n e^{-in\frac{2\pi k}{N}} \tag{68}$$

This equation can be reduced in familiar form with $2\pi k/N = (2\pi/T_o)k(T_o/N) = \omega_o k\Delta t = \omega_o t_k$

$$h_k = \frac{1}{N}\sum_{n=0}^{N-1} H_n e^{-in\omega_0 t_k} \tag{69}$$

The right-hand side is the discrete analogue to the complex form of the Fourier expansion:

$$h(t) = \sum_{n=-\infty}^{\infty} c_n e^{in\omega_0 t} \tag{70}$$

where the complex coefficients, c_n, are given by:

$$c_n = \frac{1}{T_0}\int_0^{T_0} h(t) e^{-in\omega_0 t} dt \tag{71}$$

Now, if W is defined as a complex number:

$$W \equiv e^{-2\pi i/N} \tag{72}$$

we can define H_n as:

$$H_n = \sum_{k=0}^{N-1} W^{nk} h_k \tag{73}$$

In other words, the vector of h'_ks is multiplied by a matrix whose (n,k)th element is the constant W to the power n×k. The matrix multiplication produces a vector result whose components are the H_n' s. This matrix multiplication evidently requires N^2 complex multiplications, plus a smaller number of operations to generate the required powers of W. So, the discrete Fourier transform appears to be an $O(N^2)$ process. The discrete Fourier transform can, in fact, be computed in $O(N \log_2 N)$ operations with an algorithm called the fast Fourier transform. The difference between $N \log_2 N$ and N^2 is immense. Danielson and Lanczos (1942) provided one of the clearest derivation of the algorithm. They showed that a discrete Fourier transform of length N can be rewritten as the sum of two discrete Fourier transforms, each of length N/2. One of the two is formed from the even-numbered points of the original N, the other from the odd-numbered points:

$$F_k = F_k^e + W^k F_k^0 \tag{74}$$

W is the complex constant, F_k^e denotes the kth component of the Fourier transform of length N/2 formed from the even components of the original f_j's, while F_k^o is the

corresponding transform of length N/2 formed from the odd components. Notice also that k varies from 0 to N, not just to N/2. Nevertheless, the transforms F_k^e and F_k^o are periodic in k with length N/2. So each is repeated through two cycles to obtain F_k. This procedure can be used recursively. Having reduced the problem of computing F_k to that of computing F_k^e and F_k^o. So, the same reduction of F_k^e to the problem of computing the transform of its N/4 even-numbered input data and N/4 odd-numbered data. In other words, its is possible define F_k^{ee} and F_k^{eo} to be the discrete Fourier transforms of the points that are respectively even-even and even-odd on the successive subdivisions of the data.

In this thesis post-processing analysis of data-sets were carried out with CFD-Post package of ANSYS software. Here, the discrete FFT algorithm is based on the assumption that the time-sequence data passed to the FFT corresponds to a single period of periodically repeating signal. Since in most situations the first and the last data points will not coincide, the repeating signal implied in the assumption can have a large discontinuity. The large discontinuity produce high-frequency components in the resulting Fourier modes, causing an aliasing error In this view, a windowing operation was applied to all data-sets to solve this issue.

A.1.1.6 Vortex Definition: Q-Criterion

Vortices are a special existence form of fluid motion with origin in the rotation of fluid elements. It can be possible to recognize the existence of vortices first by their intuitive streamline patterns, which are however not Galilean invariant and cannot be used to define a vortex. A natural invariant approach could be based on the vorticity, from which one can extract vorticity lines and vorticity magnitude. Saffman and Baker (1979) defined a vortex as a connected fluid region with high concentration of vorticity compared with its surrounding. In other words, a vortex is a vorticity tube surrounded by irrotational flow. But the vortex boundary becomes fuzzy in viscous flow without sharp boundary. There are a some cases where vortices are axisymmetric of which the outer boundary, of radius r_o, has the maximum value of the circumferential velocity. However, this criterion cannot be generalized to more complex and non-axisymmetric vortices.

A simple alternative to the vortex definition would be identifying the fluid region with $|\omega| \geq |\omega_0|$, where $|\omega_0|$ is a threshold magnitude. But this criterion is also inadequate because the choice of $|\omega_0|$ is subjective, and the side boundary of a vorticity tube may significantly differ from an iso-vorticity surface.

A natural basis for developing possible rational criteria is the symmetric- antisymmetric decomposition of the velocity gradient tensor, ∇u, $\nabla u = D + \Omega$, which suggests that a vortex may be defined as a flow region where the vorticity (symmetric tensor Omega) prevails over the strain rate (symmetric tensor Omega). This requires the calculation of the invariants of the velocity gradient tensor through its representative matrix, say $A\lambda$; which in cylindrical coordinates reads:

$$A_\lambda = \begin{pmatrix} u_{,r} & v_{,r} & w_{,r} \\ (u_{,\theta} - v)/r & (u_{,\theta} + u)/r & w_{,\theta}/r \\ u_{,z} & v_{,z} & w_{,z} \end{pmatrix} \tag{75}$$

where subscript ,r is the partial derivate with respect to radius, ,θ is partial derivate with respect to angular coordinate and ,z is partial derivate with respect to axial coordinate.
The first criterion to reveal vortex structures in a flow (Basdevant and Philipovitch, 1994), for two dimensional incompressible flow (u, v) based on the eigenvalues σ of ∇u, of which the characteristic equation is:

$$\sigma^2 + Q_{2D} = 0 \tag{76}$$

where Q_{2D}

$$Q_{2D} = \left(\frac{1}{2}\|\Omega\|^2 - \|D\|^2\right) \tag{77}$$

is the second invariant of ∇u (and also the negative of the discriminant Δ_{2D}; the first invariant is $\mathrm{tr}(\nabla u)=0$). When $Q_{2D} > 0$ at a point, the flow is called elliptic and we have purely imaginary eigenvalues $\pm \imath\sigma_i = \pm\sqrt{Q_{2D}}$; for the case of $Q_{2D} < 0$ the flow is called hyperbolic. Thus, a vortex is defined as a connected fluid region with:

$$Q_{2D} = (-\Delta_{2D}) = \sigma_i^2 > 0 \tag{78}$$

known as the Weiss criterion. Controversy on defining a vortex appears once three-dimensional flow is considered. The characteristic equation for the eigenvalues of ∇u is:

$$\sigma^3 + Q\sigma - R = 0 \tag{79}$$

In this case the discriminant of the equation is:

$$\Delta = \left(\frac{Q}{3}\right)^3 + \left(\frac{R}{2}\right)^2 \tag{80}$$

Consequently, in three dimensions the question on how much the vorticity should prevail over the strain rate may have two possible answers, both being within kinematics: either

$$\Delta > 0 \tag{81}$$

or

$$Q > 0 \tag{82}$$

These are known as the Δ-criterion,and Q-criterion (Hunt et al.,1988) respectively. The Q-criterion can be equally expressed in terms of the kinematic vorticity number m in both two and three dimensions:

$$m = \left(\frac{\|\Omega\|}{\|D\|}\right) > 1 \tag{83}$$

Q-criterion, is related in the literature to the family of Eulerian coherent structure criteria (together with swirling strenght criterion, vorticity and pressure criterion) for the identification of vortex structure in a flow. Such a criterion was adopted in this thesis to reveal the coherent structures in the fluid flow.

A.1.1.7 Kinetic Analysis: Numerical Tools

A part of this thesis concerns the development of novel design of combustion chambers for MILD Combustion applications. As it will pointed out in the next chapters this combustion "mode" is a very promising process in the framework of the development of new combustion technologies aimed to enhance the efficiency and reduce the environmental impact of combustion systems. In order to design and dimension novel burners concepts it is mandatory to assess the characteristic times of the chosen system in terms of the auto-ignition time and oxidation time. Kinetic analysis presented in the next chapters were carried out by means of several applications of the CHEMKIN software.

The CHEMKIN is a software developed by Sandia National Laboratories for the solution of problems and interpretation of gas phase chemical kinetics with elementary. It is a powerful and flexible tool for simulation of systems described by kinetic mechanisms detailed and complex. The software is widely used for the development and optimization of combustion processes. It allows also the study of systems not in thermal equilibrium, called plasma, where the reactions could be due to different temperatures and involve ions and electrons.

The CHEMKIN consists of four main parts: the thermodynamic database, the INTERPRETER, linking files, and the GAS-PHASE Soubroutines.

The thermodynamic database is a file that contains the declaration of many chemical species and their thermodynamic properties such as specific heat, enthalpy and entropy. These values are provided as constants which are the coefficients of polynomials in the independent variable temperature. The polynomial expression changes as a function of the temperature field analyzed. We recognize two fields, one for low temperatures and a high temperature. The cutoff between the two intervals, for most species, is 1000 K.

Thermodynamic information necessary for the study of a particular system can be declared in the file of the kinetic mechanism where are listed all the chemical reactions and rate coefficients. The reaction rate is expressed with the modified Arrhenius law:

$$K = A \cdot T^{b} \exp\left(\frac{-E \cdot a}{R \cdot T}\right) \tag{84}$$

The Interpreter is a program that can read information from the files of the kinetic mechanism and extract the necessary information from the thermodynamic database is added to a chemical species declared in the file of the reaction mechanism. It generates the files LINKING.

The latter is a binary file that contains all information relevant to the chemical species, elements and reactions that need to be sent CHEMKIN Subroutines running. Gas-phase Subroutines CHEMKIN consists of approximately 100 subroutines written in Fortran.

CHEMKIN software also has several applications designed to solve problems common chemicals.

Each of these applications can invoke the linking files and subroutines necessary for the numerical solution of the problem specified by the user.

For each sub-problem only a few, among all those available in the library of CHEMKIN, are used.

Some of the applications available are: a configuration OPPDIF to model jet opposed to plug flow reactors and piston SENKIN for batch reactors.

The user may define his alternative model through the set of equations governing the problem of interest. CHEMKIN software has also made planning somewhat simplified because the user has at his disposal routines in the Gas-Phase Library. The user only has to recall the right to define soubroutines equations, thermodynamics and combine them to define the system. The applications of the CHEMKIN used in this thesis are PLUG and AURORA. PLUG, simulates the behavior of a plug flow reactor. More specifically, the application uses a non-dispersive model, consider the one-dimensional flow of a reactant species and the mixture is assumed ideal considered. PLUG solves the differential-algebraic set of equations that describe the reactor using an implicit numerical software DASSL. PLUG solves the equations of the model to the stationary phase can be used in design, control and optimization of a tubular reactor in a flow. AURORA application was used to simulate a continuously stirred tank (CSTR) or well-mixed reactor. CSTR models have been in use for many years in the study of chemistry within a unit process for a variety of applications. For thermal (neutral) systems, perfectly stirred reactor (PSR) models are a common method for testing and developing chemical reaction mechanisms. Such reactor models are widely employed in combustion research. Well-stirred reactor modeling that includes detailed surface reaction mechanisms is applicable to thermal chemical vapor deposition (CVD) systems, as well as many other materials and catalytic processes. In the plasma simulation for microelectronics processes, global or well-mixed reactor models are used to predict average electron energies and electron densities for a variety of power-deposition mechanisms with large, to calculate thermodynamic equilibrium, to evaluate the thermodynamic and transport properties of a mixture, to assess the rate of production of chemical species and make analysis of reaction pathways to simulate processes using series of CSTR and finally to model non-ideal fluids.

A.2 Cross-interference process of multiple jets generating a cyclonic vortex flow

Nomenclature

a) Entanglement, Entrainment Engulfment , Erosion: Definition of characteristic ratios and flow rates

Table of Characteristic Ratios:

Symbol	*Definition*
K_{tgl}	Total Entanglement Ratio
K_{trn}	Total Entrainment Ratio
K_{glf}	Total Engulfment Ratio
K_{ros}	Erosion Ratio
Y_{tgl}	Entanglement Fraction
Y_{trn}	Entrainment Fraction
Y_{glf}	Engulfment Fraction
X_{tgl}	Entanglement Ratio
X_{trn}	Entrainment Ratio
X_{glf}	Engulfment Ratio

Table of Characteristic Flow Rates (by mass):

Symbol	*Definition*
$\dot{m}_0$	Initial Jet Flow Rate
$\dot{m}_{ros}$	Erosion Flow Rate
$\dot{m}_{glf}$	Engulfment Flow Rate
$\dot{m}^t{}_{glf}$	Total Engulfment Flow Rate
$\dot{m}_{trn}$	Entrainment Flow Rate
$\dot{m}^t{}_{trn}$	Total Entrainment Flow Rate
$\dot{m}_{tgl}$	Entanglement Flow Rate
$\dot{m}^t{}_{tgl}$	Total Entanglement Flow Rate

Definition of Characteristic Flow Rates:

1) $\dot{m}^t{}_{tgl} = \dot{m}_{tgl} + \dot{m}^t{}_{trn}$
2) $\dot{m}^t{}_{trn} = \dot{m}_{trn} + \dot{m}^t{}_{glf}$
3) $\dot{m}^t{}_{glf} = \dot{m}_{glf} + \dot{m}_{ros}$

Definition of Characteristic Ratios :

4) $K_{tgl} = \frac{\dot{m}^t{}_{tgl}}{\dot{m}_0}$
5) $K_{trn} = \frac{\dot{m}^t{}_{trn}}{\dot{m}_0}$

6) $K_{glf} = \frac{\dot{m}^t{}_{glf}}{\dot{m}_0}$
7) $Y_{tgl} = \frac{\dot{m}_{tgl}}{\dot{m}^t{}_{tgl}}$
8) $Y_{trn} = \frac{\dot{m}_{trn}}{\dot{m}^t{}_{trn}}$
9) $Y_{glf} = \frac{\dot{m}_{glf}}{\dot{m}^t{}_{glf}}$
10) $X_{tgl} = \frac{\dot{m}_{tgl}}{\dot{m}_0}$
11) $X_{trn} = \frac{\dot{m}_{trn}}{\dot{m}_0}$
12) $X_{glf} = \frac{\dot{m}_{glf}}{\dot{m}_0}$

All the characteristic ratios have to be related to peculiar fields of view. More specifically three fields of view can be identified with respect to the distance from jet inlet: near field, far field and total field.

A.3 MILD Vortex Burner

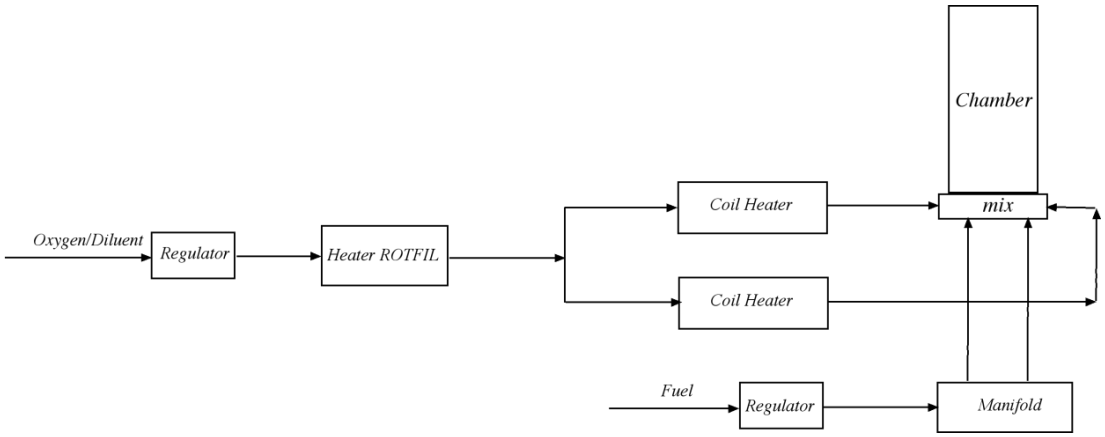

Plant layout (mix = MILD Vortex burner)

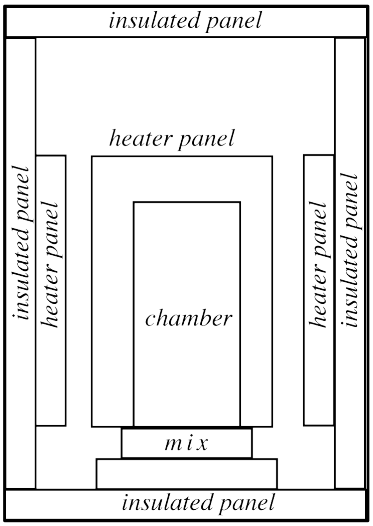

Scheme of reactor insulation

Plant: General View

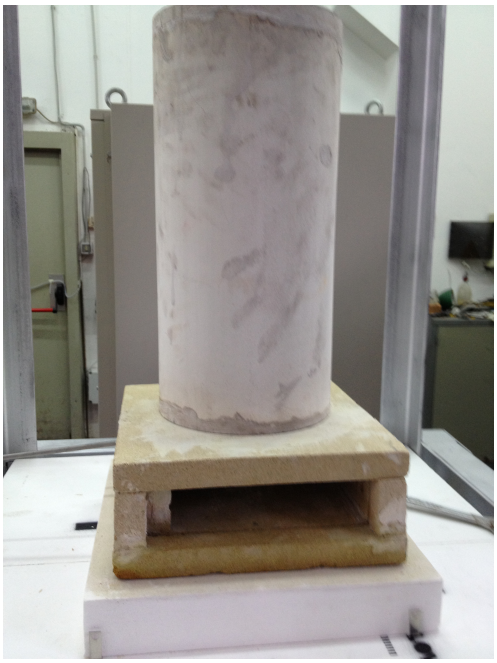

MILD Vortex burner

A.4 Test cases of conventional cyclonic apparatus

Test Case 1: 3D Turbulent Swirling Flow in a Cylinder.

Gupta and Kumar, Int. J. Heat and Fluid Flow (2007).

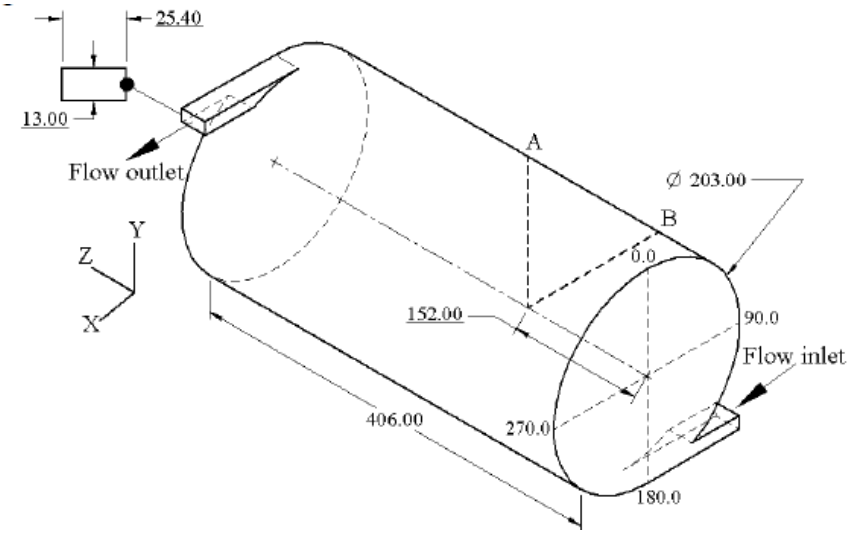

Turbulence Models	Inlet Reynolds Number
k- epsilon standard	9000
k-ω SST + curvature correction	9000
k-epsilon RNG swirl factor + curvature correction	9000
Reynolds Stress Model	9000

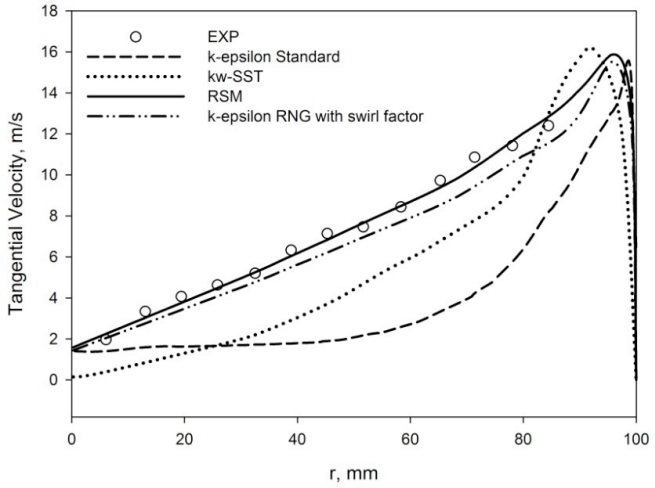

Line A

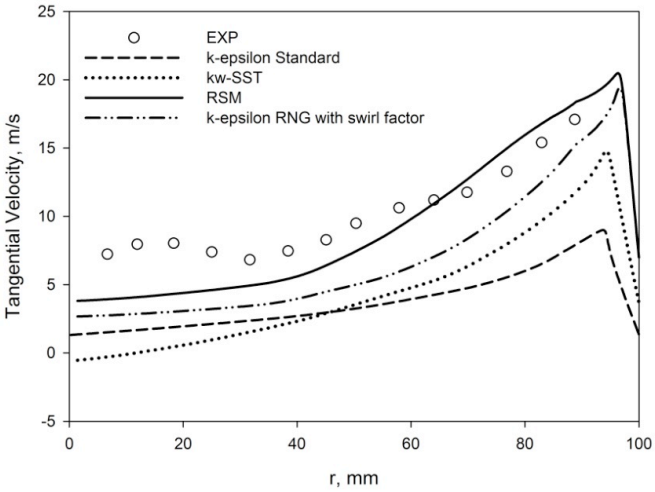

Line B

Test Case 2: Tangentially Injected Swirl Flow in a Tube

Chang and Dhir, Int. J. Heat and Fluid Flow (1994).

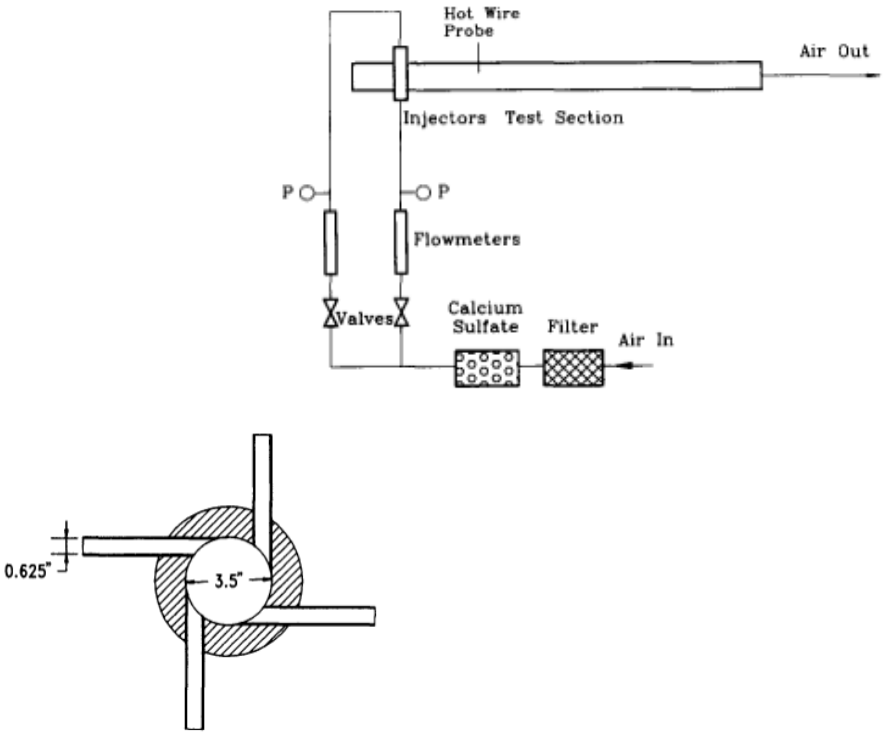

Turbulence Models	Inlet Tangential to Total Momentum Flux
k- epsilon standard	7.84
k-ω SST + curvature correction	7.84
k- epsilon RNG swirl factor + curvature correction	7.84

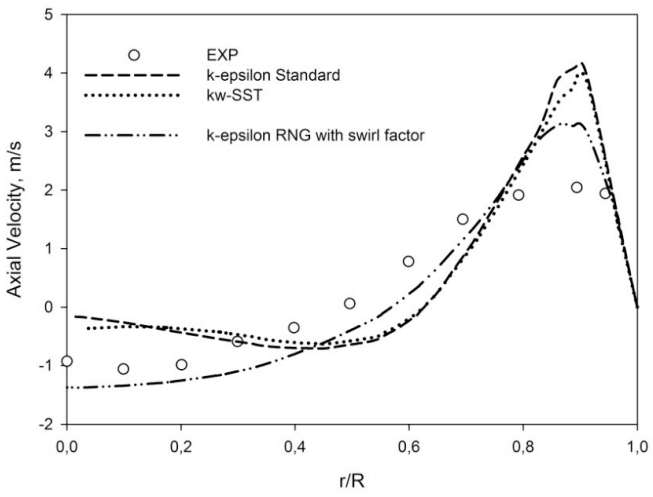

Axial Velocity, z/d = 6.

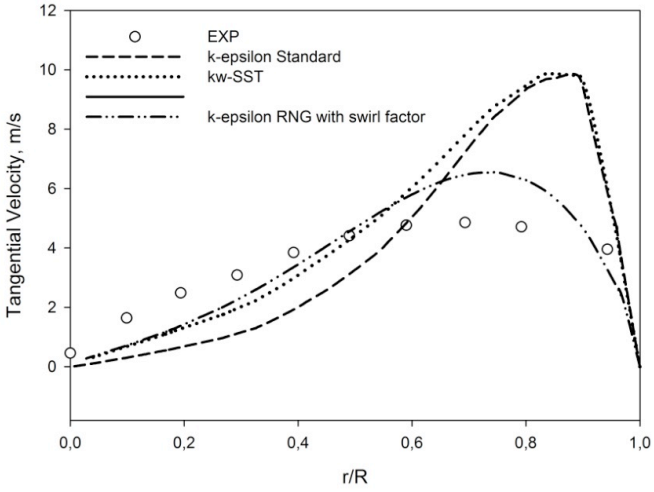

Tangential Velocity, z/d = 6.

Test Case 3: Reverse Flow Gas Cyclone Separator

Hoekstra et al., Chemical Engineering Science (1999).

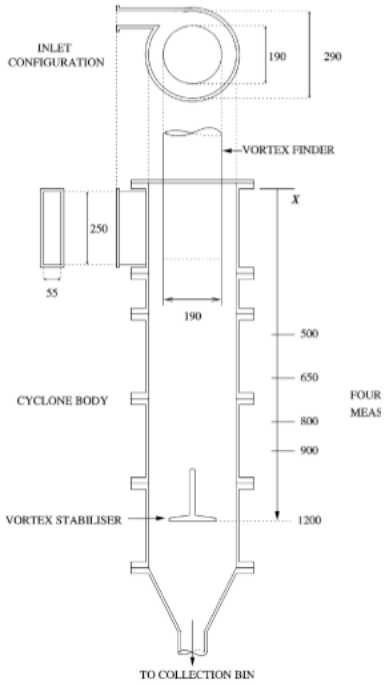

Turbulence Models	Inlet Reynolds Number	Swirl Number

k- epsilon standard	$2.5x10^4$	3.1
k- epsilon RNG swirl factor + curvature correction	$2.5x10^4$	3.1
Reynolds Stress Model	$2.5x10^4$	3.1

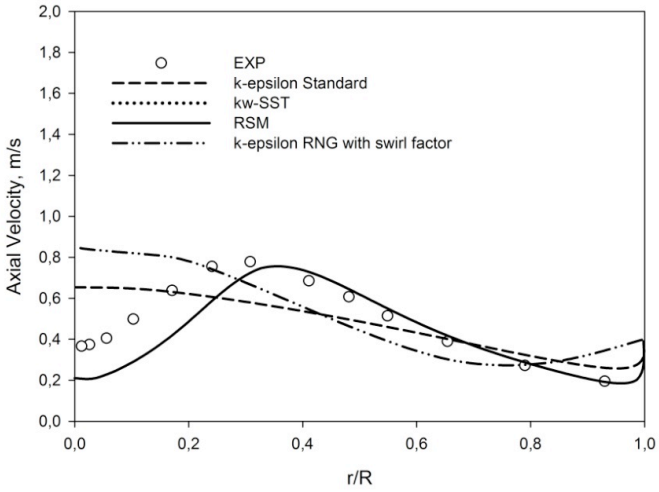

Axial Velocity, x= 650 mm.

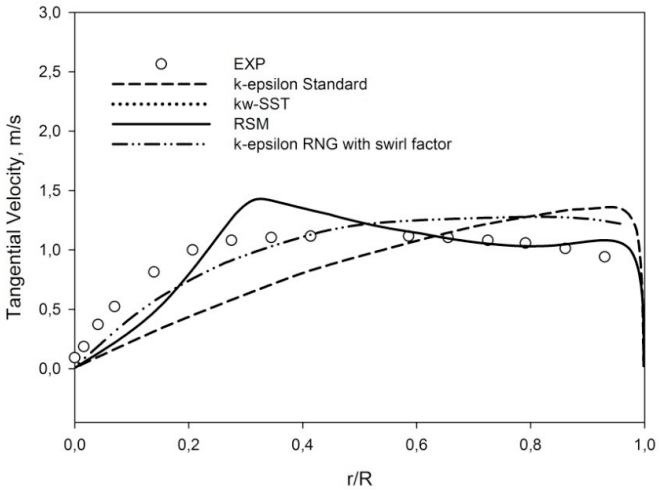

Tangential Velocity, x= 650 mm.

References

-A. Amato, B. Hudak, P. D'Carlo, D. Noble, D. Scarborough, J. Seitzman, T. Lieuwen, Methane Oxycombustion for low CO_2 cycles: Blowoff measurements and analysis, Journal of engineering for gas Turbines and Power, 133 (1) (2011).

-A. Amato, B. Hudak, P. D'Souza, P. D'Carloì, D. Noble, D. Scarborough, J. Seitzman, T. Lieuwen, Measurements and analysis of CO and O2 emissions in CH4/CO2/O2 flames, Proc. Combust. Inst. 33 (2011) 3399–3405.

-A. Cavaliere, M. de Joannon, Mild combustion, Prog. Combust. Sci. 30 (4) (2004) 329–366.

-A. Cavaliere, M. de Joannon, R. Ragucci, Highly Preheated Lean Combustion, chapter 3 in Lean Combustion: Technology and Control, (2008).

- A. Cavaliere, A. Chinnici, R. Ragucci, An Isothermal Characterization of Fluid-dynamic Configurations for ultra-lean mixture combustion Stabilization, AIDAA XXII, Naples, 2013.

- A. Chinnici, M. de Joannon, P. Sabia, A. Picarelli, R. Ragucci, CO2 Oscillations in Methane Mild Combustion, XXXIV Meeting of Italian Section of the Combustion Institute, Rome (2011).

- A. Chinnici, M. de Joannon, P. Sabia, A. Picarelli, R. Ragucci, Temperature Oscillations in CH4/O2/CO2 Mild-Oxyfuel Combustion, 11th ICCEU, Coimbra, 2012.

-A. Kather, S. Kownatzki, Assessment of the different parameters affecting the CO2 purity from coal fired oxyfuel process, Int. J. Greenhouse. Gas Con. 5 (1) (2011) 204–209.

-A. Kempf, W. Malalasekera, K.K.J. Ranga-Dinesh, and O. Stein. Large eddy simulations of swirling non-premixed flames with flamelet models: a comparison of numerical methods. Flow, Turbulence and Combustion, 81(4):523–561, 2008.

-A. Kogan, M. Kogan, The Tornado Flow Configuration:An Effective Method for Screening of a Solar Reactor Window, Transactions of the ASME, 2002.

-A. Leonard. Energy cascade in LES of turbulent fluid flows. Advances in Geophysics, 18:237–248, 1974.

-A. Mardani, S. Tabejamaat, S. Hassanpour, Numerical study of CO and CO2 formation in CH4/H2 blended flame under MILD condition, Combust. Flame, 160, 9 (2013), 1636-1649.

-A. Picarelli, P. Sabia, M. de Joannon, R. Ragucci, On the methane negative temperature coefficient behavior in Mild Combustion conditions. Water and Carbon Dioxide effects, 8th International Symposium on High Temperature Air Combustion and Gasification, Poznan, Poland, (2010).

-A. Picarelli, PhD Thesis, 2011.

-A. Sarofim, Oxy-Fuel Combustion: Progress and remaining issues, International Oxy-Combustion Research Network, 2nd Workshop, Windsor, CT, in: USA 2007.

-A. Sevault, M. Dunn, R. Barlow, M. Ditaranto, On the structure of the near field of oxy-fuel jet flames using Raman/Rayleigh laser diagnostics, Combust. Flame 159 (1), (2012), 3342-3352.

-A. Smeets, and A. Schneider. Rapid solar- thermal dissociation of natural gas in an aerosol flow reactor. Energy, 29:715– 725, 2004

-A. Spencer, J.J. McGuirk, and K. Midgley. Vortex breakdown in swirling fuel injector flows. Journal of Engineering for Gas Turbines and Power, 130:021503, 2008.

-A. Steinfeld and R. Palumbo. Encyclopedia of Physical Science & Technology, Vol. 15, chapter Solar Thermochemical Process Technology, pages 237–256. Academic Press, 2001. 1.3

-A. Z'Graggen, A. Steinfeld, Hydrogen production by steam-gasification of carbonaceous materials using concentrated solar energy – V. Reactor modeling, optimization, and scale-up, international journal of hydrogen energy 33 (2008) 5484–5492

-A. Z'Graggen, P. Haueter, D. Trommer, M. Romero, J.C. de Jesus, A. Steinfeld, Hydrogen production by steam-gasification of petroleum coke using concentrated solar power—II Reactor design, testing, and modeling, International Journal of Hydrogen Energy 31 (2006) 797–811

-A.A. Olajire, CO2 capture and separation technologies for end-of-pipe applications – a review, Energy 35 (6) (2010) 2610–2628.

-A.N. Mazas, B. Fiorina, D.A. Lacoste, T. Schuller, Effect of water vapor addition on the laminar burning velocity of oxygen-enriched methane flames, Combust. Flame 158 (12) (2011) 2428–2440.

-A.N. Mazas, D.A. Lacoste, T. Schuller, Experimental and numerical investigation on the laminar flame speed of CH_4/O_2 mixtures diluted with CO_2 and H_2O, in: Proceedings of ASME Turbo Expo, (2010).

-Adrian, Ronald J., and Westerweel J., Particle image velocimetry. Vol 30., Cambridge University Press, 2010.

-AK Gupta. Swirl flows. Technomic Publishing Co., Lancaster, PA, 1984.

-Antonia, R.A. Phys. Fluids, 23, 1980

-B. Dally, E. Riesmeier, N. Peters, Effect of fuel mixture on moderate and intense low oxygen dilution combustion, Combust.Flame 137 (4) (2004) 418-431.

-B. Thitakamol, A. Veawab, A. Aroonwilas, Environmental impacts of absorption-based CO_2 capture unit for post-combustion treatment of flue gas from coal-fired power plant, Int. J. Greenhouse Gas Control 1 (3) (2007) 318–342.

-B.E. Launder and D.B. Spalding. The numerical computation of turbulent flows. Computer Methods in Applied Mechanics and Engineering, 3(2):269–289, 1974.

-B.J.Buhre, L.K. Elliott, C.D. Sheng, R.P. Gupta, T.F. Wall, Oxy-fuel combustion technology for coal-fired power generation, Prog. Energ. Combust. Sci., 31 (4) (2005) 283-307.

-Becker, Yamazaki, Combust. Flame. 53:123–149 (1978).

-Broadwell, J. E., and Lutz, A. E., Combust. Flame 114:319–335 (1998)

-Cassidy, J J, Falvey, H T: J. Fluid Mech., 41, 4, 1970, p. 727

-C. Basdevant, T. Philipovitch, On the validity of the Weiss Criterion in two dimensional turbulence, phisica D:Non-Linear Phenomena, vol 73, Issues 1-2, pp17-30, 1994

-C. Bowman, M. Frenklach, W.R. Gardiner, G. Smith, The GRI 3.0 chemical kinetic mechanism. Berkeley, CA; University of California, (1999).

-C. Cortes, A. Gil, Modeling the gas and particle flow inside cyclone separators, Progress in Energy and Combustion Science, 33:409–452, 2007

-C. Danielson, G. and Lanczos. Some improvements in practical fourier analysis and their application to x-ray scattering from liquids. J. Franklin Inst., 233:365–380 and 435–452, 1942.

-C. Hoffmann and L. E. Stein. Gas cyclones and swirl tubes: Principle, Design and Operation. Springer, 2nd edition, 2008.

-C. Kulsheimer and H. Buchner. Combustion dynamics of turbulent swirling flames. Combustion and flame, 131[1-2]:70–84, 2002. 17

-C. Lacor. Lecture notes. Dept. Fluid Mechanics, Vrije Universiteit Brussel, Brussels, Belgium, 2007.

-C. Renard, M. Musick, P.J. Van Tiggelen, J. Vandooren, Effect of CO_2 or H_2O addition on hydrocarbon intermediates in rich C_2H_4/O_2/Ar flames, in: European Combustion Meeting, Orléans (France), (www.gfcombustion.asso.fr/ecm/2003/203_Vandooren.pdf).

-C.O.U. Umeh, Z. Rusak, E. Gutmark, R. Villalva, and D.J. Cha. Experimental and Computational Study of Non-Reacting Vortex Breakdown in a Swirl-Stabilized Combustor. In 47 th AIAA Aerospace Sciences Meeting Including the New Horizons Forum and Aerospace Exposition(Disc 1). American Institute of Aeronautics and Astronautics, 1801 Alexander Bell Drive, Suite 500, Reston, VA, 20191-4344, USA,, 2009.

-Chen, R. H., and Driscoll, J. F., Proc. Combust. Inst. 23:281–288 (1990).

-Clemens, N.T., Flow Imaging, 2002.

-D. Fritsche, Origin and Control of Thermo-Acoustic Instabilities in Lean Premixed Gas Turbine Combustion, PhD Thesis, Swiss Federal Institute of Technology Zurich, (2005).

-D. Han, M. Mungal, Comb and Flame 124:370–386 (2001)

-D. Hirsch and A. Steinfeld. Solar hydrogen production by thermal decomposition of natural gas using a vortex-flow reactor. International Journal of Hydrogen Energy, 29:47–55, 2004. 1.3

-D.C. Wilcox. Turbulence modeling for CFD. DCW Industries, Inc., La Canada, California, 2002.

-De Sa, M. S., E. Shoukry and I. Soegiarto, "Mass Transfer Enhancement in the Entrance Region for Axial and Swirling Annular Flow," Can. J. Chem. Eng. 69, 294–299 (1991).

-Derksen JJ, Akker VD. Simulation of vortex core precession in a reverse flow cyclone. AIChE J 2000;46:1317–30.

-Derksen JJ. Simulations of confined turbulent vortex flow. Comp Fluids 2005;34:301–18.

-E. A. Fletcher. Solarthermal processing: A review. Journal of Solar Energy Engineering, 123:63–74, 2001. 1.3

-E. Blomen, C. Hendriks, F. Neele, Capture technologies: improvements and promising developments, Energy Procedia 1 (1) (2009) 1505–1512.

-E. De Visser, C. Hendriks, M. Barrio, M.J. Molnvik, G. de Koeijer, S. Liljemark, Y. Le Gallo, Dynamis CO2 quality recommendations, Int. J. Greenhouse Gas Con. 2 (4) (2008) 478–484.

-E. Oldenhof, M.J. Tummers, E.H. van Veen, D.J.E.M. Roekaerts, Combustion and Flame 158 (2011) 1553–1563.

-E.L. Petersen, D.M. Kalitan, S. Simmons, G. Bourque, H.J. Curran, J.M. Simmie, Methane/Propane Oxidation at High Pressures: Experimental and Detailed Chemical Kinetic Modelling, Prog. Combust Inst., 31, (2007), 447-454.

- Biagioli, F. Guthe, and B. Schuermans. Combustion dynamics linked to flame behaviour in a partially premixed swirled industrial burner. Experimental Thermal and Fluid Science, 32[7]:1344–1353, 2008. 17, 24.

-F. Bogner and K. Wintrup. Handbook of Synfuels Technology, chapter The Fluidized-Bed Coal Gasification Process (Winkler Type), pages 111–125. McGraw-Hill, New York, 1984.

-F. Culick, Unsteady Motions in Combustion Chambers for Propulsion Systems, RTO AGARDograph, AG-AVT-039, 2006.

-F. Liu, H. Guo, G. Smallwood, O. Gulder, The chemical effect of CO_2 as an additive in a ethylene diffusion flame: Implications for soot and NOx formation, Combust. Flame 125, (2001), 778–787.

-F. Liu, H. Guo, G. Smallwood, The chemical effect of CO_2 replacement of N_2 in air on the burning velocity of CH4 and H2 premixed flames, Combust. Flame 133 (2003) 495–497.

-Fick W. PhD Thesis. Cardiff University; 1968.

- Barbieri, F.P. Di Maio, P.G. Lignola, M.L. Loiacono, Modeling methane cool flames and ignitions, Comb. Sci. Tech. 106 (1), (1995), 83-102.

-G. Borghesi, F. Biagioli, and B. Schuermans. Dynamic response of turbulent swirling flames to acoustic perturbations. Combustion Theory and Modelling, 13[3]:487–512, 2009. 16, 17, 21, 22, 24

-G. Pipitone, O. Bolland, Power generation with CO2 capture: technology for CO2 purification, Int. J. Greenhouse Gas Con. 3 (5) (2009) 528–534.

-G. Schlinger. Handbook of Synfuels Technology, chapter The Texaco Coal Gasification Process. McGraw-Hill, New York, 1984. 1.2

- Szego, B. Dally, G.J. Nathan, Scaling of NOx emissions from a laboratory-scale mild combustion furnace, Combust. Flame 154 (1) (2008) 281-295.

-G. Scheffknecht, L. Al-Makhadmeh, U. Schnell, J. Maier, Oxy-fuel coal combustion – A review of the current state-of-the-art, IJGGC 5S (1), (2011), 16-35.

-Gil A, Corte ´ s C, Romeo LM, Velilla J. Gas-particle flow inside cyclone diplegs with pneumatic extraction. Powder Technol 2002;128:78–91.

-Gil A, Romeo LM, Corte ´ s C. Cold flow model of a PFBC cyclone. Powder Technol 2001;117:207–20.

-Gupta, A. K., D. G. Lilly and N. N. Syred, "Swirl Flows," Abacus, Tunbridge Wells, England, U.K. (1984).

-Hawthorne, W. R., Weddell, D. S., and Hottel, H. C., Proc. Combust. Inst. 3:266–288 (1949).

-H. Li, J. Yan, M. Anheden, Impurity impacts on the purification process in oxy-fuel combustion based CO2 capture and storage system, Appl. Energy 86 (2009) 202–213.

-H. Li, M. Ditaranto, J. Yan, Carbon capture with low energy penalty: supplementary fired natural gas combined cycles, Appl. Energ. 97 (2012)

-H. Shalaby. On the Potential of Large Eddy Simulation to Simulate Cyclone Separators. PhD thesis, Chemnitz University of Technology, Chemnitz, Germany, 2007.

-H. Watanabe, F. Arayi, K. Okazachi, Role of CO2 in the CH4 oxidation and H2 formation during fuel-rich combustion in O2/CO2 environments, Combust. Flame, 160, 11 (2013), 2375-2385.

-H.J. Merk, Analysis of Heat-Driven Oscillations of Gas Flows. General Considerations, Applied Science Research, pp. 317-356 (1956).

-H.K. Chagger, J.M. Jones, M. Pourkashanian, A. Williams, A. Owen, G. Fynes, Emission of volatile organic compounds from coal combustion, Fuel 78 (1999) 1527–1538.

-H.M. Kvamsdal, K. Jordal, O. Bolland, A quantitative comparison of gas turbine cycles with CO2 capture, Energy 32 (2007) 10–24.

-H.M. Kvamsdal, K. Jordal, O. Bolland, A quantitative comparison of gas turbine cycles with CO2 capture, Energy 32 (2007) 10–24.

-Hawthorne, W. R., Weddell, D. S., and Hottel, H. C., Proc. Combust. Inst. 3:266–288 (1949).

-Hill, B.J., J. Fluid Mech.51:773–779 (1972).

-Hill, B.J., J. Fluid Mech.51:773–779 (1972).

-Hilsch, R., "The Use of the Expansion of Gases in a Centrifugal Field as a Cooling Process," Review of Scientific Instruments 18, 108–113 (1947).

-Holzapfel, F. (2004), "Adjustment of subgrid-scale parameterizations to strong streamline

-Hunt, J., Wray, A., Moin, P 1988 Eddies, Stream and convergence zones in turbulent flows, CTR-S88

-IEA Greenhouse Gas R&D Programme. Oxy-Combustion Processes for CO2 Capture From Power Plants, Report No. 2005/09, 2005.

-Iyougun, Birouk ,Flow Turbulence Combust (2009) 82:287–315

-J. Egret, L.R. Sochet, M. Lucquin, Bull. Soc. Chim., 2205 (1965).

-J. K. Dahl, A. W. Weimer, A. Lewandowski, C. Bingham, F. Bruetsch, and A. Steinfeld. Dry reforming of methane using a solar-thermal aerosol flow reactor. Industrial & Engineering Chemistry Research, 43:5489–5495, 2004. 1.3

-J. K. Dahl, K. J. Buechler, R. Finley, T. Stanislaus, A. W. Weimer, A. Lewandowski, C. Bingham,

-J. Park, D.J. Hwang , J.G. Choi, K.M. Lee, S.I. Keel, S.H. Shim, Chemical effects of CO_2 addition to oxidizer and fuel streams on flame structure in H_2-O_2 counterflow diffusion flames, International Journal of Energy Research, 27 (13), (2003), 1205-1220.

-J. Rezaiyan and N. P. Cheremisinoff. Gasification Technologies. Taylor & Francis, 2005. 1.2, 2.1, 4.1

-J. Wang, D. Ryan, E.J. Anthony, N. Wildgust, T. Aiken, Effect of impurities on CO2 transport injection and storage, Energy Procedia 4 (2011) 3071–3078.

-J. Warnatz, U. Maas, R. Dibble, Combustion: physical and chimica fundamentals, modeling and simulation, experiments, pollutant formayion. Berlin: Springer Verlag, (2006).

-J. Yan, M. Anheden, G. Lindgren, L. Stromberg, Conceptual development of fuel gas cleaning for CO2 capture from coal-fired oxy-fuel combustion power plant, in: 8th International Conference on GreenHouse Gas Control Technologies, Trondheim, Norway, (2006).

-J.A.Wunning, J.G. Wunning, Flameless oxidation to reduce thermal NOx formation, Prog. Energ. Combust. Sci., 23 (1) (1997) 81-94.

-J.H. Ferziger and M. Peri ´c. Computational Methods for Fluid Dynamics. Springer, Berlin, 1999.

-J.W. Deardorff. The use of subgrid transport equations in a three dimensional model of atmospheric turbulence. Journal of Fluids Engineering, 95:429–438, 1973.

-Jakirlic, S., Hanjalic, K. and Tropea, C. (2002), "Modeling rotating and swirling turbulent flows: a perpetual challenge", AIAA Journal, Vol. 40 No. 10, pp. 1984-96.

-Kanna P., Das. M, Int. J. Numer. Meth. Fluids (2005); 49:439–464

-K. Bobba, P. Gopalakrishnan, K. Periagaram, J.M. Seitzman, 45th AIAA Aerospace Sciences Meeting and Exhibit AIAA-2007-0173 Reno, Nevada, 8 - 11 (2007).

-K. Elsayed and C. Lacor. Numerical modeling of the flow field and performance in cyclones of different cone-tip diameters. Computers & Fluids, 51(1):48–59, 2011.

-Kodama, Application of an Internally Circulating Fluidized Bed for Windowed Solar Chemical Reactor with Direct Irradiation of Reacting Particles, Journal of Solar Energy Engineering, Vol. 130 / 014504-1

-K. Midgley, A. Spencer, and J.J. McGuirk. Unsteady flow structures in radial swirler fed fuel injectors. Journal of engineering for gas turbines and power, 127:755, 2005. 13

-Krishna, N.Ozalp, Numerical investigation of particle deposition inside aero-shielded solar cyclone reactor: A promising solution for reactor clogging, International Journal of Heat and Fluid Flow 40 (2013) 198–209

-Kruesi, Zoran R. Jovanovic. Aldo Steinfeld, A two-zone solar-driven gasifier concept: Reactor design and experimental evaluation with bagasse particles, Fuel 117 (2014) 680–687.

-L. B. Davis, R. M. Washam, Development of a Dry Low NOx Combustor, ASME Transactions, 89-GT-225, (1989).

-L. Chen, S. Zheng, A. Ghoniem, Oxy-fuel combustion of pulverized coal: Characterization, fundamentals, stabilization and CFD modeling, Prog. Energ. Combust. Sci., 38 (2) (2012) 156-214.

-L. Davidson. Lecture notes. Dept. of Thermo and Fluid Dynamics, Chalmers University of Technology, Go ¨teborg, Sweden, 2000.

-L. Patrignani L., M. Losurdo, C. Bruno, Journal of the International Flame Research Foundation Article Number 201003, September 2010

-L. Prandtl. Bericht uber die entstehung der turbulenz. Zeitschrift fur Angewandte Mathematik und Mechanik, 5:136–139, 1925.

-Lee SK, Lanspeary PV, Nathan GJ, Kelso RM, Mi J. Low kinetic energy loss triangular jet nozzles. Exp Therm Fluid Sci 2003;27:553–61.

-Lurgi — Kohle- und Mineral ¨oltechnik. Lurgi Handbuch. Lurgi Gesellschaften,Frankfurt a.M., 1970.

-Lieuwen, T. and V. Yang, Combustion Instabilities in Gas Turbine Engines. AIAA,

-M. Abian, J. Gimenez-Lopez, R. Bilbao, M. Alzueta, Effect of different concentration levels of CO2 and H2O on the oxidation of CO: Experiments and modeling, Prog. Combust Inst., 33, (2011), 317-323.

-M. de Joannon, A. Cavaliere, T. Faravelli, E. Ranzi, P. Sabia, A. Tregrossi, Analysis of process parameters for steady operations in methane mild combustion technology, Prog. Combust Inst., 30 (2), (2005), 2605-2612

-M. de Joannon, A. Chinnici, P. Sabia, R. Ragucci, Optimal post-combustion conditions for the purification of CO2-rich exhaust streams from non-condensable reactive species Chemical Engineering Journal, 210-211, (2012), 318-326.

-M. de Joannon, A. Matarazzo, P. Sabia, A. Cavaliere, Mild Combustion in Homogeneous Charge Diffusion Ignition (HCDI) regime, Proceedings of Combustion Institute, 31 (2), pp. 3409-3416 (2007).

-M. de Joannon, P. Sabia, A. Cavaliere, MILD Combustion, in: M. Lackner, F. Winter, A.K. Agarwal (Eds.), Handbook of combustion, Wiley-VCH, (2010).

-M. de Joannon, P. Sabia, A. Tregrossi, A. Cavaliere, Dilution effects in natural gas mild combustion, International Journal of Energy for a clean Environment, 7(2), (2007), 127-139.

-M. de Joannon, P. Sabia, A. Tregrossi, A. Cavaliere, Dynamic behavior of methane oxidation in premixed flow reactor, Comb.Sci. Tech 176 (5), (2004).

-M. de Joannon, P. Sabia, A. Tregrossi, A. Cavaliere, Periodic regimes in low molecular weight paraffin oxidation, Proceedings of the European Combustion Meeting, (2003).

-M. Germano, U. Piomelli, P. Moin, and W. H. Cabot. A dynamic subgrid-scale eddy viscosity model. Physics of Fluids A, 3(7):1760– 1765, 1991.

-M. J. Antal, L. Hofmann, and J. R. Moreira. Design and operation of a solar fired biomass flash pyrolysis reactor. Solar Energy, 30:299–312, 1983. 1.3

-M. Kiya, H. Ishikawa, and H. Sakamoto. Near-wake instabilities and vortex structures of three-dimensional bluff bodies: a review. Journal of Wind Engineering and Industrial Aerodynamics, 89[14-15]:1219–1232, 2001. 8, 9, 45

-M. Vanpee, On the cool flames of methane, Comb. Sci. Tech. 93 (1), (1993), 363-374.

-M.O ¨sterlund,A.V.Johansson,andM.N.Hassan.Anoteontheintermediate region in turbulent boundary layers. Phys. Fluids, 12(9):2360–2363, 2000.

-Manias CG, Nathan GJ. Low NOx clinker production. World Cem 1994;25(5):54–6.

-Mansurov, V I, Kuraev, Y F, Marshek, Y L, Suckkov, S I : Thermal Eng., 17, 10, 1970, p. 55

-Meier HF, Mori M. Anisotropic behavior of the Reynolds stress in gas and gas-solid flows in cyclones. Powder Technol 1999;101:108–19.

-Montavon CA, Grotjans H, Hamill IS, Philips HW, Jones IP. Mathematical modeling and experimental validation of flow in a cyclone. BHR conference on cyclone technologies, Warwick, 2000.

-Martemianov, S. and V. L Okulov, “Mass Transfer Ambiguities in Swirling Pipe Flows,” J. Applied Electroch. 32, 25–34 (2002).

-Martemianov, S. and V. L. Okulov, “On Heat Transfer Enhancement in Swirl Pipe Flows,” Int. J. Heat Mass Transfer 47, 2379–2393 (2004).

-Muniz, L.,, Ph.D. Thesis, Stanford University, Stanford, CA, 2000.

-Nasr. A, Lai J. , Experiments in Fluids 24 (1998)

-Nathan G.J., Mi, J., Alwahabi, Z.T. Newbold, G.J.R. and Nobes, D.S. (2006) Impact of a jet’s exit flow pattern on mixing and combustion performance, Prog. Energy and Combust. Sci., 32, (5-6), 496-538.

-N. Aida, T. Nishijima, S. Hayashi, H. Yamada, T. Kawakami, Combustion of lean Pre-vaporized fuel-air Mixtures mixed with hot burned gas for low-NOx emissions over an extended range of fuel-air ratios, Proceedings of Combustion Institute, 30 (1), pp. 2885-2892 (2005).

-N. Ozalp, M. Chien, G. Morrison, Fluid Dynamics and Particle Image Velocimetry Characterization of a Solar Cyclone Reactor, Journal of Solar EnergyEngineering, Vol. 135 / 031003-1

-N. Piatkowski, C.Wieckert, A. W. Weimer, A. Steinfeld, Solar-driven gasification of carbonaceous feedstock—a review, Environ. Sci., 2011, 4, 73

-Nathan GJ, Hill SJ, Luxton RE. An axisymetric ‘fluidic’ nozzle to generate jet precession. J Fluid Mech 1998;370:347–80.

-Newbold GJR, Nathan RE, Luxton RE. Large scale dynamics of an unconfined precessing jet flame. Combust Sci Technol 1997; 126:71–95.

-Nicholas, S., A review of oscillation mechanisms and the role of the precessing vortex core (PVC) in swirl combustion systems. Progress in Energy and Combustion Science, 2006. 32(2): p. 93-161.

-N. Syred and J.M. Beer. Combustion in swirling flows- A review. Combustion and Flame, 23:143–201, 1974. 11

-- N. Syred and J.M. Beer. The damping of precessing vortex cores by combustion in swirl generators. Astronautica Acta, 17[4/5]:78, 1972. 13

-O. Bolland, Outlook for CO2 capture technologies, in: IARU International Scientific Congress on Climate Change, Copenaghen, Denmark, (2009).

-O. Marzouk, D. Huckaby, Engineering Letters, 18:1, EL_18_1_07

-Ocampo, E. Arenas, F. Chejne, J. Espinel, C. London, J. Aguirre, J.D. Perez 82 An experimental study on gasification of Colombian coal in fluidised bed (2003) Fuel 82 (2003) 161–164–164.

-Ottino J.M.,J.Fluid Mech.,1982.

-O. Iyogun, · M. Birouk, ‚Flow Turbulence Combust (2009) 82:287–315

-O. Lucca-Negro and T. O'Doherty. Vortex breakdown: a review. Progress in Energy and Combustion Science, 27[4]:431–481, 2001. 11, 13, 126, 131

-O. Marzouk, D. Huckaby, Engineering Letters, 18:1, EL_18_1_07

-P. G. Saffman and G. R. Baker. Vortex interactions. Annual Review of Fluid Mechanics, 11:95–122, 1979.

-P. Glarborg, L.L.B. Bentzen, Chemical effects of high CO2 concentration in Oxy-Fuel combustion of methane, Energy Fuels, 22 (1) (2008), 291-296.

-P. Gray, J.H. Griffiths, S.M. Hasko, P.G. Lignola, Proc.R.Soc.Lond. 374 (1981), 313-339.

-P. Heil, D. Toporov, M. Forster, R. Kneer, Experimental investigation on the effect of O2 and CO2 on burning rates during oxyfuel combustion of methane, Proc. Combust. Inst 33 (2011) 3407–3413.

-P. Heil, D. Toporov, M. Forster, R. Kneer, Experimental investigation on the effect of O2 and CO_2 on burning rates during oxyfuel combustion of methane, Proc. Combust. Inst 33, (2011), 3407–3413.

-P. Jones and B. E. Launder. The prediction of laminarization with a two-equation model of turbulence. Int. J. Heat Mass Transfer, 15:301–314, 1972.

- Moin and J. Kim. Numerical investigation of turbulent channel flow. Journal of Fluid Mechanics, 155:441, 1982.

-P.L. Woodfield et al., International Journal of Heat and Mass Transfer 46 (2003) 2655–2663

-Patrignani L., M. Losurdo, C. Bruno, Journal of the International Flame Research Foundation Article Number 201003, September 2010

-Peters, N., Turbulent Combustion, institute für Technische Mechanik, Rheinisch-

-P. Sabia, F. Romeo, M. de Joannon, A. Cavaliere, VOC destruction by water diluted hydrogen mild combustion, Chemosphere 68 (2006) 330–337.

-P. Sabia, M. de Joannon, A. Picarelli, R. Ragucci, Methane autoignition times and oxidation regimes in MILD combustion at atmospheric pressure, Combust. Flame (2012)

-P. Sabia, M. de Joannon, A. Picarelli, A. Chinnici, R. Ragucci, Modeling negative temperature coefficient region in methane oxidation, Fuel 91 (1) (2012) 238–245.

-P. Sabia, M. de Joannon, S. Fierro, A. Tregrossi, A. Cavaliere, Hydrogen-enriched methane Mild Combustion in a well stirred reactor, Experimental Thermal and Fluid Science 31 (1), (2007), 469-475.

-P. Sagaut. Large-Eddy Simulation for Incompressible Flows. Scientific Computation, Springer, 2002.

-P. Schmitt, T. Poinsot, B. Schuermans, and KP Geigle. Large-eddy simulation and experimental study of heat transfer, nitric oxide emis- sions and combustion instability in a swirled turbulent high-pressure burner. Journal of Fluid Mechanics, 570:17–46, 2007. xiv, 17, 18, 20, 21, 23, 25

-P. von Zedtwitz, J. Petrasch, D. Trommer, and A. Steinfeld. Hydrogen production via the solar thermal decarbonization of fossil fuels. Solar Energy, 80:1333–1337, 2006.

-P.L. Woodfield et al., International Journal of Heat and Mass Transfer 46 (2003) 2655–2663

-P.S. Yarlagadda, A.M. Lawrence, R.H. Norman, D.G. Hyman, Temperature oscillations during the high-pressure partial oxidation of methane in a tubular flow reactor, Combust. Flames 79 (2), (1990), 216-218.

-Peng W, Boot P, Udding A, Hoffmann AC, Dries HWA, Ekker A, et al. Determining the best modelling assumptions for cyclones and swirl tubes by CFD and LDA. International Congress for Particle Technology; 2001. p. 1–8.

-Peng W, Hoffmann AC, Boot PJAJ, Udding A, Dries HWA, Ekker A, et al. Flow pattern in reverse-flow centrifugal separators. Powder Technol 2002;127:212–22.

-Progress in Astronautics and Aeronautics, USA, 2005. 210.

- Berber and E. A. Fletcher. Extracting oil from shale using solar energy. Energy, 13:12–23, 1988. 1.3

-Ricou, F. P., and Spalding, D. B., J. Fluid Mech.11:21–32 (1961).

-R. Steeneveldt, B. Berger, CO2 capture and storage: closing the knowing-doing gap, Chem. Eng. Prog. 84 (9) (2006) 739–763.

-R. Vicquelin, B. Fiorina, O. Gicquel, G. Lartigue, T. Poinsot, LES COST 2007

-R. Vicquelin, B. Fiorina, O. Gicquel, G. Lartigue, T. Poinsot, LES COST 2007.

- Weber, S. Orsino, N. Lallemant, A. Verlaan, Combustion of natural gas with high-temperature air and large quantities of flue gas, Proc. Combust Inst., 28 (1) (2000) 1315-1321

-R. Buck, J. F. Muir, R. E. Hogan, and R. D. Skocypec. Carbon dioxide reforming of methane in a solar volumetric receiver/reactor: the CAESAR project. Solar Energy Materials, 24:449–463, 1991. 1.3

-R.E. Foglesong, T.R. Frazier, L.M. Flamand, J.E. Peters, R.P. Luchi, Flame Structure and Emissions Characteristics of a Lean Premixed Gas Turbine Combustor, 99-2399 (1999).

-R.J. Kee, F.M. Rupley, J.A. Miller, M.E. Coltrin, J.F. Grcar, E. Meeks, H.K. Moffat, A.E. Lutz, G. Dixon-Lewis, M.D. Smooke, J. Warnatz, G.H. Evans, R.S. Larson, R.E. Mitchell, L.R. Petzold, W.C. Reynolds, M. Caracotsios, W.E. Stewart, P. Glarborg, C. Wang, O. Adigun, W.G. Houf, C.P. Chou, S.F. Miller, CHEMKIN Collection, Release 3.7, Reaction Design, Inc., San Diego, CA, 2003.

-Rumsey, C.L., Gatski, T.B. and Morrison, J.H. (2000), "Turbulence model predictions of strongly curved flow in a U duct", AIAA Journal, Vol. 38 No. 8, pp. 1394-402.

-S. Abanades and G. Flamant. Solar hydrogen production from the thermal splitting of methane in a high temperature solar chemical reactor. Solar Energy, 80:1321–1332, 2006. 1.3

-S. B. Pope. Turbulent flows. Cambridge university press, New York, 2000.

-S. Candel, Combustion dynamics and control: Progress and challenges, Proceedings of Combustion Institute, 29 (1), pp. 1-28 (2002).

- Seepana, S. Jayanti, Optimized enriched CO_2 recycle oxy-fuel combustion for high ash coals, Fuel 102 (1) (2012), 32-40.

-S.T.. Jayaraju. Study of the air flow and aerosol transport in the human upper airway using LES and DES methodology. PhD thesis, Vrije Universiteit Brussel, 2009.

-S. Seo, Combustion Instability Mechanism of a Lean Premixed Gas Turbine Combustor, KSME International Journal, 17 (6), pp.906-913, (2003).

-S. Wang-Ping, L. Jong Guen, D.A. Santavicca, Stability and Emissions Characteristics of a Lean Premixed Gas Turbine Combustor, XXVI International Symposium on Combustion, pp. 2771-2778 (1996).

-Schmidt, K R: V.D.I. ·Berichte, 146, 1970, p. 90.

-Schneider W., , J. Fluid Mech. Vol 154, pp 91-110

-Shilapuram, D. J. Krishna, N. Ozalp , IResidence time distribution and flow field study of aero-shielded solar cyclone reactor for emission-free generation of Hydrogen, International journal of hydrogen energy 36 (2011)

-Slack MD, Prasad RO, Bakker A, Boysan F. Advances in cyclone modelling using unstructured grids. Trans I Chem 2000;78:1098–104.

-Speziale, C.G., Younis, B.A. and Berger, S.A. (2000), "Analysis and modeling of turbulent flow in an axially rotating pipe", J. of Fluid Mechanics, Vol. 407, pp. 1-26.

-Syred N, Beer JM. Combustion in swirling Flows: a review. Combustion and Flame, 1974;23:143201.

-Syred N, Dahmen K, Styles AC, Najim SE. A review of combustion problems associated with low calorific value gases. J Inst Energy (ISSN: 0144-2600) 1997;50:195–207.

-Syred, N, Dahmen, K R, Styles, A C, Najim, S E: J. Inst. Fuel, 50, 405, 1977, p. 195.

-S.T.. Jayaraju. Study of the air flow and aerosol transport in the human upper airway using LES and DES methodology. PhD thesis, Vrije Universiteit Brussel, 2009.

-S. Wang, V. Yang, G. Hsiao, S.Y. Hsieh, and H.C. Mongia. Large-eddy simulations of gas-turbine swirl injector flow dynamics. Journal of Fluid Mechanics, 583:99–122, 2007.

-Schneider W. J. Fluid Mech. Vol 154, pp 91-110

-Smith NL, Megalos NP, Nathan GJ, Zhang DK, Smart JP. Precessing jet burners for stable and low NOx pulverized fuel flames—preliminary results from small scale trials. Fuel 1998; 77(9/10):1013–6.

-Smith, J L: J. Basic Eng., Trans. ASME, D84, 1962, p. 602.

-Suzuki, M: Scientific Papers Institute Physics and Chemistry Research, Tokyo, 54, 1, 1960, p. 44.

- Swithenbank J, Chigier NA. Vortex mixing for supersonic combustion. 21st International Symposium on Combustion, 1969. p. 1154±62.

-Symons E., Labus T., NASA Report 1971

-Tanasana. Y. and K. Nakamira. "On the Vortex Combustor as Applied to the Gas Turbine." JSME-15 paper presented at the Tokyo Joint JSME-ASME International Gas Turbine Conference and Product Show, Tokyo, Japan, Cot. 4–7, (1971).

-Tsarev, V K, Troyankin, Y V: Thermal Eng., 18, 12, 1971, p. 84.

-T. C. Lieuwen. Physics of premixed combustion-acoustic wave interac- tions. In T. C. Lieuwen and V. Yang, editors, Combustion Instabilities in Gas Turbine Engines, 210 of Progress in Astronautics and Aeronautics, pages 315–366. AIAA, 2005. 16

-T. Kodama, A. Kiyama, T. Moriyama, and O. Mizuno. Solar methane reform- ing using a new type of catalytically-activated metallic foam absorber. Journal of Solar Energy Engineering, 126:808–811, 2004. 1.3

-T. Kodama. High-temperature solar chemistry for converting solar heat to chemical fuels. Progress in Energy and Combustion Science, 29:567–597, 2003. 1.3

-T. Le Cong, P. Dagaut, Effect of water vapor on the kinetics of combustion of hydrogen and natural gas: experimental and detailed modeling study, ASME Paper GT, 50272, (2008).

-T. Le Cong, P. Dagaut, G. Dayma, Oxidation of natural gas, natural gas/syngas mixtures, and effect of burnt gas recirculation: experimental and detailed kinetic modeling, J. Eng. Gas Turb. Power 130, (2008), 041502–041512.

-T. Le Cong, P. Dagaut, Oxidation of H_2/CO_2 mixtures and effect of hydrogen initial concentration on the combustion of CH_4 and CH_4/CO_2 mixtures: Experiments and modeling, Proc. Combust. Inst. 32, (2009), 427–435.

-T. Lieuwen, H. Torres, C. Johnson, B.T. Zinn, A mechanism of Combustion Instability in Lean Premixed Gas Turbine, ASME Transactions, 123 (1), pp. 182-189 (2001).

-T. Lieuwen, Modeling Premixed Combustion-Acoustic Wave Interactions: A Review Journal of Propulsion and Power, 19 (5), pp. 765-781 (2003).

-T. Wada, F. Jarmolowitz, D. Abel, N. Peters, An instability of diluted lean methane/air combustion: Modeling and Control, Comb.Sci. Tech 183 (1), (2010), 1-19.

-T. Wada, G. Pazcko, N. Peters, Numerical investigations of high diluted lean CH4/air oscillations at low temperatures, ECM 2009 Fourth European Combustion Meeting, Vienna University of Technology, Vienna, Austria, 14 - 17 April, (2009).

-T.F. Fric, Effects of Fuel-Air Unmixedness on NOx Emissions, Journal of Propulsion and Power, 9 (1), pp. 708-713 (1993).

-T.F. Wall, Combustion processes for carbon capture, Proc. Combust Inst., 31 (1) (2007) 31-47.

-Taylor, R. Berjoan, J.P. Courtes, Solar Gasification of Carbonaceous Materials, Energy, Vol.30,No.6,pp.513-525,1983.

-U. Piomelli, Y. Yu, and R. J. Adrain. Sub-grid scale energy transfer and near-wall turbulence structure. Physics of Fluids, 8:215 –224, 1996.

-Valera-Medina, A., Coherent Structures and Their Effects on Process Occurring in

- Valera-Medina, N. Syred, and A. Griffiths. Characterization of Large Coherent Structures in a Swirl Burner under Combustion Conditions. In 47 th AIAA aerospace sciences meeting including the new horizons forum and aerospace exposition. American Institute of Aeronautics and Astronautics, 1801 Alexander Bell Drive, Suite 500, Reston, VA, 20191-4344, USA,, 2009.

- Valera-Medina, N. Syred, and A. Griffiths. Characterization of Large Coherent Structures in a Swirl Burner under Combustion Conditions. In 47 th AIAA aerospace sciences meeting including the new horizons forum and aerospace exposition. American Institute of Aeronautics and Astronautics, 1801 Alexander Bell Drive, Suite 500, Reston, VA, 20191-4344, USA,, 2009. 1, 10, 11, 13, 15

-V. Vogt, M. J. V. D. Burgt, J. H. Chesters, and J. C. Hoogendoorn. De- velopment of the Shell-Koppers coal gasification process. Philosophical Transactions of the Royal Society of London. Series A, Mathematical and Physical Sciences, 300:111–120, 1981.

-V. White, R. Allam, E. Miller, Purification of Oxyfuel-derived CO2 for sequestration or EOR, 8th International Conference on GreenHouse Gas Control Technologies, Trondheim, Norway, (2006).

-V.C Patel, W. Rodi, and J. Schneider. Turbulence models for near-wall and low-Reynolds-number flows: A review. AIAA j., 23:1308–1319, 1985.

-V.K. Arghode, A.K. Gupta, Investigation of Reverse Flow Distributed Combustion for Gas Turbine Application, Applied Energy, 88, pp. 1096-1104 (2011).

-Valera-Medina, A., et al., Flame Stabilization and Flashback Avoidance using Passive Nozzle Constrictions, in IFRF International Meeting. June 8th-10th, 2009: Boston, USA.

-Velilla J. Study of the flow at a PFBC cyclone dipleg. PhD thesis, University of Zaragoza, 2005.

-W. H. Beattie, R. Berjoan, and J.-P. Coutures. High temperature solar pyrolysis of coal. Solar Energy, 31:137–143, 1983. 1.3

-W. P. Jones and M. Wille. Large-eddy simulation of a plane jet in a cross-flow. International Journal of Heat and Fluid Flow, 17-3:296– 306, 1995.

-W. Vicente, S. Ocho, J. Aguillo, E. Barrios, An Eulerian model for the simulation of an entrained flow coal gasifier, Applied Thermal Engineering 23 (2003) 1993–2008.

-Wang B, Xu DL, Chu KW, Yu AB. Numerical study of gas–solid flow in a cyclone separator. Appl Math Model 2006;30:1326–42.

-Wang, PhD Thesis 2004.

-Weber R, Boysan F, Swithenbank J, Roberts PA. Computation of near ®eld aerodynamics of swirling expanding Flows. 21st International Symposium on Combustion, 1986. p. 1435-1443.

-Wilk, H. Hofbauer ,Influence of fuel particle size on gasification in a dual fluidized bed steam gasifier, Fuel Processing Technology 115 (2013) 139–151

-Williams F. <http://maeweb.ucsd.edu/~combustion.cermech>.

-Witt PJ, Mittoni LJ. Validation of a CFD model for predicting gas flow in a cyclone. CHEMECA 99, Newcastle, Australia, 1999.

-Wong CY, Lanspeary PV, Nathan GJ, Kelso RM, O'Doherty T. Phase averaged velocity in a fluidic precessing jet nozzle and in the near external field. Exp Therm Fluid Sci 2003;27:515–24

-Y.V. Basevic, S.M. Kogarko, The mechanism of methane combustion: cool flame oxidation, Oxidation Communications, 3 (4), (1983), 199.

-Yang, Z.Y., Priestman, G.H. and Boysan, H.F. (1991), "Internal flow modeling of vortex throttles", Proceedings of Institute of Mechanical Engineers, Part C, J. of Mechanical Engineering Science, Vol. 205, pp. 405-13.

-Y.M. Al-Abdeli and A.R. Masri. Turbulent swirling natural gas flames: Stability characteristics, unsteady behavior and vortex breakdown. Combustion Science and Technology, 179[1]:207–225, 2007. 15

-Z'Graggen, 2008 PhD Thesis.

-Z. Rusak and S. Wang. Review of theoretical approaches to the vortex breakdown phenomenon. AIAA Pap, pages 96–2126, 1996. 12, 13